The monitoring and modelling of the impacts of storms under sea-level rise on a breached coastal dune-barrier system

VOLUME II

FIGURES AND TABLES

A thesis submitted for the degree of PhD in the College of Arts, Celtic Studies, and Social Sciences, National University of Ireland, Cork

By Sarah Kandrot

September 2016

Department of Geography

National University of Ireland, Cork, Ireland

Head of Department: Professor Donald Lyons

Supervisors: Professor Robert Devoy and Dr. Fiona Cawkwell

Table of Contents – Volume II

Figures and Tables

1 Introduction

Figure 2.1 Study area showing location of Inch and Rossbehy beach-dune barriers within Dingle Bay, Co. Kerry. Data source: OSI 1

2 Theoretical Background

Figure 2.1 Sedimentary environments present at study site. Data sources: OSI; Guilcher et al. (1960) 2
Figure 2.2 Idealised model of barrier spit development. LST = longshore sediment transport. A reduction in wave energy at the updrift corner of a headland due to wave refraction results in the deposition of sediment, which initiates spit growth. Source: Davis and FitzGerald (2004) 2
Figure 2.3 Foredune and storm built beach ridge at Inch. Hesp et al. (2005) defined foredunes as accumulations of sand formed by aeolian processes and beach ridges as wave built accumulations of sediment. Image source: author's own. 3
Figure 2.4 Historical recurves (circled) at Rossbehy (left) and Inch (right) may represent eirlier limits of dune progression due to a historical breaching event. Minor drift aligned recurves are present at both sites adjacent to the main inlet. Source: Google Earth (Rossbehy) and OSI (Inch). 3
Figure 2.5 Plan form orientation of drift-aligned vs. swash-aligned barriers. Drift alignment occurs when the down-drift sediment supply is sufficient to fulfil the longshore power for transport, while swash-alignment occurs where the downdrift supply is limited or non-existent. Figure modified from Sala (2009) and Stéphan (2009). 4
Figure 2.6 Phases of spit restructuring after a decrease in longshore sediment supply. Refraction induced changes in the longshore power gradients result in the development of sediment cells. As additional cells develop, breaching may occur at weaker points (along the up-drift cell boundary). If the breach enlarges, it becomes the focus for a transverse transport corridor. Source: Orford et al. (1996). 5
Figure 2.7 Cross section of a breach channel area against water levels showing types of breach, according to
Hartley and Pontee (2008). Modified from Sala (2009). 5
Figure 2.8 Cross-sectional inlet stability relationship of Escoffier (1940). Modified from Escoffier (1940) and van de Kreeke (1992). 6
Figure 2.9 Incipient or embryo dunes at Inch, Co. Kerry. Dune hummocks, like those shown here, are also termed nebkha or coppice dunes. Source: author's own. 6
Figure 2.10 Established foredune at Inch, Co. Kerry. The wooden posts on the ridge are approximately 1 m high. High water mark (not shown) is approximately 15-20 m behind the point from which the photograph was taken. Source: author's own. 7
Figure 2.11 Saucer blowout (width = approximately 15-20 m) at Rossbehy, Co. Kerry. Source: author's own. 7
Figure 2.12 Relict dune ridges at Inch, Co. Kerry. Source: author's own. 8
Figure 2.13 Parabolic (U-shaped) dunes at Inch, Co. Kerry. Source: OSI (2005) 8
Figure 2.14 Conceptual model of the relationship between dune morphology and sediment budget. See text for explanation. Source: Psuty (2004) 9
Figure 2.15 Pre- and post- storm beach profiles. Source: Van Thiel de Vries (2009) 9
Figure 2.16 Dune erosion mechanisms described by Nishi and Kraus (2001). Source: Nishi and Kraus (2001) 10
Figure 2.17 Example of layer separation and collapsing at Rossbehy, Co. Kerry. Source: author's own. 10
Figure 2.18 Phases leading up to post-storm dune recovery. Source: Carter et al . (1990). 11

Figure 2.19 Evidence of slope failure of a dune scarp (height = approximately 5 m) at Rossbeigh, Co. Kerry. Slump blocks held together by vegetation litter the foredune. Source: author's own. 11
Figure 2.20 Morphological components of a typical tidal inlet. Source: Schrader et al. (2000) 12
Figure 2.21 Ebb-tidal delta fronting Inch and Rossbehy barriers. Source of aerial imagery: Google Earth. 12
Figure 2.22 Multiple inlet system at the Nauset barrier system, Cape Cod MA. Dominant longshore transport is southerly. Source: Giese et al. (2009). 13
Figure 2.23 Multiple inlet system at Ria Formosa, Portugal. Source: Salles (2001). 14
Figure 2.24 Categorisation of a typical beach-dune profile. Modified from Schwartz (2006) and Beaugrand (2010). 14
Figure 2.25 Nearshore wave processes. Source: Svendsen (2006) 15
Figure 2.26 Hjulstrom curve showing critical velocities for erosion, transport, and deposition as a function of sediment grain size. Source: http://en.wikipedia.org/wiki/Hjulstr%C3%B6m_curve - Original: Hjulstrom (1939) later modified by Sundborg (1956) 16
Figure 2.27 Forces responsible for sediment entrainment. Modified from MIT OpenCourseWare (available from: http://ocw.mit.edu/courses/earth-atmospheric-and-planetary-sciences/12-090-introduction-to-fluidmotions-sediment-transport-and-current-generated-sedimentary-structures-fall-2006/course-textbook/ch9.pdf) 16
Figure 2.28 Shield's diagram modified by Miller et al. (1977) showing the boundary Reynold's number as a function of the critical Shield's stress for experimental data. Entrainment occurs for conditions above the curve. Source: MIT OpenCourseWare 17
Figure 2.29 Sedimentary cells and sediment budgets near Point Arguello, California, USA. Source: Bowen and Inman (1966) 18

3 The Inch-Rossbehy barrier system

Table 3.1 Previous research undertaken at Inch-Rossbehy 19
Figure 3.1 Ebb shoals fronting Inch and Rossbehy. Imagery obtained 30 August 2010. Source**:** Google Earth 20
Figure 3.2 Seabed substrate within Dingle Bay. Map layer generated from Geological Survey of Ireland (GSI) multibeam echosounder data and seabed sampling data acquired during the INFOMAR and INSS national seabed mapping programmes. 21
Figure 3.3 Dingle Bay bathymetry. Map layer generated from Geological Survey of Ireland (GSI) multibeam echosounder data acquired during the INFOMAR and INSS national seabed mapping programmes. Depth is shown in metres below LAT (according to data obtained from the GSI, LAT is 2.85±0.13metres below ODM at Rossbehy). 21
Figure 3.4 Castlemaine Harbour depth contours. Map layer generated from interpolation of depth soundings published on Navionics free webapp (http://webapp.navionics.com/?lang=en). The data is crowd sourced from recreational boaters using mobile technology to ensure it remains up to date. Units are in metres below LAT. 21
Table 3.2 Paleoenvironmental chronology of Inch-Rossbehy and surrounding environs. 22
Figure 3.5 Exposed peat on the beach face (left, 16 January 2014) and beneath the dune sands (right; 14 April 2015) provides evidence of barrier rollover at Rossbehy. The truncated upper contact of similar woody, monocot peat from a core in the back barrier saltmarsh has been dated by Delaney *et al.* (2012) to 2781-2000 BP. Source: author's own 23
Figure 3.6 Extract of study area from the Down Survey Maps published in 1673. Both Inch and Rossbehy are depicted. Source: http://downsurvey.tcd.ie/down-survey-maps.php 23
Table 3.3 Recent (500 years BP to present) chronology of Inch-Rossbehy. Continued on next page. 24
Figure 3.7 Historical shoreline variations at Inch. Source: Cooper *et al.* (1995) 26
Figure 3.8 Historical shoreline variation at Rossbehy. Source: Cooper *et al.* (1995) 26

Figure 3.9 Results of shoreline change analysis undertaken by O'Shea *et al*. (2011) superimposed on an aerial photograph from 2010. Yellow = 1842; Red = 1894; Black = 2000. Source: O'Shea *et al*. (2011) 27
Figure 3.10 Aerial photographs (1995, 2005, and 2010) and Landsat 8 imagery (2015) of Inch, illustrating the relative stability of its shoreline. Source of imagery: 1995 and 2005 = OSI; 2010 = Google Earth; 2015 = USGS LandsatLook viewer 27
Figure 3.11 Aerial photographs (1997, 1995, 2005, 2010, and 2012) and Landsat 8 imagery (2015) of Rossbehy, illustrating recent changes along its distal shoreline. Source of imagery: 1977, 1995, and 2005 = OSI; 2010 = Google Earth; 2012 = ESRI World Imagery / Microsoft; 2015 = USGS LandsatLook viewer 28
Figure 3.12 Aerial photographs of Rossbehy prior to (September 2008) and after (July 2009) breaching in December 2008. Source: John Herriott aerial photography 29
Figure 3.13 Damage to main road providing access to Rossbehy strand following the winter storms of 2013/2014. Looking north toward the children's play area. Source: The Kerryman (2014) 29
Figure 3.14 Sunbeam shipwreck before 2013/2014 storms (in its original position since 1903; top), after first displacement in December 2013 (middle; lying parallel to foredune ridge) and after final displacement in February 2014 (bottom; lying oblique to foredune ridge). For scale, the boat's maximum width is approximately 5 m and maximum length is approximately 22 m. Source: author's own 30
Figure 3.15 Historic maps (1842, 1894), aerial photographs (1977, 1995, 2005, 2010, 2011, and 2014) and Landsat 8 imagery illustrating changes in the shape and position of ebb shoals off Inch and Rossbehy from 1842 to 2015. Source of maps and 1977 and 1995 imagery: OSI; source of 2010 and 2011 imagery: GoogleEarth; source of 2014 imagery: Irish Air Corps; source of 2015 imagery: USGS LandsatLook viewer. 31
Figure 3.16 Dune blowout at the entrance to Rossbehy strand. Source: author's own 32
Figure 3.17 Annotated DEM illustrating dunescape at Inch, which is characterised by parabolics and transverse ridges. Data derived from aerial LiDAR data provided by the Kerry County Council and flown in April 2011. Box indicates area covered by beach-dune topographic surveys. Adapted from Devoy (2013). 33
Figure 3.18 Annotated DEM illustrating dunescape at Rossbehy, which, like Inch, is characterised by parabolics and transverse ridges. Data derived from aerial LiDAR data provided by the Kerry County Council and flown in April 2011. Box indicates area covered by beach-dune topographic surveys. 34
Figure 3.19 Geotagged panorama showing scarping on the southwestern side of Inch. Map, inset, shows location of photo. Photo source: author's own; Map source: Google Maps 35
Figure 3.20 High foredune ridge in active, southern zone of Inch. Wooden posts on dune ridge are approx. 1 metre in height. Source: author's own (6 October 2012). 35
Figure 3.21 Ephemeral embryonic dunes at southern tip of Inch (looking south towards Dooks golf course). 20 June 2013 Source: author's own 36
Figure 3.22 Transverse ridges in southern and middle interior of Rossbehy. Looking north towards Inch. Source: John Coveney 36
Figure 3.23 Dune slack in middle interior of Rossbehy. Looking south. Source: author's own 37
Figure 3.24 Valentia windrose 1940-2010. Source: Met Éireann 37
Table 3.4 Tidal ranges at Inch Beach based on predictions for a total tidal cycle (20 years). Source: Vial (2008) and Sala (2010) 38
Figure 3.25 Conceptual model of inferred morphological changes in Inch beach and dunes proposed by Orford *et al*. (1999a). Source: Orford *et al*. (1999a) 39
Figure 3.26 Distribution of wave energy dissipation at Inch and Rossbehy under (A) modal swell (H=0.04 m, T = 7 s) and (B) large swell waves (H=6.6 m, T = 13.6 s). Extracted from Cooper *et al*. (2004) 39
Figure 3.27 Wave orbital velocities at Inch and Rossbehy under (A) modal swell conditions and (B) Hurricane Debbie wind-generated waves, indicating relative ability of waves to transport sediment under storm conditions. Extracted from Cooper *et al*. (2004) 39

Figure 3.28 Significant wave heights associated with a 100-year return storm coming from an angle of 240° for (a) mean high water, (b) mean sea level, and (c) mean low water. Extracted from Vial (2008) 40
Figure 3.29 Historical recurves (blue) at Rossbehy represent either earlier northern limits of dune progression or southern limits to a historical breaching event. Figure adapted from O'Shea (2015). 41
Figure 3.30 Sedimentary cells at Rossbehy as defined within the short-term conceptual model of Sala (2010). Looking south. Source: Sala (2010). 41
Figure 3.31 Five-step conceptual model of O'Shea (2015) for breach evolution at Rossbehy. Graphics for stage 1 extracted from O'Shea *et al.* (2013) 42

4 Sea-level change: past, present and future

Figure 3.1 Phanerozoic global sea-level curves derived from the stratigraphic record. Source: http://en.wikipedia.org/wiki/Sea-level_curve - after Vail *et al.* (1977) and Hallam (1981). 43
Figure 4.2 Global sea-level change from coastal tide gauge records - 1870 to 2000. Source**:** CSIRO (2014) 44
Figure 4.3 Multi-mission ocean altimeter data showing global mean sea-levels from 1993 to 2014. Data is with respect to the 1993-2002 mean and plotted every 10 days. Source: NASA Goddard Space Flight Center (2014) 44
Figure 4.4 Modelled and observed GMSL rise from IPCC AR5. Modelled data was computed from the Coupled Model Intercomparison Project (CMIP5) and shows good agreement with observations. Source: Church *et al.* (2013). 45
Figure 4.5 Derived projected RSL increases under the IPCC AR4 medium emissions scenario for the year 2095. Projections take into account both absolute SLR and vertical land movement due to glacial isostatic adjustment. Source: Lowe *et al.* (2009) 45
Figure 4.6 Oblique aerial photos of Portballintrae Beach in 1938 (top) and 1999 (bottom) illustrating beach narrowing as a result of the installation of a pier in its western section. Source: Jackson (2012) 46

6 Terrestrial laser scanning: a new approach to monitoring beach morphodynamics

Figure 6.1 Airborne LiDAR systems work by sending out multiple laser pulses and recording the time it takes for the signal to be reflected off the ground and returned to the sensor. These systems consist of three main parts: the sensor, the inertial measurement unit, and a GPS. Source: Heritage and Large (2009) 47
Figure 6.2 Ground-based LiDAR systems use the same basic technology as airborne systems, but are deployed on the ground. While they are limited in terms of coverage area compared to airborne systems, they are capable of capturing higher resolution data and are easier to deploy at short notice (*e.g.* in the aftermath of a storm). 47
Figure 6.3 Point cloud showing beach and foredunes (centre) at the terminal margin of the Rossbehy barrier (looking south). The dune scarp (centre right) is the on seaward side of barrier, with the vegetated lee side shown centre left. The track marks are from the wheels of the trolley used to transport equipment to the field site, which are approx. 7 cm in width. This figure illustrates the fine detail that can be captured using this survey technique. 48
Figure 6.4 Shadow zones - zones of missing data located behind obstructions to the laser scanners field of view, resulting in 'gaps' in the point cloud. These can be minimised by obtaining multiple surveys over the same area from different angles. Source: author's own data obtained at Rossbehy field site 48
Figure 6.5 Survey target, as seen in a point cloud, used for referencing multiple scans to one common coordinate system. Source: author's own data obtained at Rossbehy field site 49

Figure 6.6 DEMs generated from TLS data collected at monthly intervals at Rehoboth Beach, North Carolina, USA from January 2006-April 2007. Areas of maximum erosion are shown in black and grade to areas of maximum accretion, shown in white. The data was collected at 0.20 m resolution over an area of approximately 500 m x 70 m and reduced to 1 m x 1 m grid cells. Source: Pietro *et al*. (2008) 49
Figure 6.7 Digital elevation model of embryo dunes in North Lincolnshire, UK. Elevation in metres. Source: Montreuil *et al*. (2013) 50
Figure 6.8 Rendered triangular irregular network (TIN) showing a hard rock cliff face in North Yorkshire, UK (left) and close up (right) showing triangular faces. TLS data form the nodes of the TIN. Source: Rosser *et al*. (2005) 50
Figure 6.9 Graphic illustrating how natural neighbour interpolation works. See text for explanation. Image source: ESRI ArcGIS 9.2 Desktop Help (http://webhelp.esri.com/arcgisdesktop/9.2/index.cfm?TopicName=Natural%20Neighbor%20Interpolation) 51
Figure 6.10 Graphic illustrating how inverse distance weighting interpolation works. See text for explanation. Image source: ESRI ArcGIS 9.2 Desktop Help (http://webhelp.esri.com/arcgisdesktop/9.2/index.cfm?TopicName=Implementing_Inverse_Distance_Weighted_(IDW)) 51
Figure 6.11 DEMs of difference showing seasonal changes to embryo dunes for three periods between October 2009 and October 2010. Source: Montreuil *et al*. (2013) 52
Figure 6.12 Example of compartments (top) generated in TOPCAT for a case study at Dog Beach, Del Mar California (Oct 2005–March 2007). Compartments are overlain on elevation change map. Graphs show cliff face retreat rate (centre) and volumetric change (bottom) for each compartment along the length of the cliff. F1, F2, and F3 are major cliff failure events. Source: Olsen *et al*. (2012) 52
Figure 6.13 Results of classification using a multi-scale dimensionality criterion for a steep river bank (left, classes labelled) and a tidal marsh (right, green = vegetation, white = soil). Source: Brodu (2012) 53

7 Observations of morphodynamic behaviour under the influence of storms

Figure 7.1 General locations of field sites at Rossbehy and Inch. Source: Modified from OSI vector coastline data and 2010 OSI aerial photography. 54
Figure 7.2 High foredune at Inch field site (looking North). Source: author's own (6 October 2012) 54
Figure 7.3 Ephemeral embryo dune field and beach fronting foredune at Inch field site. Looking southeast. Rossbehy can be seen in the distance. Source: author's own (20 June 2013) 55
Figure 7.4 Oblique aerial view of Inch field site, looking north-northwest. Source: coastalhelicopterview.ie 55
Figure 7.5 General location of Rossbehy field site. Looking south. Source: Google Earth (2012) 56
Figure 7.6 Main section of Rossbehy field site, consisting of upper beach and foredune scarp. Barrier terminus is at left. Looking east. Source: author's own (8 October 2012) 56
Figure 7.7 Terminus of mainland section of barrier (centre). Looking south. Foredune scarp is hidden by shadow (right of centre). Some scans covered part of vegetated dunes (left of centre) and back barrier beach. Source: author's own (15 April 2012) 56
Figure 7.8 Leica ScanStation components. NB: Figure was extracted from Leica ScanStation2 model manual
(Leica Geosystems, 2007), but ScanStation setup is more or less the same. 57
Figure 7.9 Leica ScanStation setup at Rossbehy field site. Looking north at main dune barrier terminus. Source: author's own (15 November 2012) 57
Figure 7.10 Field equipment being transported via tractor and trolley at Inch. Photo: Valerie Heffernan 58
Figure 7.11 Leica HDS registration target – for registration of multiple same-date scans. 58

Figure 7.12 Leica HDS target as seen in section of photo mosaic (inset) and in the point cloud (main). From the mosaic, targets can be identified ('fenced') and the scanner can then be directed to scan only the fenced areas in high resolution for scan registration. 59
Table 7.1 Summary of data obtained during field surveys completed at Rossbehy field site. 60
Table 7.2 Summary of data obtained during field surveys completed at Inch field site. 60
Figure 7.13 Example from Inch field site illustrating same-date scan registration for two point clouds obtained from two stations (S1 and S2). Following registration of the S2 cloud to the S1 cloud using the Leica HDS targets, the clouds are in the coordinate system of the S1 cloud. 61
Figure 7.14 Distribution of registration errors between same-date scans at Inch 62
Figure 7.15 Distribution of registration errors between same-date scans at Rossbehy 62
Figure 7.16 Example of semi-permanent wooden posts set up in the field for registering multi-temporal scans. The tips of the nails act as control points from which the successive scans are registered to one common coordinate system. 63
Figure 7.17 RMS Errors of registration associated with multi-temporal constraints (Post 1, Post 2, and Post 3) for May 2012 and August 2012 at Inch. Left: Post 3 in the May 2012 cloud; Right: Post 3 in the August 2012 cloud. 63
Figure 7.18 Distribution of registration errors between scans registered using semi-permanent targets at Rossbehy. Inset: Population (N), mean, min, and max errors and standard deviation. 64
Figure 7.19 Distribution of registration errors between scans registered using semi-permanent targets at Inch. Inset: Population (N), mean, min, and max errors. 64
Figure 7.20 Distribution of registration errors between scans registered using dGPS coordinates at Rossbehy. Inset: Population (N), mean, min, and max errors. 65
Figure 7.21 Before (top) and after (bottom) vegetation filtering using lowest points analysis on a subset of the May 2012 point cloud from Inch. Subset shown left, with cross section through centre shown right. 65
Figure 7.22 Subset of May 2012 point cloud from Inch on which initial vegetation classification tests were performed. Colours represent laser scanned intensity values, which correspond to the distribution shown in figure 7.23. 66
Figure 7.23 Laser scanned intensity distribution of cloud shown in figure 7.22. Intensity values (x axis) are based on the capabilities of the scanner and are scaled to a range of -2048 to +2048. Y axis represents frequency. 66
Figure 7.24 Result of filtering points with laser scanned intensity values outside -233 to -156 (light blue peak shown in fig. 7.23) from test patch. Close up of ground surface with multiple non-ground points shown top right. 67
Figure 7.25 Histogram showing the distribution of manually sampled ground and vegetation point intensities. 67
Figure 7.26 Mean intensity variation (and standard error bars) with distance from the scanner for 200 manually selected ground points plotted at 5 m intervals up to a distance of 50 m from the position of the scanner. 68
Figure 7.27 Mean intensity variation (and standard error bars) with distance from the scanner for 200 manually selected vegetation points plotted at 5 m intervals up to a distance of 50 m from the position of the scanner. 68
Figure 7.28 Workflow for classifier construction using CANPO. See text for explanation. 69
Figure 7.29 Foredune scarp and upper beach at Rossbehy in November 2012 and January 2013. The distance between the two points shown is 44 m. 70
Figure 7.30 Graphic illustrating the process of coordinate system rotation for foredune point clouds at Rossbehy. In this example, two point clouds are shown, one captured at time t_1 (red) and another captured at a later date, t_2 (blue). These are shown in plan view – e.g. looking down from above (top). Using CloudCompare software, it is possible to rotate the clouds along a rotation axis using the rotate/translate tool. An oblique view of the clouds captured as they were being rotated is shown (middle). The clouds were rotated 90 degrees about this axis, such that their final orientation was as shown (bottom). This was performed for the foredune because few scans overlapped in plan view due to considerable foredune recession over the course of study period. 70

Figure 7.31 Example of classified (top) and filtered (bottom) cloud from May 2012 Inch dataset. 71
Figure 7.32 Example of classified (top) and filtered (bottom) cloud from Rossbehy foredune scarp (June 2012) 71
Figure 7.33 Schematic diagram showing how elevation (z) values from overlapping DEMs can be subtracted to produce DEMs of difference (DODs) for beach at Inch and Rossbehy 72
Figure 7.34 Schematic diagram showing how elevation (z) values from overlapping DEMs can be subtracted to produce DEMs of difference (DODs) for foredune at Rossbehy. 72
Figure 7.35 Cartographic model illustrating GIS workflow for generating elevation/distance change maps and volume change maps. 73
Figure 7.36 Distribution of February 2013 EDM ground truthing points (red) for Inch (top) and Rossbehy (bottom). Basemaps shown are natural neighbour interpolations of unfiltered TLS point clouds where green is low (flat beach) and purple/white is high (foredune crest). 74
Figure 7.37 Error distribution for unfiltered (top) and filtered (bottom) clouds at Inch. 75
Figure 7.38 Error distribution for unfiltered (top) and filtered (bottom) clouds at Rossbehy. 76
Figure 7.39 Voronoi map for Inch data symbolised by standard deviation. The pattern shown suggests the data is non-stationary. As a result, kriging was deemed an inappropriate interpolation method for this data. 77
Table 7.3 Residual errors for February 2013 Inch DEMs generated using unfiltered and filtered TLS point clouds and interpolated using NN, IDW, and EBK. Results of paired t-test demonstrating significant differences between unfiltered and filtered clouds also shown. 77
Figure 7.40 Areal photograph of Rossbehy field site indicating general location of TLS surveys. Locations A and B correspond generally to the maps shown in figures 7.41 to 7.58 and represent the dune barrier terminus (A) and the southern periphery of the surveyed area (B) at the time of the corresponding survey. Source of areal photography: ESRI 78
Figure 7.41 Rossbehy beach elevation change (DOD) between 2012-06-28 and 2012-08-05. Elevation change across the majority of the surveyed area lies below the level of detectable change (±0.41 m) and ranged from -0.27 m to +1.08 m. Locations A and B correspond with those shown in figure 7.42. The coordinate marked with the triangle is at the same location as that shown in figure 7.43 (the DOD for the subsequent survey period) for reference. Mean sea level (MSL) is equal to +2.3 m ODM. 79
Figure 7.42 Rossbehy foredune distance change between 2012-06-28 and 2012-08-05. Dune recession is shown in varying shades of red and advance in varying shades of blue. Distance change below the level of detectable change (±0.41 m) is shown in gray. Distance change across the surveyed area ranged from -5.74 m to +4.20 m. Locations A and B correspond with those shown in figure 7.41. Mean sea level (MSL) is equal to +2.3 m ODM. 80
Figure 7.43 Rossbehy beach elevation change (DOD) between 2012-08-05 and 2012-10-07. Beach erosion is shown in red, while accretion is shown in blue. Elevation changes below the level of detectable change (±0.41 m) are shown in gray. Elevation change ranged from -2.15 m to +5.49 m. The coordinate marked with the triangle is at the same location as that shown in figure 7.41 (the DOD for the previous period) for reference. Locations A and B correspond (in a general way) with those shown in figure 7.40. Mean sea level (MSL) is equal to +2.3 m ODM. 81
Figure 7.44 Rossbehy foredune distance change between 2012-08-05 and 2012-11-15. Dune recession is shown in varying shades of red and advance in varying shades of blue. Distance change below the level of detectable change (±0.41 m) is shown in gray. Distance change across the surveyed area ranged from -18.28 m to +5.05 m. For reference, locations A and B correspond (in a general way) with those shown in figure 7.40. Mean sea level (MSL) is equal to +2.3 m ODM. 82
Figure 7.45 Rossbehy foredune distance change between 2012-11-15 and 2013-01-30. Dune recession is shown in varying shades of red. Distance change across the surveyed area ranged from -16.95 m to -44.97 m. For reference, locations A and B

correspond (in a general way) with those shown in figure 7.40. Mean sea level (MSL) is equal to +2.3 m ODM. 83
Figure 7.46 Rossbehy beach elevation change (DOD) between 2013-01-30 and 2013-02-28. Accretion occurred across the majority of the surveyed area (varying shades of blue). Area in gray lies below the level of detectable change (±0.41 m). Elevation change ranged from +0.18 m to +0.99 m. Locations A and B correspond with those shown in figure 7.47. The coordinate marked with the circle is at the same location as that shown in figures 7.48, 7.50, and 7.52 (the DODs for the subsequent survey periods) for reference. Mean sea level (MSL) is equal to +2.3 m ODM. 84
Figure 7.47 Rossbehy foredune distance change between 2013-01-30 and 2013-02-28. Dune recession is shown in varying shades of red and advance in varying shades of blue. Distance change below the level of detectable change (±0.41 m) is shown in gray. Distance change across the surveyed area ranged from -2.80 m to +2.34 m. For reference, locations A and B correspond with those shown in figure 7.46. Mean sea level (MSL) is equal to +2.3 m ODM. 85
Figure 7.48 Rossbehy beach elevation change (DOD) between 2013-02-28 and 2013-04-19. Beach erosion occurred across the entire survey area (varying shades of red). Beach elevation change ranged from -1.94 m to -0.62 m. Locations A and B correspond with those shown in figure 7.49. The coordinate marked with the circle is at the same location as that shown in figures 7.46, 7.50, and 7.52 (the DODs for the previous and subsequent survey periods) for reference. Mean sea level (MSL) is equal to +2.3 m ODM. 86
Figure 7.49 Rossbehy foredune distance change between 2013-02-28 and 2013-04-19. Dune recession, which occurred across the entire length of the surveyed area, is shown in varying shades of red. Distance change ranged from -1.39 m to -6.40 m. For reference, locations A and B correspond with those shown in figure 7.48. Mean sea level (MSL) is equal to +2.3 m ODM. 87
Figure 7.50 Rossbehy beach elevation change (DOD) between 2013-04-19 and 2013-06-05. Elevation change across the majority of the site lies below the level of detectable change (±0.41 m) and ranges from -0.17 m to +0.51 m. Locations A and B correspond with those shown in figure 7.51. The coordinate marked with the circle is at the same location as that shown in figures 7.46, 7.48, and 7.52 (the DODs for the previous and subsequent survey periods) for reference. Mean sea level (MSL) is equal to +2.3 m ODM. 88
Figure 7.51 Rossbehy foredune distance change between 2013-04-19 and 2013-06-05. Distance change across the majority of the surveyed area lies below the level of detectable change (±0.41 m) and ranges from -2.16 m to +2.34 m. For reference, locations A and B correspond with those shown in figure 7.50. Mean sea level (MSL) is equal to +2.3 m ODM. 89
Figure 7.52 Rossbehy beach elevation change (DOD) between 2013-06-05 and 2013-12-11. Elevation change across the majority of the site lies below the level of detectable change (±0.44 m) and ranges from -0.13 m and +0.88 m. Locations A and B correspond with those shown in figure 7.53. The coordinate marked with the circle is at the same location as that shown in figures 7.46, 7.48, and 7.50 (the DODs for the previous survey periods) for reference. Mean sea level (MSL) is equal to +2.3 m ODM. 90
Figure 7.53 Rossbehy foredune distance change between 2013-06-05 and 2013-12-11. Dune recession is shown in varying shades of red and advance in varying shades of blue. Distance change below the level of detectable change (±0.44 m) is shown in gray. Distance change across the surveyed area ranged from -3.62 m to +7.15 m. For reference, locations A and B correspond with those shown in figure 7.52. Mean sea level (MSL) is equal to +2.3 m ODM. 91
Figure 7.54 Rossbehy foredune distance change between 2013-12-11 and 2014-01-16. Dune recession, which occurred across the entire length of the surveyed area, is shown in varying shades of red. Distance change ranged from -54.33 m to -33.06 m. For reference, locations A and B correspond (in a general way) with those shown in figure 7.40. Mean sea level (MSL) is equal to +2.3 m ODM. 92
Figure 7.55 Rossbehy beach elevation change (DOD) between 2014-06-16 and 2014-05-04. Elevation change across the majority of the site lies below the level of

detectable change (±0.44 m) and ranges from -0.42 m to +1.42 m. Locations A and B correspond with those shown in figure 7.56. The coordinate marked with the square is at the same location as that shown in figure 7.57 (the DOD for the subsequent survey period) for reference. Mean sea level (MSL) is equal to +2.3 m ODM. 93

Figure 7.56 Rossbehy foredune distance change between 2014-01-16 and 2014-05-04. Dune recession, which occurred across the entire length of the surveyed area, is shown in varying shades of red. Distance change ranged from -6.41 m to -0.29 m. For reference, locations A and B correspond with those shown in figure 7.55. Mean sea level (MSL) is equal to +2.3 m ODM. 94

Figure 7.57 Rossbehy beach elevation change (DOD) between 2014-05-04 and 2014-07-29. Accretion (varying shades of blue) occurred across the majority of the site. Elevation change below the level of detectable change (±0.44 m) is shown in gray. Elevation change across the surveyed area ranged from -0.87 m to +1.40 m. Locations A and B correspond with those shown in figure 7.58. The coordinate marked with the square is at the same location as that shown in figure 7.55 (the DOD for the previous survey period) for reference. Mean sea level (MSL) is equal to +2.3 m ODM. 95

Figure 7.58 Rossbehy foredune distance change between 2014-05-04 and 2014-07-29. Distance change across much of the surveyed area lies below the level of detectable change (±0.44 m) and ranges from -2.91 m to +2.47 m. For reference, locations A and B correspond with those shown in figure 7.57. Mean sea level (MSL) is equal to +2.3 m ODM. 96

Table 7.4 Summary of elevation and volume changes for beach at Rossbehy field site. 97

Table 7.5 Summary of distance and volumetric changes for foredune at Rossbehy field site. 98

Figure 7.59 Shoreline positions at Rossbehy during TLS monitoring campaign. The shoreline is defined as position of the dune toe, or the line along which there is an abrupt change in slope, marking the boundary between the beach and dune. The March 2012 shoreline was digitized from an aerial photograph (for reference), while the others were digitized from TLS data. 99

Figure 7.60 Areal photographs of Inch field site indicating location of TLS surveys. The area enclosed by the green polygon is the area over which all surveys overlap. Source of areal photography: ESRI 100

Figure 7.61 Inch beach elevation change (DOD) between 2012-05-24 and 2012-08-06. Beach erosion is shown in varying shades of red and accretion in varying shades of blue. Elevation change below the level of detectable change (±0.05 m) is shown in gray. Elevation change ranged from -3.00 m to +2.76 m. The coordinate marked with the star is at the same location as that shown in figures 7.62-7.68 (the DODs for the subsequent survey periods) for reference. The area enclosed by the gray polygon is the area across which all surveys overlap. Mean sea level (MSL) is equal to +2.3 m ODM. 101

Figure 7.62 Inch beach elevation change (DOD) between 2012-08-06 and 2012-10-06. Beach erosion is shown in varying shades of red and accretion in varying shades of blue. Elevation change below the level of detectable change (±0.05 m) is shown in gray. Elevation change ranged from -5.42 m to +4.43 m. The coordinate marked with the star is at the same location as that shown in figures 7.61-7.68 (the DODs for the previous and subsequent survey periods) for reference. The area enclosed by the gray polygon is the area across which all surveys overlap. Mean sea level (MSL) is equal to +2.3 m ODM. 102

Figure 7.63 Inch beach elevation change (DOD) between 2012-10-06 and 2013-01-09. Beach erosion is shown in varying shades of red and accretion in varying shades of blue. Elevation change below the level of detectable change (±0.05 m) is shown in gray. Elevation change ranged from -1.78 m to +2.41 m. The coordinate marked with the star is at the same location as that shown in figures 7.61-7.68 (the DODs for the previous and subsequent survey periods) for reference. The area enclosed by the gray polygon is the area across which all surveys overlap. Mean sea level (MSL) is equal to +2.3 m ODM. 103

Figure 7.64 Inch beach elevation change (DOD) between 2013-01-09 and 2013-02-27. Beach erosion is shown in varying shades of red and accretion in varying shades of

blue. Elevation change below the level of detectable change (±0.05 m) is shown in gray. Elevation change ranged from -2.11 m to +1.96 m. The coordinate marked with the star is at the same location as that shown in figures 7.61-7.68 (the DODs for the previous and subsequent survey periods) for reference. The area enclosed by the gray polygon is the area across which all surveys overlap. Mean sea level (MSL) is equal to +2.3 m ODM. 104

Figure 7.65 Inch beach elevation change (DOD) between 2013-02-27 and 2013-05-02. Beach erosion is shown in varying shades of red and accretion in varying shades of blue. Elevation change below the level of detectable change (±0.05 m) is shown in gray. Elevation change ranged from -2.00 m to +1.96 m. The coordinate marked with the star is at the same location as that shown in figures 7.61-7.68 (the DODs for the previous and subsequent survey periods) for reference. The area enclosed by the gray polygon is the area across which all surveys overlap. Mean sea level (MSL) is equal to +2.3 m ODM. 105

Figure 7.66 Inch beach elevation change (DOD) between 2013-05-02 and 2013-06-20. Beach erosion is shown in varying shades of red and accretion in varying shades of blue. Elevation change below the level of detectable change (±0.05 m) is shown in gray. Elevation change ranged from -5.29 m to +3.09 m. The coordinate marked with the star is at the same location as that shown in figures 7.61-7.68 (the DODs for the previous and subsequent survey periods) for reference. The area enclosed by the gray polygon is the area across which all surveys overlap. Mean sea level (MSL) is equal to +2.3 m ODM. 106

Figure 7.67 Inch beach elevation change (DOD) between 2013-06-20 and 2014-03-12. Beach erosion is shown in varying shades of red and accretion in varying shades of blue. Elevation change below the level of detectable change (±0.05 m) is shown in gray. Elevation change ranged from -3.56 m to +2.84 m. The coordinate marked with the star is at the same location as that shown in figures 7.61-7.68 (the DODs for the previous and subsequent survey periods) for reference. The area enclosed by the gray polygon is the area across which all surveys overlap. Mean sea level (MSL) is equal to +2.3 m ODM. 107

Figure 7.68 Inch beach elevation change (DOD) between 2014-03-12 and 2014-08-28. Beach erosion is shown in varying shades of red and accretion in varying shades of blue. Elevation change below the level of detectable change (±0.05 m) is shown in gray. Elevation change ranged from -1.26 m to +2.34 m. The coordinate marked with the star is at the same location as that shown in figures 7.61-7.67 (the DODs for the previous survey periods) for reference. The area enclosed by the gray polygon is the area across which all surveys overlap. Mean sea level (MSL) is equal to +2.3 m ODM. 108

Figure 7.69 Embryo dune field at Inch on 20 June 2013 (top) and 12 March 2014 (bottom). The embryo dune field likely shielded the foredune from extreme waves during the winter 2013/2014 storms. Source: author's own 109

Table 7.6 Summary of elevation and volume changes at Inch field site. 110

Figure 7.70 Rates of volume change for Rossbehy (top) and Inch (bottom) for TLS monitoring periods. Note the large difference in scale between rates of volume change for Rossbehy beach and scarp and between Rossbehy and Inch generally. 111

8 Relationships between observed morphological change and storms

Figure 8.1 Model domain and flexible mesh on which WAM was run. Extracted from O'Shea *et al*. (2011) 112

Figure 8.2 Five points in WAM model domain for which outputs (significant wave height, wave period, and wave direction) were extracted. 112

Table 8.1 Summary of event information extracted from WAM data. Events are described as times when the significant wave height, H_s, exceeded the critical wave height, h_{crit} (see text for explanation), for a minimum duration of 12 hours. 113

Figure 8.3 Breakdown of storm events identified using WAM data by event duration. 116

Figure 8.4 Modelled event frequency by month during morphologic monitoring period. 116

Figure 8.5 Excel spreadsheet and formulae used to identify storm events and extract storm characteristics from simulated WAM data. Records (rows) extend below the window shown. Formulae examples are for the first entry and were applied to each subsequent entry (*eg.* the cells below). 117
Figure 8.6 Excel worksheets and formulae used to extract storm characteristics from Ventry weather station data. Records (rows) extend below the windows shown. Formulae examples are for the first entry and were applied to each subsequent entry (*eg.* the cells below). 118
Figure 8.7 Location of weather station set up near Inch field site. 119
Figure 8.8 Wind roses and wind speeds for Inch and Ventry from 6 August 2012 to 5 September 2012. Wind speeds were derived from instantaneous wind speeds averaged at half hourly (or approximately half hourly) intervals. Running means (with 48 hour periods) have been superimposed on the wind speed graph for visual clarity. 120
Figure 8.9 Wind roses and wind speeds for Inch and Ventry from 15 October 2012 to 26 October 2012. Wind speeds were derived from instantaneous wind speeds averaged at half hourly (or approximately half hourly) intervals. Running means (with 48 hour periods) have been superimposed on the wind speed graph for visual clarity. 121
Figure 8.10 Wind roses and wind speeds for Inch and Ventry from 21 August 2013 to 3 September 2013. Wind speeds were derived from instantaneous wind speeds averaged at half hourly (or approximately half hourly) intervals. Running means (with 48 hour periods) have been superimposed on the wind speed graph for visual clarity. 122
Table 8.2 Summary of event information extracted from Ventry weather station data. 123
Figure 8.11 Histogram showing frequency of storm events with a range of mean wind speeds. 126
Figure 8.12 Histogram showing frequency of storm events with a range of maximum gust speeds. 126
Figure 8.13 Frequency of events with prevailing wind directions from the north, northeast, east, southeast, south, southwest, west, and northwest. 126
Figure 8.14 (a.) Rates of volume change at Rossbehy beach broken down by morphological monitoring period. (b.) Event frequency for storm events occurring during corresponding morphological monitoring periods. (c.) There was a very weak positive relationship between rate of beach volume change and event frequency (n=7, r=0.09). This relationship was not statistically significant (p=0.85). Negative rates of beach volume change are associated with net volume losses; positive rates of beach volume change are associated with net volume gains. 127
Figure 8.15 (a.) Rates of foredune volume change at Rossbehy broken down by morphological monitoring period. (b.) Event frequency for storm events occurring during corresponding morphological monitoring periods. (c.) There was a very weak positive relationship between rate of foredune volume change and event frequency (n=9, r=0.12). This relationship was not statistically significant (p=0.76). Negative rates of dune volume change are associated with net volume losses; positive rates of dune volume change are associated with net volume gains. 128
Figure 8.16 (a.) Rates of volume change at Inch broken down by morphological monitoring period. (b.) Event frequency for storm events occurring during corresponding morphological monitoring periods. (c.) There was a weak positive relationship between rate of volume change and event frequency (n=8, r=0.3). This relationship was not statistically significant (p=0.47). Negative rates of volume change are associated with net volume losses; positive rates of volume change are associated with net volume gains. 129
Figure 8.17 (a.) Rates of volume change at Rossbehy beach broken down by morphological monitoring period. (b.) Mean duration of storm events that occurred during corresponding morphological monitoring periods. (c.) There was a moderate negative relationship between rate of beach volume change and mean duration of events (n=7, r=-0.59). This relationship was not statistically significant (p=0.17). Negative rates of beach volume change are associated with net volume

losses; positive rates of beach volume change are associated with net volume gains. 130

Figure 8.18 (a.) Rates of foredune volume change at Rossbehy broken down by morphological monitoring period. (b.) Mean duration of storm events occurring during corresponding morphological monitoring periods. (c.) There was a very strong negative relationship between rate of foredune volume change and mean duration of events (n=9, r=-0.96). This relationship was statistically significant (p<0.001). Negative rates of dune volume change are associated with net volume losses; positive rates of dune volume change are associated with net volume gains. This result indicates longer duration events are associated with higher rates of dune volume loss. 131

Figure 8.19 (a.) Rates of volume change at Rossbehy beach broken down by morphological monitoring period. (b.) Maximum duration of storm events that occurred during corresponding morphological monitoring periods. (c.) There was a weak negative relationship between rate of beach volume change and max duration of events (n=7, r=-0.39). This relationship was not statistically significant (p=0.40). Negative rates of beach volume change are associated with net volume losses; positive rates of beach volume change are associated with net volume gains. 132

Figure 8.20 (a.) Rates of foredune volume change at Rossbehy broken down by morphological monitoring period. (b.) Maximum durations of storm events occurring during corresponding morphological monitoring periods. (c.) There was a very strong negative relationship between rate of foredune volume change and maximum duration of events (n=9, r=-0.93). This relationship was statistically significant (p<0.001). Negative rates of dune volume change are associated with net volume losses; positive rates of dune volume change are associated with net volume gains. This result indicates longer duration events are associated with higher rates of dune volume loss. 133

Figure 8.21 (a.) Rates of volume change at Inch broken down by morphological monitoring period. (b.) Mean duration of storm events which occurred during corresponding morphological monitoring periods. (c.) There was a moderate positive relationship between rate of beach volume change and mean duration of events (n=8, r=0.51). This relationship was not statistically significant (p=0.20). Negative rates of volume change are associated with net volume losses; positive rates of volume change are associated with net volume gains. 134

Figure 8.22 (a.) Rates of volume change at Inch broken down by morphological monitoring period. (b.) Maximum duration of storm events which occurred during corresponding morphological monitoring periods. (c.) There was a weak positive relationship between rate of beach volume change and max duration of events (n=8, r=0.37). This relationship was not statistically significant (p=0.37). Negative rates of volume change are associated with net volume losses; positive rates of volume change are associated with net volume gains. 135

Figure 8.23 (a.) Rates of volume change at Rossbehy beach broken down by morphological monitoring period. (b.) Max tidal level for events that occurred during corresponding morphological monitoring periods. (c.) There was a moderate negative relationship between rate of beach volume change and max tidal levels associated with events (n=7, r=-0.45). This relationship was not statistically significant (p=0.31). Negative rates of beach volume change are associated with net volume losses; positive rates of beach volume change are associated with net volume gains. 136

Figure 8.24 (a.) Rates of foredune volume change at Rossbehy broken down by morphological monitoring period. (b.) Maximum tidal levels associated with events that occurred during corresponding morphological monitoring periods. (c.) There was a moderate negative relationship between rate of foredune volume change and max tidal levels associated with events (n=9, r=-0.48). This relationship was not statistically significant (p=0.19). Negative rates of dune volume change are associated with net volume losses; positive rates of dune volume change are associated with net volume gains. 137

Figure 8.25 (a.) Rates of volume change at Inch broken down by morphological monitoring period. (b.) Max tidal levels associated with storm events that

occurred during corresponding morphological monitoring periods. (c.) There was a weak positive relationship between rate of volume change and mean time between events (n=8, r=0.33). This relationship was not statistically significant (p=0.42). Negative rates of volume change are associated with net volume losses; positive rates of volume change are associated with net volume gains. 138

Figure 8.26 (a.) Rates of volume change at Rossbehy beach broken down by morphological monitoring period. (b.) Mean time betwen storm events that occurred during corresponding morphological monitoring periods. (c.) There was a weak negative relationship between rate of beach volume change and mean time between events (n=7, r=-0.32). This relationship was not statistically significant (p=0.48). Negative rates of beach volume change are associated with net volume losses; positive rates of beach volume change are associated with net volume gains. 139

Figure 8.27 (a.) Rates of foredune volume change at Rossbehy broken down by morphological monitoring period. (b.) Mean time between storm events that occurred during corresponding morphological monitoring periods. (c.) There was a moderate positive relationship between rate of foredune volume change and mean time between events (n=9, r=0.56). This relationship was not statistically significant (p=0.11). Negative rates of dune volume change are associated with net volume losses; positive rates of dune volume change are associated with net volume gains. 140

Figure 8.28 (a.) Rates of volume change at Inch broken down by morphological monitoring period. (b.) Mean time between storm events that occurred during corresponding morphological monitoring periods. (c.) There was a moderate negative relationship between rate of volume change and mean time between events (n=8, r=-0.44). This relationship was not statistically significant (p=0.27). Negative rates of volume change are associated with net volume losses; positive rates of volume change are associated with net volume gains. 141

Figure 8.29 (a.) Rates of volume change at Rossbehy beach broken down by morphological monitoring period. (b.) Mean significant wave height associated with storm events that occurred during corresponding morphological monitoring periods. (c.) There was a strong negative relationship between rate of beach volume change and mean H_s associated with events (n=7, r=-0.67). This relationship was not statistically significant (p=0.10). Negative rates of beach volume change are associated with net volume losses; positive rates of beach volume change are associated with net volume gains. 142

Figure 8.30 (a.) Rates of foredune volume change at Rossbehy broken down by morphological monitoring period. (b.) Mean significant wave height associated with storm events that occurred during corresponding morphological monitoring periods. (c.) There was a moderate negative relationship between rate of foredune volume change and mean H_s associated with events (n=9, r=-0.5). This relationship was not statistically significant (p=0.17). Negative rates of dune volume change are associated with net volume losses; positive rates of dune volume change are associated with net volume gains. 143

Figure 8.31 (a.) Rates of volume change at Rossbehy beach broken down by morphological monitoring period. (b.) Maximum significant wave height associated with storm events that occurred during corresponding morphological monitoring periods. (c.) There was a moderate negative relationship between rate of beach volume change and max H_s associated with events (n=7, r=-0.56). This relationship was not statistically significant (p=0.20). Negative rates of beach volume change are associated with net volume losses; positive rates of beach volume change are associated with net volume gains. 144

Figure 8.32 (a.) Rates of foredune volume change at Rossbehy broken down by morphological monitoring period. (b.) Maximum significant wave height associated with storm events that occurred during corresponding morphological monitoring periods. (c.) There was a moderate negative relationship between rate of foredune volume change and max H_s associated with events (n=9, r=-0.58). This relationship was not statistically significant (p=0.10). Negative rates of dune volume change are associated with net volume losses; positive rates of dune volume change are associated with net volume gains. 145

Figure 8.33 (a.) Rates of volume change at Inch broken down by morphological monitoring period. (b.) Mean significant wave height associated with storm events that occurred during corresponding morphological monitoring periods. (c.) There was a strong positive relationship between rate of volume change and mean H_s associated with events (n=8, r=0.74). This relationship was statistically significant ($p<0.05$). Negative rates of volume change are associated with net volume losses; positive rates of volume change are associated with net volume gains. This result indicates higher significant wave heights during storms are associated with higher rates of volume gain at the site. 146

Figure 8.34 (a.) Rates of volume change at Inch broken down by morphological monitoring period. (b.) Maximum significant wave height associated with storm events that occurred during corresponding morphological monitoring periods. (c.) There was a strong positive relationship between rate of volume change and max H_s associated with events (n=8, r=0.62). This relationship was not statistically significant (p=0.10). Negative rates of volume change are associated with net volume losses; positive rates of volume change are associated with net volume gains. 147

Figure 8.35 (a.) Rates of volume change at Rossbehy beach broken down by morphological monitoring period. (b.) Mean peak wave period associated with storm events that occurred during corresponding morphological monitoring periods. (c.) There was a weak negative relationship between rate of beach volume change and mean peak period associated with events (n=7, r=-0.34). This relationship was not statistically significant (p=0.46). Negative rates of beach volume change are associated with net volume losses; positive rates of beach volume change are associated with net volume gains. 148

Figure 8.36 (a.) Rates of foredune volume change at Rossbehy broken down by morphological monitoring period. (b.) Mean peak wave period associated with storm events that occurred during corresponding morphological monitoring periods. (c.) There was a very weak relationship (neither positive or negative) between rate of foredune volume change and mean peak period associated with events (n=9, r=0). This relationship was not statistically significant (p=0.998). Negative rates of dune volume change are associated with net volume losses; positive rates of dune volume change are associated with net volume gains. 149

Figure 8.37 (a.) Rates of volume change at Inch broken down by morphological monitoring period. (b.) Mean peak wave period associated with storm events that occurred during corresponding morphological monitoring periods. (c.) There was a moderate positive relationship between rate of volume change and mean peak period associated with events (n=8, r=0.57). This relationship was not statistically significant (p=0.14). Negative rates of volume change are associated with net volume losses; positive rates of volume change are associated with net volume gains. 150

Figure 8.38 (a.) Rates of volume change at Rossbehy beach broken down by morphological monitoring period. (b.) Mean wind speed associated with storm events that occurred during corresponding morphological monitoring periods. (c.) There was a very weak positive relationship between rate of beach volume change and mean wind speed associated with events (n=7, r=0.09). This relationship was not statistically significant (p=0.84). Negative rates of beach volume change are associated with net volume losses; positive rates of beach volume change are associated with net volume gains. 151

Figure 8.39 (a.) Rates of foredune volume change at Rossbehy broken down by morphological monitoring period. (b.) Mean wind speeds associated with storm events that occurred during corresponding morphological monitoring periods. (c.) There was a very weak positive relationship between rate of foredune volume change and mean wind speed associated with events (n=9, r=0.17). This relationship was not statistically significant (p=0.66). Negative rates of dune volume change are associated with net volume losses; positive rates of dune volume change are associated with net volume gains. 152

Figure 8.40 (a.) Rates of volume change at Rossbehy beach broken down by morphological monitoring period. (b.) Max gust speed associated with storm events that occurred during corresponding morphological monitoring periods. (c.)

There was a weak negative relationship between rate of beach volume change and mean wind speed associated with events (n=7, r=-0.39). This relationship was not statistically significant (p=0.39). Negative rates of beach volume change are associated with net volume losses; positive rates of beach volume change are associated with net volume gains. 153

Figure 8.41 (a.) Rates of foredune volume change at Rossbehy broken down by morphological monitoring period. (b.) Maximum gust speeds associated with storm events that occurred during corresponding morphological monitoring periods. (c.) There was a weak negative relationship between rate of foredune volume change and max gust speed associated with events (n=9, r=-0.29). This relationship was not statistically significant (p=0.45). Negative rates of dune volume change are associated with net volume losses; positive rates of dune volume change are associated with net volume gains. 154

Figure 8.42 (a.) Rates of volume change at Inch broken down by morphological monitoring period. (b.) Mean wind speed associated with storm events that occurred during corresponding morphological monitoring periods. (c.) There was a very weak negative relationship between rate of beach volume change and mean wind speeds associated with events (n=8, r=-0.04). This relationship was not statistically significant (p=0.92). Negative rates of volume change are associated with net volume losses; positive rates of volume change are associated with net volume gains. 155

Figure 8.43 (a.) Rates of volume change at Inch broken down by morphological monitoring period. (b.) Maximum gust speed associated with storm events that occurred during corresponding morphological monitoring periods. (c.) There was a moderate positive relationship between rate of beach volume change and max gust speeds associated with events (n=8, r=0.46). This relationship was not statistically significant (p=0.24). Negative rates of volume change are associated with net volume losses; positive rates of volume change are associated with net volume gains. 156

Figure 8.44 (a.) Rates of volume change at Rossbehy beach broken down by morphological monitoring period. (b.) Prevailing wind directions for events occurring during each corresponding morphological monitoring period. 157

Figure 8.45 (a.) Rates of foredune volume change at Rossbehy broken down by morphological monitoring period. (b.) Prevailing wind directions for events occurring during each corresponding morphological monitoring period. 158

Figure 8.46 (a.) Rates of volume change at Inch broken down by morphological monitoring period. (b.) Prevailing wind directions for events occurring during each corresponding morphological monitoring period. 159

Table 8.3 Rates of beach volume change for each of the morphological monitoring periods at Rossbehy and event characteristics used to test for the existence of simple linear relationships. No statistically significant correlations were observed between rate of beach volume change and any of these variables. 160

Table 8.4 Rates of scarp volume change for each of the morphological monitoring periods at Rossbehy and event characteristics used to test for the existence of simple linear relationships. Strong negative statistically significant correlations were observed between mean duration of events and rate of scarp volume change and maximum duration of events and rate of scarp volume change (p-values highlighted in blue). 161

Table 8.5 Rates of volume change for each of the morphological monitoring periods at Inch and event characteristics used to test for the existence of simple linear relationships. A strong positive statistically significant correlation was observed between mean H_s associated with events and rate of volume (p-value highlighted in blue). 162

Figure 8.47 Residual scatterplot showing predicted scores against errors of prediction for Rossbehy foredune rate of change multiple regression analysis. The plot confirms that the homoscedasticity assumption is met. 163

Figure 8.48 Distribution of residuals for Rossbehy scarp rate of change multiple regression analysis. The distribution is close to normal, satisfying a principal assumption for multiple regression analysis. 163

9 Investigation of sediment transport pathways at Rossbehy using a sediment tracer method

Figure 9.1 Methods of tracer injection 164
Figure 9.2 Dry tracer particles used in this experiment. 165
Figure 9.3 Tracer/sand mix under UV light at injection site. 165
Figure 9.4 Sites of sediment tracer injection and locations of core samples for December 2013 tracer experiment. The shoreline at distal end of the barrier has been updated to reflect the dune toe position on 11 December 2013, at which time a TLS survey was also carried out. The 2 kg injection site was at an elevation of 2.91 m ODM and the 0.5 kg injection site was at an elevation of 2.50 m. 166
Figure 9.5 Sampling with half pipes and trowel. 166
Figure 9.6 December sediment tracer experiment timeline in relation to tidal cycle. Source of tide data: Marine Institute 167
Figure 9.7 Wind speeds and directions during December 2012 tracer experiment. Winds were predominantly southwesterly, with average speeds of 5.5 m/s. Hourly data obtained from Ventry weather station. 168
Figure 9.8 Samples from the December tracer experiment were analysed in 1.5 cm layers, whereby each layer was carefully removed, broken, and sifted through. The presence and number of individual tracer particles was noted for each layer. 169
Figure 9.9 Individual tracer particles in a core sample. 170
Figure 9.10 Tracer distribution after first tidal cycle following first injection. 171
Table 9.1 Tracer distribution with depth for each sample collected on 11 Dec. 172
Figure 9.11 Tracer distribution after third tidal cycle following first injection and second tidal cycle following second injection. 173
Table 9.2 Tracer distribution with depth for each sample collected on 12 Dec. 174
Figure 9.12 Sites of sediment tracer injection and locations of core samples for June 2014 tracer experiment. The shoreline at distal end of the barrier has been updated to reflect the dune toe position on 4 May 2014 (the last TLS survey before the experiment). It should be noted that the dune toe here had receded by approximately 50 m since the last experiment in December 2013. 175
Figure 9.13 June sediment tracer experiment timeline in relation to tidal cycle. Source of tide data: Marine Institute 176
Figure 9.14 Wind speeds and directions during June 2014 tracer experiment. Winds were predominantly southeasterly, with average speeds of 8.6 m/s. Hourly data obtained from Ventry weather station. 177
Figure 9.15 Tracer particles in a June 2013 core under ordinary and UV light. 178
Figure 9.16 Tracer distribution after first tidal cycle following injection. Small (top) and large (bottom) scale views of the site are shown to better illustrate sample distribution. 179
Table 9.3 Tracer distribution with depth for each sample collected after the first tidal cycle. Maps showing the locations of samples (labeled with corresponding sample IDs) are shown in figure 9.17. 180
Figure 9.17 Locations of samples labeled with sample IDs, which correspond to those in table 9.3. Small (top) and large (bottom) scale views of the site are shown to better illustrate sample distribution. 181
Figure 9.18 Tracer distribution in top 0-4 cm layer for samples collected after first tidal cycle following injection. Only area where samples containing positively identified tracer are shown. 182
Figure 9.19 Tracer distribution in 4-8 cm depth layer for samples collected after first tidal cycle following injection. 182
Figure 9.20 Tracer distribution in 8-12 cm depth layer for samples collected after first tidal cycle following injection. 183
Table 9.4 Longshore position of tracer cloud centroids and velocities of transport for sample layers 0-4 cm, 4-8 cm, and 8-12 cm. (Samples collected after 1st tidal cycle) 183
Figure 9.21 Tracer distribution after second tidal cycle following injection. 184
Table 9.4 Tracer distribution with depth for each sample collected after the second tidal cycle. A map showing the locations of samples (labeled with corresponding sample IDs) is shown in figure 9.22. 185

Figure 9.22 Locations of samples labeled with sample IDs, which correspond to those in table 9.4. 186
Figure 9.23 Tracer distribution in top 0-4 cm layer in samples collected after second tidal cycle following injection. 186
Figure 9.24 Tracer distribution in 4-8 cm layer in samples collected after second tidal cycle following injection. 187
Figure 9.25 Tracer distribution in 8-12 cm layer in samples collected after second tidal cycle following injection. 187
Table 9.5 Longshore position of tracer cloud centroids and velocities of transport for sample layers 0-4 cm, 4-8 cm, and 8-12 cm. (Samples collected after 2nd tidal cycle) 188
Figure 9.26 Tracer distribution after third tidal cycle following injection. 188
Table 9.6 Tracer distribution with depth for each sample collected after the third tidal cycle. A map showing the locations of samples (labeled with corresponding sample IDs) is shown in figure 9.27. 189
Figure 9.27 Locations of samples labeled with sample IDs, which correspond to those in table 9.6. 189
Figure 9.28 Tracer distribution in top 0-4 cm layer in samples collected after third tidal cycle following injection. 190
Figure 9.29 Tracer distribution in 4-6 cm layer in samples collected after third tidal cycle following injection. 190
Figure 9.30 Tracer distribution in 8-12 cm layer in samples collected after third tidal cycle following injection. 191
Table 9.7 Longshore position of tracer cloud centroids and velocities of transport for sample layers 0-4 cm, 4-8 cm, and 8-12 cm. (Samples collected after 3rd tidal cycle) 191
Table 9.8 Longshore position of tracer cloud centroids and velocities of transport for subsample layers 0-4 cm, 4-8 cm, and 8-12 cm from samples collected after each of the three tidal cycles. 192

10 Process-based modelling of the impacts of storms under SLR

Figure 10.1 MIKE21 nearshore mesh 193
Figure 10.2 INFOMAR Bathymetry Data for Dingle Bay used in model set-up. Extracted from INFOMAR (2015b) 193
Figure 10.3 Aerial LiDAR data used in model set-up. The survey took place in April 2011. Data was provided by Kerry County Council. 194
Table 10.1 Measured versus calculated rates of dune recession using the cross-shore formula of van Rijn (2009) from a study by O'Shea and Murphy (2013). In that study, an evaluation of the effectiveness of various transport formulae was carried out in an effort to choose the most appropriate one for the Dingle Bay model set-up used in this PhD research. There was good agreement between modeled dune recession using the cross-shore formula of van Rijn (2009) and measurements for the swash-aligned zone. Data source: O'Shea and Murphy (2013). 195
Table 10.2 Measured versus calculated rates of dune recession using the alongshore formula of van Rijn (1998) from a study by O'Shea and Murphy (2013). In that study, an evaluation of the effectiveness of various transport formulae was carried out in an effort to choose the most appropriate one for the Dingle Bay model set-up used in this PhD research. There was some agreement between modeled dune recession using the alongshore formula of van Rijn (1998) and measurements for the drift-aligned zone. Data source: O'Shea and Murphy (2013). 196
Table 10.3 Characteristics associated with all storm events that occurred during the period 2011-2014 that were characterized by modal wave conditions. Data extracted from nearshore wave hindcast data. 196
Table 10.4 Characteristics of event chosen to represent "typical" storm conditions. Data extracted from nearshore wave hindcast data. 196
Figure 10.4 Wind speeds used to drive typical event scenario. 197
Figure 10.5 Wind directions used to drive typical event scenario. 197

Figure 10.6 Surge heights used to drive typical event scenario. 197
Table 10.5 Characteristics of most extreme event to have occurred during period over which data was available (2011-2014). Data extracted from nearshore wave hindcast data. 198
Figure 10.7 Storm power (in terms of minimum pressure and wind speed) for extreme events that have affected Ireland compared to the 26/27 December and 23/24 December 2013 events. Data for historic events compiled by Orford *et al*. (1999). 198
Figure 10.8 Wind speeds used to drive extreme event scenario. 199
Figure 10.9 Wind directions used to drive extreme event scenario. 199
Figure 10.10 Surge heights used to drive extreme event scenario. 199
Figure 10.11 Wind speeds used to drive fair-weather scenario. 200
Figure 10.12 Wind directions used to drive fair-weather scenario. 200
Table 10.6 Model inputs for extreme event scenario, typical event scenario, and fair-weather event scenario. Inputs were derived from simulated nearshore wave data and local weather station data. Each scenario was run under sea-levels of 0 cm, 10 cm, and 50 cm. 200
Figure 10.13 Coordinate at which time series of sediment transport magnitude and direction and water levels were extracted for each scenario. Injection of sediment tracer took place at this same coordinate during the June 2014 sediment tracer experiment. Bed levels are shown relative to LAT. UTM coordinate 433532.807, 5770466.742 201
Figure 10.14 Second coordinate at which time series of water levels were extracted to give full picture of tidal state during simulations. Bed levels are shown relative to LAT. 201
Figure 10.15 Aerial view of the area covered by the maps presented in section 10.3.1 relative to the 0 m and -5 m depth contours and the site of the sediment tracer experiment. 202
Figure 10.16 Bed level change for the fair-weather, 0 m SLR scenario. Contours are relative to LAT. 203
Figure 10.17 Volume gains and losses for the fair-weather, 0 m SLR scenario. Contours are relative to LAT. 204
Figure 10.18 Bed level change for the fair-weather, 0.1 m SLR scenario. Contours are relative to LAT. 205
Figure 10.19 Volume gains and losses for the no event, 0.1 m SLR scenario. Contours are relative to LAT. 206
Figure 10.20 Bed level change for the no event, 0.5 m SLR scenario. Contours are relative to LAT. 207
Figure 10.21 Volume gains and losses for the no event, 0.5 m SLR scenario. Contours are relative to LAT. 208
Figure 10.22 Volume change above the 0 m bathymetric contour (top) and between the -5 to 0 m bathymetric contours (bottom) for the 3 SLR scenarios run over the course of the fair-weather scenario at Rossbehy. 0 m contour is equal to LAT. 209
Figure 10.23 Bed level change for the typical event, 0 m SLR scenario. The polygons representing the 0 m and -5 m contours were extracted from the initial bathymmetry. Net volume change was calculated within the bounds of these polygons. Contours are relative to LAT. 210
Figure 10.24 Volume gains and losses for the typical event, 0 m SLR scenario. Contours are relative to LAT. 211
Figure 10.25 Bed level change for the typical event, 0.1 m SLR scenario. Contours are relative to LAT. 212
Figure 10.26 Volume gains and losses for the typical event, 0.1 m SLR scenario. Contours are relative to LAT. 213
Figure 10.27 Bed level change for the typical event, 0.5 m SLR scenario. Contours are relative to LAT. 214
Figure 10.28 Volume gains and losses for the typical event, 0.5 m SLR scenario. Contours are relative to LAT. 215
Figure 10.29 Volume change above the 0 m bathymetric contour (top) and between the -5 to 0 m bathymetric contours (bottom) for the 3 SLR scenarios run over the course of the "typical event" scenario at Rossbehy. 0 m contour is equal to LAT. 216

Figure 10.30 Bed level change for the extreme event, 0 m SLR scenario. Contours are relative to LAT. 217
Figure 10.31 Volume gains and losses for the extreme event, 0 m SLR scenario. Contours are relative to LAT. 218
Figure 10.32 Bed level change for the extreme event, 0.1 m SLR scenario. Contours are relative to LAT. 219
Figure 10.33 Volume gains and losses for the extreme event, 0.1 m SLR scenario. Contours are relative to LAT. 220
Figure 10.34 Bed level change for the extreme event, 0.5 m SLR scenario. Contours are relative to LAT. 221
Figure 10.35 Volume gains and losses for the extreme event, 0.5 m SLR scenario. Contours are relative to LAT. 222
Figure 10.36 Volume change above the 0 m bathymetric contour (top) and between the -5 to 0 m bathymetric contours (bottom) for the 3 SLR scenarios run over the course of the extreme event scenario at Rossbehy. 0 m contour is equal to LAT. 223
Figure 10.37 Graphic summary of net volume change above the -5 m depth contour for each model scenario. 0 m contour is equal to LAT. 223
Figure 10.38 Nearshore water levels for UTM coordinate 431732.69, 5770864.57 – shown in fig. 10.14 - during the three fair-weather simulations (0 m SLR, 0.1 m SLR, and 0.5 m SLR). **NB:** While the simulation began on 1 Feb 2012 at 00:00, a 24 hour spin-up meant water levels did not reach statistical equilibrium until 2 Feb 2012 at 01:00. Water levels are relative to MSL. 224
Figure 10.39 Water levels for nearshore coordinate (UTM coordinate 431732.69, 5770864.57 – shown in fig. 10.14) and sediment tracer injection point coordinate (UTM coordinate 433532.807, 5770466.742 – shown in fig. 10.13) during the three typical event simulations (0 m SLR, 0.1 m SLR, and 0.5 m SLR). NB: While the simulation began on 24 Jan 2012 at 18:00, a 24 hour spin-up meant water levels did not reach statistical equilibrium until 25 Jan 2012 at 18:15. Water levels are relative to MSL. 224
Figure 10.40 Time series showing transport magnitude at the sediment tracer injection point during the typical event simulation for all three SLR scenarios. 225
Figure 10.41 Mean and max bed load transport for typical event simulations for 0 m, 0.1 m, and 0.5 m SLR scenarios. 225
Figure 10.42 Compass rose plot illustrating direction of sediment transport at the sediment tracer injection point during the typical event simulation for all three SLR scenarios. **NB:** While in many cases, wind and wave directions are defined positive clockwise from true North (coming from), in MIKE 21 load directions are defined positive clockwise from true North (going against). For clarity, the output was adjusted to reflect load directions coming from, as opposed to going against. This means that, for example, for the 0 m SLR scenario, for 20% of the time, transport was from southeast to northwest and for 80% of the time, transport was from west to east (onshore). 226
Figure 10.43 Time series showing water levels at the sediment tracer injection point during the extreme event simulation for all three SLR scenarios. Water levels are relative to MSL. 226
Figure 10.44 Maximum water levels reached at sediment tracer injection point coordinate for all nine scenarios. Water levels are relative to MSL. 227
Figure 10.45 Duration of inundation at sediment tracer injection point coordinate for all nine scenarios. Water levels are relative to MSL. 227
Figure 10.46 Time series showing transport magnitude at the sediment tracer injection point during the extreme event simulation for all three SLR scenarios. 228
Figure 10.47 Mean and max bed load transport for extreme event simulations for 0 m, 0.1 m, and 0.5 m SLR scenarios. 228
Figure 10.48 Compass rose plot illustrating direction of sediment transport at the sediment tracer injection point during the extreme event simulation for all three SLR scenarios. 229

11 Discussion

Figure 11.1 S-SLR conceptual model of evolution of Rossbehy in response to storms under a rising sea-level 230

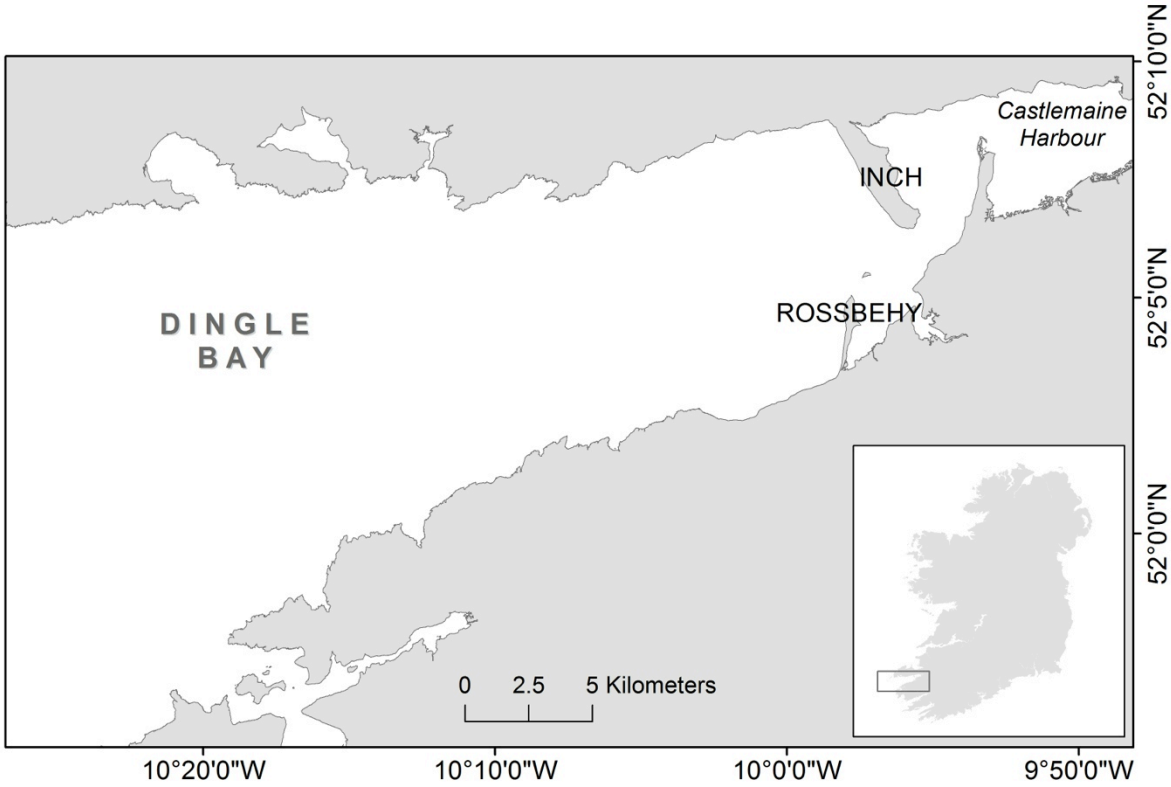

Figure 1.1 Study area showing location of Inch and Rossbehy beach-dune barriers within Dingle Bay, Co. Kerry. Data source: OSI

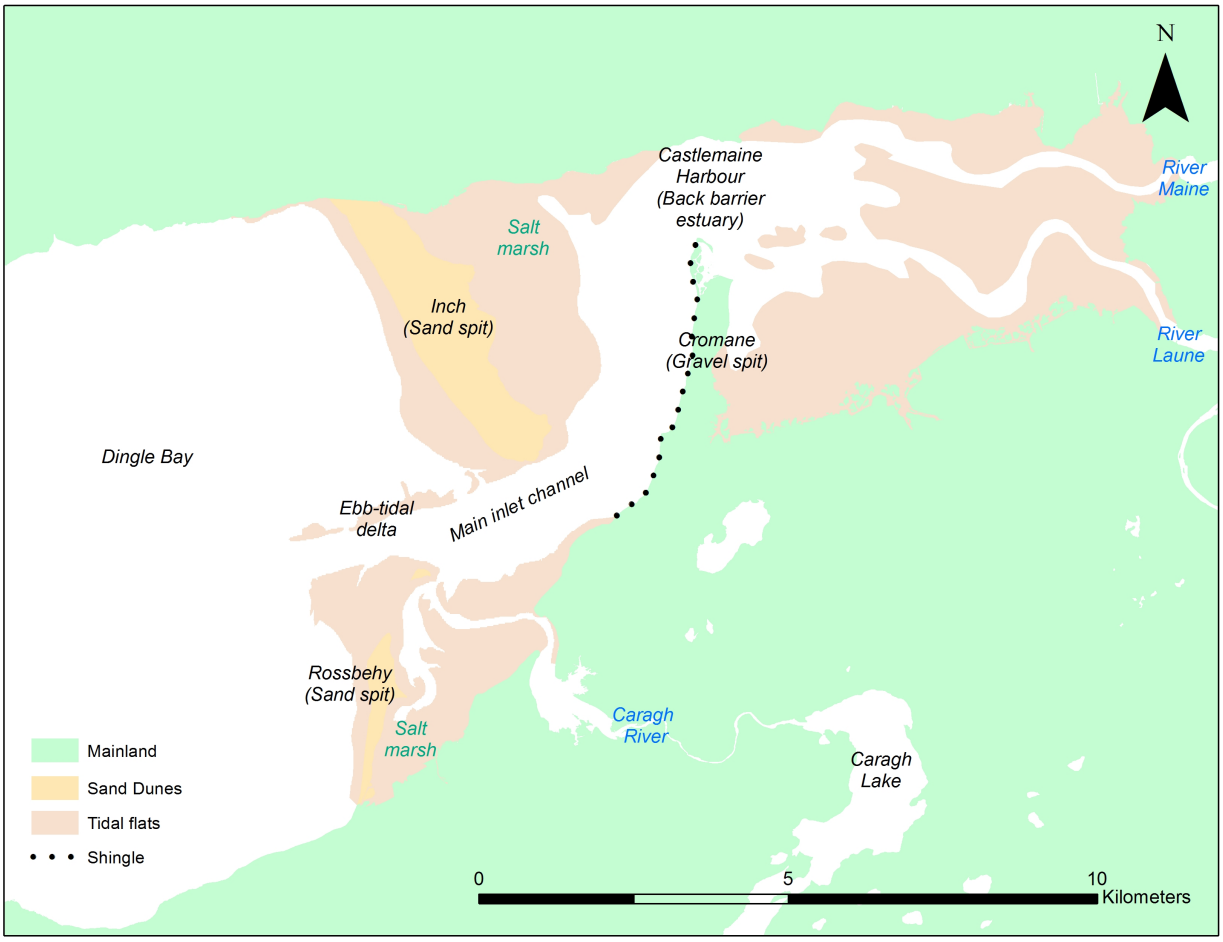

Figure 2.1 Sedimentary environments present at study site. Data sources: OSI; Guilcher *et al*. (1960)

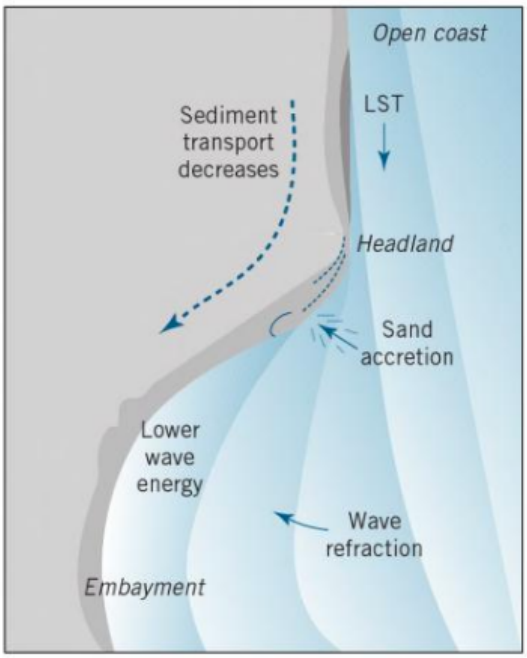

Figure 2.2 Idealised model of barrier spit development. LST = longshore sediment transport. A reduction in wave energy at the updrift corner of a headland due to wave refraction results in the deposition of sediment, which initiates spit growth. Source: Davis and FitzGerald (2004).

Figure 2.3 Foredune and storm built beach ridge at Inch. Hesp *et al*. (2005) defined foredunes as accumulations of sand formed by aeolian processes and beach ridges as wave built accumulations of sediment. Image source: author's own.

Figure 2.4 Historical recurves (circled) at Rossbehy (left) and Inch (right) may represent eirlier limits of dune progression due to a historical breaching event. Minor drift aligned recurves are present at both sites adjacent to the main inlet. Source: Google Earth (Rossbehy) and OSI (Inch).

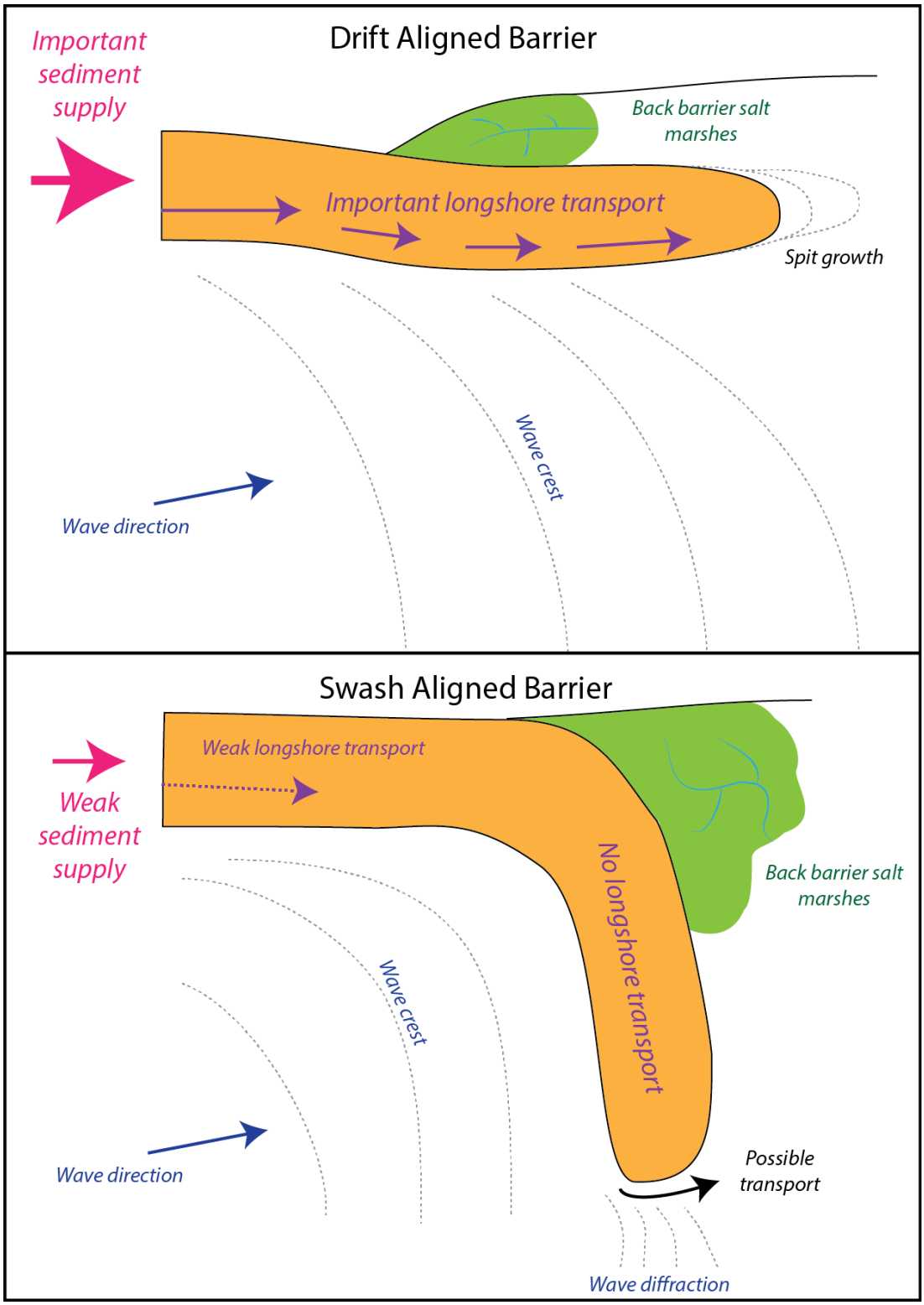

Figure 2.5 Plan form orientation of drift-aligned vs. swash-aligned barriers. Drift alignment occurs when the down-drift sediment supply is sufficient to fulfil the longshore power for transport, while swash-alignment occurs where the downdrift supply is limited or non-existent. Figure modified from Sala (2009) and Stéphan (2009).

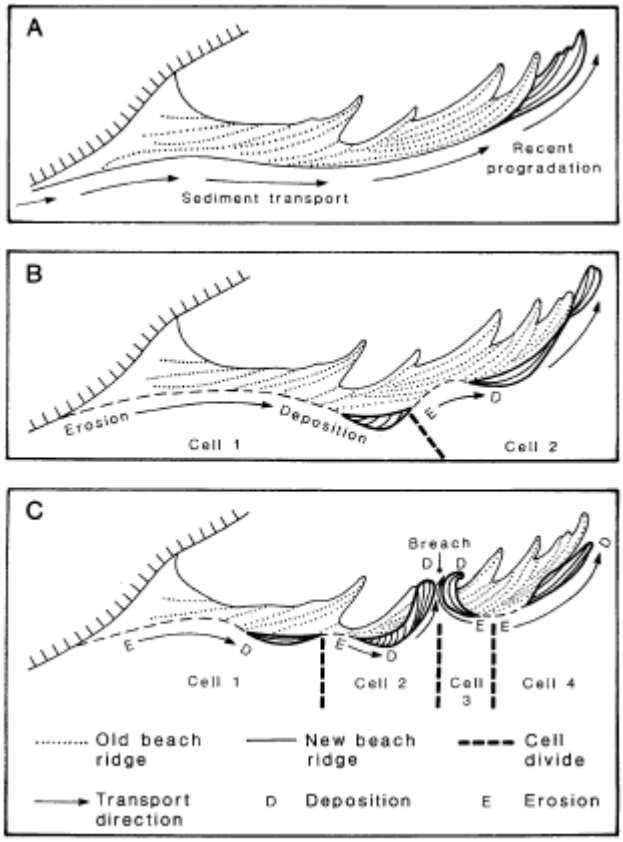

Figure 2.6 Phases of spit restructuring after a decrease in longshore sediment supply. Refraction induced changes in the longshore power gradients result in the development of sediment cells. As additional cells develop, breaching may occur at weaker points (along the up-drift cell boundary). If the breach enlarges, it becomes the focus for a transverse transport corridor. Source: Orford *et al.* (1996).

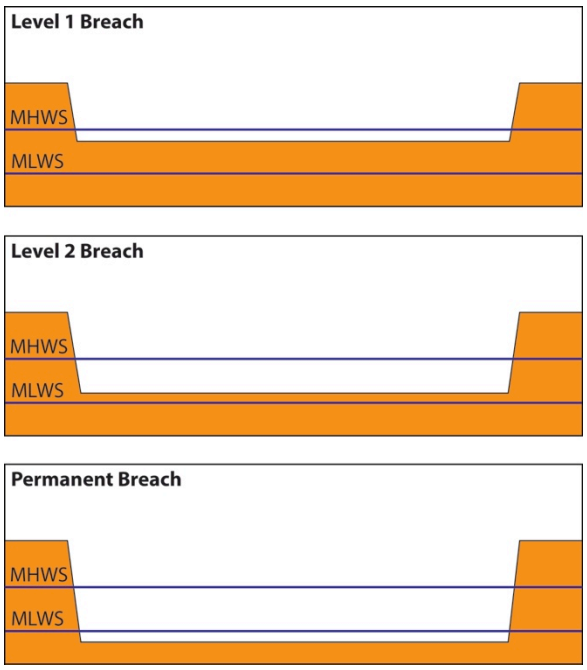

Figure 2.7 Cross section of a breach channel area against water levels showing types of breach, according to Hartley and Pontee (2008). Modified from Sala (2009).

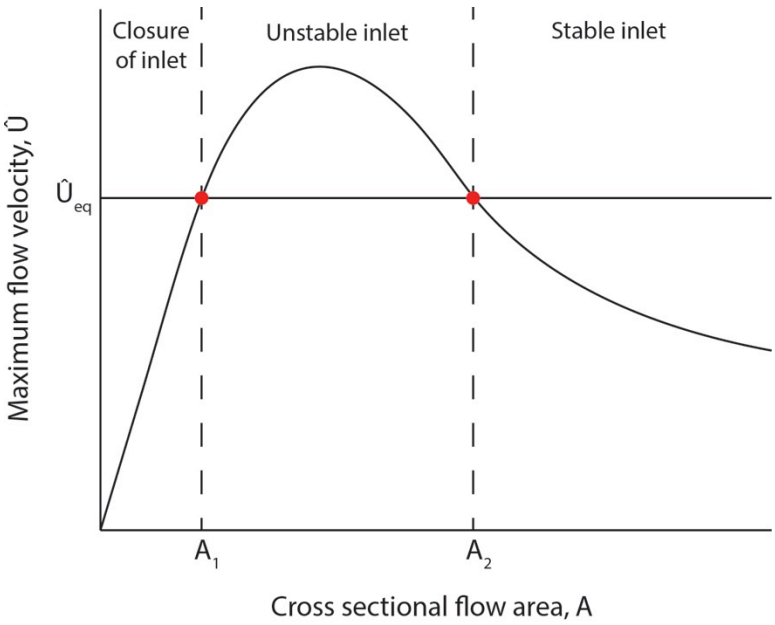

Figure 2.8 Cross-sectional inlet stability relationship of Escoffier (1940). Modified from Escoffier (1940) and van de Kreeke (1992).

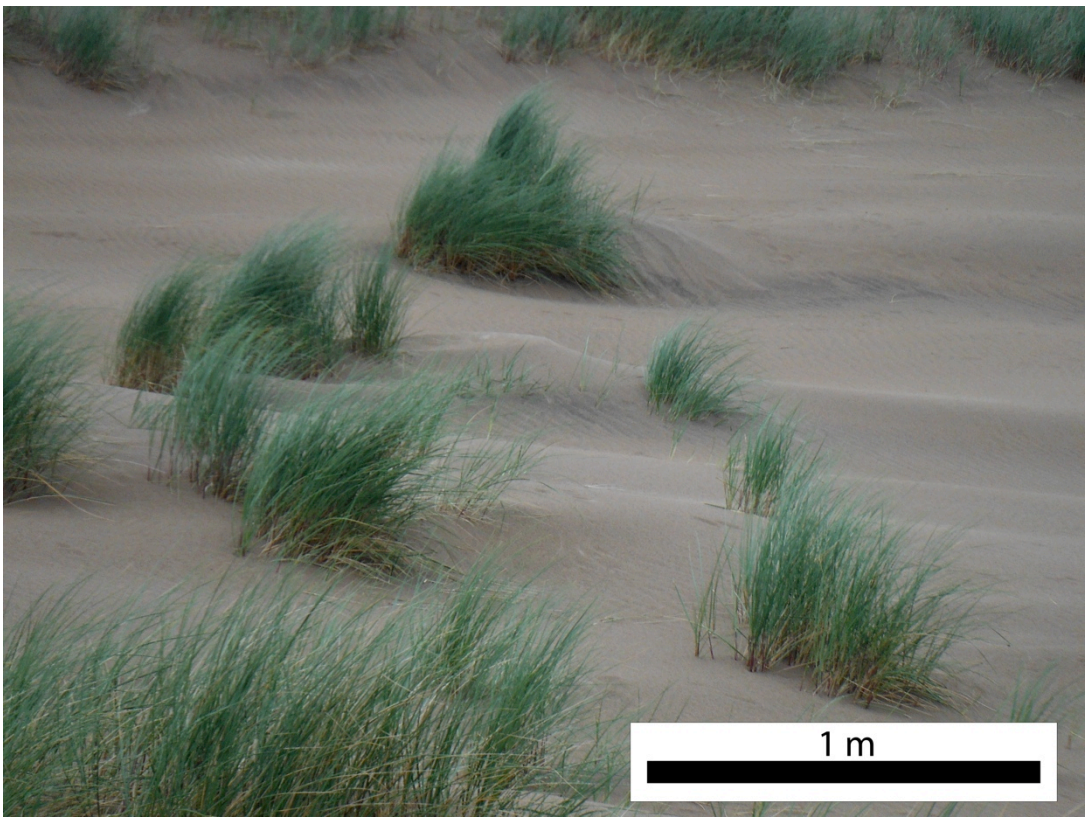

Figure 2.9 Incipient or embryo dunes at Inch, Co. Kerry. Dune hummocks, like those shown here, are also termed nebkha or coppice dunes. Source: author's own.

Figure 2.10 Established foredune at Inch, Co. Kerry. The wooden posts on the ridge are approximately 1 m high. High water mark (not shown) is approximately 15-20 m behind the point from which the photograph was taken. Source: author's own.

Figure 2.11 Saucer blowout (width = approximately 15-20 m) at Rossbehy, Co. Kerry. Source: author's own.

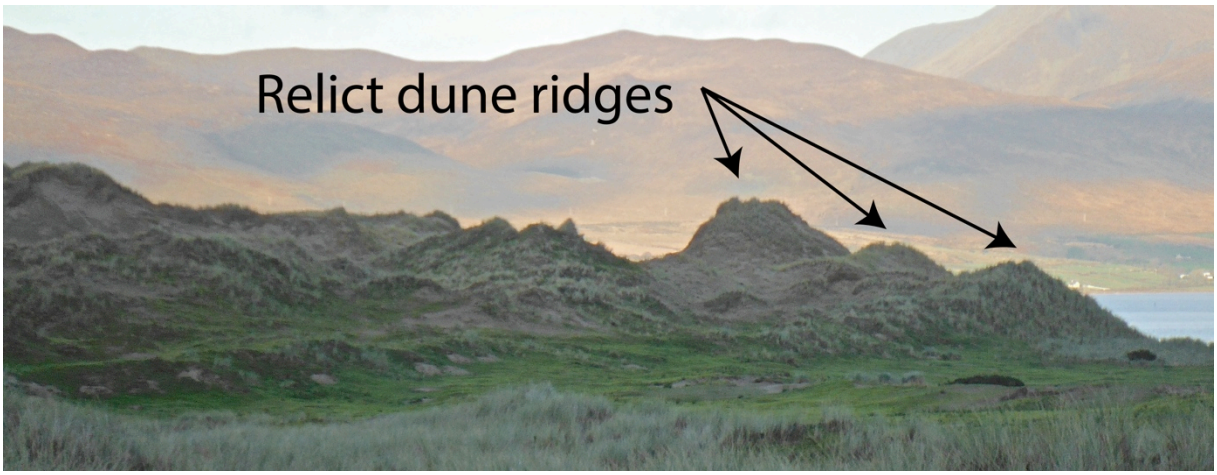

Figure 2.12 Relict dune ridges at Inch, Co. Kerry. Source: author's own.

Figure 2.13 Parabolic (U-shaped) dunes at Inch, Co. Kerry. Source**:** OSI (2005)

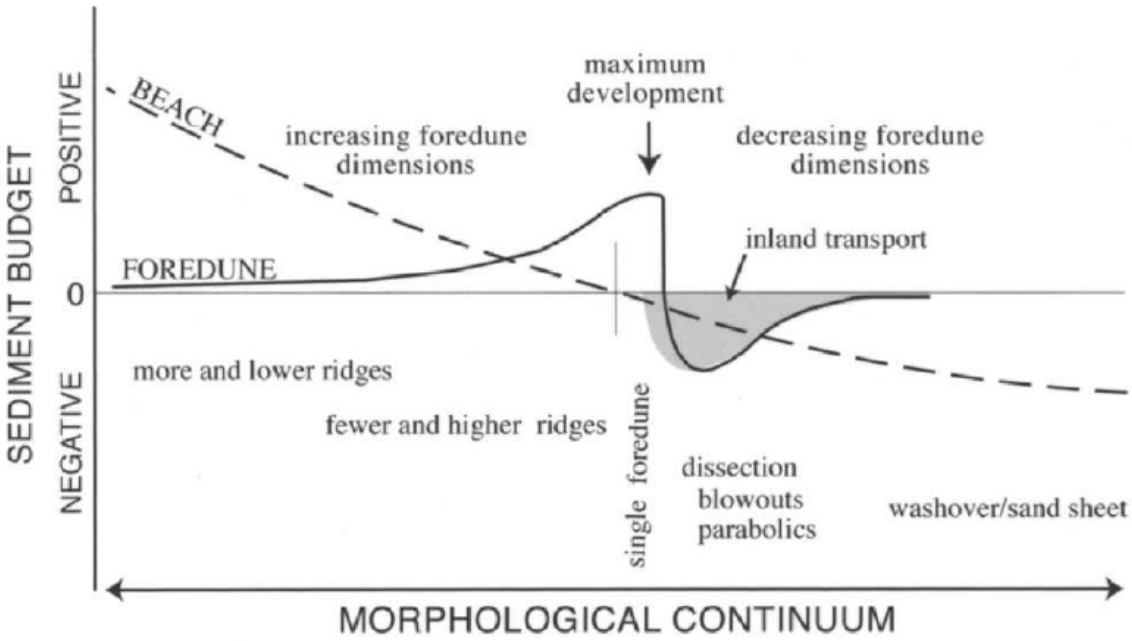

Figure 2.14 Conceptual model of the relationship between dune morphology and sediment budget. See text for explanation. Source: Psuty (2004)

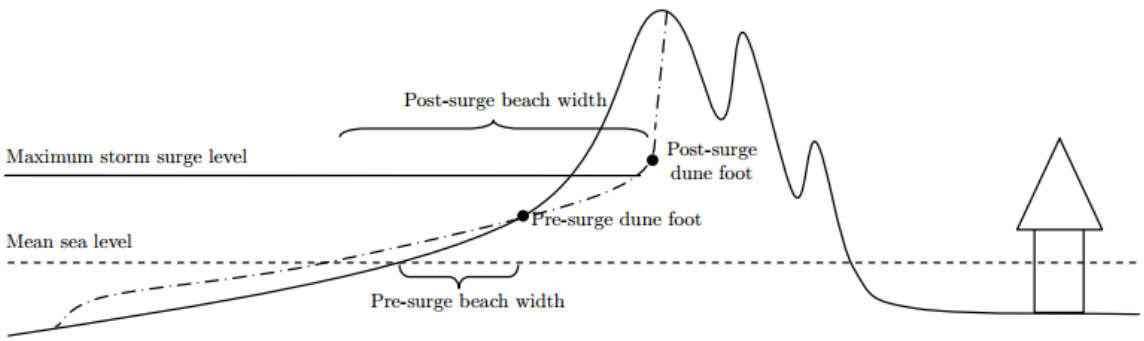

Figure 2.15 Pre- and post- storm beach profiles. Source: Van Thiel de Vries (2009)

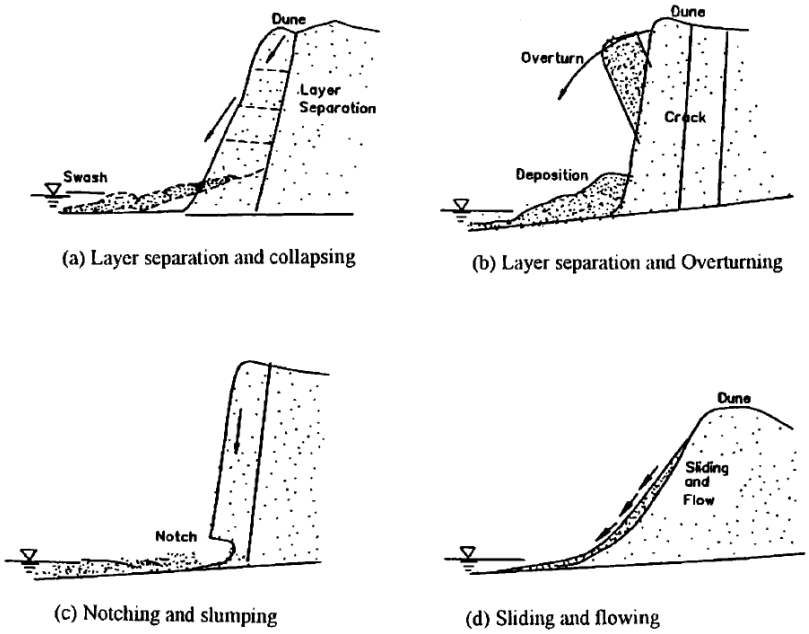

Figure 2.16 Dune erosion mechanisms described by Nishi and Kraus (2001). Source: Nishi and Kraus (2001)

Figure 2.17 Example of layer separation and collapsing at Rossbehy, Co. Kerry. Source: author's own.

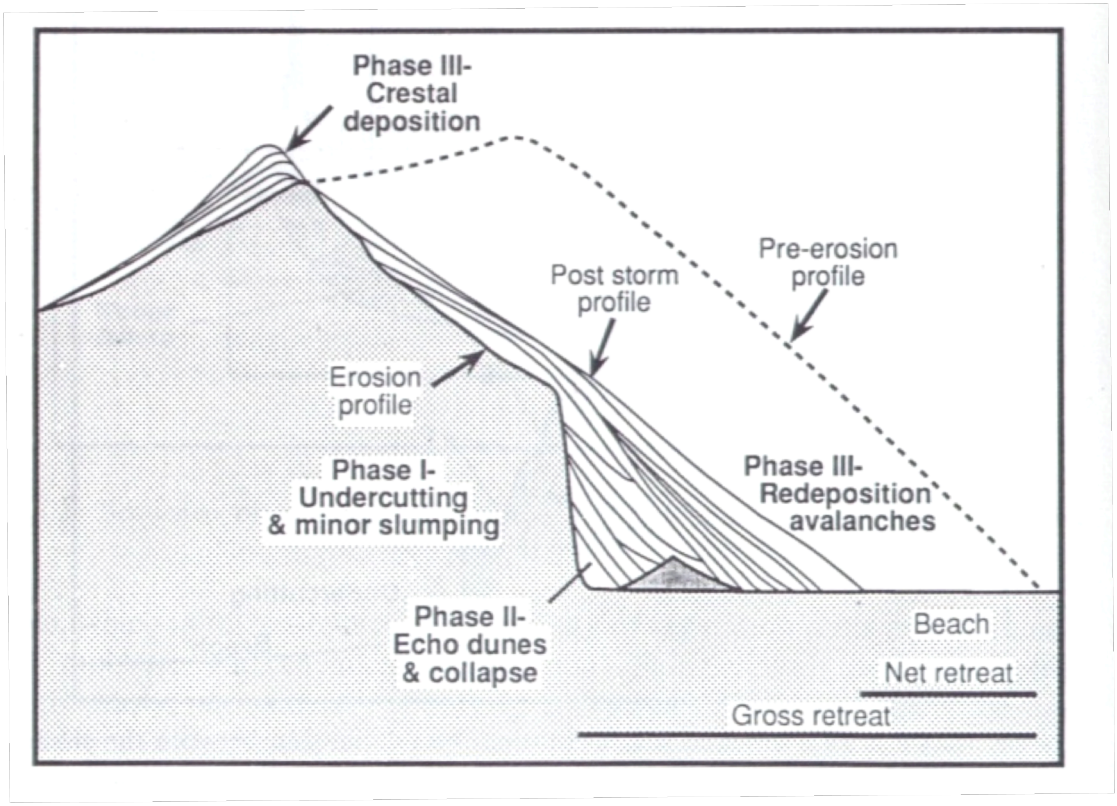

Figure 2.18 Phases leading up to post-storm dune recovery. Source: Carter *et al*. (1990).

Figure 2.19 Evidence of slope failure of a dune scarp (height = approximately 5 m) at Rossbeigh, Co. Kerry. Slump blocks held together by vegetation litter the foredune. Source: author's own.

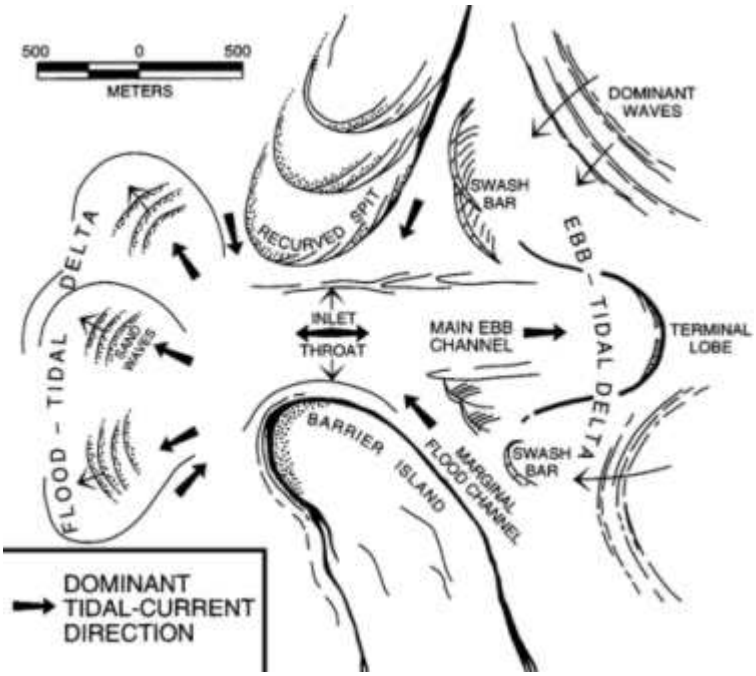

Figure 2.20 Morphological components of a typical tidal inlet. Source: Schrader *et al.* (2000)

Figure 2.21 Ebb-tidal delta fronting Inch and Rossbehy barriers. Source of aerial imagery: Google Earth.

Figure 2.22 Multiple inlet system at the Nauset barrier system, Cape Cod MA. Dominant longshore transport is southerly. Source: Giese *et al*. (2009).

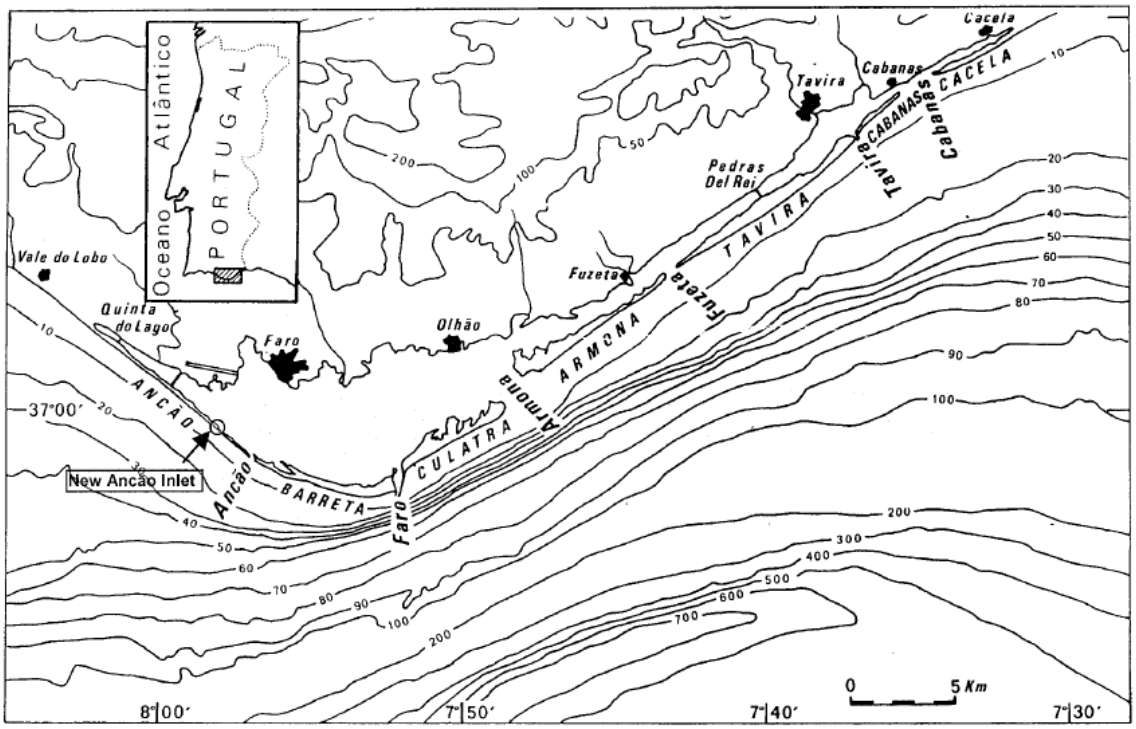

Figure 2.23 Multiple inlet system at Ria Formosa, Portugal. Source: Salles (2001).

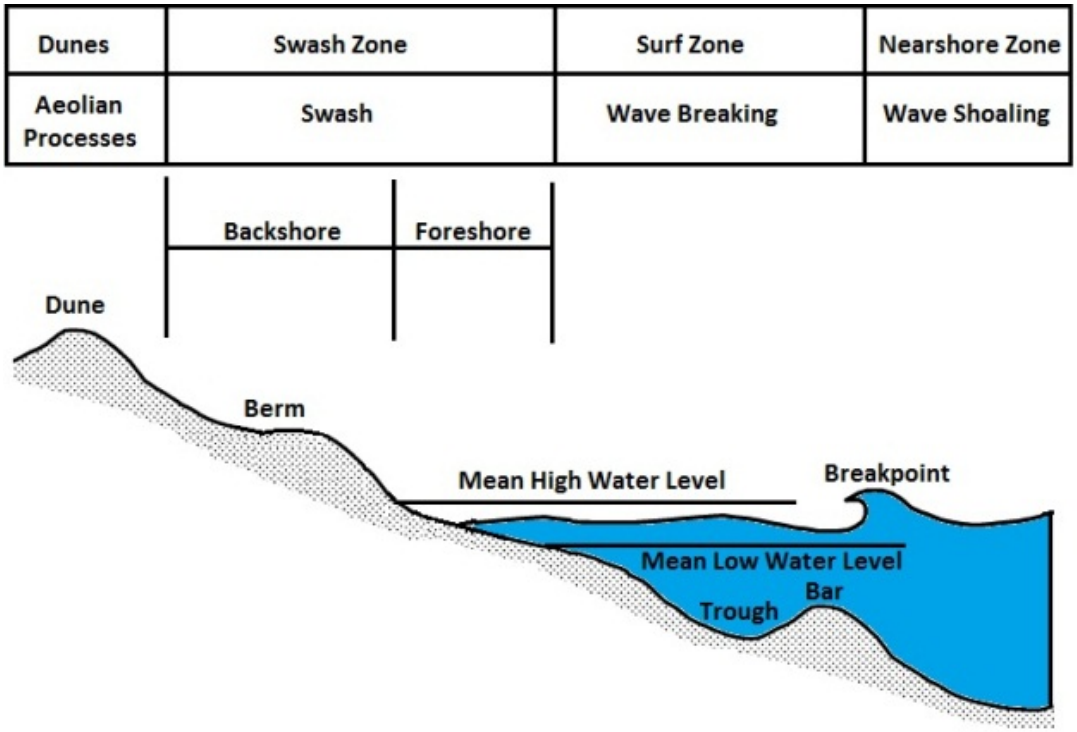

Figure 2.24 Categorisation of a typical beach-dune profile. Modified from Schwartz (2006) and Beaugrand (2010).

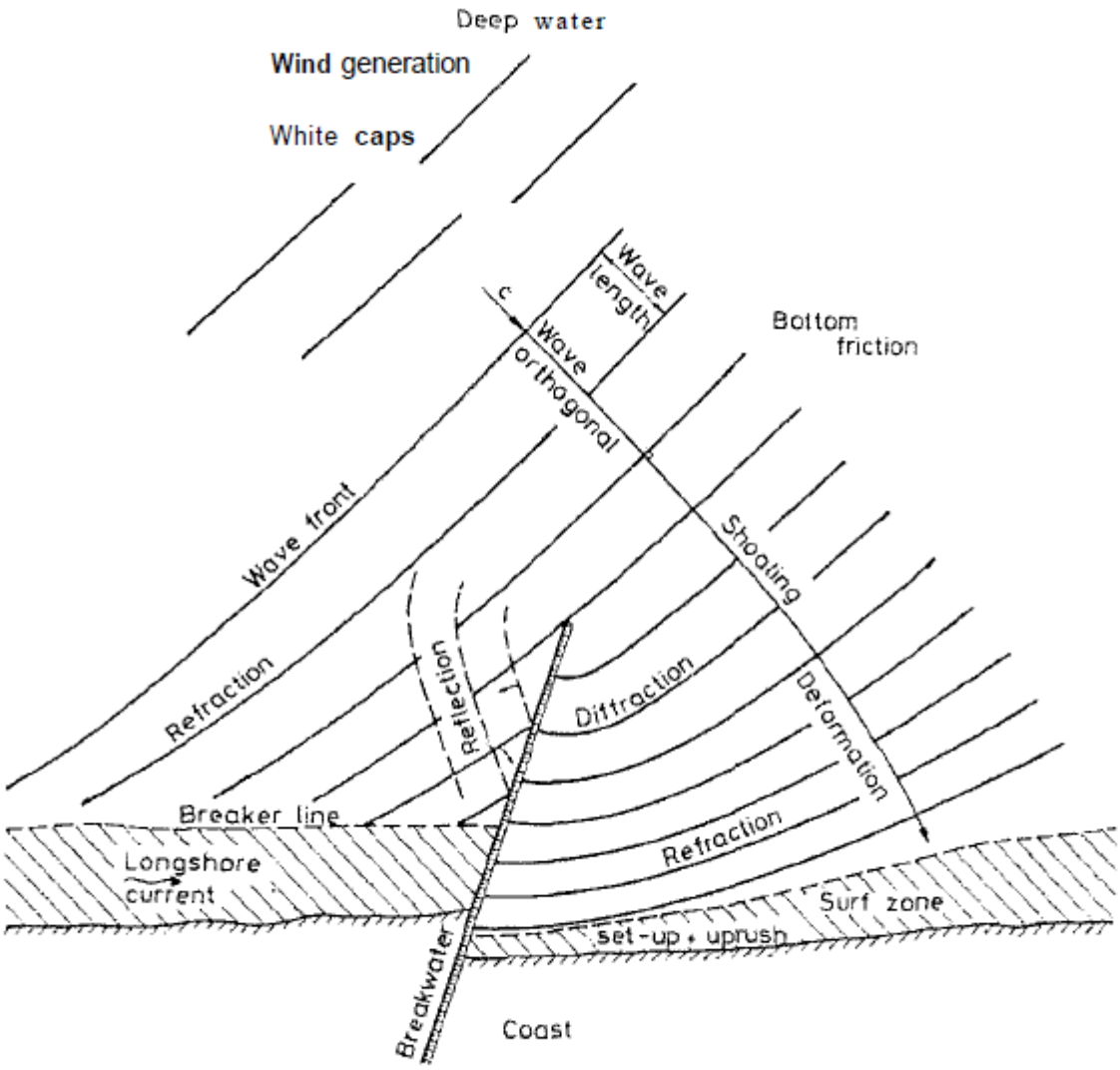

Figure 2.25 Nearshore wave processes. Source: Svendsen (2006)

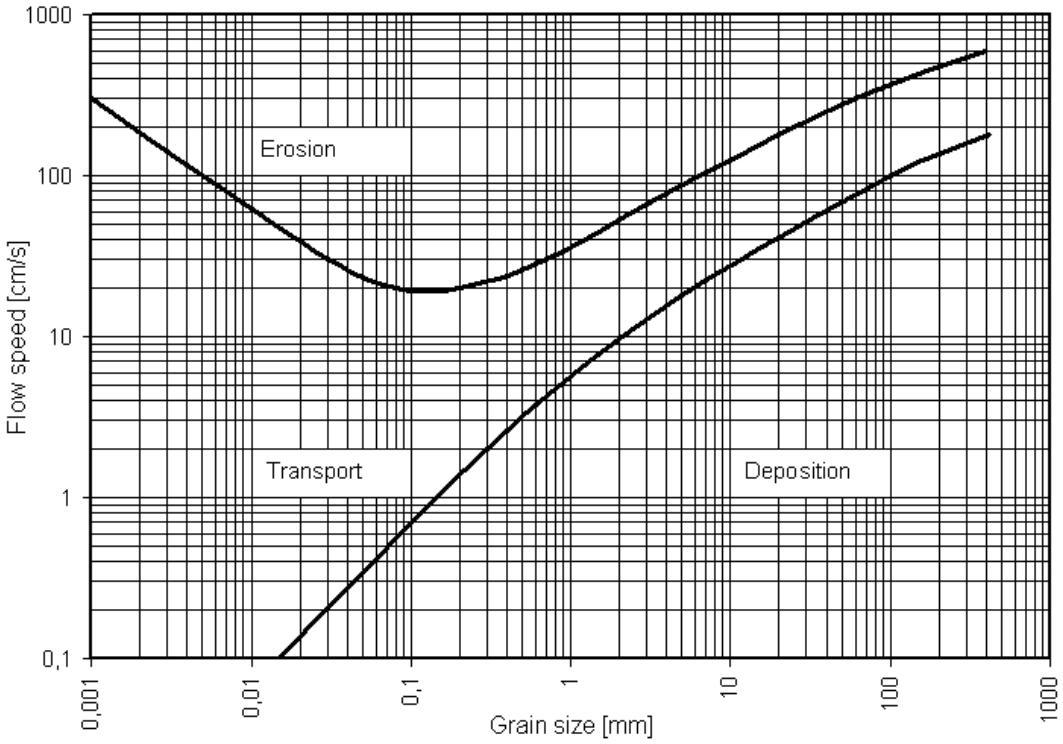

Figure 2.26 Hjulstrom curve showing critical velocities for erosion, transport, and deposition as a function of sediment grain size. Source**:** http://en.wikipedia.org/wiki/Hjulstr%C3%B6m_curve - **Original**: Hjulstrom (1939) later modified by Sundborg (1956)

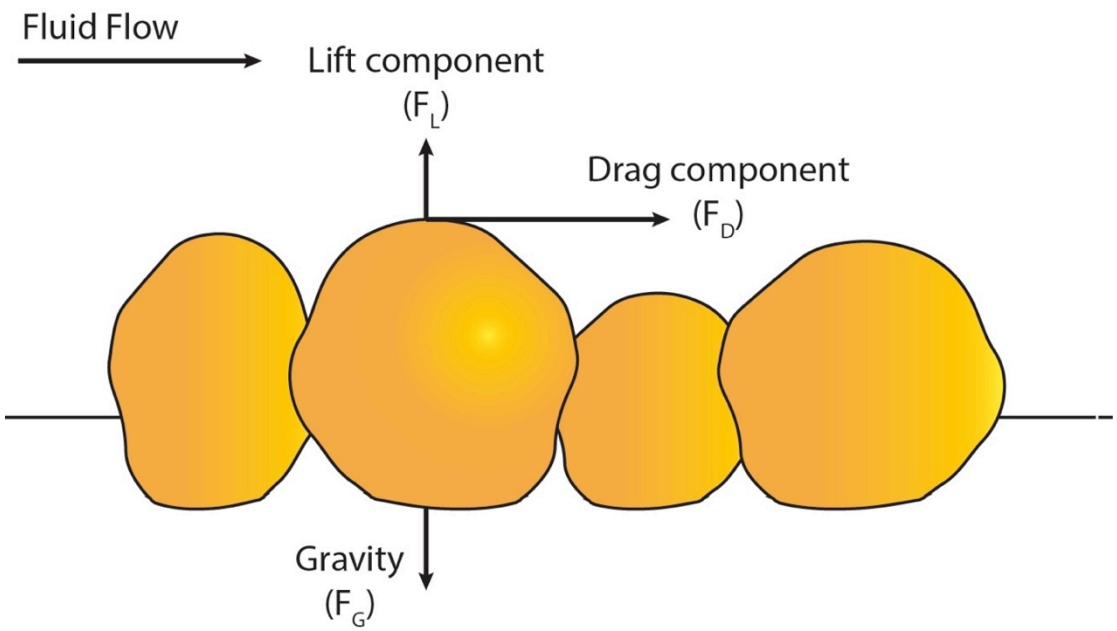

Figure 2.27 Forces responsible for sediment entrainment. Modified from MIT OpenCourseWare (available from: http://ocw.mit.edu/courses/earth-atmospheric-and-planetary-sciences/12-090-introduction-to-fluid-motions-sediment-transport-and-current-generated-sedimentary-structures-fall-2006/course-textbook/ch9.pdf)

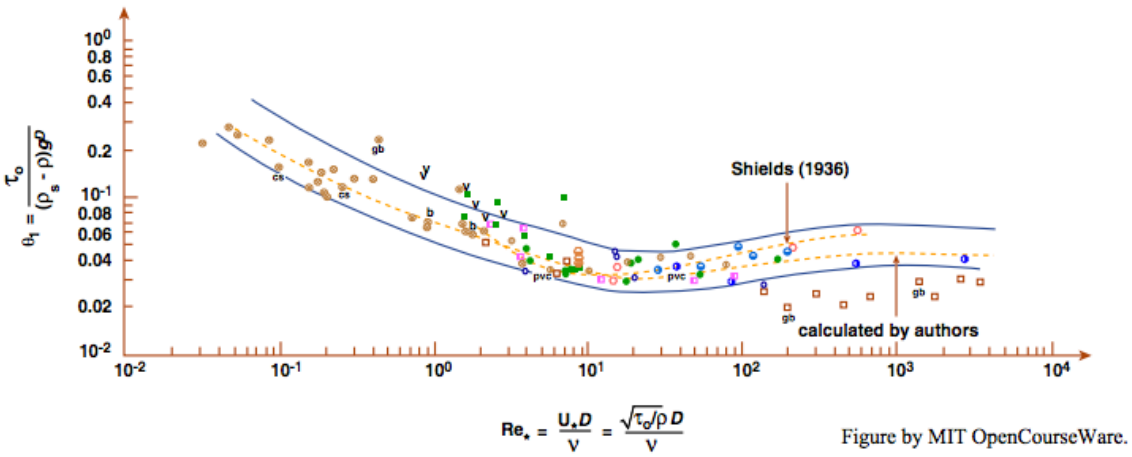

Figure 2.28 Shield's diagram modified by Miller *et al*. (1977) showing the boundary Reynold's number as a function of the critical Shield's stress for experimental data. Entrainment occurs for conditions above the curve. Source**:** MIT OpenCourseWare

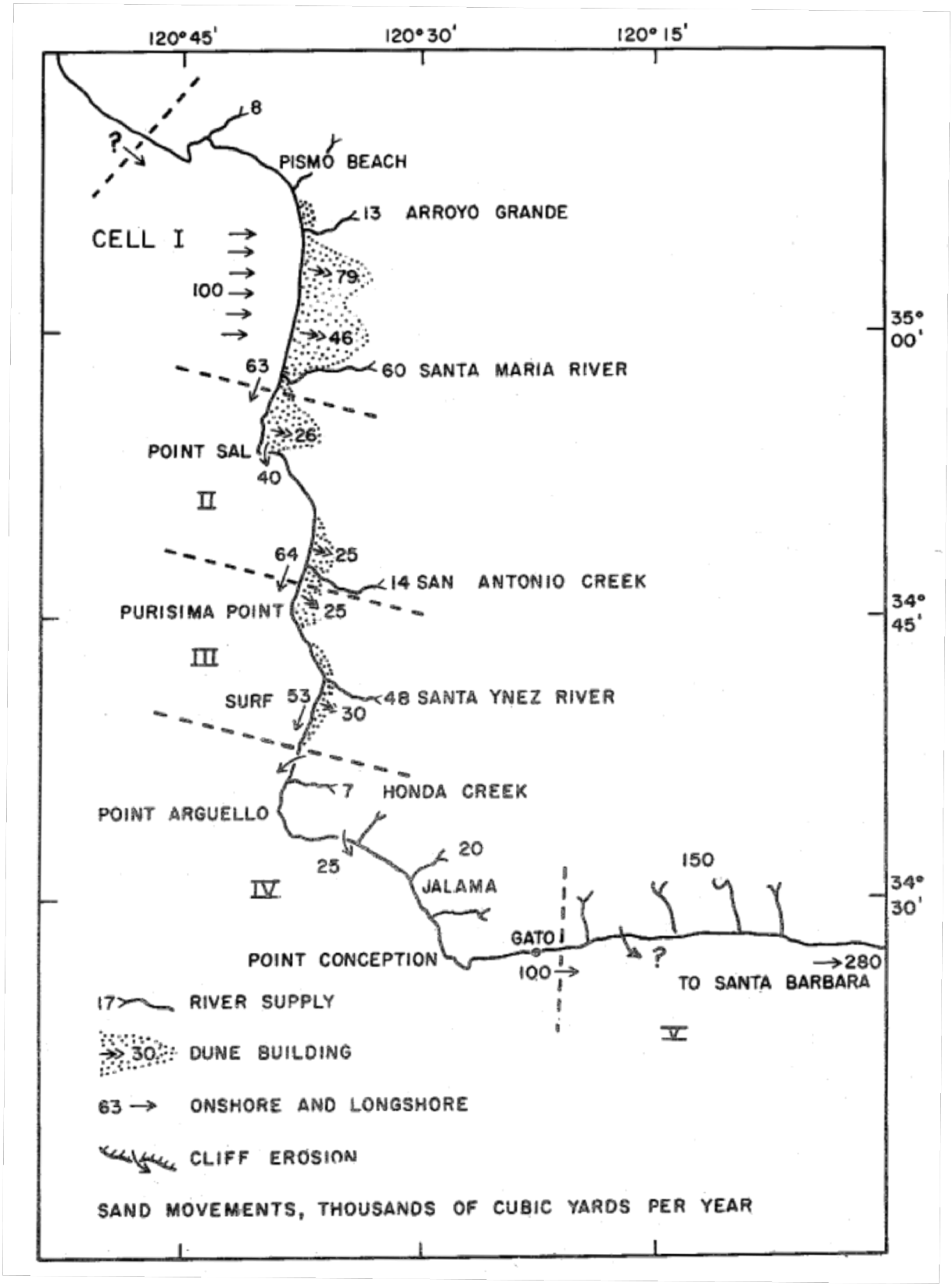

Figure 2.29 Sedimentary cells and sediment budgets near Point Arguello, California, USA. Source: Bowen and Inman (1966)

Guilcher *et al*., 1960	Provided initial descriptive geomorphology of Inch & Rossbehy
Shaw *et al*., 1986	Provided summary of RSL changes based on pollen analysis
Taylor *et al*., 1986 & Carter *et al*., 1989a	Investigated the impact of RSL change & sediment supply on gravel barriers
Shaw *et al*., 1994	Performed marine geological surveys of Dingle Bay
Devoy, 1995 & Cooper *et al*., 1995	Related meso-scale morphological change during the mid- to late- Holocene to sea-level, sediment supply, & extreme storms
MacClenahan, 1997	Investigated variations in meso-scale morphological change at Inch in relation to climate, sea-level & human impact
Sherman *et al.*, 1998 & 2012	Used Inch as a laboratory to study Aeolian transport models
Wintle *et al*., 1998	Used IRSL dating to date dune sediments at Inch (oldest = 600 yrs)
Orford *et al*., 1999 & Orford, Cooper & McKenna, 1999	Related dune morphodynamics at Inch with extreme storms & associated surge
Jackson & Cooper, 1999	Documented & described the formation of ephemeral bedform turrets at Inch
Cooper *et al*., 2004	Assessed the impacts of storms as drivers to change at Inch/Rossbehy & other sites on the Irish coast
Vial, 2008	Investigated morphological response of Inch to storms & waves
Sala, 2010	Used numerical modelling to investigate breach risk & formation
Gault *et al*., 2011	Evaluated effectiveness of CONSCIENCE Frame of Reference as an erosion management tool at Inch
O'Shea *et al*., 2011	Used numerical modelling to investigate impacts of breaching on estuary
Delaney *et al*., 2012	Provided an account of mid- to late- Holocene RSL based on stratigraphical record in Castlemaine Harbour
Devoy, 2013	Evaluated the potential physical and geomorphological impacts of proposed golf course development at Inch
O'Shea *et al*., 2013	Related variations in incident wave directionality along Rossbehy over the tidal cycle with changes to the size, shape, and orientation of ebb-tidal bar
Devoy, 2015	Provided an account of the micro- to meso-scale development of Inch/Rossbehy and the controls on their development, and speculated on the future of the barriers in response to sea-level change
O'Shea, 2015	Used numerical modelling techniques to speculate on the future morphodynamic behaviour of the barrier
Williams *et al*., 2015	Assessed threshold conditions for dune recession, overwashing and breaching at Rossbehy using Xbeach

Table 3.1 Previous research undertaken at Inch-Rossbehy

Figure 3.1 Ebb shoals fronting Inch and Rossbehy. Imagery obtained 30 August 2010. Source**:** Google Earth

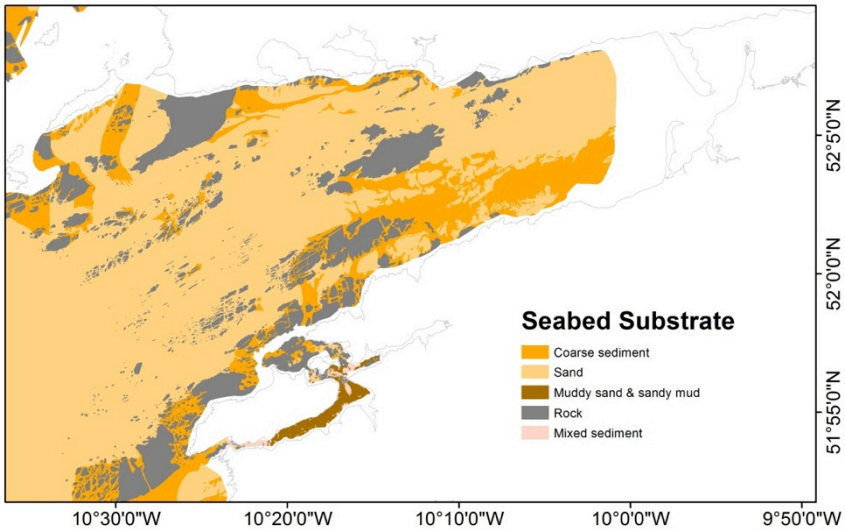

Figure 3.2 Seabed substrate within Dingle Bay. Map layer generated from Geological Survey of Ireland (GSI) multibeam echosounder data and seabed sampling data acquired during the INFOMAR and INSS national seabed mapping programmes.

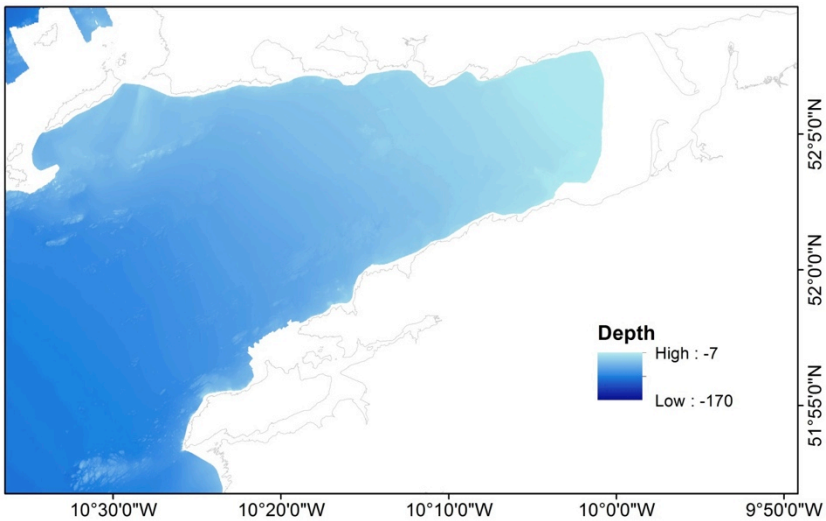

Figure 3.3 Dingle Bay bathymetry. Map layer generated from Geological Survey of Ireland (GSI) multibeam echosounder data acquired during the INFOMAR and INSS national seabed mapping programmes. Depth is shown in metres below LAT (according to data obtained from the GSI, LAT is 2.85±0.13metres below ODM at Rossbehy).

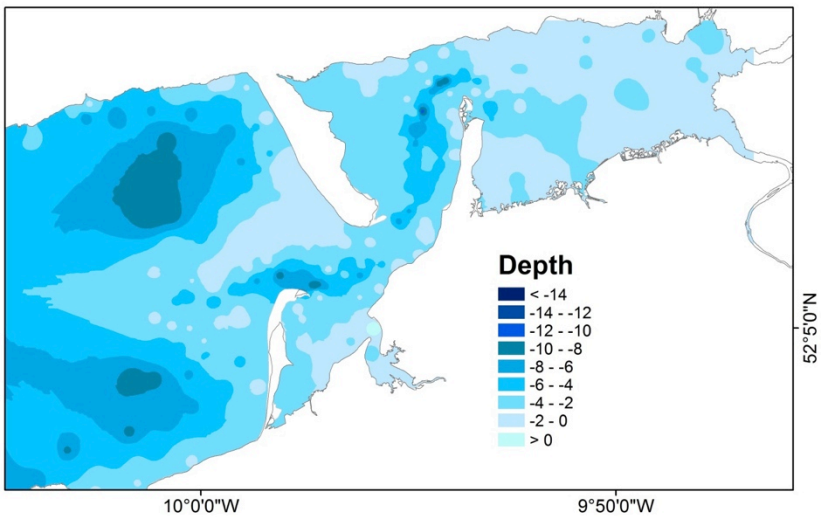

Figure 3.4 Castlemaine Harbour depth contours. Map layer generated from interpolation of depth soundings published on Navionics free webapp (http://webapp.navionics.com/?lang=en). The data is crowd sourced from recreational boaters using mobile technology to ensure it remains up to date. Units are in metres below LAT.

Table 3.2 Paleoenvironmental chronology of Inch-Rossbehy and surrounding environs.

Dingle Bay Chronology - 5,000 to 500 years BP

Date	Location	Description
19,000 BP	South shore of Bay	Extensive glacigenic deposits, including a series of arcuate moraines, formed along south shore of Dingle Bay (Delaney *et al*., 2012)
6100 BP	Rossbeigh	Date of freshwater organics beneath modern beach at Rossbeigh; indicates proto-barrier was probably seaward of its present position (Delaney *et al*., 2012)
6000-5000 BP	Ireland	Deceleration phase of Atlantic RSL; Initiation of Primary dune emplacement in Ireland (Shaw & Carter, 1994)
6000-3000 BP	Knockaunnaglashy, Garrane, and elsewhere	Palynological results from (inner harbour) cores show a mid-Holocene progressive marine inundation of earlier freshwater environments; palynological evidence for the development of locally extensive shrub-woodlands (Delaney *et al*., 2012)
5500 BP	Knockaunnaglashy	Palynological results from core at Knockaunnaglashy (southern shore of Castlemaine Harbour) suggest gradual flooding of estuary from a sea level about 5m below that of present (Shaw *et al*., 1986)
5000 BP - Present	Southwest Ireland	RSL rising showly (0.6-1.1 mm/yr) (Delaney *et al*., 2012)
4700 BP	Outer harbour	Strong marine influence detectable in biogenic sediments (Delaney *et al*., 2012)
2749 BC	Inch	Radiocarbon age of oldest gravel/sand ridge (underlying dune sediments) (MacClenahan, 1997)
2749 BC - AD 916	Inch	Inch Peninsula retreats landwards and develops as a longshore, prograding spit (MacClenahan, 1997)
2978-3362 BP	Knockaunnaglashy	Radiocarbon date of core indicates average accretion rate for peat between 0.43 - 0.55 mm/yr (Delaney *et al*., 2012)
3000 BP	Rossbeigh / inner harbour	Probable barrier breaching led to abrupt and permanent switch to intercalated and heterogeneous biogenic/minerogenic sedimentation in inner harbour; Lithostratigraphic evidence suggests repeated episodes of marine flooding of shrub-woodlands and marshes beginning pre-3000 BP; species of diatoms found indicative of tidal and storm-driven inundation; shrub-woodlands replaced by grass and sedge dominated reedswamp type wetlands, together with open salt marsh and high marsh environments (Delaney et al., 2012)
3000-1200 BP	Cromane	Core indicates gradual change from terrestrial to marine conditions was punctuated by three clear marine inundations (possibly storm surges) (Shaw et al., 1986)
2781-2000 BP	Rossbeigh	Age of truncated upper contact of woody, monocot peat from core in saltmarsh (Delaney *et al*., 2012)
2800 BP	Rossbeigh	Marine conditions established here; after 2800 BP, re-establishment of barrier occurs (Delaney *et al*., 2012)
2500-500 BP	Cromane	Pollen analysis of core at Cromane point suggests waning of terrestrial dominated environment, giving way to marine (Shaw et al., 1986)
2352-2162 BP	Rossbeigh	Age of sediments overlying truncated woody peat horizon in core from saltmarsh (Delaney *et al*., 2012)
After 2300 BP	Rossbeigh	Salt marsh appears to be well developed (Delaney *et al*., 2012)
1500 BP	Inch	Establishment of a hydraulically efficient inlet (Cooper *et al*., 1995)
1000-1500 BP	Inch	Development of ebb-tidal delta depletes spit of sediment; increased rate of cannibalisation of proximal end forces formation of spit, eventual rotation to the east, and switching of dominant longshore transport to an offshore & cross barrier transport, resulting in large dune development (Cooper et al., 1995; MacClenahan, 1997)
800 BP	Rossbeigh	Possible breaching event (O'Shea *et al*., 2011)
600 BP	Inch	Radiocarbon age of oldest dune sediments (Wintle *et al*., 1998)
500 BP	Inch	Beach barrier sediments overwhelm site (Shaw et al., 1986); swash-aligned equilibrium attained (Cooper et al., 1995)

Timescale columns of the chart:

Cal BP	Cal (BC/AD)
>5000	>BC 3050
5000	BC 3050
4900	2950
4800	2850
4700	2750
4600	2650
4500	BC 2550
4400	2450
4300	2350
4200	2250
4100	2150
4000	BC 2050
3900	1950
3800	1850
3700	1750
3600	1650
3500	BC 1550
3400	1450
3300	1350
3200	1250
3100	1150
3000	BC 1050
2900	950
2800	850
2700	750
2600	650
2500	BC 550
2400	450
2300	350
2200	250
2100	150
2000	BC 50
1900	0
1800	150
1700	250
1600	350
1500	AD 450
1400	550
1300	650
1200	750
1100	850
1000	AD 950
900	1050
800	1150
700	1250
600	1350
500	AD 1450
400	1550
300	1650
200	1750
100	1850
0	AD 1950

Figure 3.5 Exposed peat on the beach face (left, 16 January 2014) and beneath the dune sands (right; 14 April 2015) provides evidence of barrier rollover at Rossbehy. The truncated upper contact of similar woody, monocot peat from a core in the back barrier saltmarsh has been dated by Delaney *et al.* (2012) to 2781-2000 BP. **Source:** author's own

Figure 3.6 Extract of study area from the Down Survey Maps published in 1673. Both Inch and Rossbehy are depicted. Source: http://downsurvey.tcd.ie/down-survey-maps.php

Dingle Bay Chronology 500 years BP to Present		
500-450 BP	Inch	Period of sand influx into dunes (MacClenahan, 1997)
300 BP	Inch	Period of sand influx into dunes (Cooper *et al*., 1995)
1673	Ireland	Inch and Rossbehy depicted on historic map by Sir William Petty
18th Century	Inch	Documentary evidence of major barrier breaching (Delaney *et al*., 2012, p. 36)
200 BP	Inch	Period of sand influx into dunes (Cooper *et al.* 1995)
1750 - Present	Castlemaine Harbour	Documentary evidence of direct agricultural activity from before 1750 until recently on coastal wetlands around Castlemaine Harbour (Delaney *et al*., 2012)
1756	Inch	According to Cooper *et al*. (1995), Smith (1756) provided an account of the morphology of the area: Inch was an elongated spit topped by vegetated dunes 30-40 ft high and an ebb-tidal delta and tidal inlet were present in a configuration similar to the present.
19th century until 1950s	Castlemaine harbour	Abstraction of beach and dune sands for agriculture common (Delaney *et al*., 2012)
150 BP	Inch	Period of sand influx into dunes (MacClenahan, 1997)
19th century	Inner harbour (Tullig to Cromane Point)	Piecemeal embanking and subsequent abandonment of marshes (Delaney *et al*., 2012)
1800-1960s	Rossbehy	Cutting of marram and lyme grasses for thatching (Quinn, 1977)
1819-1822	Rossbehy	162 ha embanked and drained behind Rossbehy by local landowner Lord Headley; Behy river permanently rerouted (Delaney et al., 2012)
1842	Rossbehy	Barrier breaching almost occurred at distal neck (Delaney *et al*., 2012)
1842 - 1894	Caragh River	Wetlands on left bank of river cut for fuel (Delaney *et al*., 2012)
1842-1894	Inch	Seaward progradation of dunes and shoreline (O'Shea *et al*., 2011)
1844	Rossbehy	1822 embankment breached and was subsequently abandoned (Delaney *et al*., 2012)

Table 3.3 Recent (500 years BP to present) chronology of Inch-Rossbehy. Continued on next page.

pre-1845	Inch / Rossbehy	Abstraction of beach and dune sands for agriculture likeley reached peak here in pre-famine years (Delaney et al., 2012)
1894-1977	Inch	Recession of shoreline further leeward than 1842 position (O'Shea *et al*., 2011)
1894-1977	Rossbehy	1894 and 1977 shorelines similar in position; slight erosion in area that is presently breached (O'Shea *et al*., 2011)
1895-1897	Rossbehy	Storms and high tides increase rate of erosion (Allanson-Winn, 1899)
1897	Rossbehy	R.G. Allanson-Will called in by the trustees of Lord Headley's estate to devise a scheme to prevent further coastal erosion at the neck of Rossbehy, which was threatening the road and some local properties (Allanson-Winn, 1899)
1903	Rossbehy	Allanson-Winn installs three groynes at proximal end of Rossbehy beach (Allanson-Winn, 1899)
1949	Rossbehy	Account of sand removal from Rossbehy for use on golf greens in Killarney (Anonymous, 1949)
1958	Inner harbour	Embanking by OPW limits tidal inundation to a narrow strip of salt marsh <500 m wide (Delaney et al., 2012)
1977	Rossbehy	Quinn (1977) notes: Rossbehy is "now known as the 'island' because the sea breached its narrow neck."
1977-2000	Inch	Growth in dune line (O'Shea *et al.*, 2011)
1977-2000	Rossbehy	Increase in erosion of area that is presently breached; little change in dune line
approx. 1980s-Present	North Atlantic	Increase in current regional SLR rate to 2-3 mm/yr (Delaney *et al*., 2012; NOAA)
15-17 Oct 1982	Rossbehy	Rate of erosion reported by the department of the Marine to be 0.45 to 1.23 ft per year (0.14 to 0.37 m)
1993	Rossbehy	National Coastal Erosion Committee (1993) reports erosion on seaward side is 0.1 to 0.5 m per year
2000-2006	Inch	Slight erosion of distal end of barrier (O'Shea *et al*., 2011)
2008 AD	Rossbehy	Barrier breach occurs; initiation of new tidal inlet

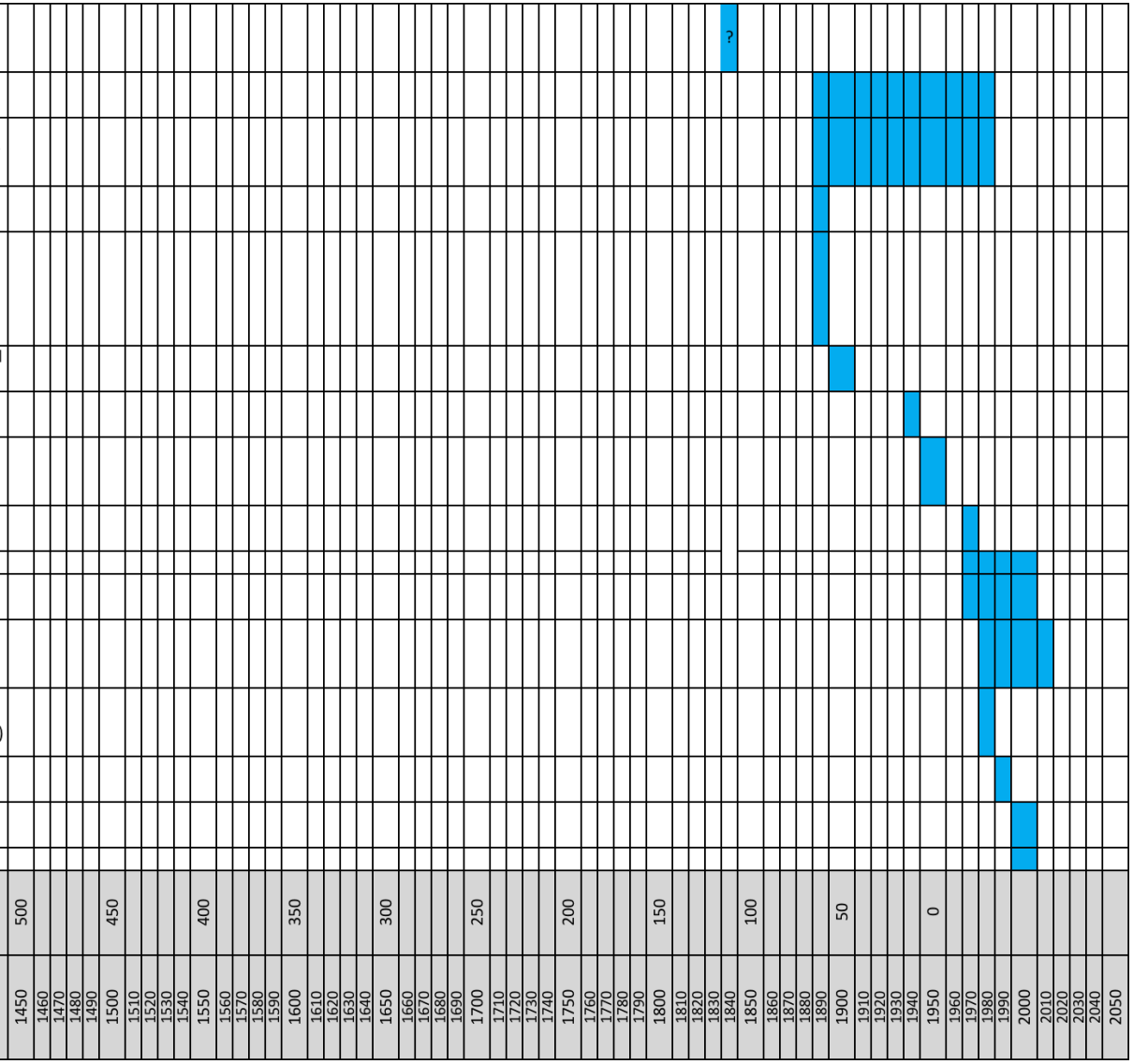

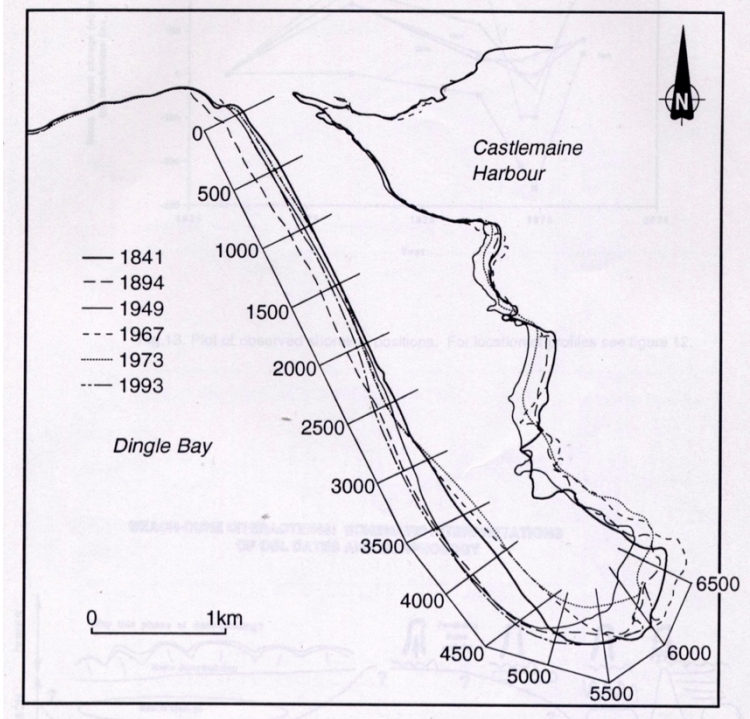

Figure 3.7 Historical shoreline variations at Inch. Source: Cooper *et al.* (1995)

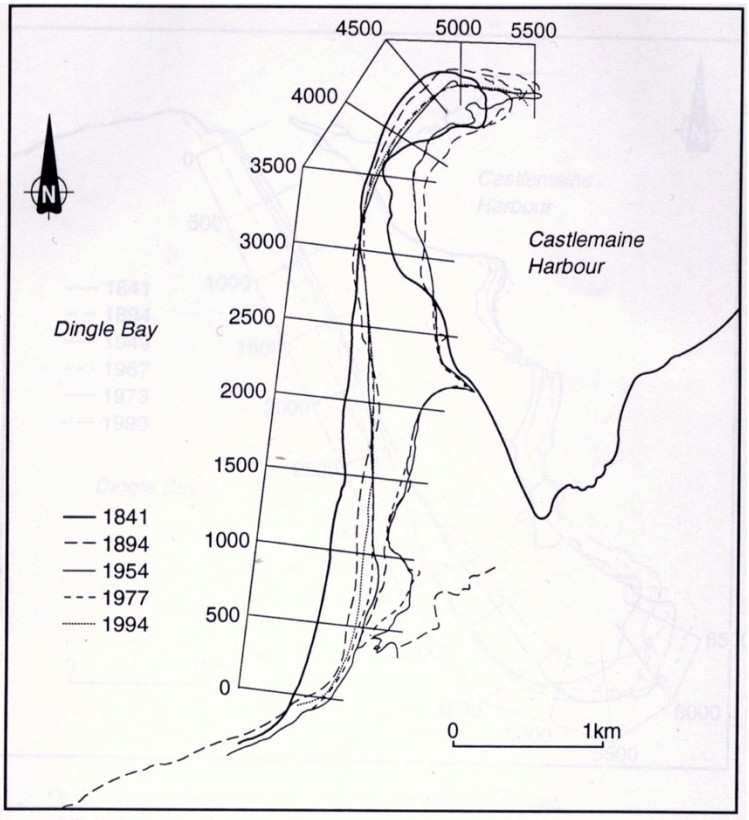

Figure 3.8 Historical shoreline variation at Rossbehy. Source: Cooper *et al.* (1995)

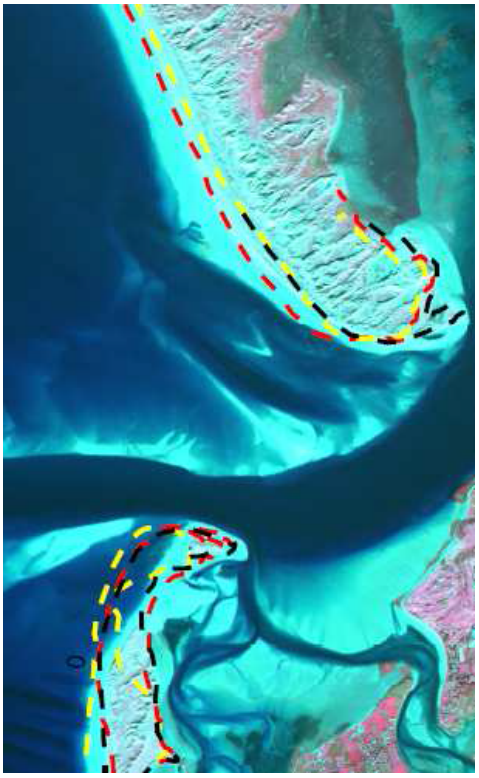

Figure 3.9 Results of shoreline change analysis undertaken by O'Shea *et al*. (2011) superimposed on an aerial photograph from 2010. Yellow = 1842; Red = 1894; Black = 2000. **Source**: O'Shea *et al*. (2011)

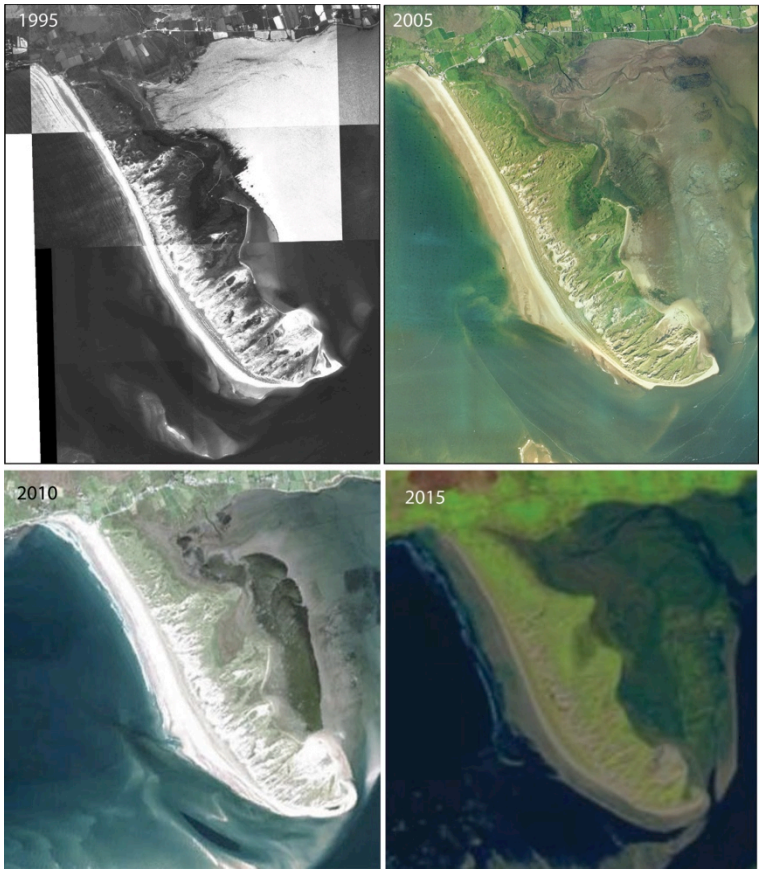

Figure 3.10 Aerial photographs (1995, 2005, and 2010) and Landsat 8 imagery (2015) of Inch, illustrating the relative stability of its shoreline. Source of imagery: 1995 and 2005 = OSI; 2010 = Google Earth; 2015 = USGS LandsatLook viewer

Figure 3.11 Aerial photographs (1997, 1995, 2005, 2010, and 2012) and Landsat 8 imagery (2015) of Rossbehy, illustrating recent changes along its distal shoreline. Source of imagery: 1977, 1995, and 2005 = OSI; 2010 = Google Earth; 2012 = ESRI World Imagery / Microsoft; 2015 = USGS LandsatLook viewer

Figure 3.12 Aerial photographs of Rossbehy prior to (September 2008) and after (July 2009) breaching in December 2008. Source: John Herriott aerial photography

Figure 3.13 Damage to main road providing access to Rossbehy strand following the winter storms of 2013/2014. Looking north toward the children's play area. Source: The Kerryman (2014)

Figure 3.14 Sunbeam shipwreck before 2013/2014 storms (in its original position since 1903; top), after first displacement in December 2013 (middle; lying parallel to foredune ridge) and after final displacement in February 2014 (bottom; lying oblique to foredune ridge). For scale, the boat's maximum width is approximately 5 m and maximum length is approximately 22 m. Source: author's own

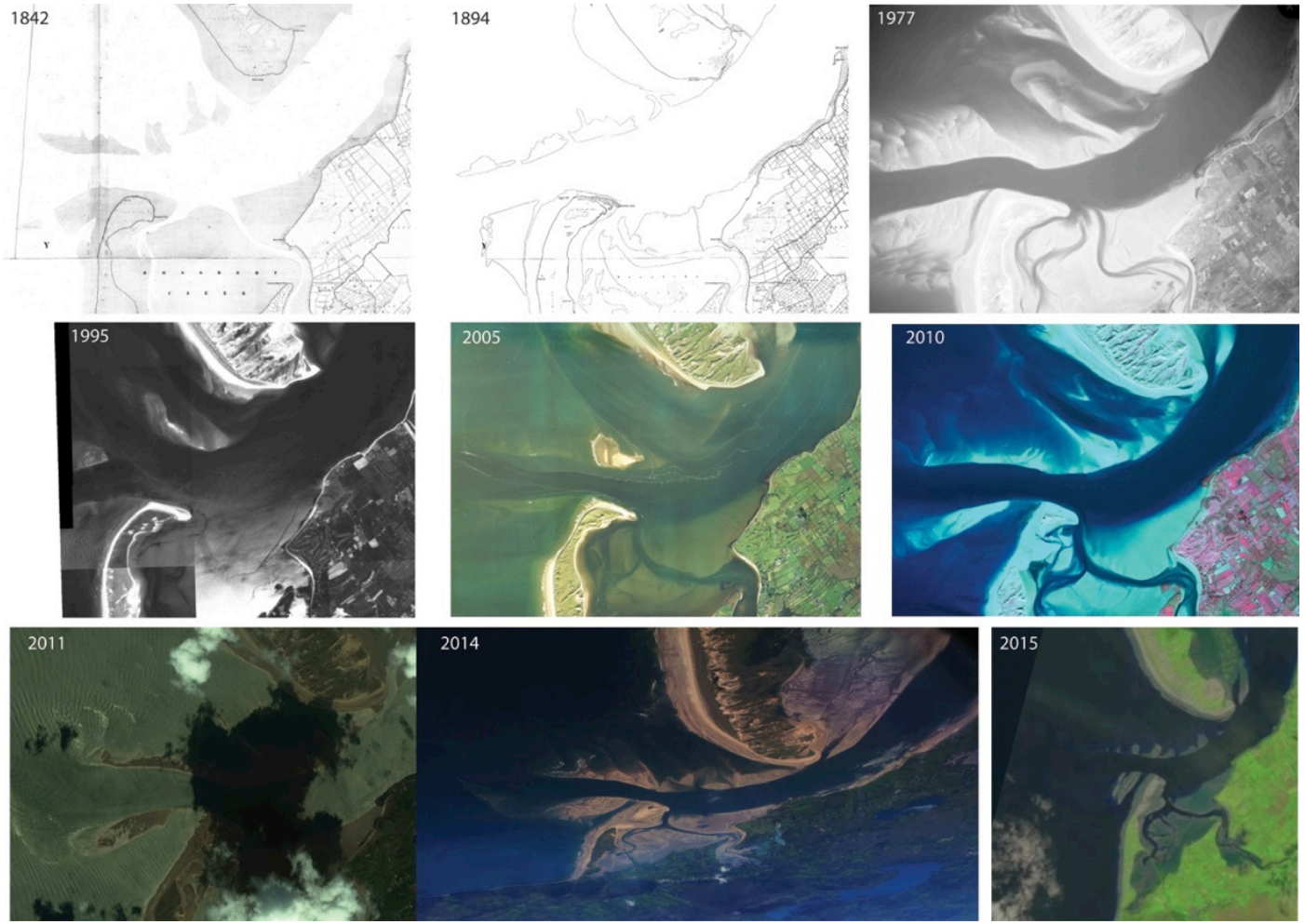

Figure 3.15 Historic maps (1842, 1894), aerial photographs (1977, 1995, 2005, 2010, 2011, and 2014) and Landsat 8 imagery illustrating changes in the shape and position of ebb shoals off Inch and Rossbehy from 1842 to 2015. Source of maps and 1977 and 1995 imagery: OSI; source of 2010 and 2011 imagery: GoogleEarth; source of 2014 imagery: Irish Air Corps; source of 2015 imagery: USGS LandsatLook viewer.

Figure 3.16 Dune blowout at the entrance to Rossbehy strand. Source: author's own

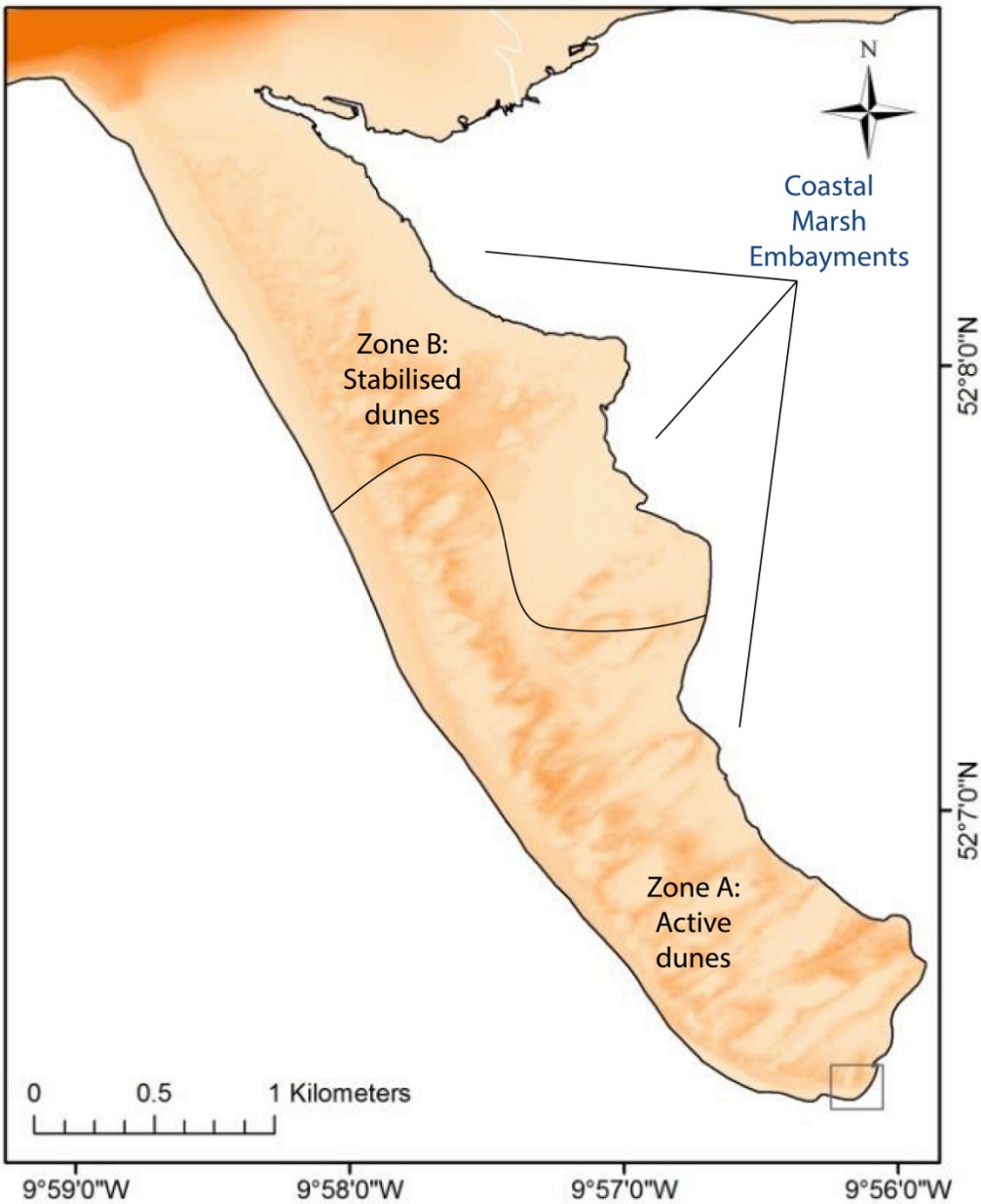

Figure 3.17 Annotated DEM illustrating dunescape at Inch, which is characterised by parabolics and transverse ridges. Data derived from aerial LiDAR data provided by the Kerry County Council and flown in April 2011. Box indicates area covered by beach-dune topographic surveys. Adapted from Devoy (2013).

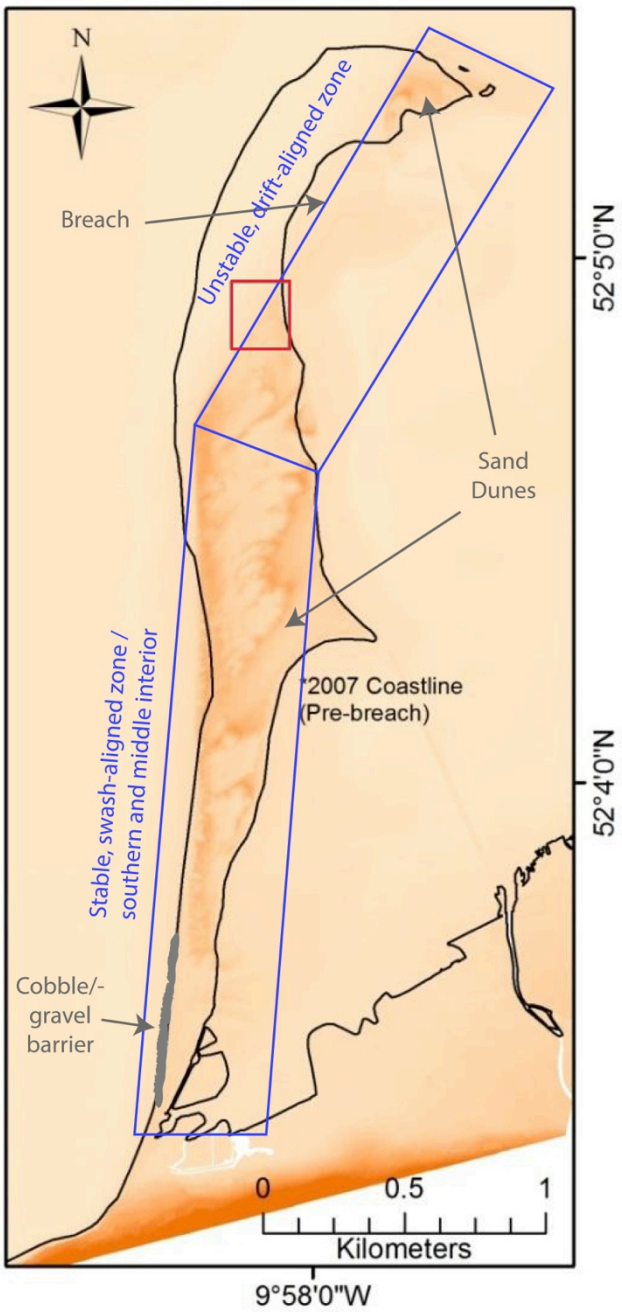

Figure 3.18 Annotated DEM illustrating dunescape at Rossbehy, which, like Inch, is characterised by parabolics and transverse ridges. Data derived from aerial LiDAR data provided by the Kerry County Council and flown in April 2011. Box indicates area covered by beach-dune topographic surveys.

Figure 3.19 Geotagged panorama showing scarping on the southwestern side of Inch. Map, inset, shows location of photo. Photo source: author's own; Map source: Google Maps

Figure 3.20 High foredune ridge in active, southern zone of Inch. Wooden posts on dune ridge are approx. 1 metre in height. Source: author's own (6 October 2012).

Figure 3.21 Ephemeral embryonic dunes at southern tip of Inch (looking south towards Dooks golf course). 20 June 2013 Source: author's own

Figure 3.22 Transverse ridges in southern and middle interior of Rossbehy. Looking north towards Inch. Source: John Coveney

Figure 3.23 Dune slack in middle interior of Rossbehy. Looking south. Source: author's own

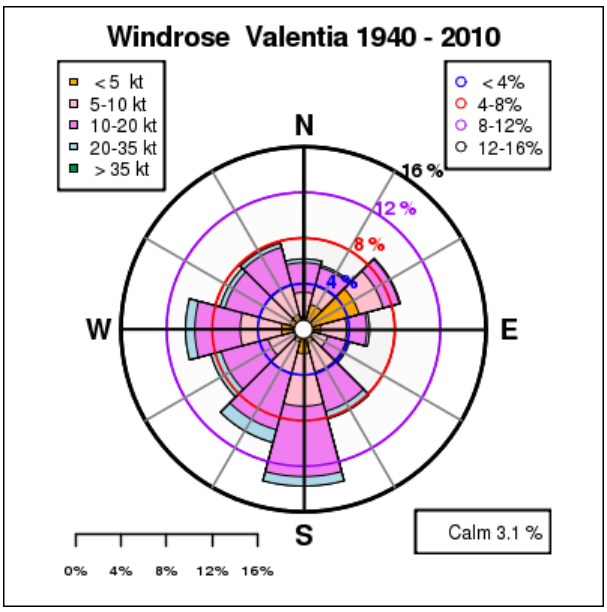

Figure 3.24 Valentia windrose 1940-2010. Source: Met Éireann

Highest Astronomical Tide	+4.36 m
Mean High Water Spring	+3.76 m
Mean High Water Neap	+3.15 m
Mean Sea Level (0 m at Malin Head)	+2.3 m (Ordnance Datum Malin)
Mean Low Water Neap	+1.17 m
Mean Low Water Spring	+0.58 m
Lowest Astronomical Tide	0 m

Table 3.4 Tidal ranges at Inch Beach based on predictions for a total tidal cycle (20 years). Source: Vial (2008) and Sala (2010)

Figure 3.25 Conceptual model of inferred morphological changes in Inch beach and dunes proposed by Orford *et al*. (1999a). Source: Orford *et al*. (1999a)

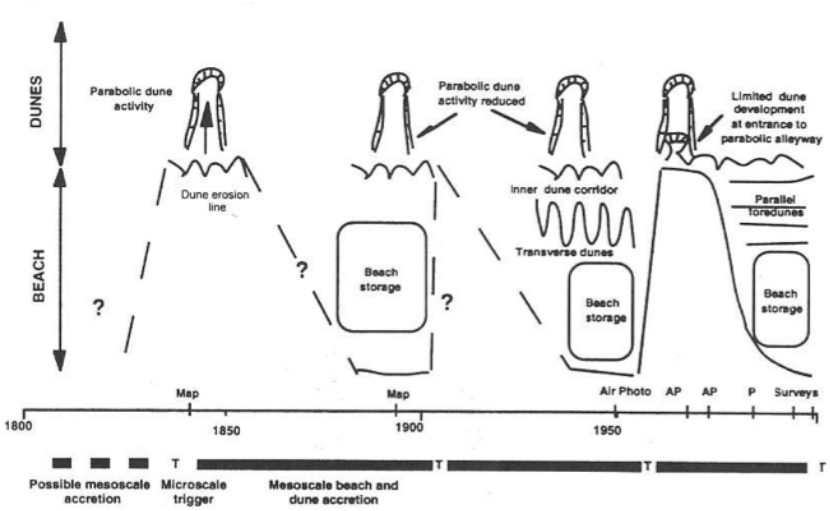

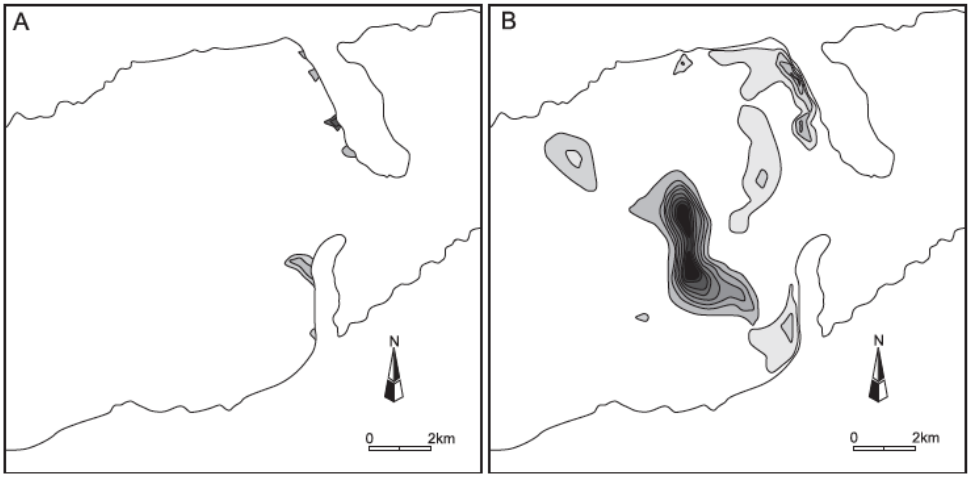

Figure 3.26 Distribution of wave energy dissipation at Inch and Rossbehy under (A) modal swell (H=0.04 m, T = 7 s) and (B) large swell waves (H=6.6 m, T = 13.6 s). Extracted from Cooper *et al*. (2004)

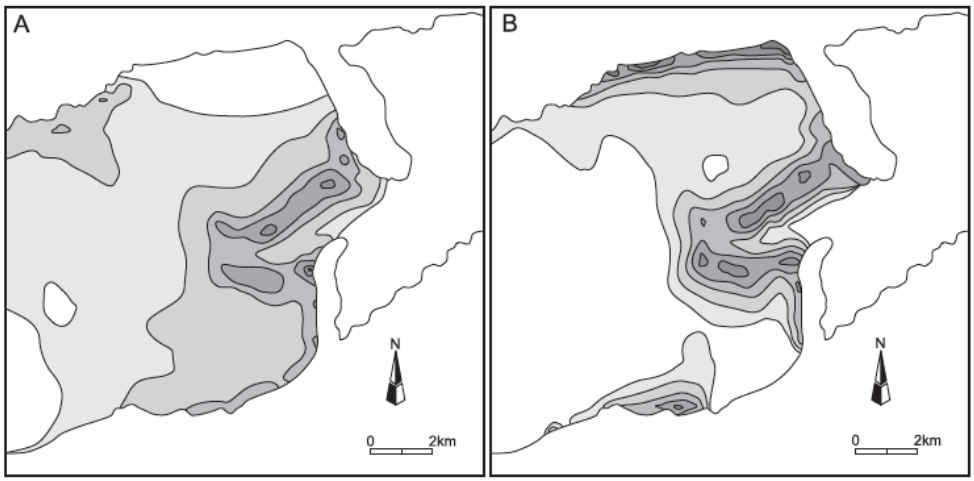

Figure 3.27 Wave orbital velocities at Inch and Rossbehy under (A) modal swell conditions and (B) Hurricane Debbie wind-generated waves, indicating relative ability of waves to transport sediment under storm conditions. Extracted from Cooper *et al*. (2004)

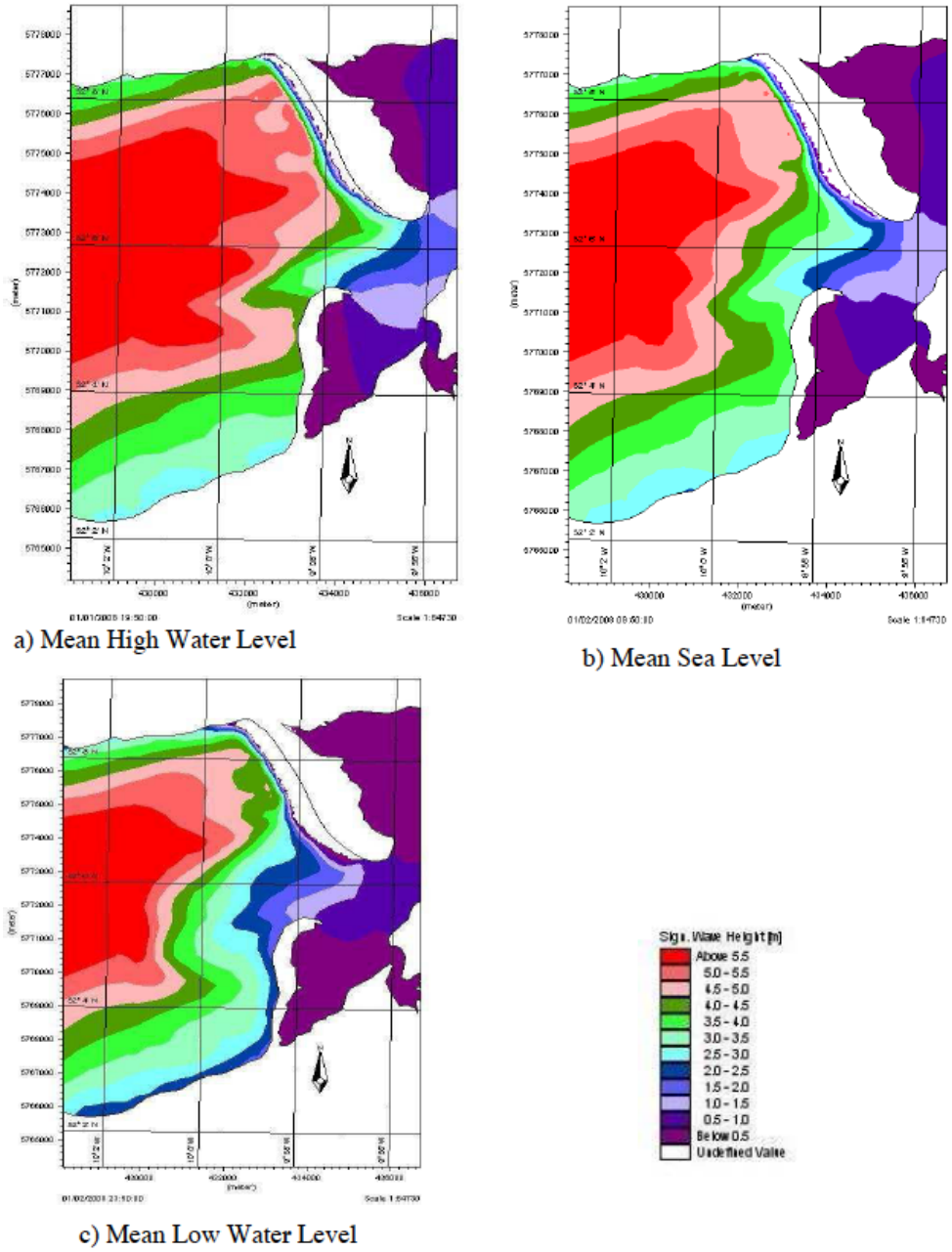

Figure 3.28 Significant wave heights associated with a 100-year return storm coming from an angle of 240° for (a) mean high water, (b) mean sea level, and (c) mean low water. Extracted from Vial (2008)

Figure 3.29 Historical recurves (blue) at Rossbehy represent either earlier northern limits of dune progression or southern limits to a historical breaching event. Figure adapted from O'Shea (2015).

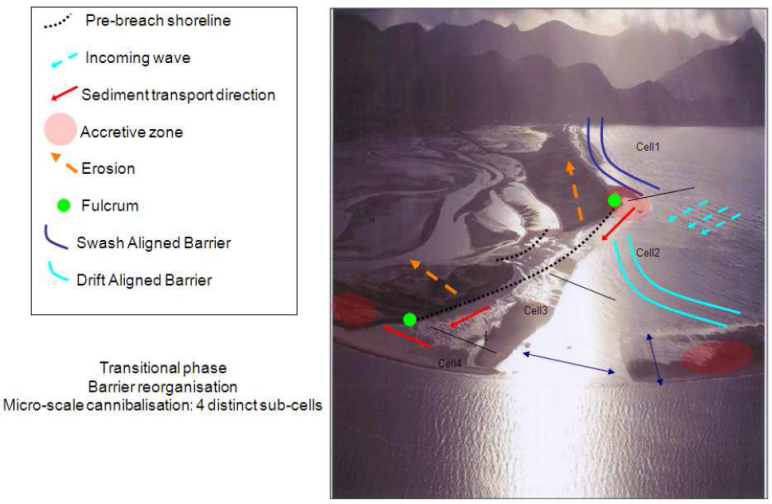

Figure 3.30 Sedimentary cells at Rossbehy as defined within the short-term conceptual model of Sala (2010). Looking south. Source: Sala (2010).

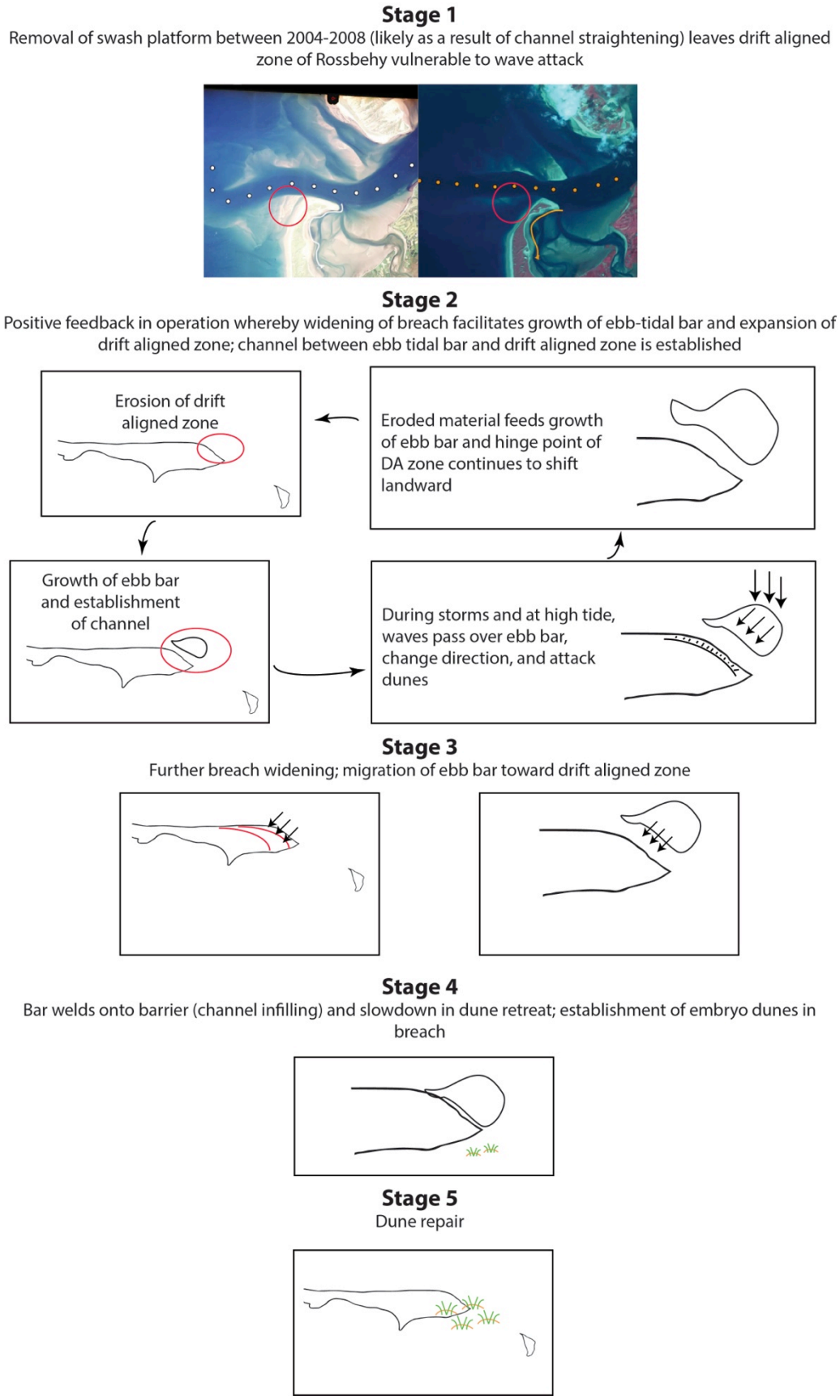

Figure 3.31 Five-step conceptual model of O'Shea (2015) for breach evolution at Rossbehy. Graphics for stage 1 extracted from O'Shea *et al.* (2013)

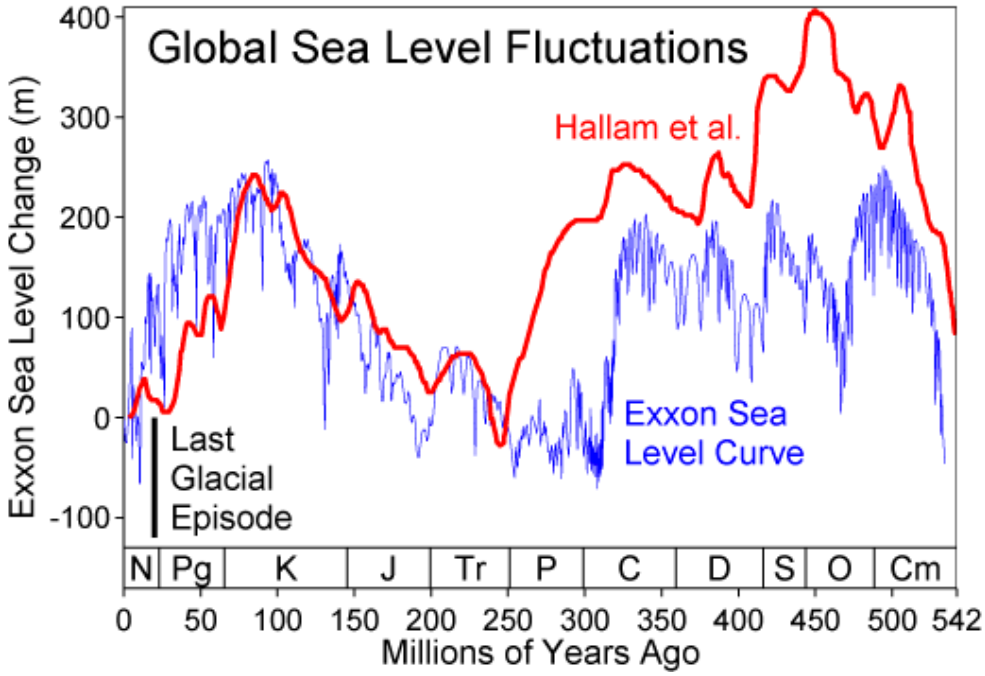

Figure 4.1 Phanerozoic global sea-level curves derived from the stratigraphic record. Source: http://en.wikipedia.org/wiki/Sea-level_curve - after Vail *et al.* (1977) and Hallam (1981).

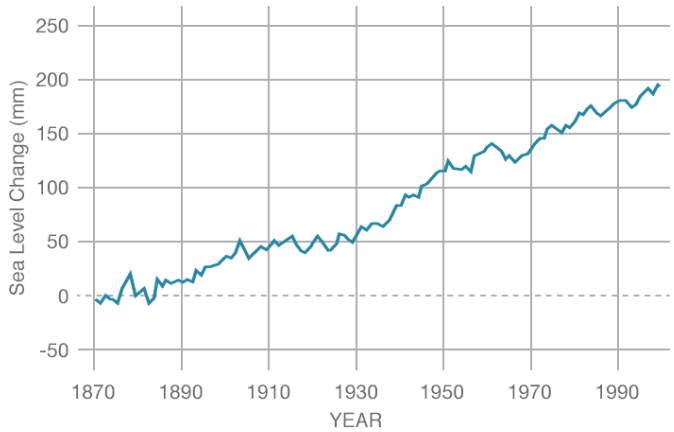

Figure 4.2 Global sea-level change from coastal tide gauge records - 1870 to 2000. Source**:** CSIRO (2014)

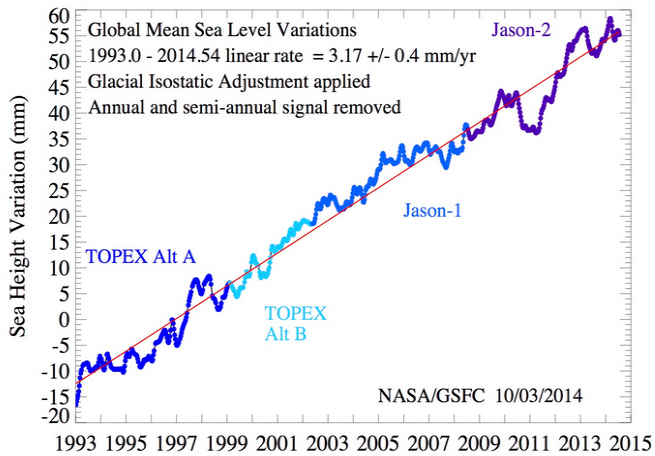

Figure 4.3 Multi-mission ocean altimeter data showing global mean sea-levels from 1993 to 2014. Data is with respect to the 1993-2002 mean and plotted every 10 days. Source: NASA Goddard Space Flight Center (2014)

Source	1901–1990	1971–2010	1993–2010
Observed contributions to global mean sea level (GMSL) rise			
Thermal expansion	–	0.8 [0.5 to 1.1]	1.1 [0.8 to 1.4]
Glaciers except in Greenland and Antarctica[a]	0.54 [0.47 to 0.61]	0.62 [0.25 to 0.99]	0.76 [0.39 to 1.13]
Glaciers in Greenland[b]	0.15 [0.10 to 0.19]	0.06 [0.03 to 0.09]	0.10 [0.07 to 0.13][b]
Greenland ice sheet	–	–	0.33 [0.25 to 0.41]
Antarctic ice sheet	–	–	0.27 [0.16 to 0.38]
Land water storage	−0.11 [−0.16 to −0.06]	0.12 [0.03 to 0.22]	0.38 [0.26 to 0.49]
Total of contributions	–	–	**2.8 [2.3 to 3.4]**
Observed GMSL rise	**1.5 [1.3 to 1.7]**	**2.0 [1.7 to 2.3]**	**3.2 [2.8 to 3.6]**
Modelled contributions to GMSL rise			
Thermal expansion	0.37 [0.06 to 0.67]	0.96 [0.51 to 1.41]	1.49 [0.97 to 2.02]
Glaciers except in Greenland and Antarctica	0.63 [0.37 to 0.89]	0.62 [0.41 to 0.84]	0.78 [0.43 to 1.13]
Glaciers in Greenland	0.07 [−0.02 to 0.16]	0.10 [0.05 to 0.15]	0.14 [0.06 to 0.23]
Total including land water storage	**1.0 [0.5 to 1.4]**	**1.8 [1.3 to 2.3]**	**2.8 [2.1 to 3.5]**
Residual[c]	**0.5 [0.1 to 1.0]**	**0.2 [−0.4 to 0.8]**	**0.4 [−0.4 to 1.2]**

Notes:

[a] Data for all glaciers extend to 2009, not 2010.

[b] This contribution is not included in the total because glaciers in Greenland are included in the observational assessment of the Greenland ice sheet.

[c] Observed GMSL rise – modelled thermal expansion – modelled glaciers – observed land water storage.

Figure 4.4 Modelled and observed GMSL rise from IPCC AR5. Modelled data was computed from the Coupled Model Intercomparison Project (CMIP5) and shows good agreement with observations. Source: Church *et al.* (2013).

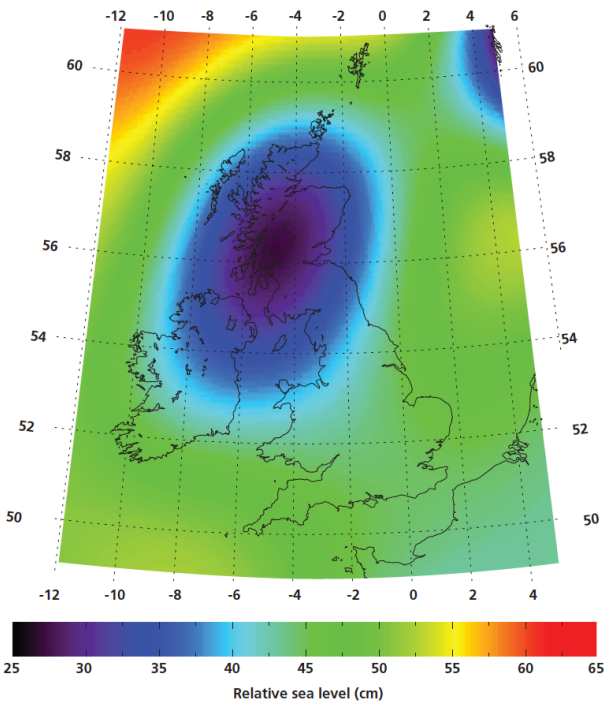

Figure 4.5 Derived projected RSL increases under the IPCC AR4 medium emissions scenario for the year 2095. Projections take into account both absolute SLR and vertical land movement due to glacial isostatic adjustment. Source: Lowe *et al.* (2009)

Figure 4.6 Oblique aerial photos of Portballintrae Beach in 1938 (top) and 1999 (bottom) illustrating beach narrowing as a result of the installation of a pier in its western section. Source: Jackson (2012)

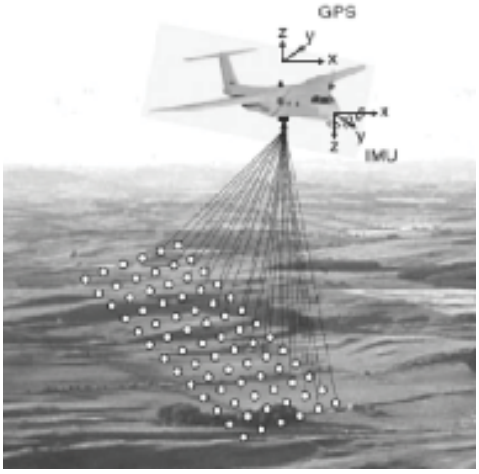

Figure 6.1 Airborne LiDAR systems work by sending out multiple laser pulses and recording the time it takes for the signal to be reflected off the ground and returned to the sensor. These systems consist of three main parts: the sensor, the inertial measurement unit, and a GPS. Source: Heritage and Large (2009)

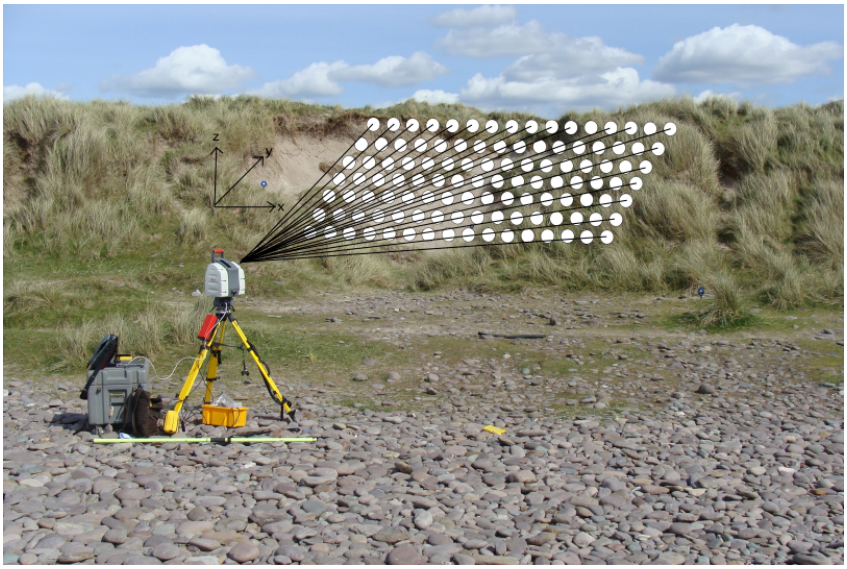

Figure 6.2 Ground-based LiDAR systems use the same basic technology as airborne systems, but are deployed on the ground. While they are limited in terms of coverage area compared to airborne systems, they are capable of capturing higher resolution data and are easier to deploy at short notice (*e.g.* in the aftermath of a storm).

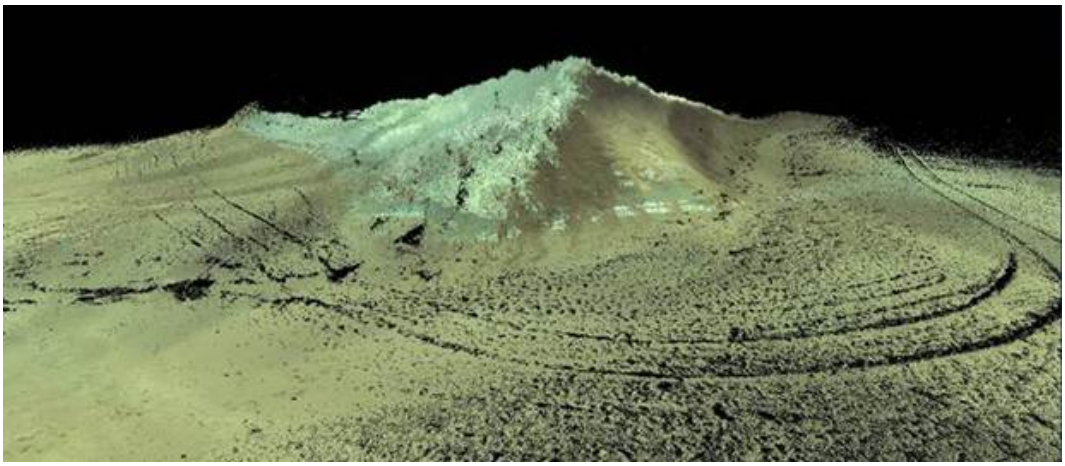

Figure 6.3 Point cloud showing beach and foredunes (centre) at the terminal margin of the Rossbehy barrier (looking south). The dune scarp (centre right) is the on seaward side of barrier, with the vegetated lee side shown centre left. The track marks are from the wheels of the trolley used to transport equipment to the field site, which are approx. 7 cm in width. This figure illustrates the fine detail that can be captured using this survey technique.

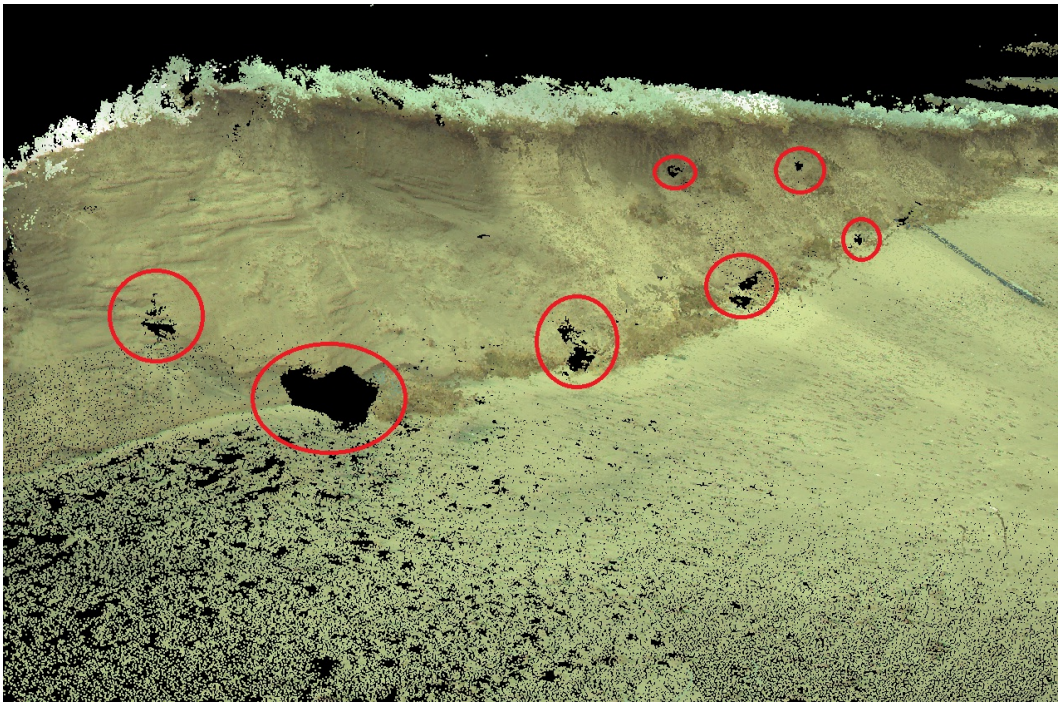

Figure 6.4 Shadow zones - zones of missing data located behind obstructions to the laser scanners field of view, resulting in 'gaps' in the point cloud. These can be minimised by obtaining multiple surveys over the same area from different angles. Source: author's own data obtained at Rossbehy field site

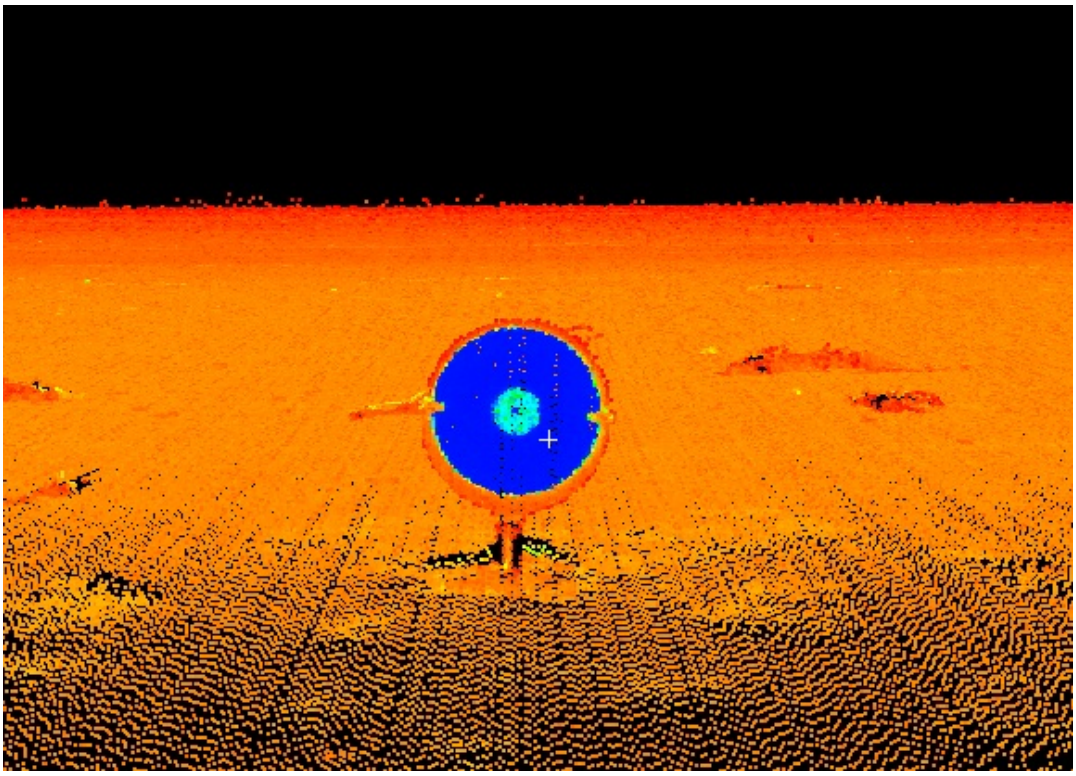

Figure 6.5 Survey target, as seen in a point cloud, used for referencing multiple scans to one common coordinate system. Source: author's own data obtained at Rossbehy field site

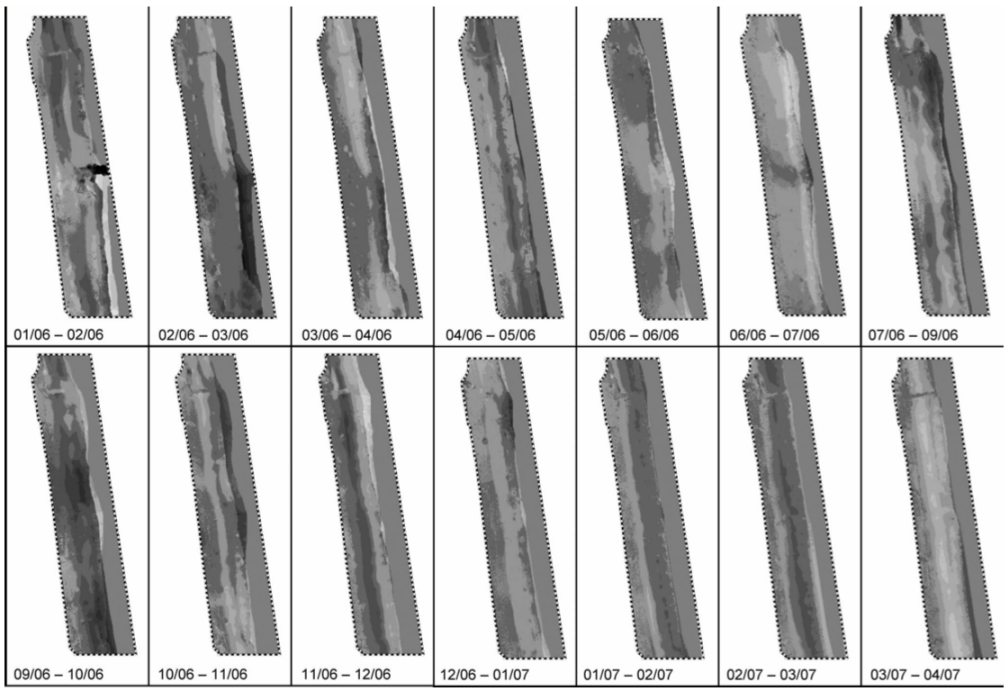

Figure 6.6 DEMs generated from TLS data collected at monthly intervals at Rehoboth Beach, North Carolina, USA from January 2006-April 2007. Areas of maximum erosion are shown in black and grade to areas of maximum accretion, shown in white. The data was collected at 0.20 m resolution over an area of approximately 500 m x 70 m and reduced to 1 m x 1 m grid cells. Source: Pietro *et al*. (2008)

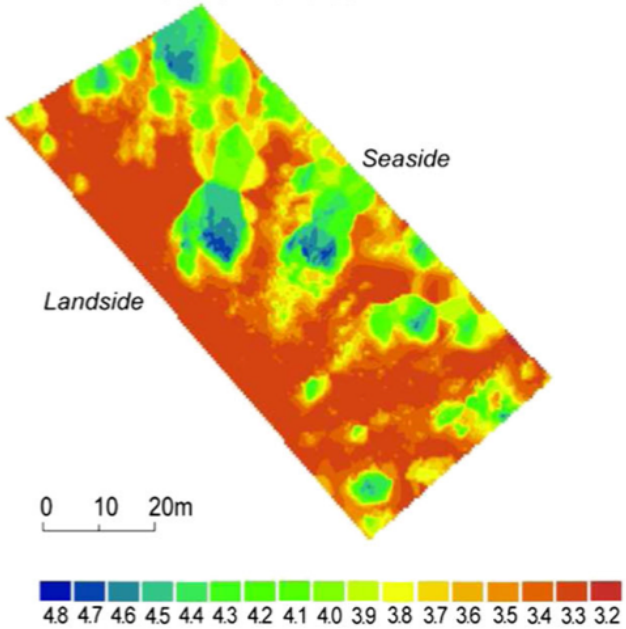

Figure 6.7 Digital elevation model of embryo dunes in North Lincolnshire, UK. Elevation in metres. Source: Montreuil *et al*. (2013)

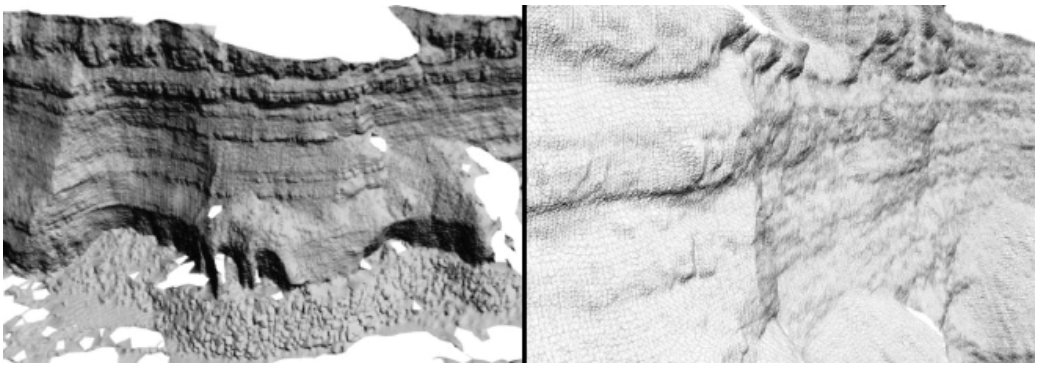

Figure 6.8 Rendered triangular irregular network (TIN) showing a hard rock cliff face in North Yorkshire, UK (left) and close up (right) showing triangular faces. TLS data form the nodes of the TIN. Source: Rosser *et al*. (2005)

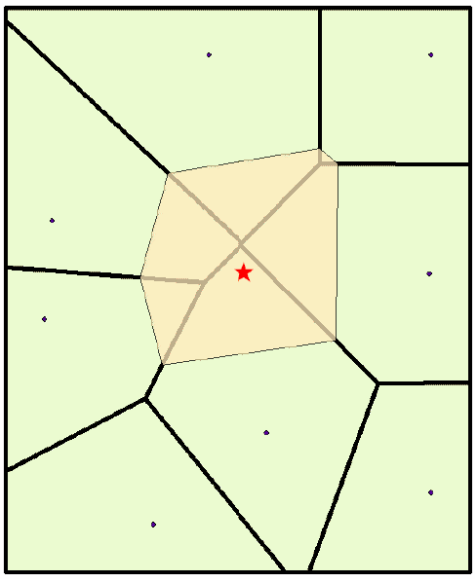

Figure 6.9 Graphic illustrating how natural neighbour interpolation works. See text for explanation. Image source: ESRI ArcGIS 9.2 Desktop Help (http://webhelp.esri.com/arcgisdesktop/9.2/index.cfm?TopicName=Natural%20Neighbor%20Interpolation)

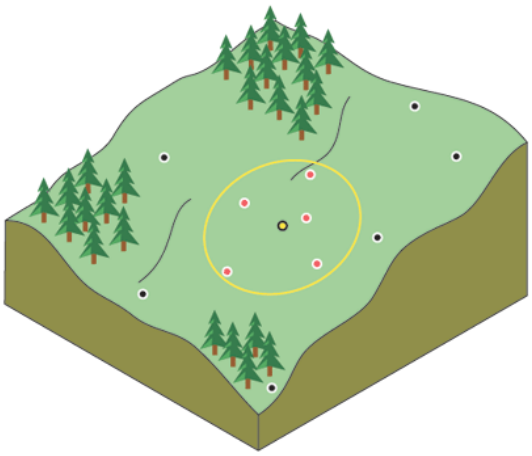

Figure 6.10 Graphic illustrating how inverse distance weighting interpolation works. See text for explanation. Image source: ESRI ArcGIS 9.2 Desktop Help (http://webhelp.esri.com/arcgisdesktop/9.2/index.cfm?TopicName=Implementing_Inverse_Distance_Weighted_(IDW))

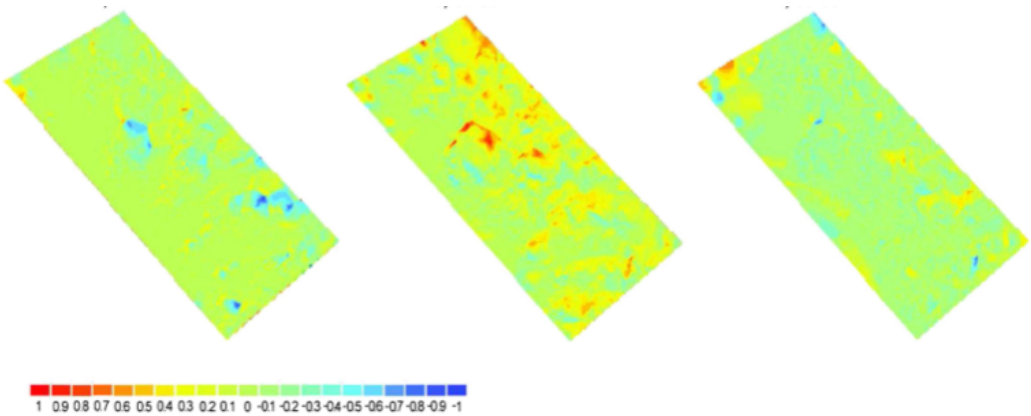

Figure 6.11 DEMs of difference showing seasonal changes to embryo dunes for three periods between October 2009 and October 2010. Source: Montreuil *et al*. (2013)

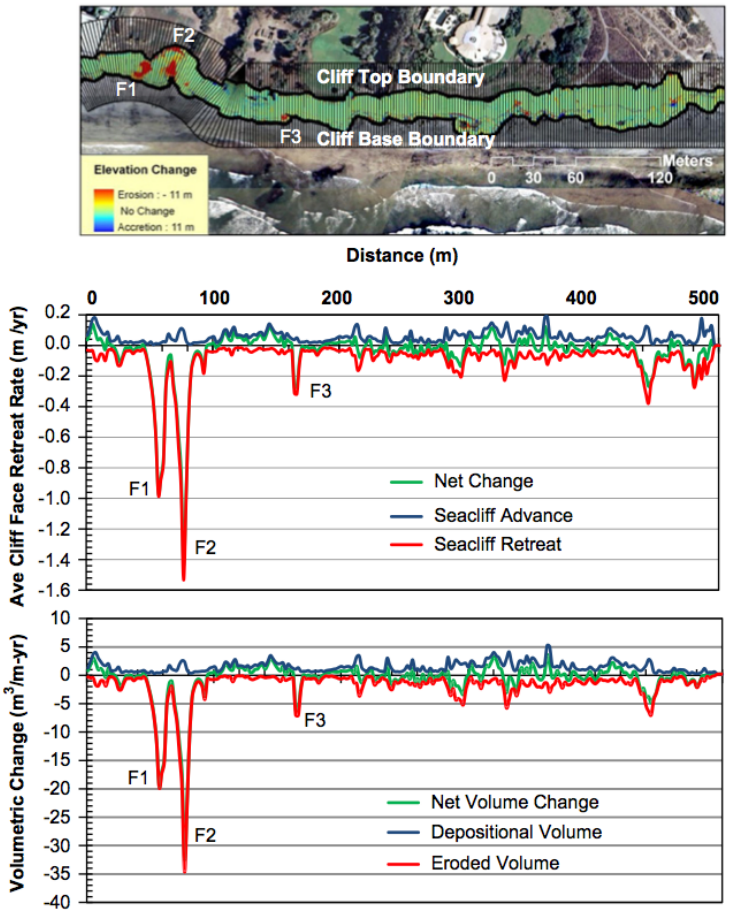

Figure 6.12 Example of compartments (top) generated in TOPCAT for a case study at Dog Beach, Del Mar California (Oct 2005–March 2007). Compartments are overlain on elevation change map. Graphs show cliff face retreat rate (centre) and volumetric change (bottom) for each compartment along the length of the cliff. F1, F2, and F3 are major cliff failure events. Source: Olsen *et al*. (2012)

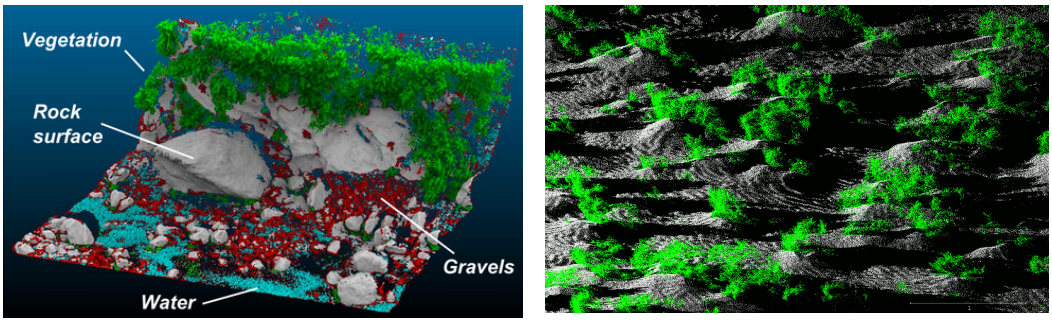

Figure 6.13 Results of classification using a multi-scale dimensionality criterion for a steep river bank (left, classes labelled) and a tidal marsh (right, green = vegetation, white = soil). Source: Brodu (2012)

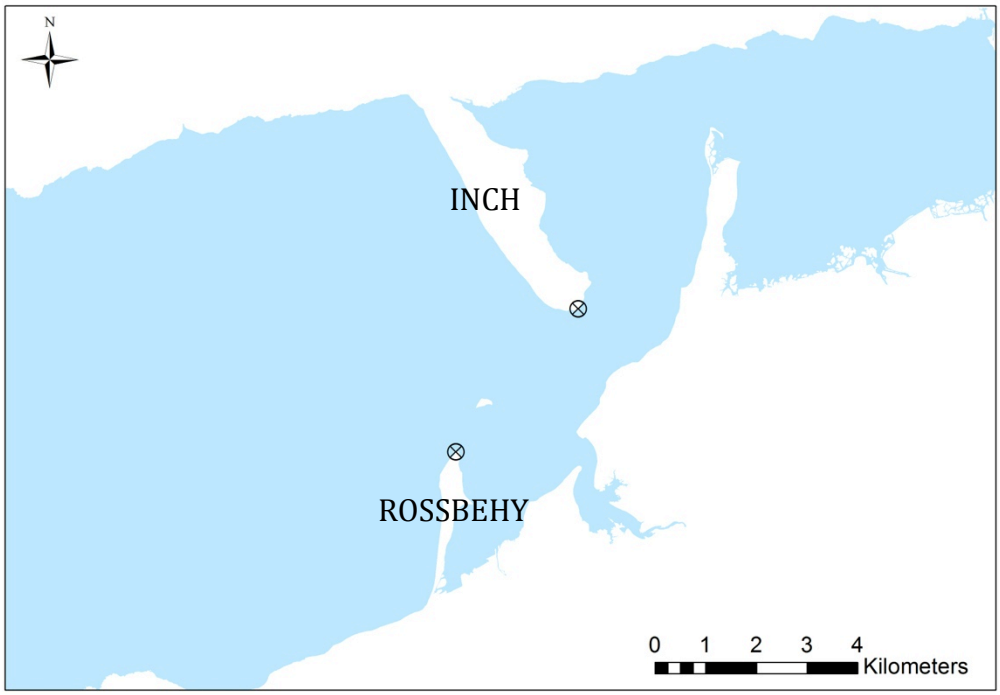

Figure 7.1 General locations of field sites at Rossbehy and Inch. Source: Modified from OSI vector coastline data and 2010 OSI aerial photography.

Figure 7.2 High foredune at Inch field site (looking North). Source: author's own (6 October 2012)

Figure 7.3 Ephemeral embryo dune field and beach fronting foredune at Inch field site. Looking southeast. Rossbehy can be seen in the distance. Source: author's own (20 June 2013)

Figure 7.4 Oblique aerial view of Inch field site, looking north-northwest. Source: coastalhelicopterview.ie

Figure 7.5 General location of Rossbehy field site. Looking south. Source: Google Earth (2012)

Figure 7.6 Main section of Rossbehy field site, consisting of upper beach and foredune scarp. Barrier terminus is at left. Looking east. Source: author's own (8 October 2012)

Figure 7.7 Terminus of mainland section of barrier (centre). Looking south. Foredune scarp is hidden by shadow (right of centre). Some scans covered part of vegetated dunes (left of centre) and back barrier beach. Source: author's own (15 April 2012)

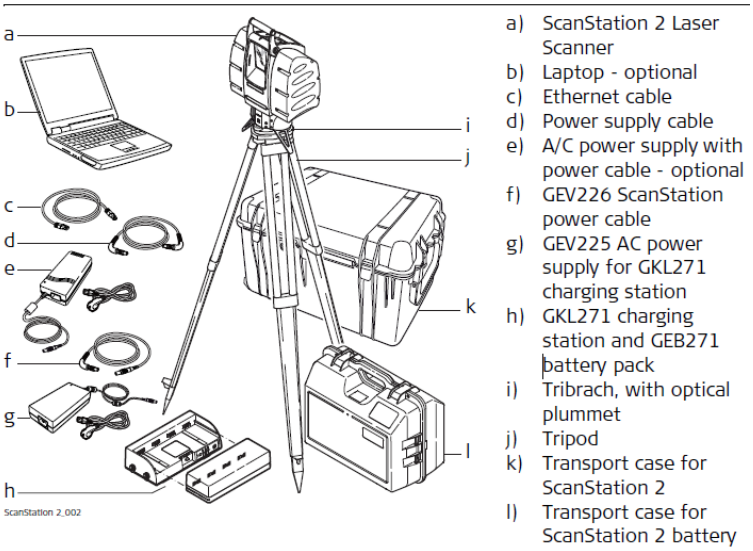

Figure 7.8 Leica ScanStation components. NB: Figure was extracted from Leica ScanStation2 model manual (Leica Geosystems, 2007), but ScanStation setup is more or less the same.

Figure 7.9 Leica ScanStation setup at Rossbehy field site. Looking north at main dune barrier terminus. Source: author's own (15 November 2012)

Figure 7.10 Field equipment being transported via tractor and trolley at Inch. Photo: Valerie Heffernan

Figure 7.11 Leica HDS registration target – for registration of multiple same-date scans.

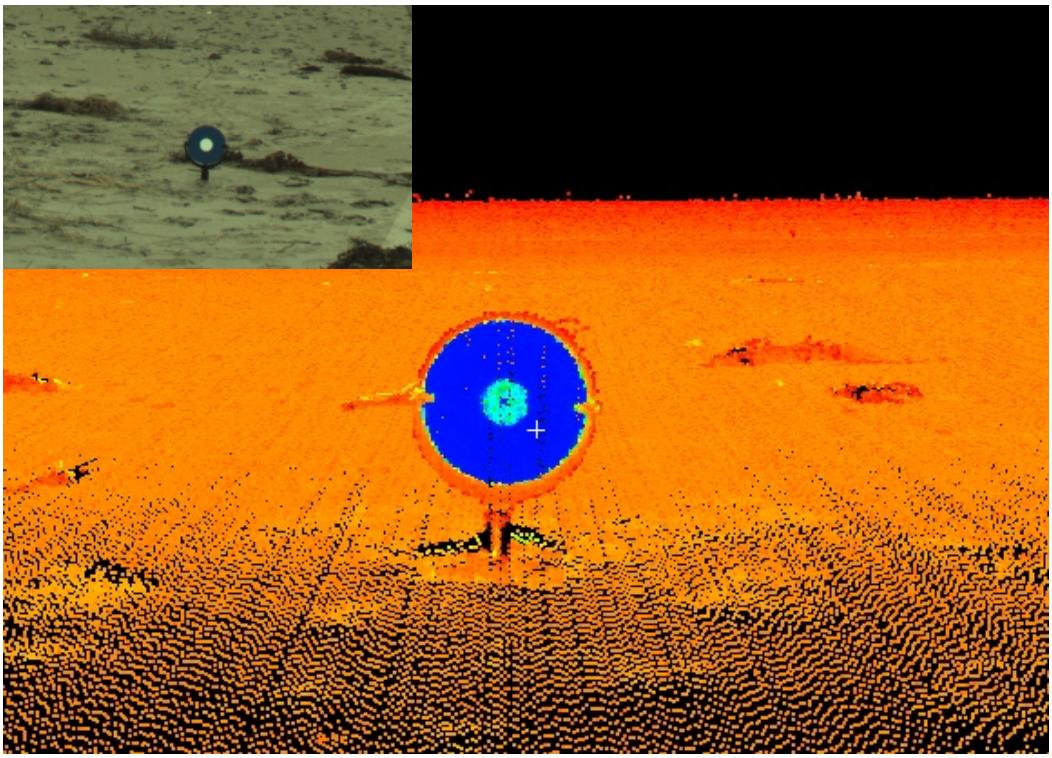

Figure 7.12 Leica HDS target as seen in section of photo mosaic (inset) and in the point cloud (main). From the mosaic, targets can be identified ('fenced') and the scanner can then be directed to scan only the fenced areas in high resolution for scan registration.

Date	Site	Resolution	Total number of points in cloud
2012-06-28*	Rossbehy	2 cm	67420725
2012-08-05*	Rossbehy	2.5 cm	97274308
2012-10-07*	Rossbehy	2.5 cm	43358639
2012-11-15	Rossbehy	2.5 cm	4267504
2013-01-30	Rossbehy	2.5 cm	4699073
2013-02-28	Rossbehy	2.5 cm	7609265
2013-04-19	Rossbehy	2 cm	7459604
2013-06-05	Rossbehy	2.5 cm	6794554
2013-08-06	Rossbehy	2.5 cm	5023912
2013-12-11	Rossbehy	10 cm	4104385
2014-01-16	Rossbehy	15 cm	1573813
2014-05-04	Rossbehy	2.5 cm	22997536
2014-07-29	Rossbehy	2.5 cm	16386541

Table 7.1 Summary of data obtained during field surveys completed at Rossbehy field site.
*Data obtained using Leica C10 instrument.

Date	Site	Resolution	Total number of points in cloud
2012-05-24	Inch	1 cm	8367215
2012-08-06	Inch	2.5 cm	30972308
2012-10-06	Inch	2.5 cm	47232935
2013-01-09	Inch	2.5 cm	10058134
2013-02-27	Inch	2.5 cm	4843043
2013-05-02	Inch	2.5 cm	7804177
2013-06-20	Inch	2.5 cm	24366526
2014-03-12	Inch	2.5 cm	23432492
2014-08-28	Inch	2.5 cm	2358641

Table 7.2 Summary of data obtained during field surveys completed at Inch field site.
*Data obtained using Leica C10 instrument.

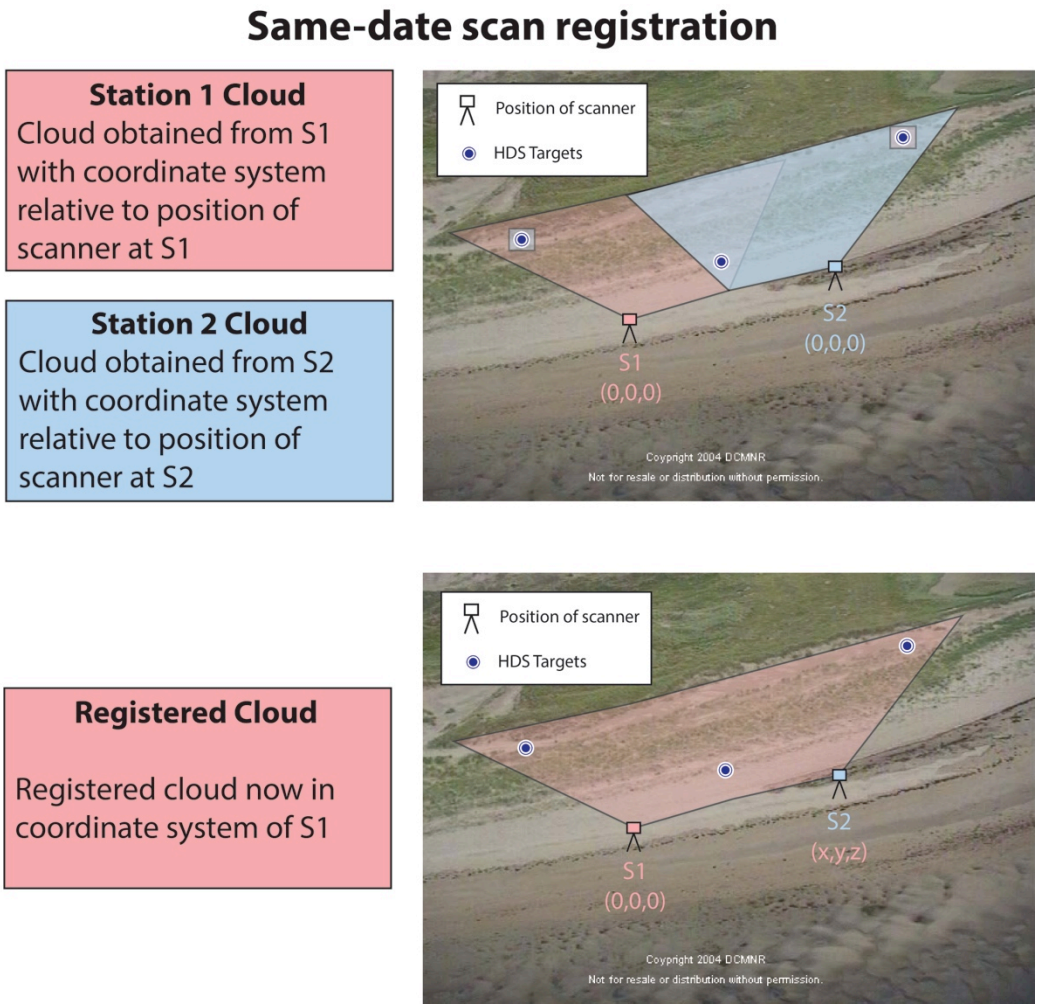

Figure 7.13 Example from Inch field site illustrating same-date scan registration for two point clouds obtained from two stations (S1 and S2). Following registration of the S2 cloud to the S1 cloud using the Leica HDS targets, the clouds are in the coordinate system of the S1 cloud.

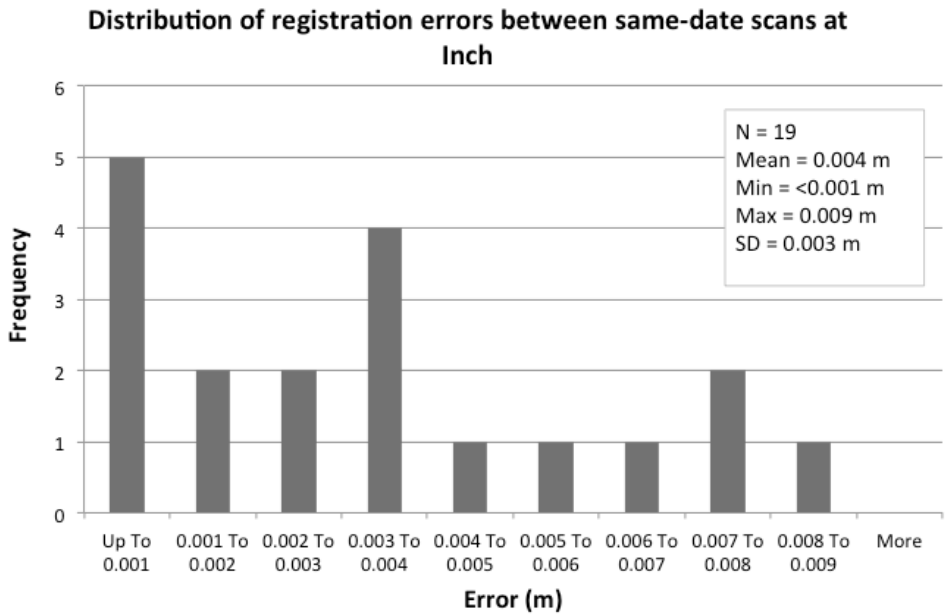

Figure 7.14 Distribution of registration errors between same-date scans at Inch. Inset: Population (N), mean, min, and max errors and standard deviation.

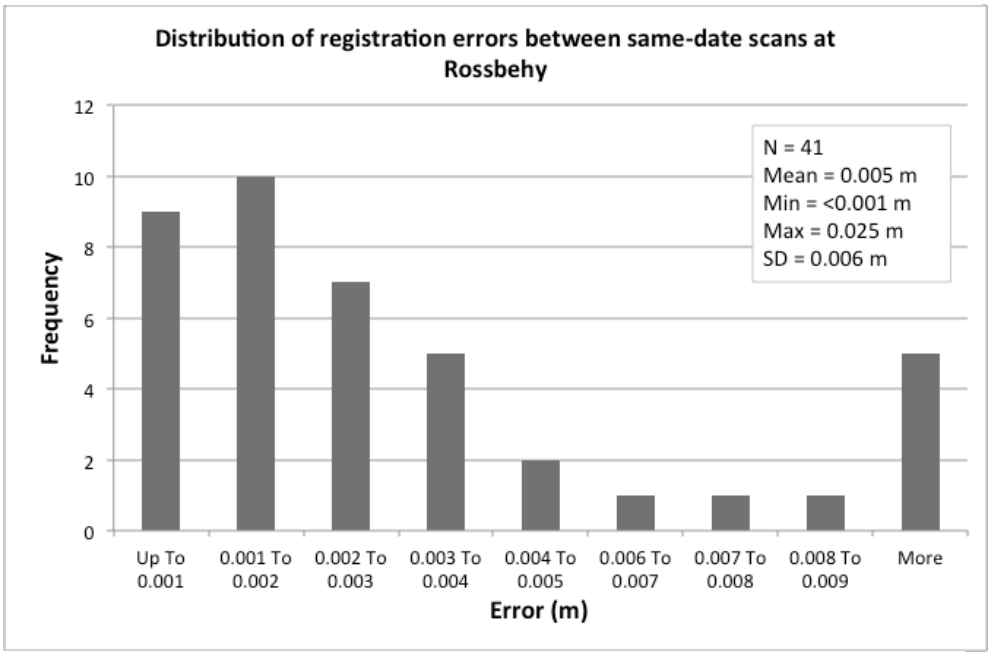

Figure 7.15 Distribution of registration errors between same-date scans at Rossbehy. Inset: Population (N), mean, min, and max errors and standard deviation.

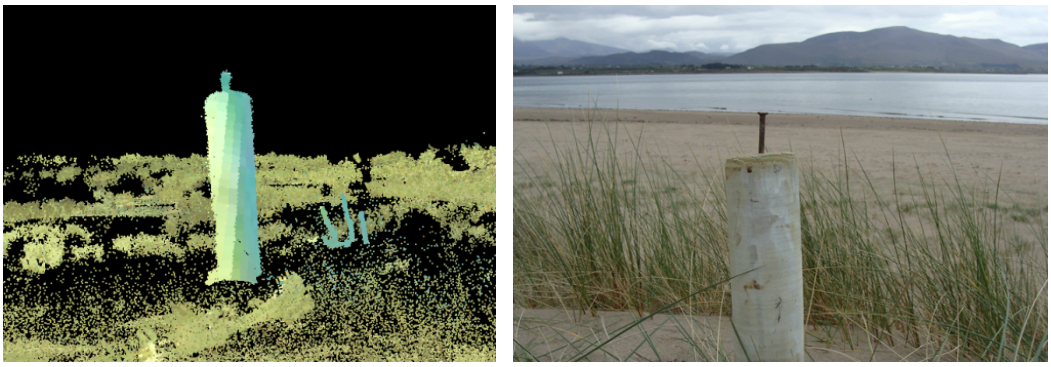

Figure 7.16 Example of semi-permanent wooden posts set up in the field for registering multi-temporal scans. The tips of the nails act as control points from which the successive scans are registered to one common coordinate system.

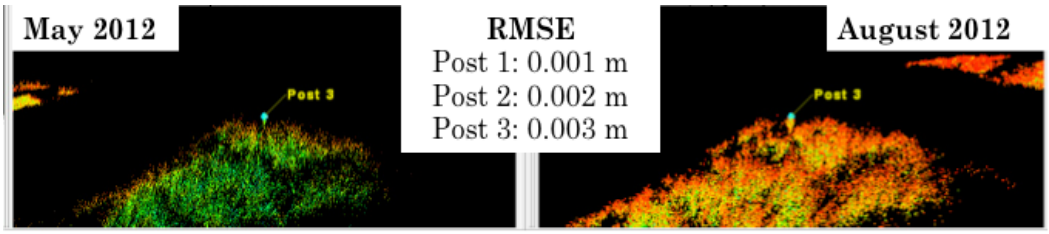

Figure 7.17 RMS Errors of registration associated with multi-temporal constraints (Post 1, Post 2, and Post 3) for May 2012 and August 2012 at Inch. Left: Post 3 in the May 2012 cloud; Right: Post 3 in the August 2012 cloud.

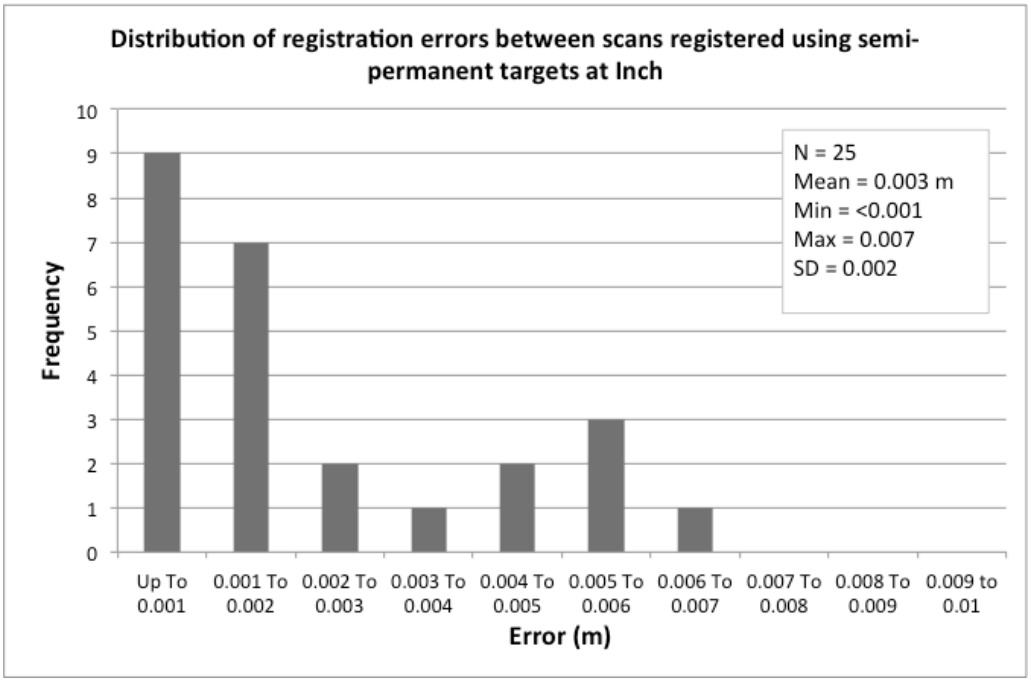

Figure 7.18 Distribution of registration errors between scans registered using semi-permanent targets at Rossbehy. Inset: Population (N), mean, min, and max errors and standard deviation.

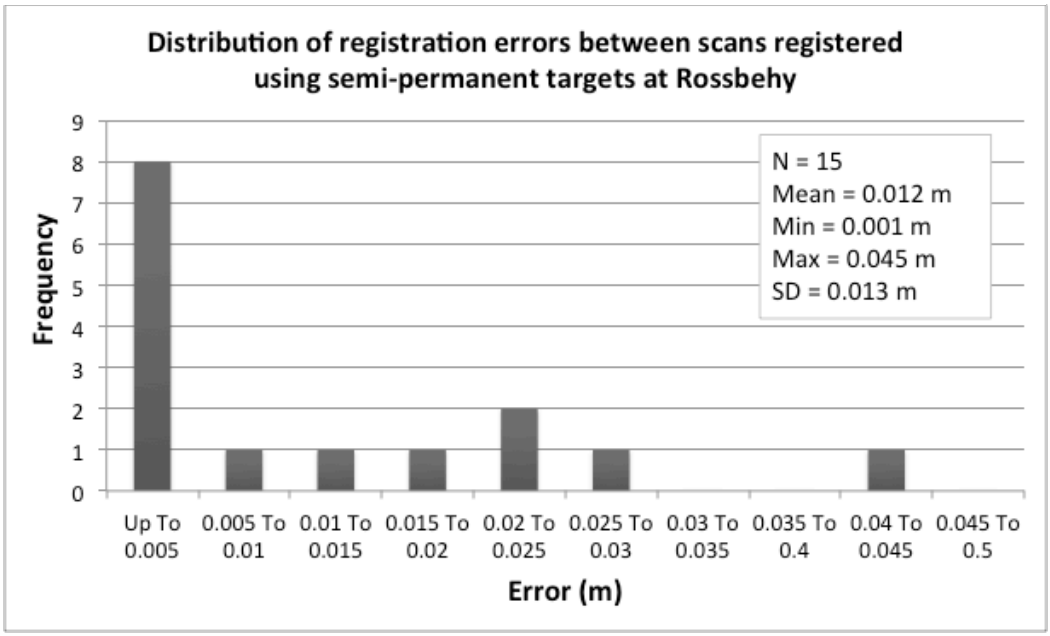

Figure 7.19 Distribution of registration errors between scans registered using semi-permanent targets at Inch. Inset: Population (N), mean, min, and max errors.

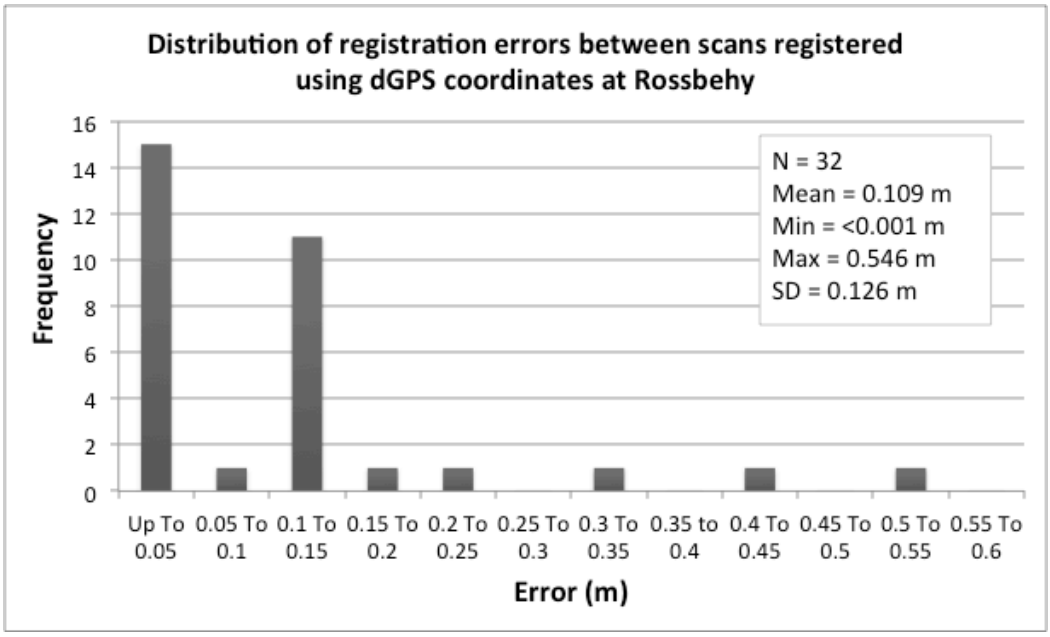

Figure 7.20 Distribution of registration errors between scans registered using dGPS coordinates at Rossbehy. Inset: Population (N), mean, min, and max errors.

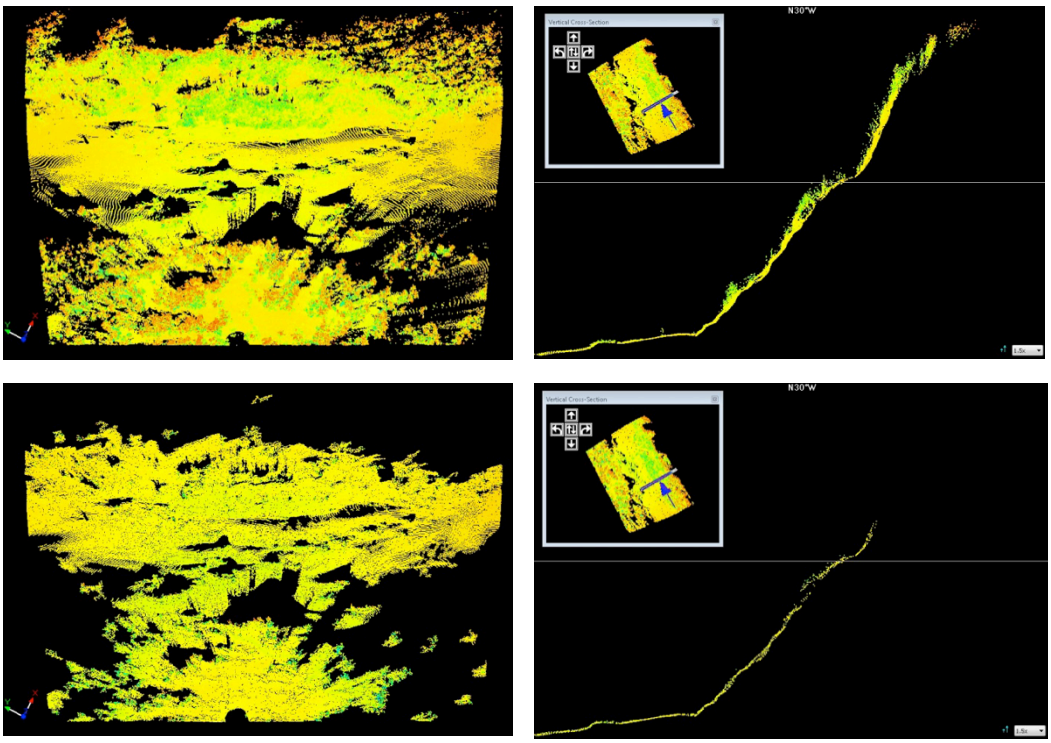

Figure 7.21 Before (top) and after (bottom) vegetation filtering using lowest points analysis on a subset of the May 2012 point cloud from Inch. Subset shown left, with cross section through centre shown right.

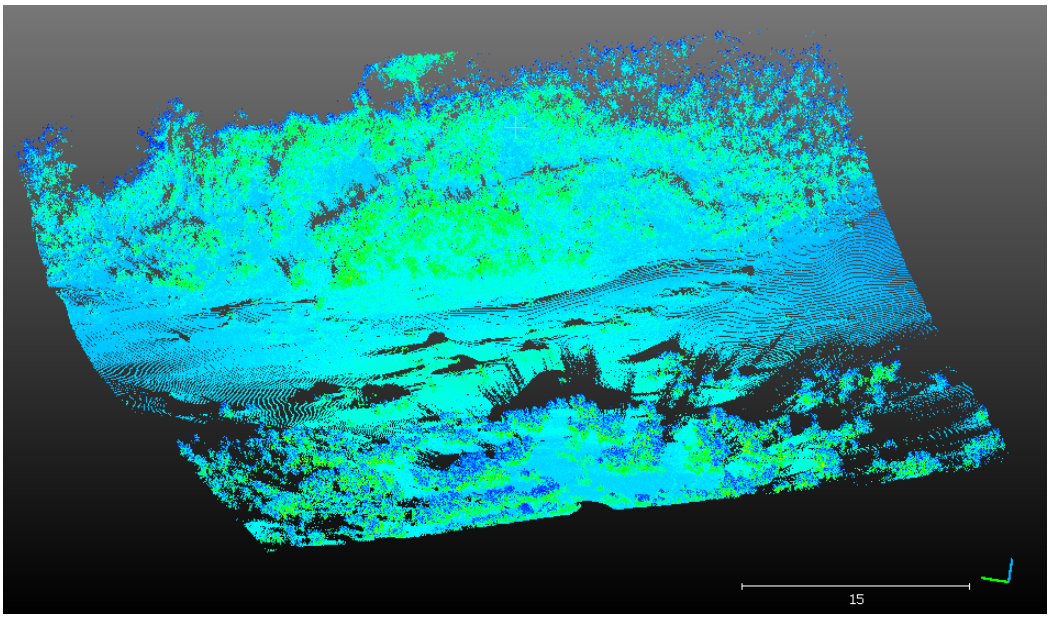

Figure 7.22 Subset of May 2012 point cloud from Inch on which initial vegetation classification tests were performed. Colours represent laser scanned intensity values, which correspond to the distribution shown in figure 7.23.

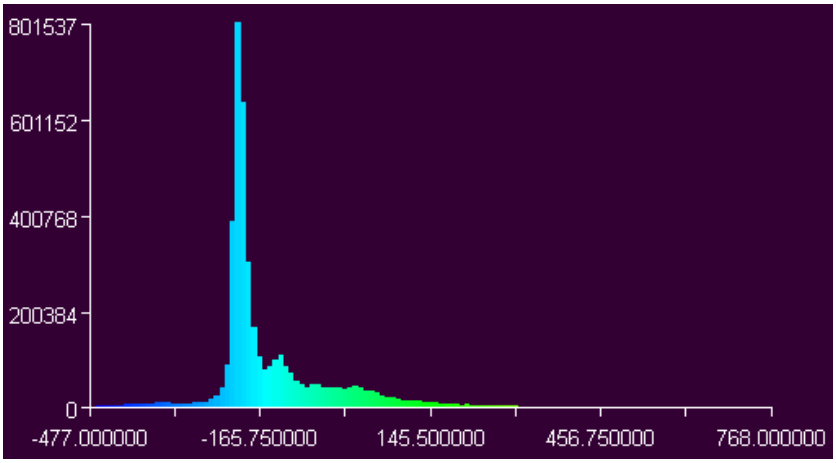

Figure 7.23 Laser scanned intensity distribution of cloud shown in figure 7.22. Intensity values (x axis) are based on the capabilities of the scanner and are scaled to a range of -2048 to +2048. Y axis represents frequency.

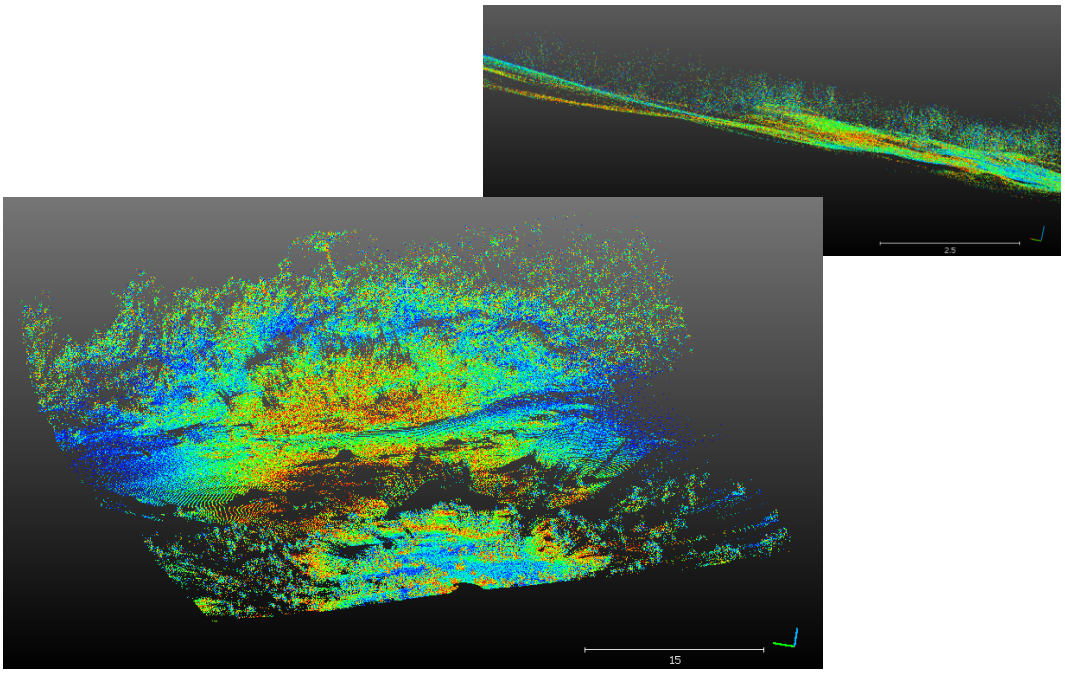

Figure 7.24 Result of filtering points with laser scanned intensity values outside -233 to -156 (light blue peak shown in fig. 7.23) from test patch. Close up of ground surface with multiple non-ground points shown top right.

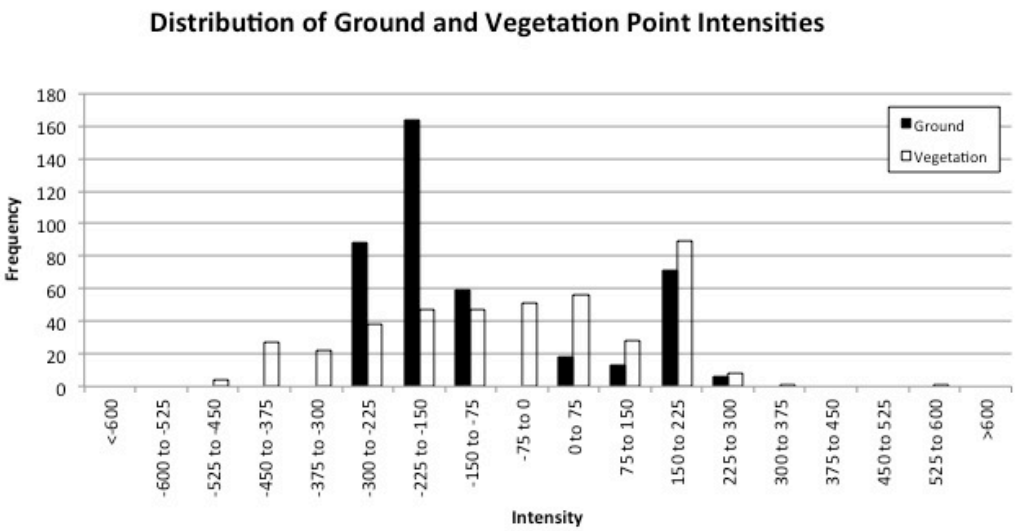

Figure 7.25 Histogram showing the distribution of manually sampled ground and vegetation point intensities.

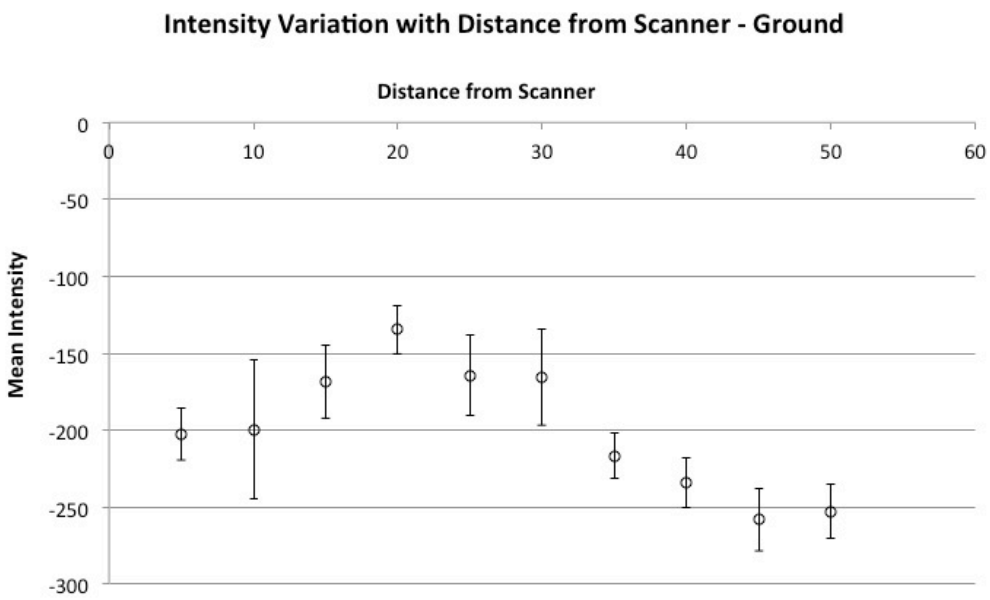

Figure 7.26 Mean intensity variation (and standard error bars) with distance from the scanner for 200 manually selected ground points plotted at 5 m intervals up to a distance of 50 m from the position of the scanner.

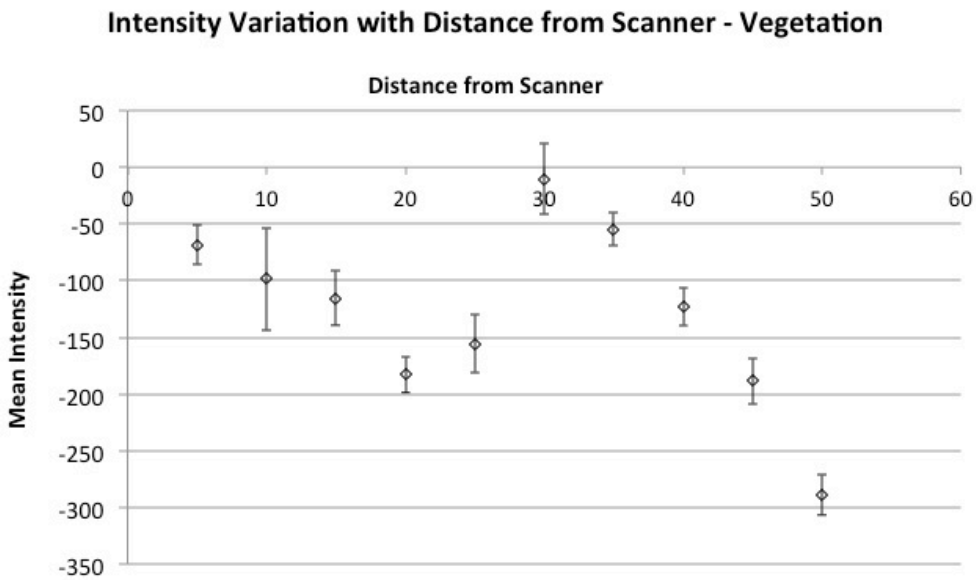

Figure 7.27 Mean intensity variation (and standard error bars) with distance from the scanner for 200 manually selected vegetation points plotted at 5 m intervals up to a distance of 50 m from the position of the scanner.

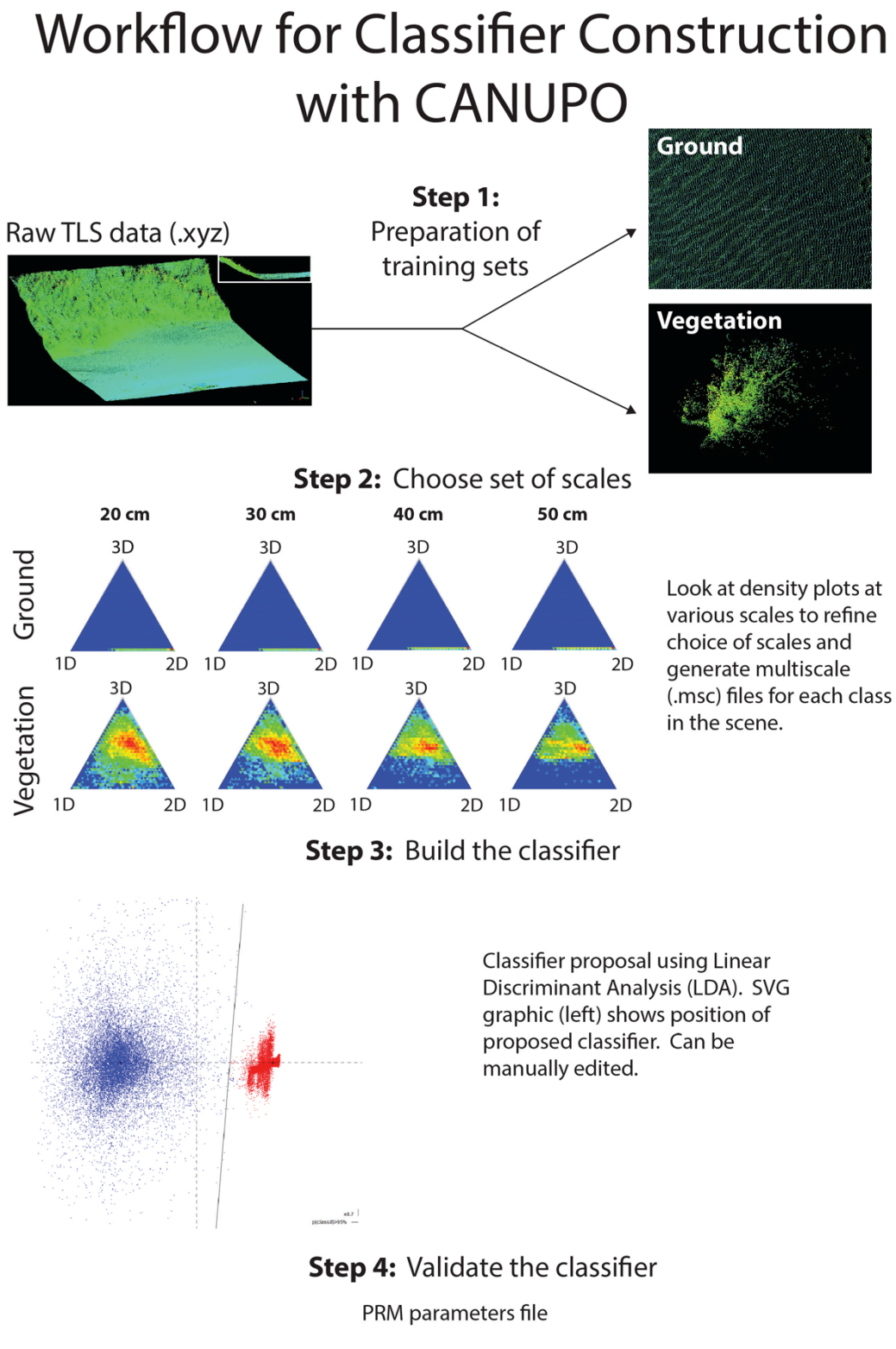

Figure 7.28 Workflow for classifier construction using CANPO. See text for explanation.

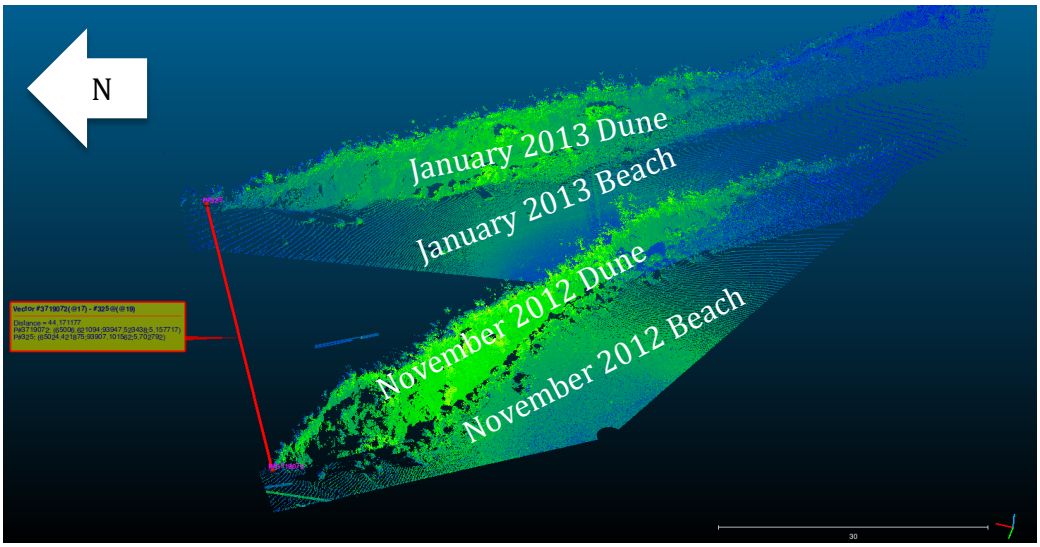

Figure 7.29 Foredune scarp and upper beach at Rossbehy in November 2012 and January 2013. The distance between the two points shown is 44 m.

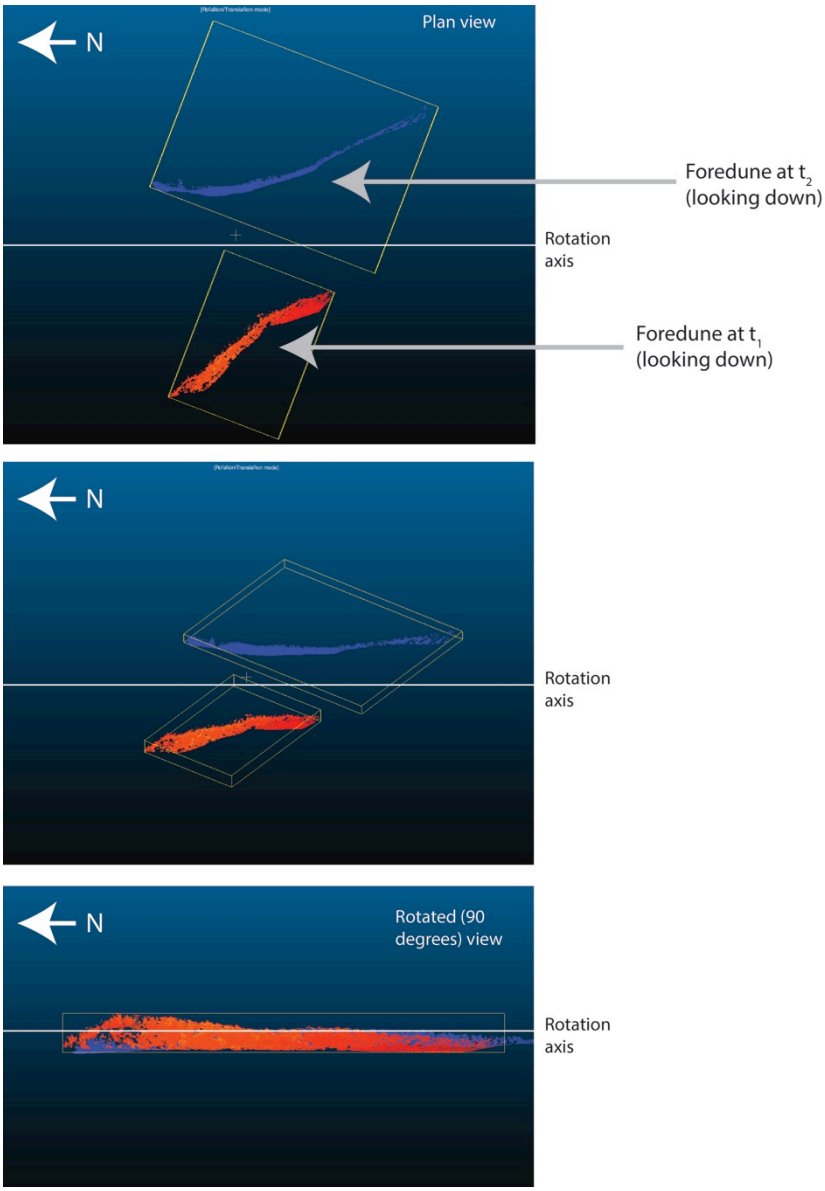

Figure 7.30 Graphic illustrating the process of coordinate system rotation for foredune point clouds at Rossbehy. In this example, two point clouds are shown, one captured at time t_1 (red) and another captured at a later date, t_2 (blue). These are shown in plan view – e.g. looking down from above (top). Using CloudCompare software, it is possible to rotate the clouds along a rotation axis using the rotate/translate tool. An oblique view of the clouds captured as they were being rotated is shown (middle). The clouds were rotated 90 degrees about this axis, such that their final orientation was as shown (bottom). This was performed for the foredune because few scans overlapped in plan view due to considerable foredune recession over the course of study period.

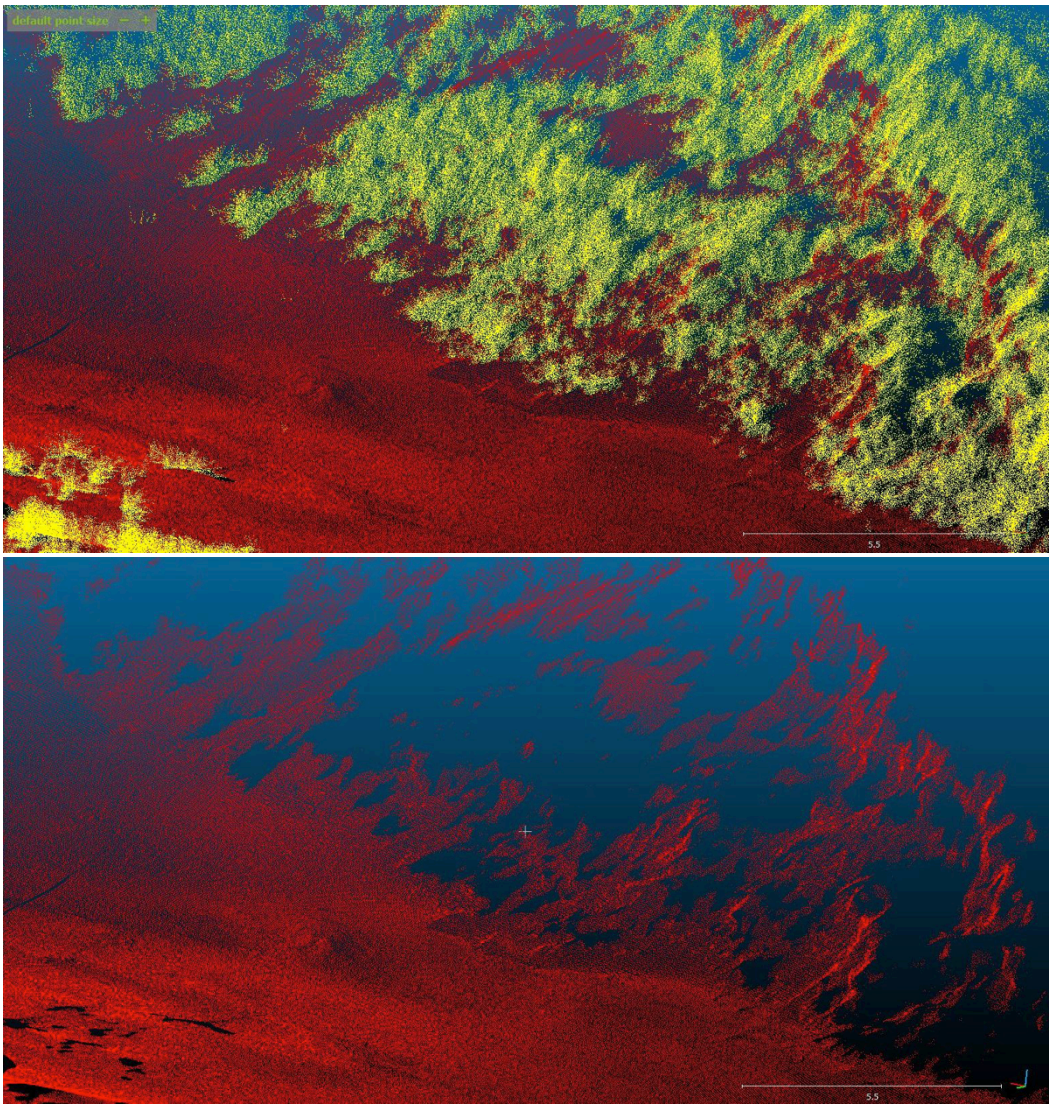

Figure 7.31 Example of classified (top) and filtered (bottom) cloud from May 2012 Inch dataset.

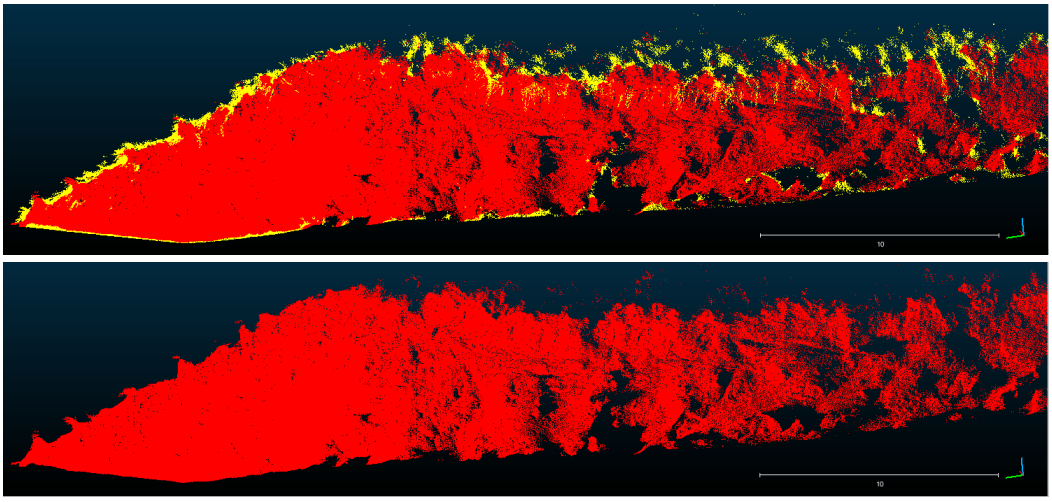

Figure 7.32 Example of classified (top) and filtered (bottom) cloud from Rossbehy foredune scarp (June 2012)

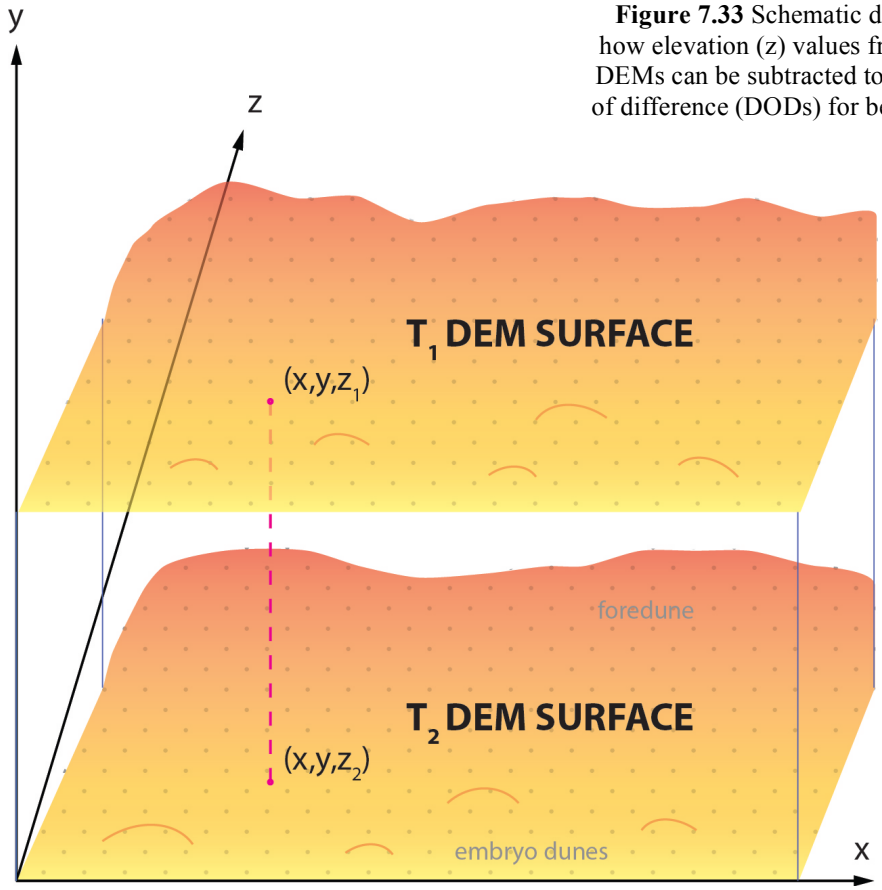

Figure 7.33 Schematic diagram showing how elevation (z) values from overlapping DEMs can be subtracted to produce DEMs of difference (DODs) for beach at Inch and Rossbehy.

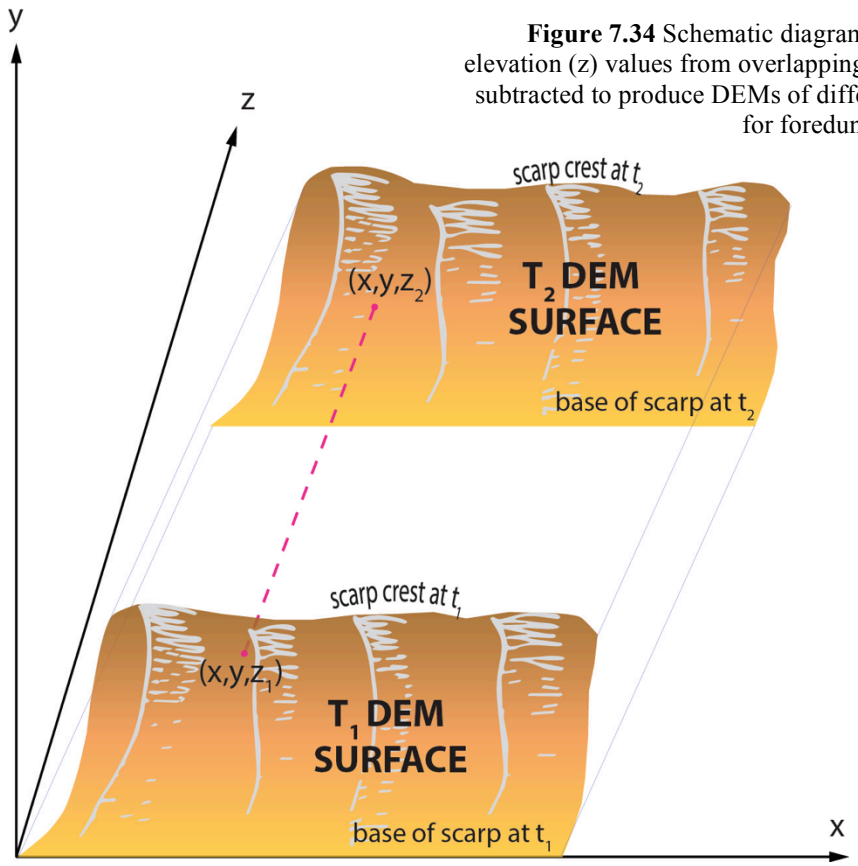

Figure 7.34 Schematic diagram showing how elevation (z) values from overlapping DEMs can be subtracted to produce DEMs of difference (DODs) for foredune at Rossbehy.

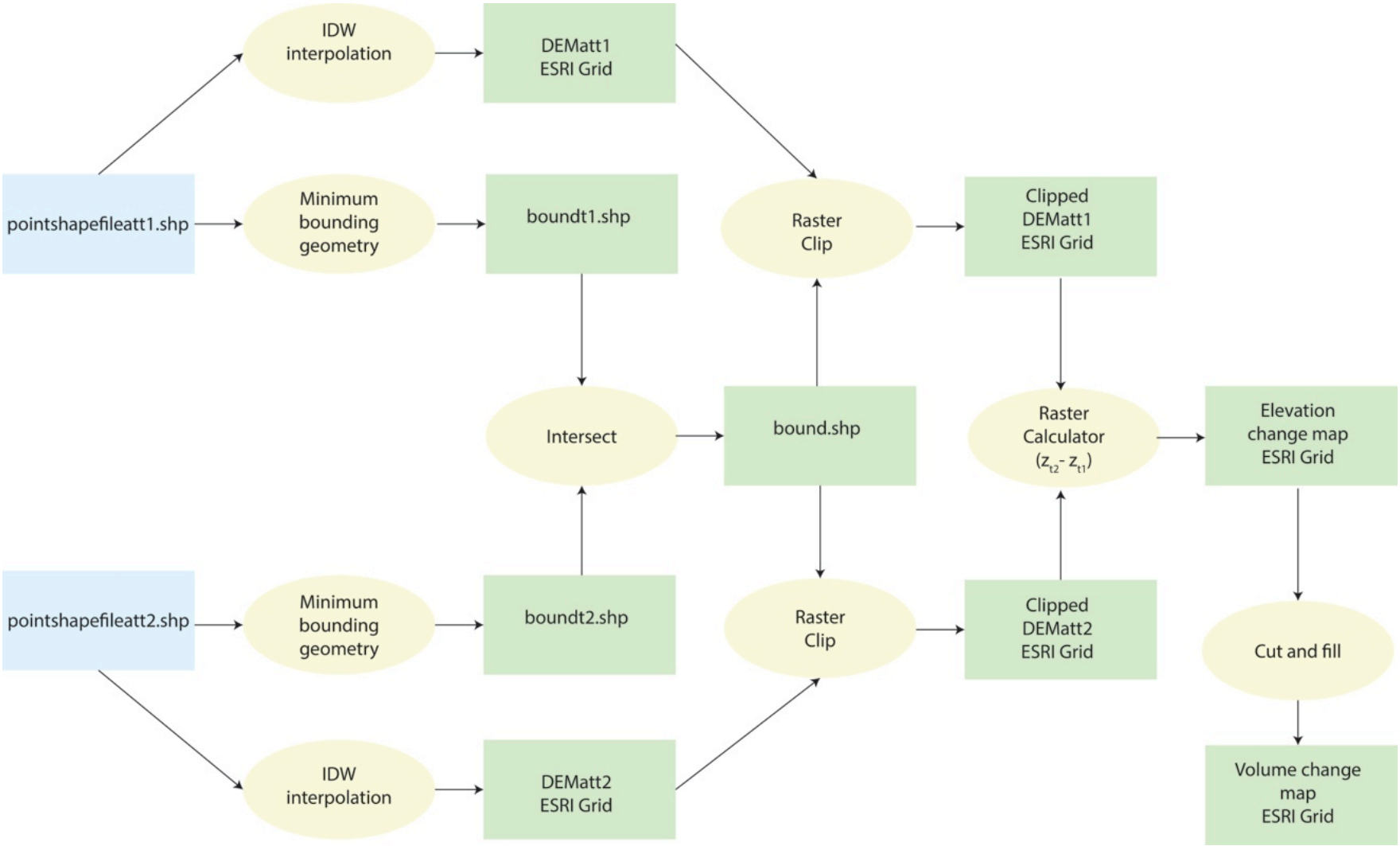

Figure 7.35 Cartographic model illustrating GIS workflow for generating elevation/distance change maps and volume change maps.

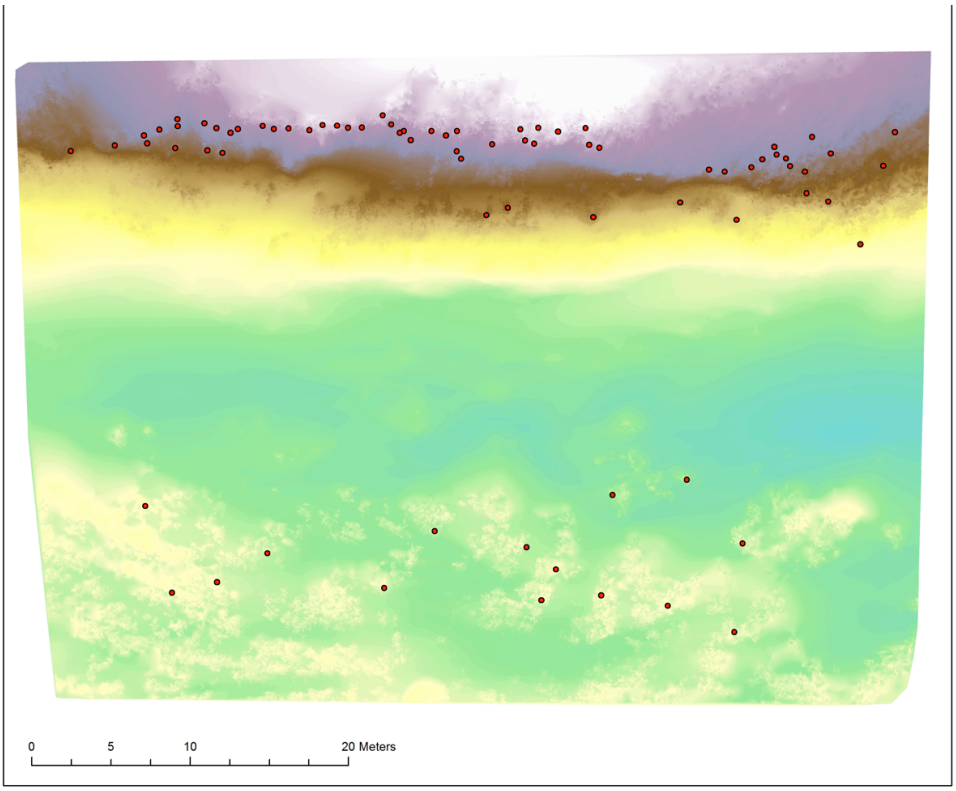

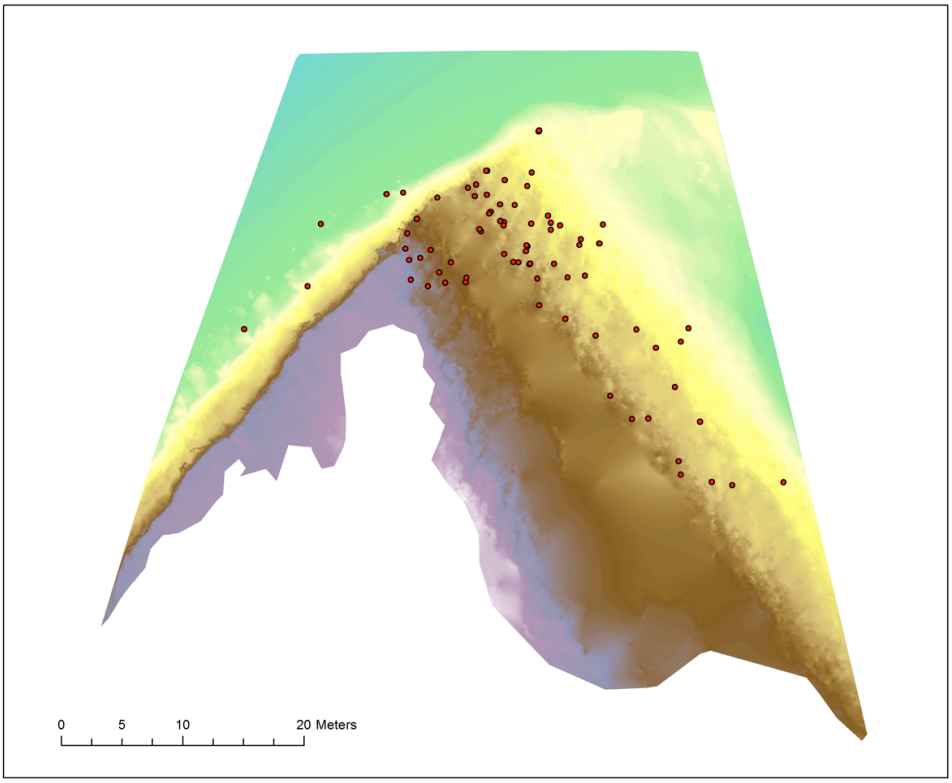

Figure 7.36 Distribution of February 2013 EDM ground truthing points (red) for Inch (top) and Rossbehy (bottom). Basemaps shown are natural neighbour interpolations of unfiltered TLS point clouds where green is low (flat beach) and purple/white is high (foredune crest).

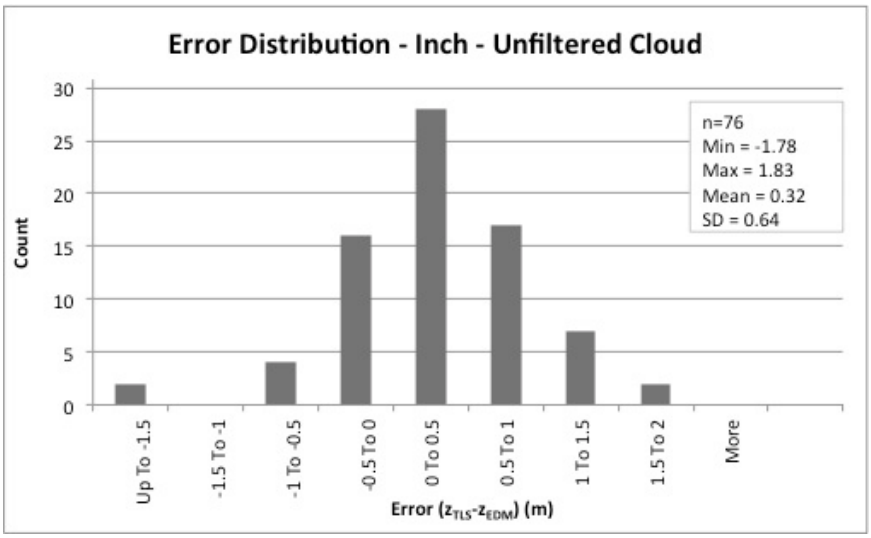

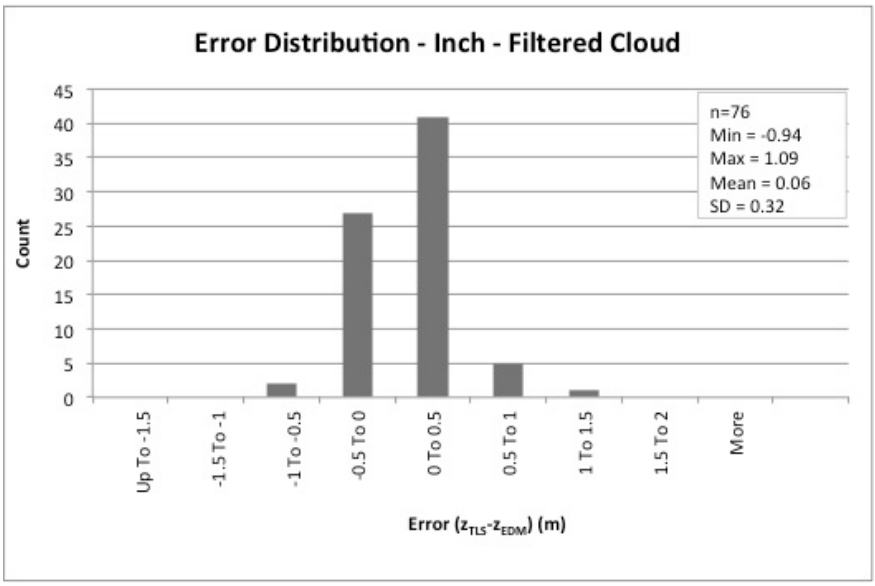

Figure 7.37 Error distribution for unfiltered (top) and filtered (bottom) clouds at Inch.

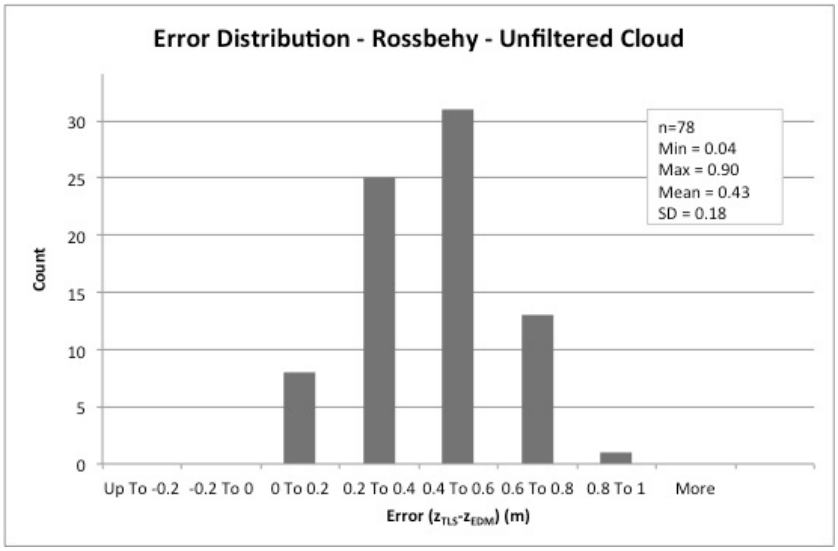

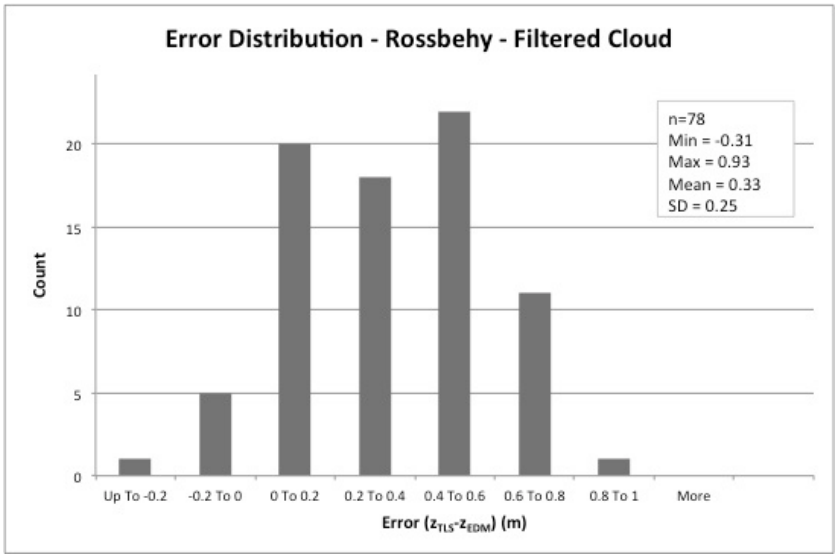

Figure 7.38 Error distribution for unfiltered (top) and filtered (bottom) clouds at Rossbehy.

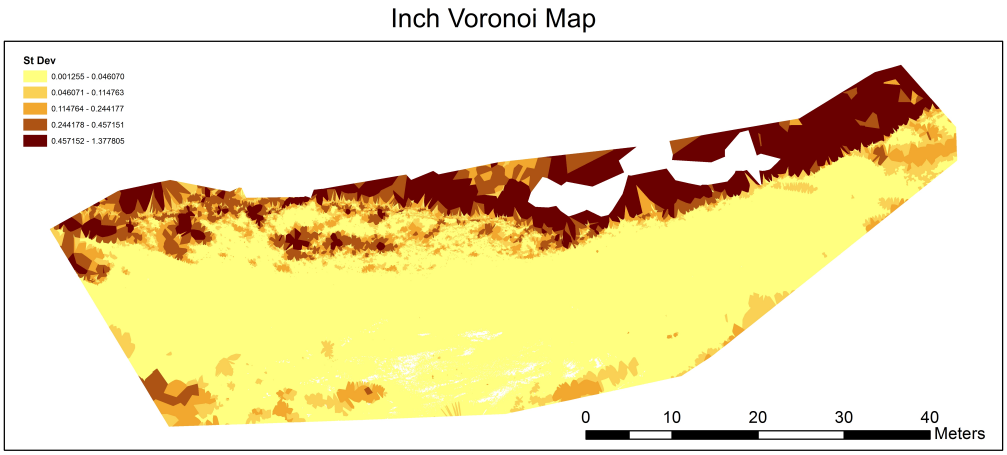

Figure 7.39 Voronoi map for Inch data symbolised by standard deviation. The pattern shown suggests the data is non-stationary. As a result, kriging was deemed an inappropriate interpolation method for this data.

	NN	**IDW**	**EBK**
Unfiltered	0.537 mm	0.539 m	0.540 m
Filtered	0.183 m	-0.037 m	0.147 m
	t(76)=15.536, p<0.001	t(76)=14.801, p<0.001	t(76)=13.952, p<0.001

Table 7.3 Residual errors for February 2013 Inch DEMs generated using unfiltered and filtered TLS point clouds and interpolated using NN, IDW, and EBK. Results of paired t-test demonstrating significant differences between unfiltered and filtered clouds also shown.

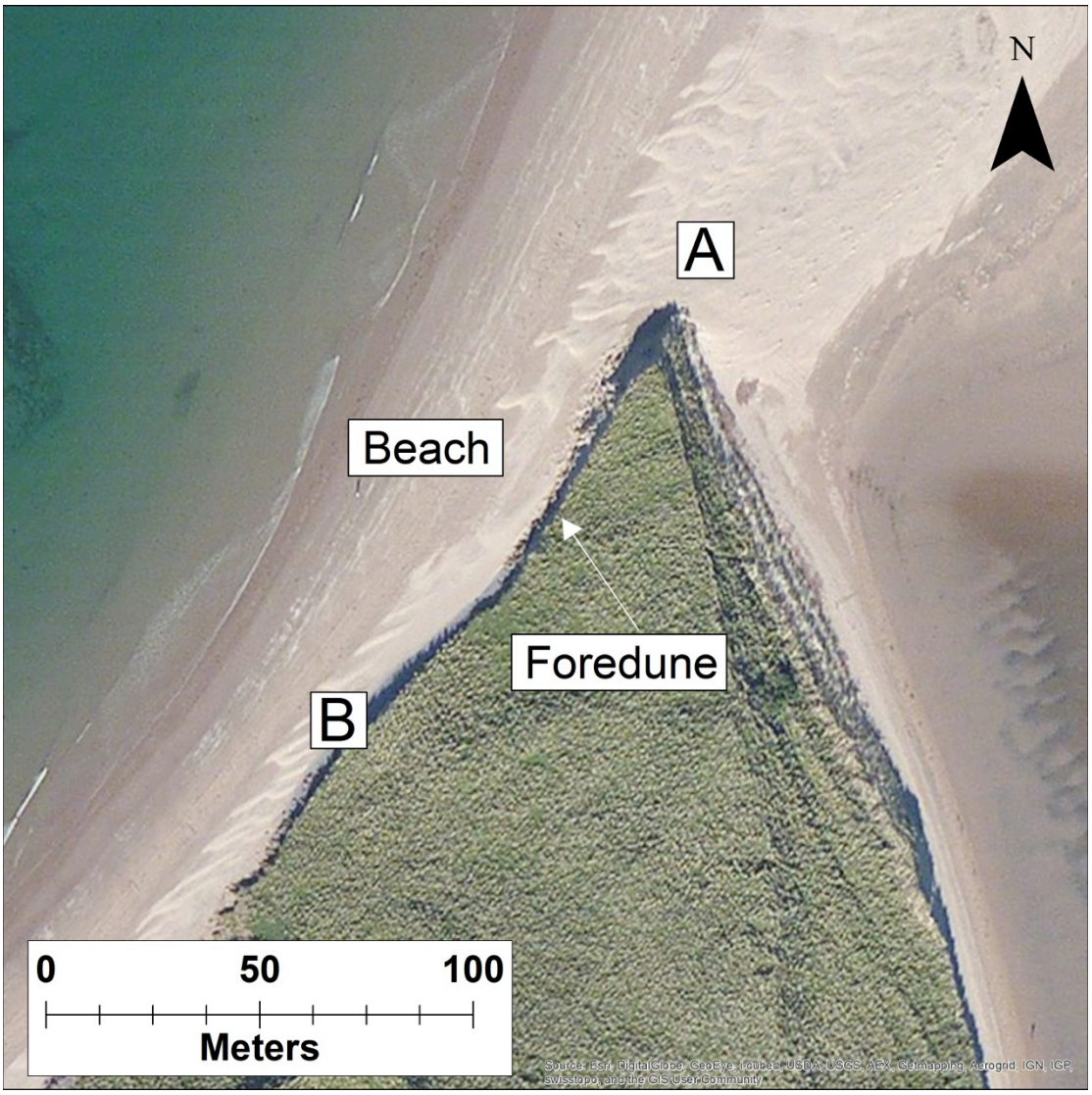

Figure 7.40 Areal photograph of Rossbehy field site indicating general location of TLS surveys. Locations A and B correspond generally to the maps shown in figures 7.41 to 7.58 and represent the dune barrier terminus (A) and the southern periphery of the surveyed area (B) at the time of the corresponding survey. Source of areal photography: ESRI

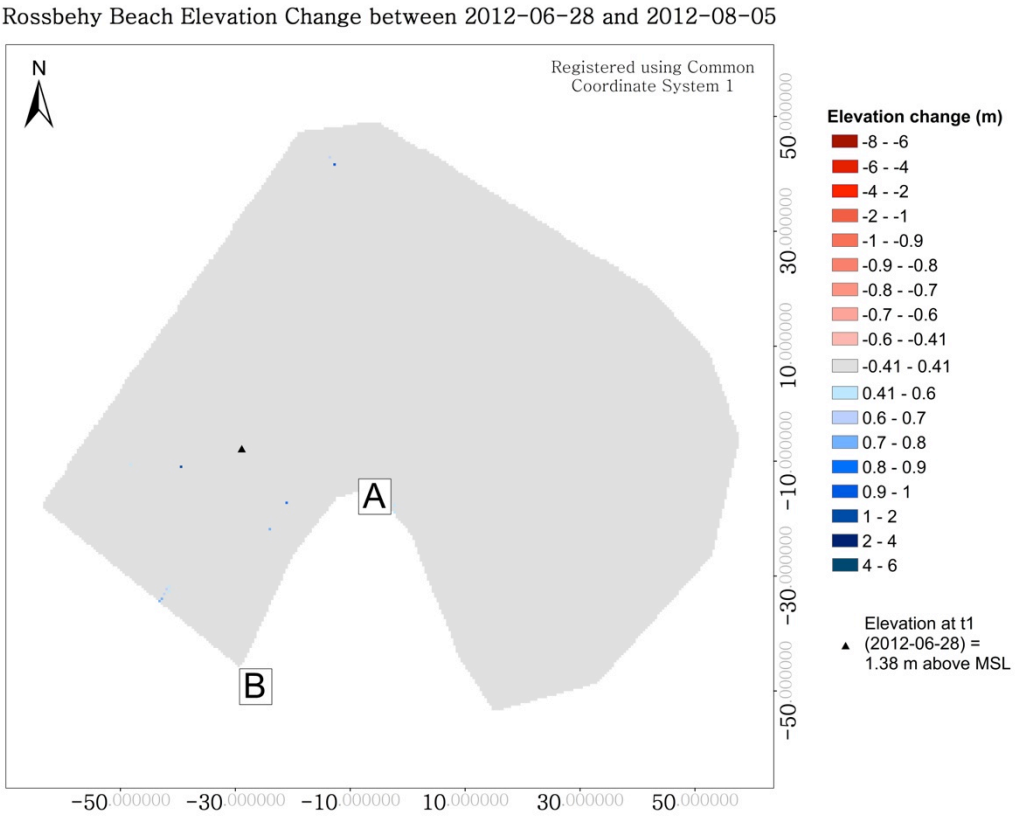

Figure 7.41 Rossbehy beach elevation change (DOD) between 2012-06-28 and 2012-08-05. Elevation change across the majority of the surveyed area lies below the level of detectable change (±0.41 m) and ranged from -0.27 m to +1.08 m. Locations A and B correspond with those shown in figure 7.42. The coordinate marked with the triangle is at the same location as that shown in figure 7.43 (the DOD for the subsequent survey period) for reference. Mean sea level (MSL) is equal to +2.3 m ODM.

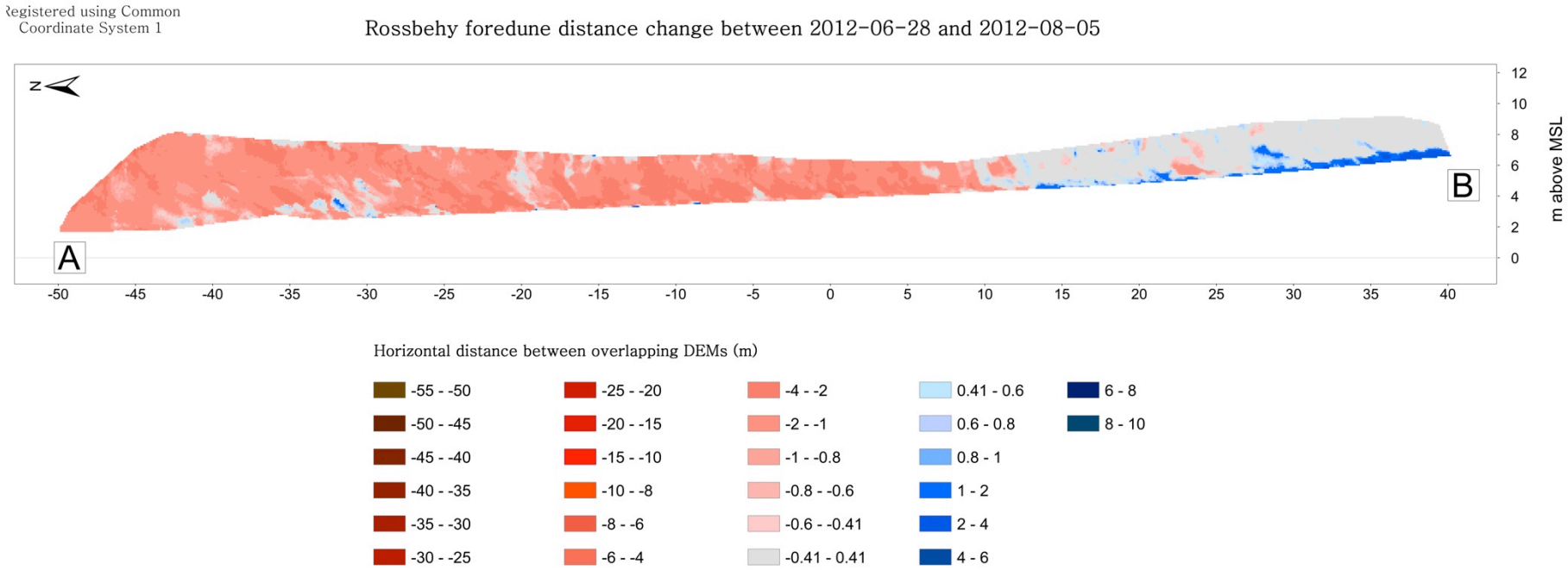

Figure 7.42 Rossbehy foredune distance change between 2012-06-28 and 2012-08-05. Dune recession is shown in varying shades of red and advance in varying shades of blue. Distance change below the level of detectable change (±0.41 m) is shown in gray. Distance change across the surveyed area ranged from -5.74 m to +4.20 m. Locations A and B correspond with those shown in figure 7.41. Mean sea level (MSL) is equal to +2.3 m ODM.

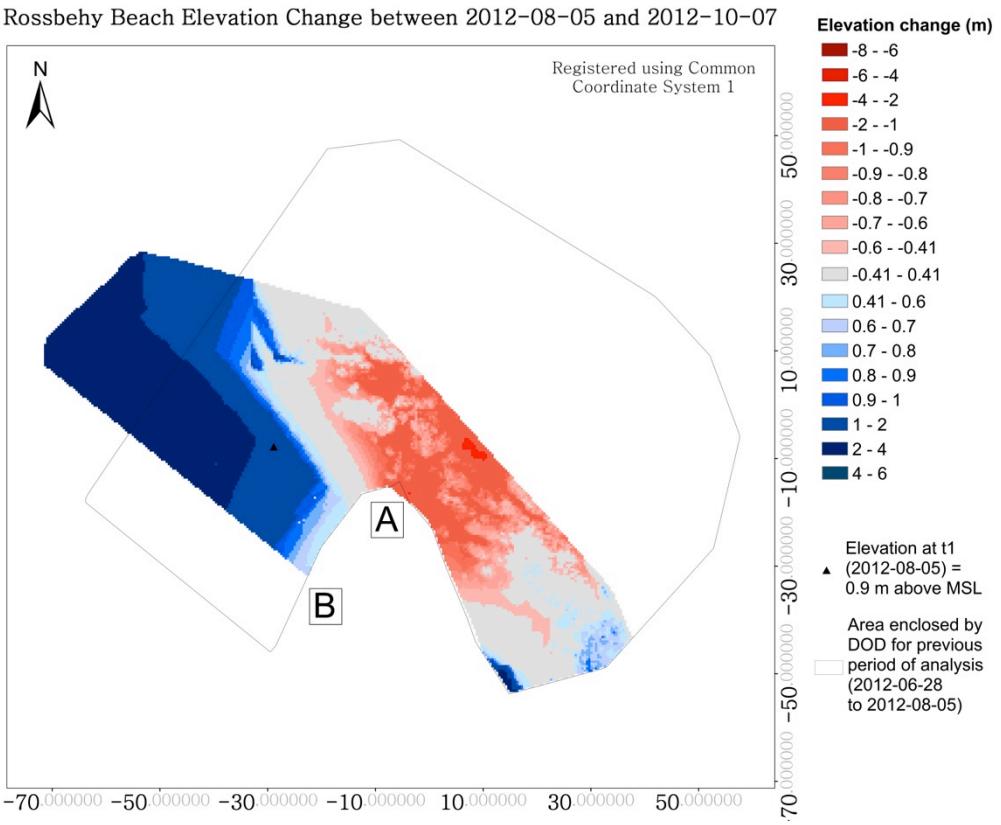

Figure 7.43 Rossbehy beach elevation change (DOD) between 2012-08-05 and 2012-10-07. Beach erosion is shown in red, while accretion is shown in blue. Elevation changes below the level of detectable change (±0.41 m) are shown in gray. Elevation change ranged from -2.15 m to +5.49 m. The coordinate marked with the triangle is at the same location as that shown in figure 7.41 (the DOD for the previous period) for reference. Locations A and B correspond (in a general way) with those shown in figure 7.40. Mean sea level (MSL) is equal to +2.3 m ODM.

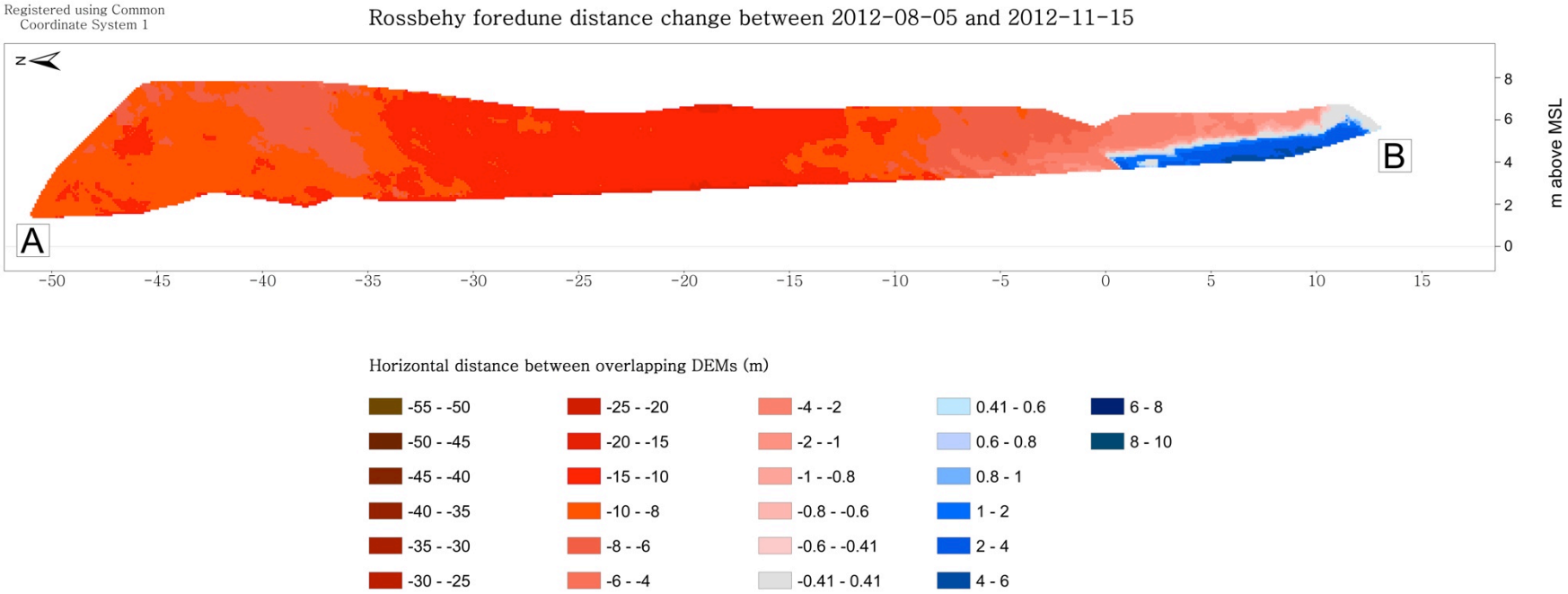

Figure 7.44 Rossbehy foredune distance change between 2012-08-05 and 2012-11-15. Dune recession is shown in varying shades of red and advance in varying shades of blue. Distance change below the level of detectable change (±0.41 m) is shown in gray. Distance change across the surveyed area ranged from -18.28 m to +5.05 m. For reference, locations A and B correspond (in a general way) with those shown in figure 7.40. Mean sea level (MSL) is equal to +2.3 m ODM.

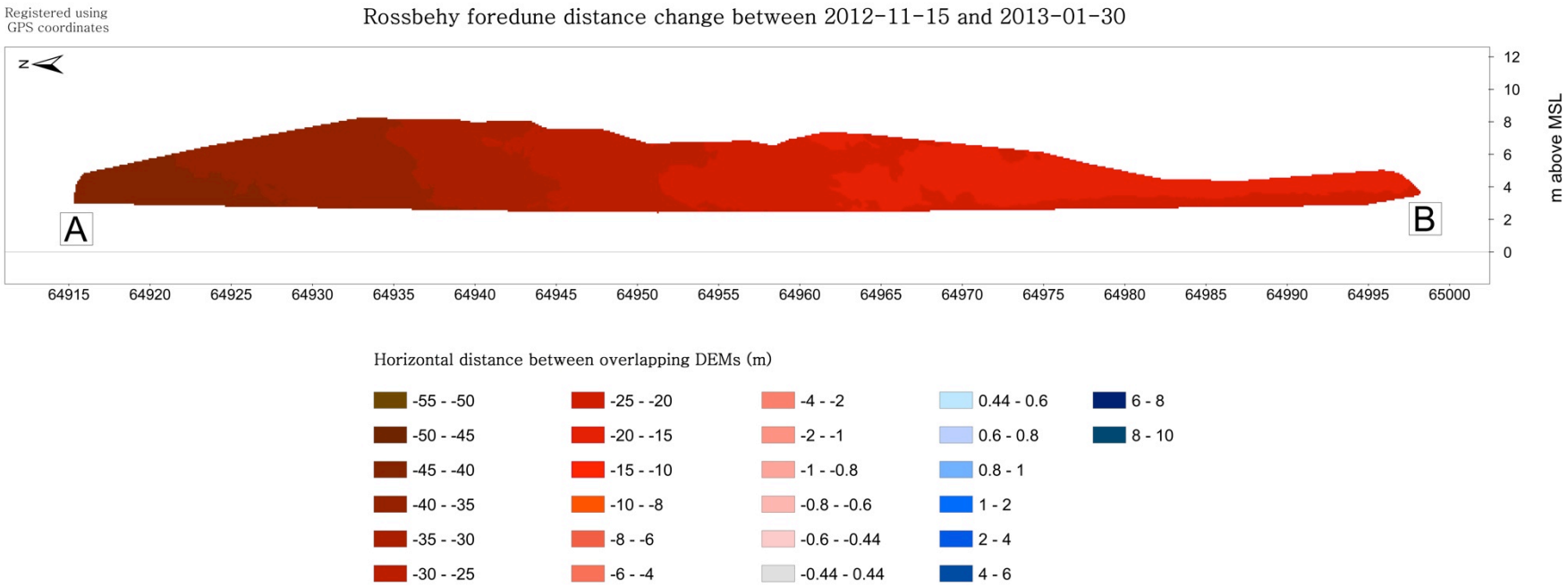

Figure 7.45 Rossbehy foredune distance change between 2012-11-15 and 2013-01-30. Dune recession is shown in varying shades of red. Distance change across the surveyed area ranged from -16.95 m to -44.97 m. For reference, locations A and B correspond (in a general way) with those shown in figure 7.40. Mean sea level (MSL) is equal to +2.3 m ODM.

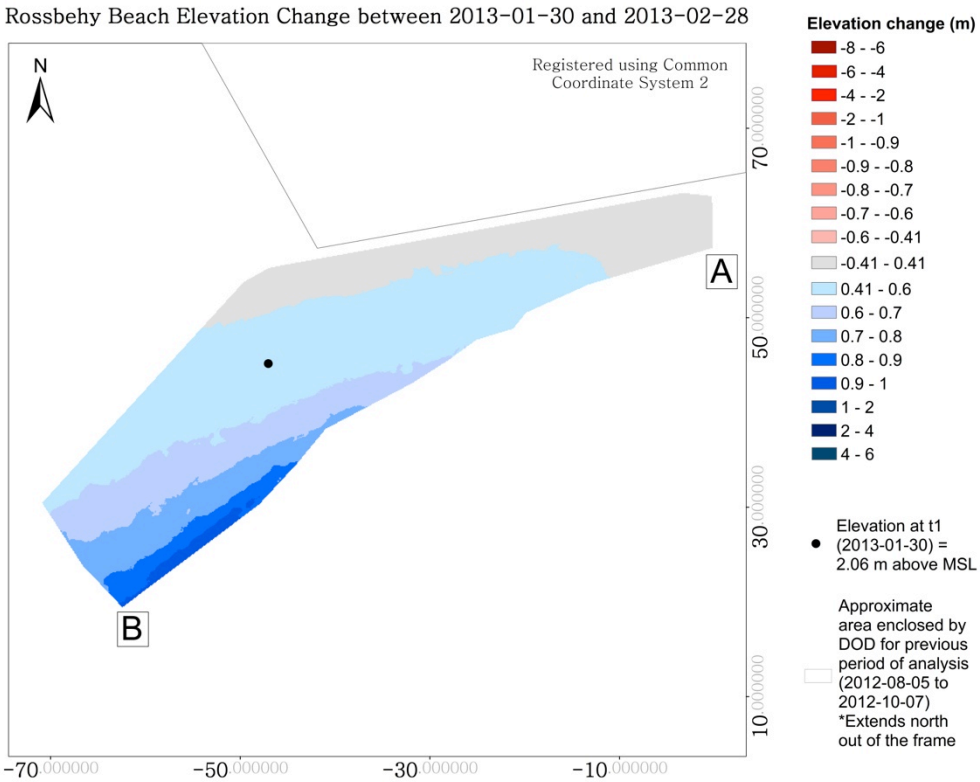

Figure 7.46 Rossbehy beach elevation change (DOD) between 2013-01-30 and 2013-02-28. Accretion occurred across the majority of the surveyed area (varying shades of blue). Area in gray lies below the level of detectable change (±0.41 m). Elevation change ranged from +0.18 m to +0.99 m. Locations A and B correspond with those shown in figure 7.47. The coordinate marked with the circle is at the same location as that shown in figures 7.48, 7.50, and 7.52 (the DODs for the subsequent survey periods) for reference. Mean sea level (MSL) is equal to +2.3 m ODM.

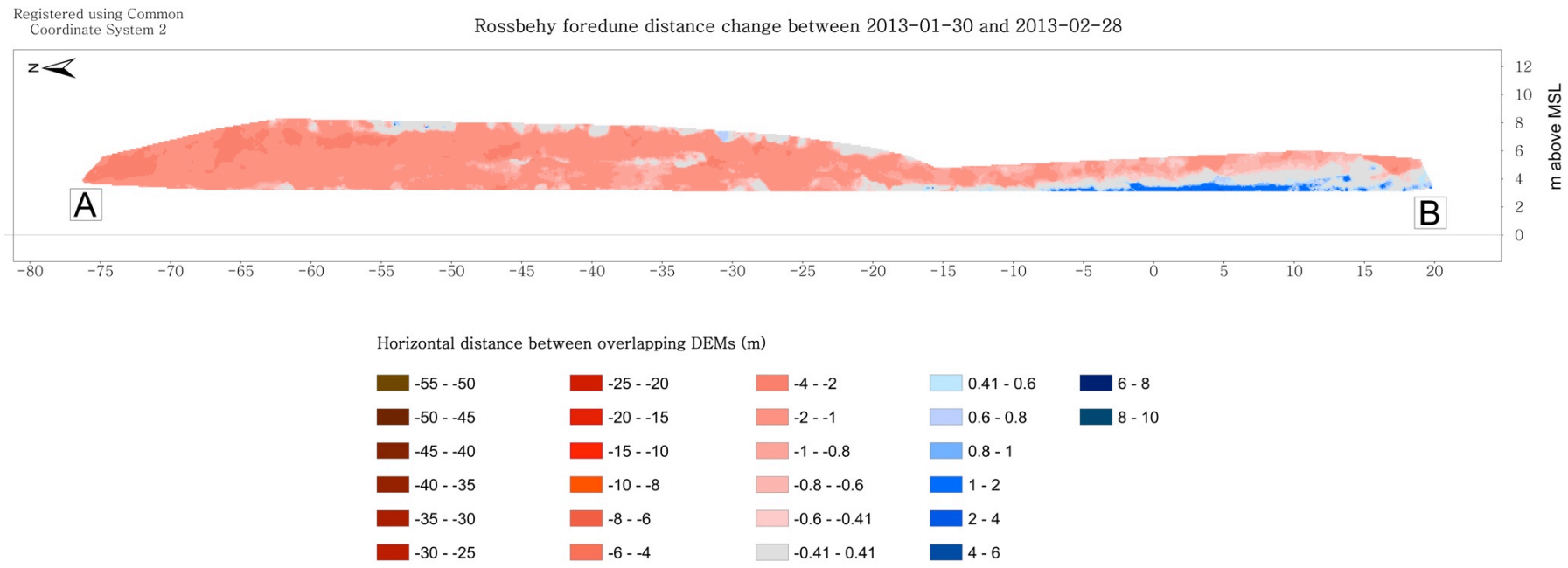

Figure 7.47 Rossbehy foredune distance change between 2013-01-30 and 2013-02-28. Dune recession is shown in varying shades of red and advance in varying shades of blue. Distance change below the level of detectable change (±0.41 m) is shown in gray. Distance change across the surveyed area ranged from -2.80 m to +2.34 m. For reference, locations A and B correspond with those shown in figure 7.46. Mean sea level (MSL) is equal to +2.3 m ODM.

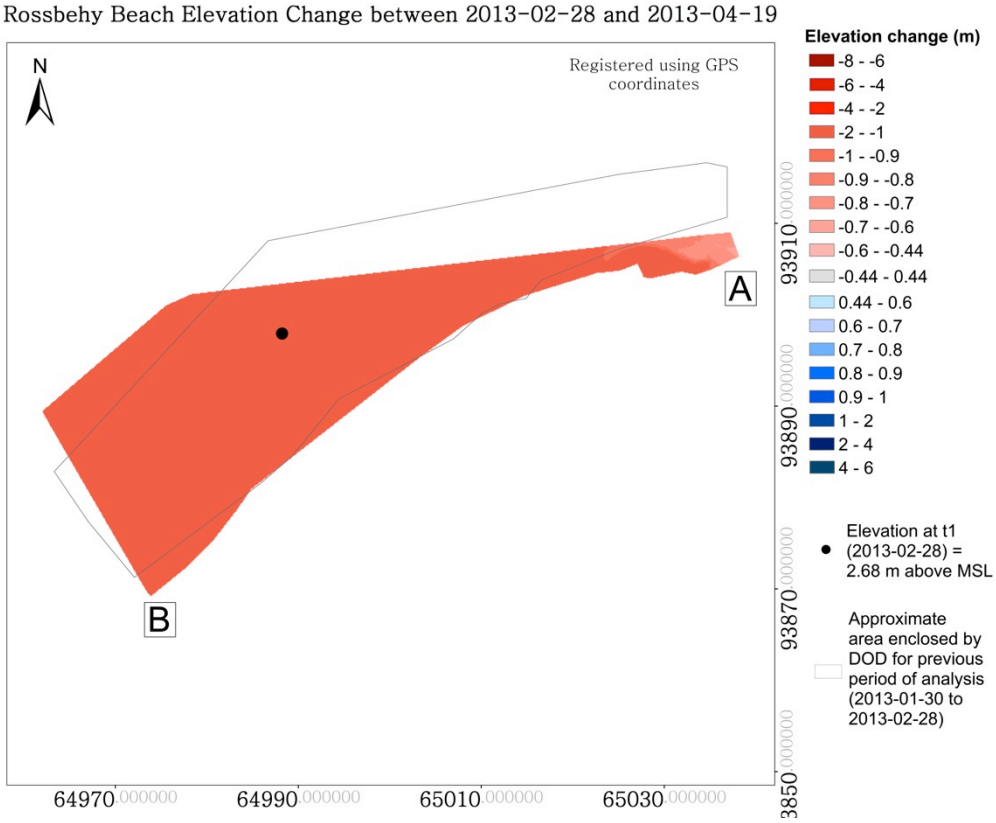

Figure 7.48 Rossbehy beach elevation change (DOD) between 2013-02-28 and 2013-04-19. Beach erosion occurred across the entire survey area (varying shades of red). Beach elevation change ranged from -1.94 m to -0.62 m. Locations A and B correspond with those shown in figure 7.49. The coordinate marked with the circle is at the same location as that shown in figures 7.46, 7.50, and 7.52 (the DODs for the previous and subsequent survey periods) for reference. Mean sea level (MSL) is equal to +2.3 m ODM.

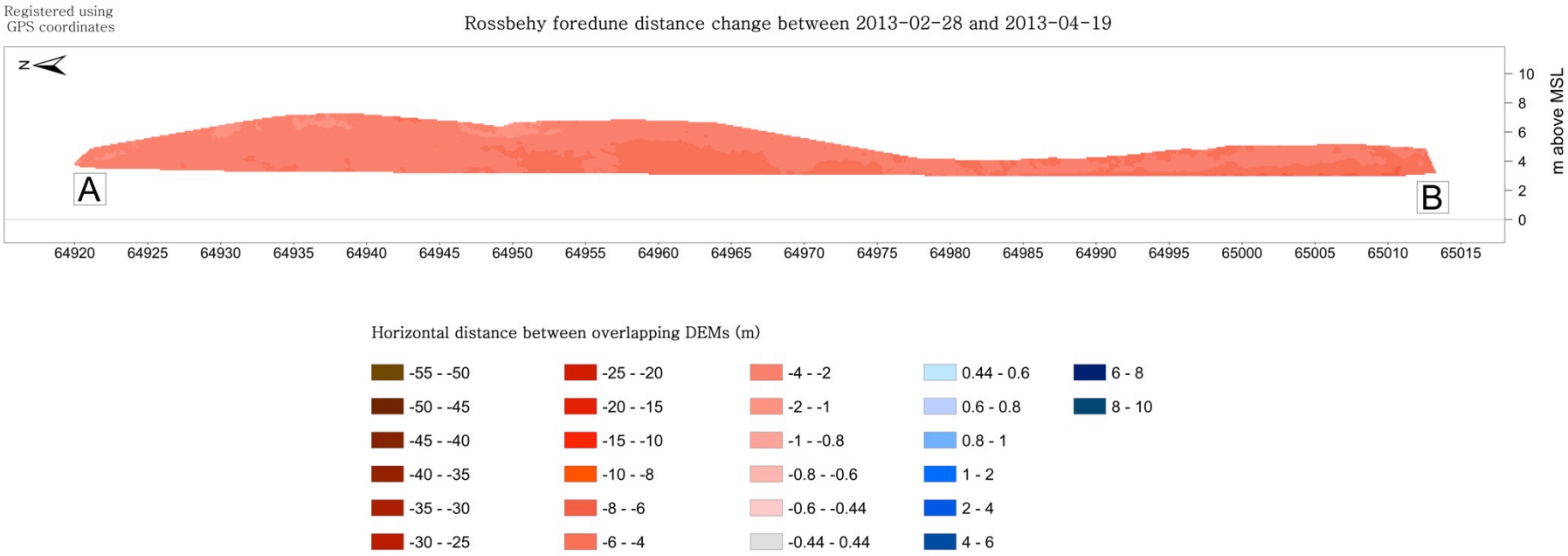

Figure 7.49 Rossbehy foredune distance change between 2013-02-28 and 2013-04-19. Dune recession, which occurred across the entire length of the surveyed area, is shown in varying shades of red. Distance change ranged from -1.39 m to -6.40 m. For reference, locations A and B correspond with those shown in figure 7.48. Mean sea level (MSL) is equal to +2.3 m ODM.

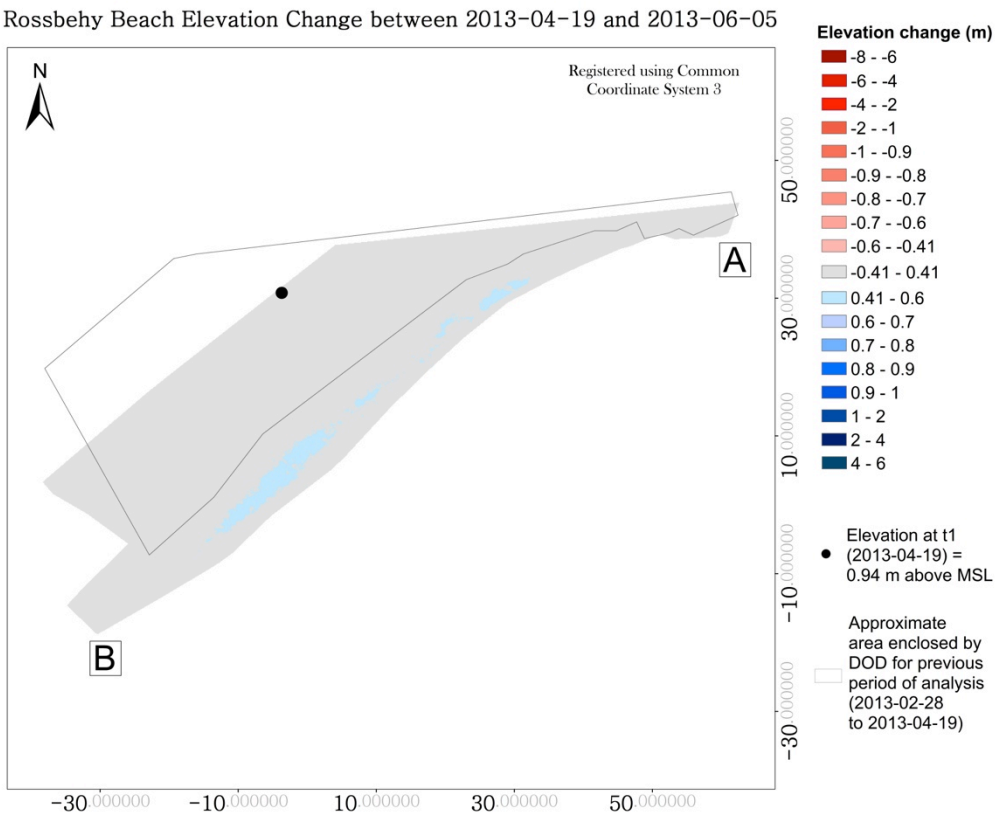

Figure 7.50 Rossbehy beach elevation change (DOD) between 2013-04-19 and 2013-06-05. Elevation change across the majority of the site lies below the level of detectable change (±0.41 m) and ranges from -0.17 m to +0.51 m. Locations A and B correspond with those shown in figure 7.51. The coordinate marked with the circle is at the same location as that shown in figures 7.46, 7.48, and 7.52 (the DODs for the previous and subsequent survey periods) for reference. Mean sea level (MSL) is equal to +2.3 m ODM.

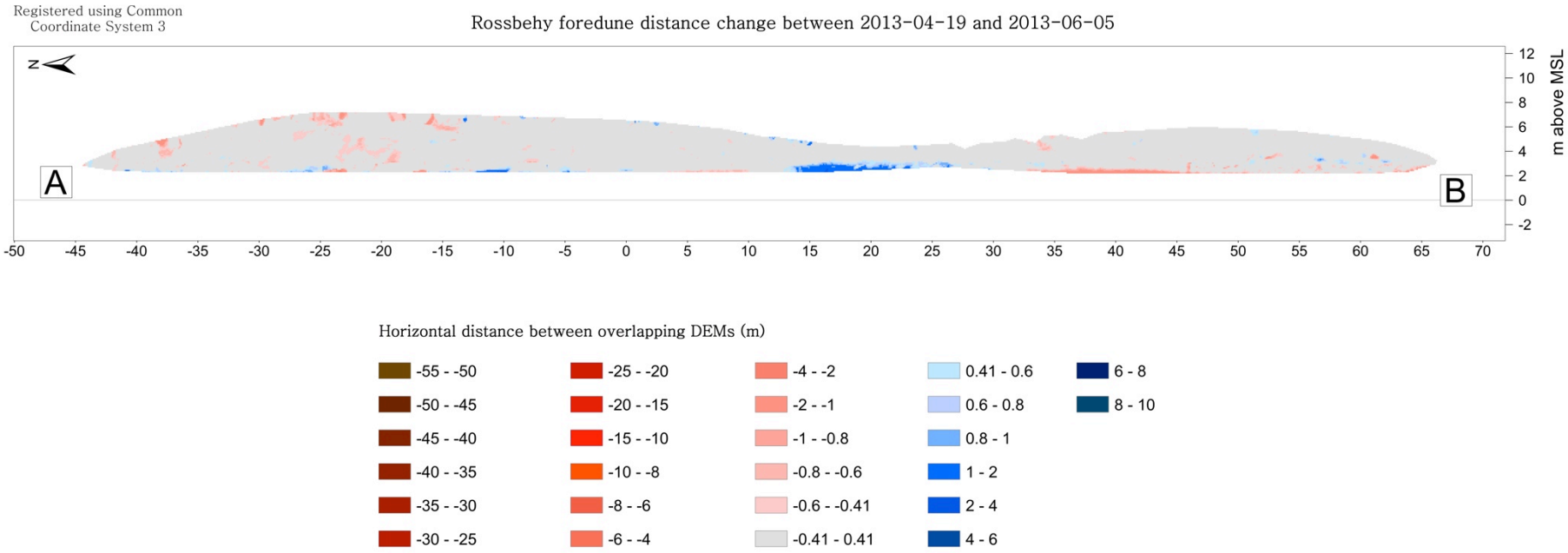

Figure 7.51 Rossbehy foredune distance change between 2013-04-19 and 2013-06-05. Distance change across the majority of the surveyed area lies below the level of detectable change (±0.41 m) and ranges from -2.16 m to +2.34 m. For reference, locations A and B correspond with those shown in figure 7.50. Mean sea level (MSL) is equal to +2.3 m ODM.

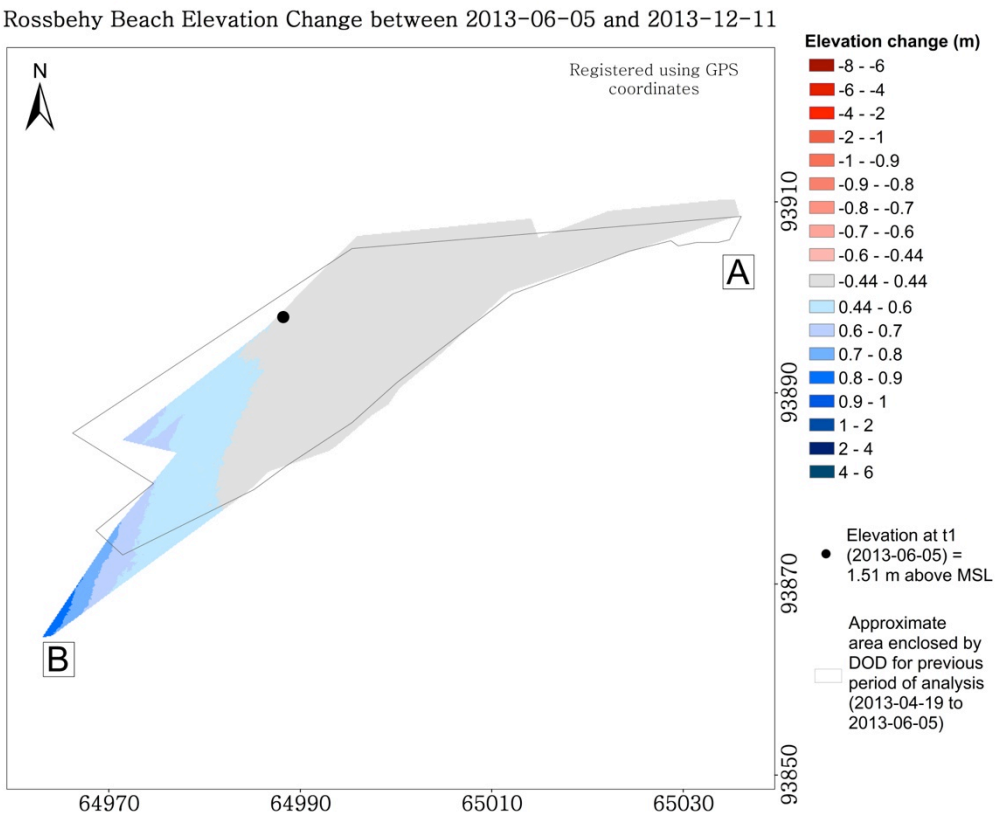

Figure 7.52 Rossbehy beach elevation change (DOD) between 2013-06-05 and 2013-12-11. Elevation change across the majority of the site lies below the level of detectable change (±0.44 m) and ranges from -0.13 m and +0.88 m. Locations A and B correspond with those shown in figure 7.53. The coordinate marked with the circle is at the same location as that shown in figures 7.46, 7.48, and 7.50 (the DODs for the previous survey periods) for reference. Mean sea level (MSL) is equal to +2.3 m ODM.

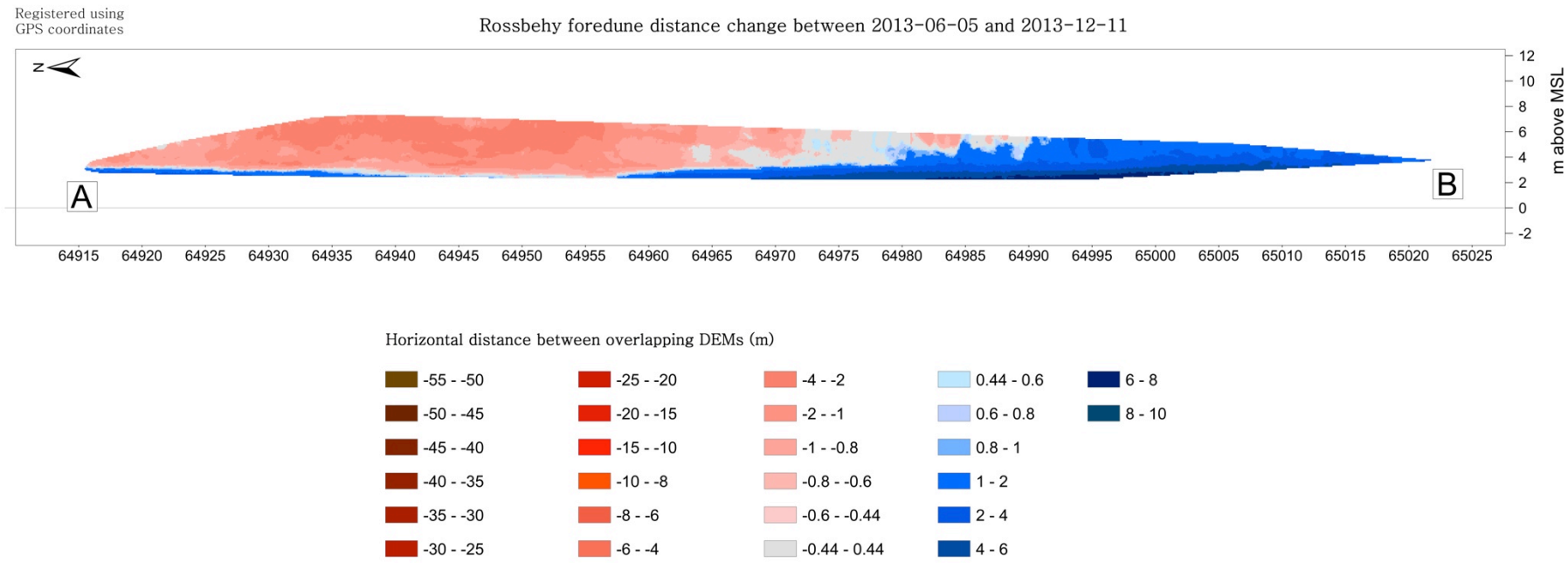

Figure 7.53 Rossbehy foredune distance change between 2013-06-05 and 2013-12-11. Dune recession is shown in varying shades of red and advance in varying shades of blue. Distance change below the level of detectable change (±0.44 m) is shown in gray. Distance change across the surveyed area ranged from -3.62 m to +7.15 m. For reference, locations A and B correspond with those shown in figure 7.52. Mean sea level (MSL) is equal to +2.3 m ODM.

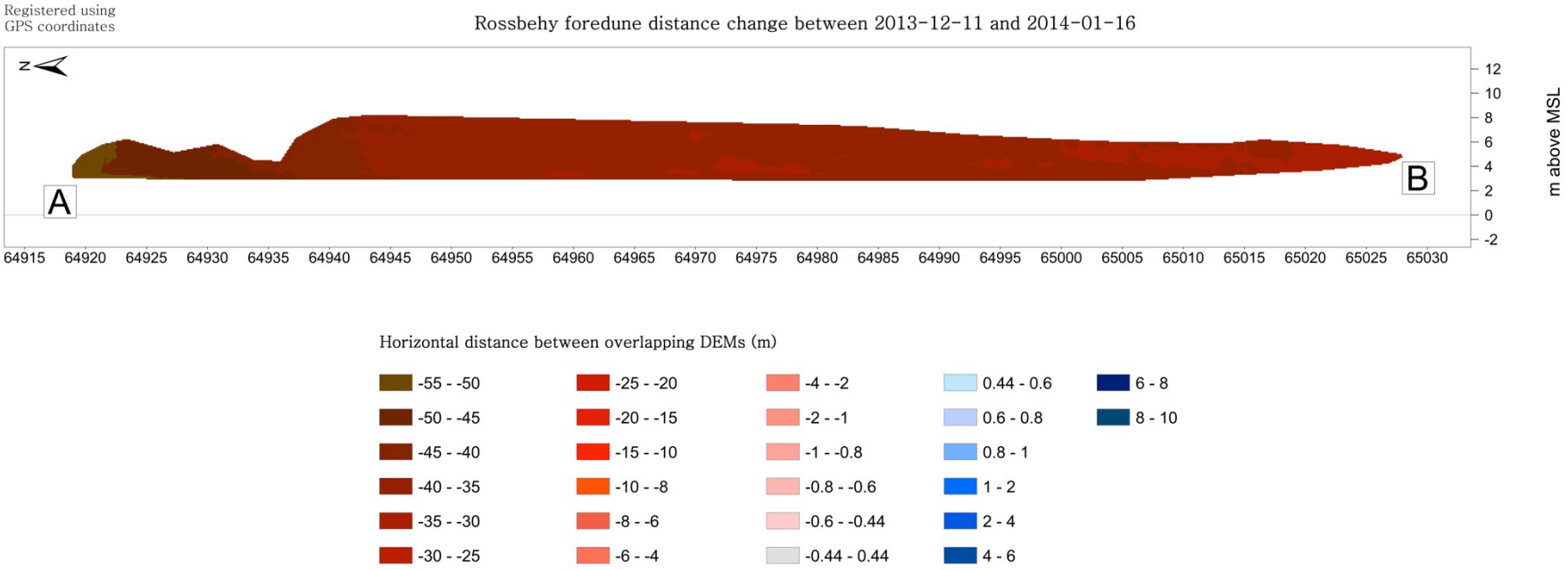

Figure 7.54 Rossbehy foredune distance change between 2013-12-11 and 2014-01-16. Dune recession, which occurred across the entire length of the surveyed area, is shown in varying shades of red. Distance change ranged from -54.33 m to -33.06 m. For reference, locations A and B correspond (in a general way) with those shown in figure 7.40. Mean sea level (MSL) is equal to +2.3 m ODM.

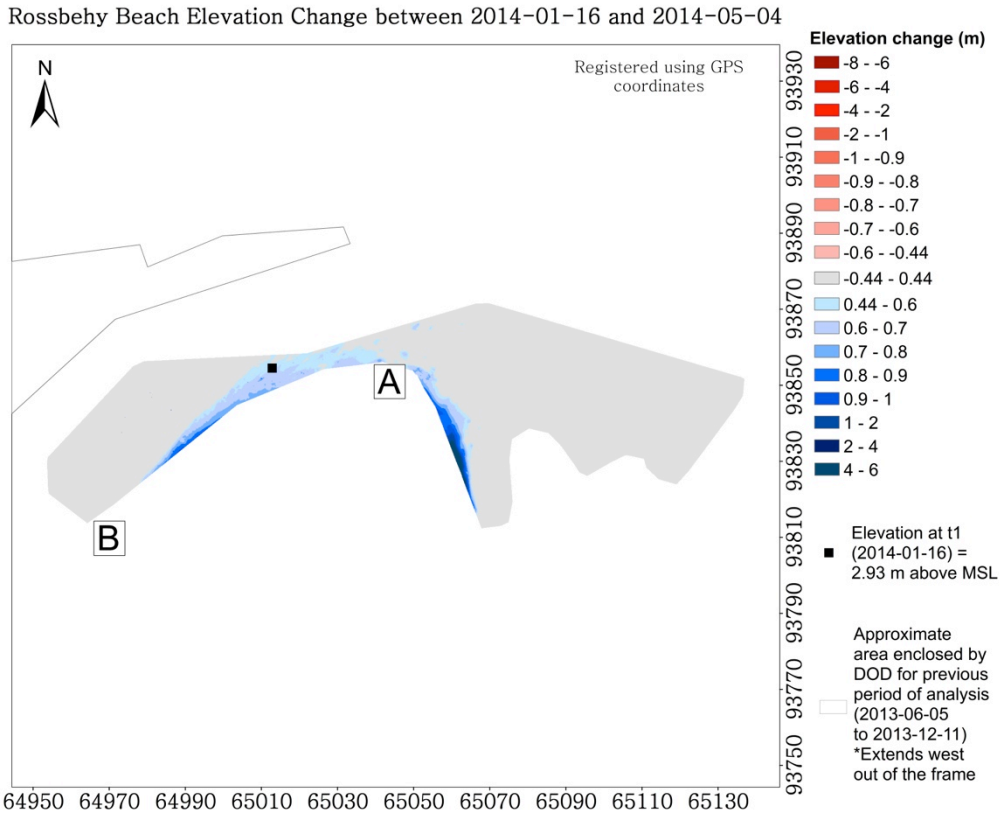

Figure 7.55 Rossbehy beach elevation change (DOD) between 2014-06-16 and 2014-05-04. Elevation change across the majority of the site lies below the level of detectable change (±0.44 m) and ranges from -0.42 m to +1.42 m. Locations A and B correspond with those shown in figure 7.56. The coordinate marked with the square is at the same location as that shown in figure 7.57 (the DOD for the subsequent survey period) for reference. Mean sea level (MSL) is equal to +2.3 m ODM.

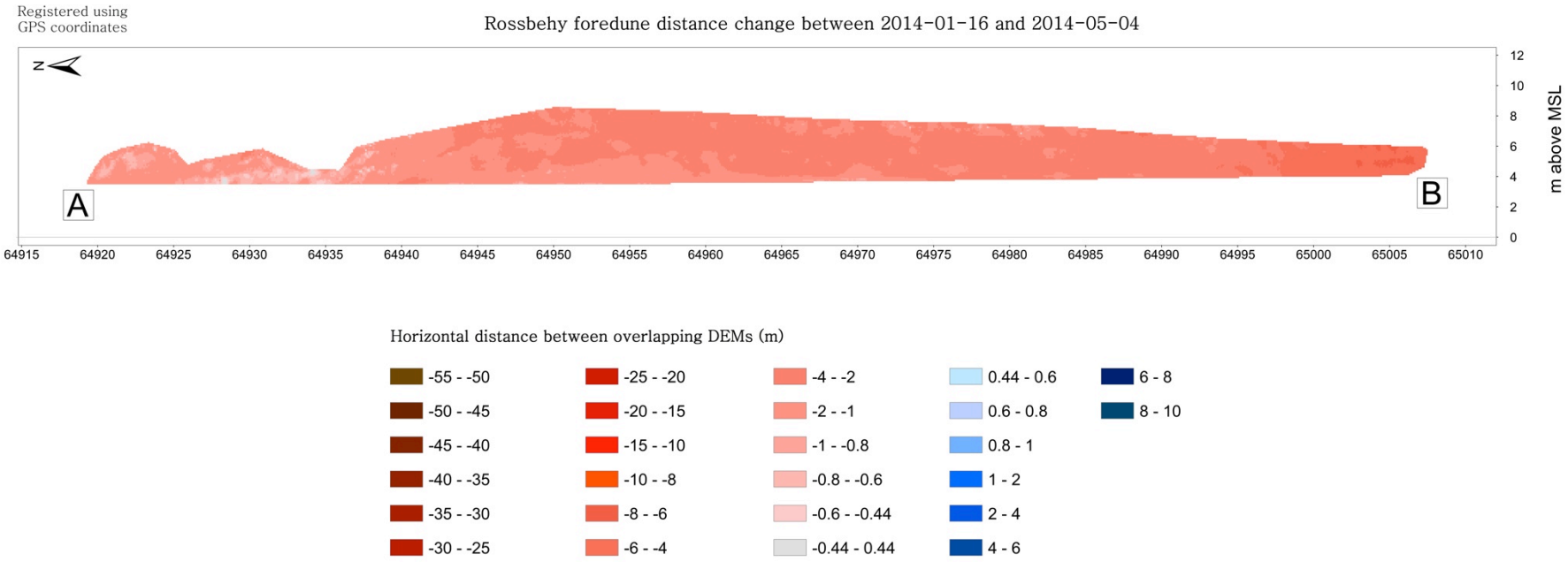

Figure 7.56 Rossbehy foredune distance change between 2014-01-16 and 2014-05-04. Dune recession, which occurred across the entire length of the surveyed area, is shown in varying shades of red. Distance change ranged from -6.41 m to -0.29 m. For reference, locations A and B correspond with those shown in figure 7.55. Mean sea level (MSL) is equal to +2.3 m ODM.

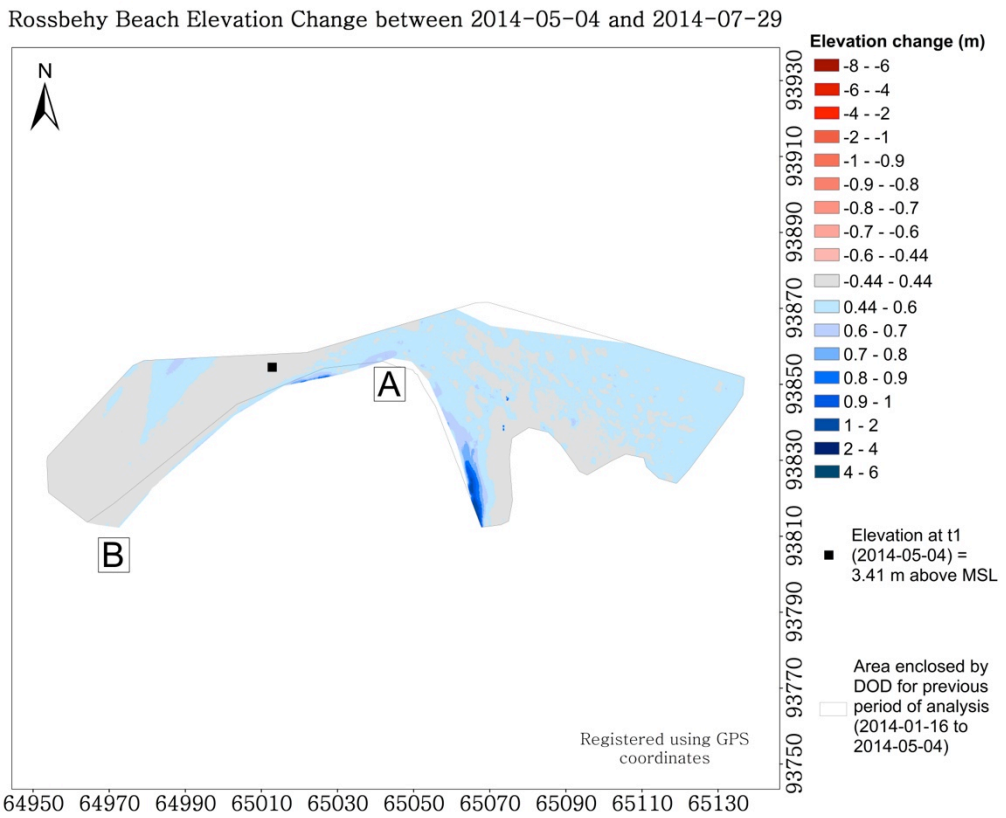

Figure 7.57 Rossbehy beach elevation change (DOD) between 2014-05-04 and 2014-07-29. Accretion (varying shades of blue) occurred across the majority of the site. Elevation change below the level of detectable change (±0.44 m) is shown in gray. Elevation change across the surveyed area ranged from -0.87 m to +1.40 m. Locations A and B correspond with those shown in figure 7.58. The coordinate marked with the square is at the same location as that shown in figure 7.55 (the DOD for the previous survey period) for reference. Mean sea level (MSL) is equal to +2.3 m ODM.

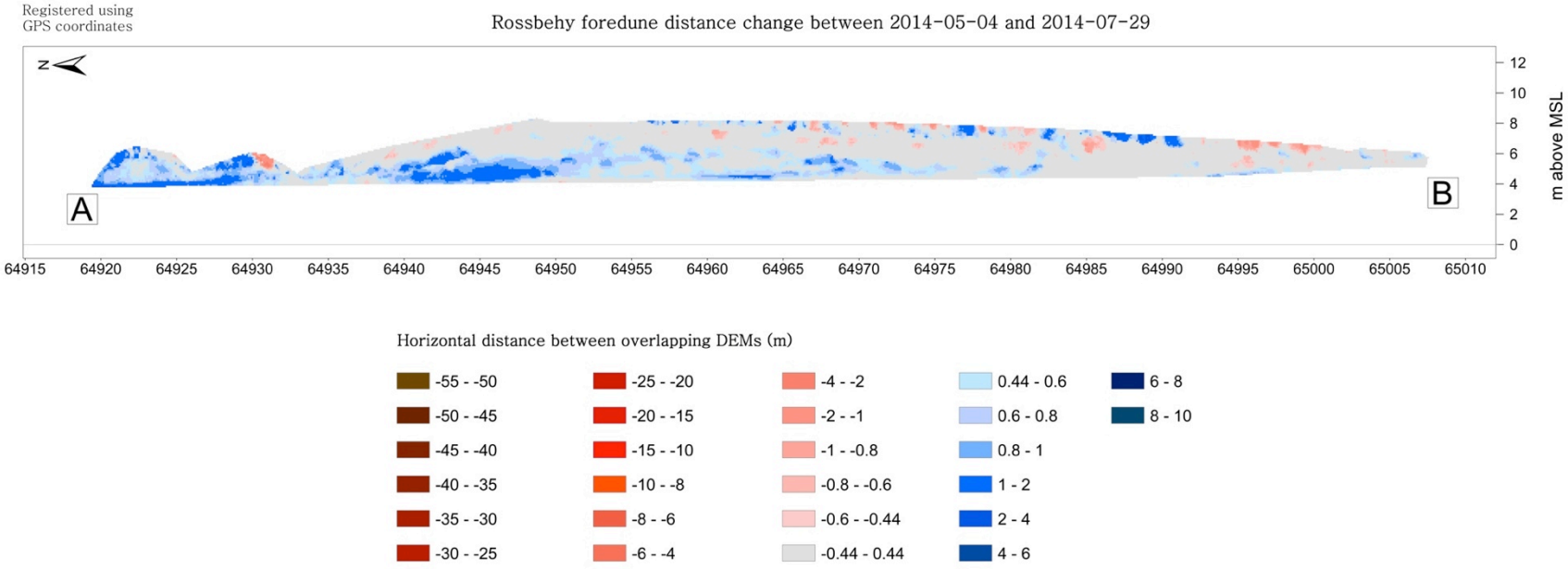

Figure 7.58 Rossbehy foredune distance change between 2014-05-04 and 2014-07-29. Distance change across much of the surveyed area lies below the level of detectable change (±0.44 m) and ranges from -2.91 m to +2.47 m. For reference, locations A and B correspond with those shown in figure 7.57. Mean sea level (MSL) is equal to +2.3 m ODM.

Survey start/end dates	Mean elevation change between DEMs (m)	Elevation change error margin (m)	Volume Gain (m^3)	Volume Loss (m^3)	Net volume change (V_s) (m^3)	Volumetric error margin (m^3)	Area of Survey (A) (m^2)	Time between surveys (days)	Rate of volume change (R_{vs}) (m^3 m^2 day)	Volumetric error margin associated with rate of volume change (m^3 m^2 day)	Remark
2012-06-28 2012-08-05	0.02	±0.41	320.6	171.4	149.2	±2983	7275.9	58	0.0004	±0.007	Inconclusive
2012-08-05 2012-10-07	0.80	±0.41	3844.1	973.2	2870.9	±1468	3581.5	43	0.0186	±0.003	Net gain
2013-01-30 2013-02-28	0.54	±0.41	544.9	0.0	544.9	±417	1017.2	29	0.0185	±0.014	Net gain
2013-02-28 2013-04-19	-1.50	±0.44	0.0	1369.6	-1369.6	±412	938.1	50	-0.0292	±0.009	Net loss
2013-04-19 2013-06-05	0.19	±0.41	363.7	9.8	353.9	±764	1865.5	47	0.0040	±0.009	Inconclusive
2013-06-05 2013-12-11	0.30	±0.44	219.7	2.5	217.2	±321	731.6	189	0.0016	±0.002	Inconclusive
2014-01-16 2014-05-04	0.17	±0.44	788.0	62.4	725.6	±1931	4390.7	108	0.0015	±0.004	Inconclusive
2014-05-04 2014-07-29	0.41	±0.44	1818.2	4.2	1813.9	±1936	4402.2	86	0.0048	±0.005	Inconclusive

Table 7.4 Summary of elevation and volume changes for beach at Rossbehy field site.

Survey start/end dates	Mean change in distance between DEMs (m)	Distance change error margin (m)	Volume Gain (m^3)	Volume Loss (m^3)	Net volume change (V_s) (m^3)	Volumetric error margin (m^3)	Area of Survey (A) (m^2)	Time between surveys (days)	Rate of volume change (R_{vs}) (m^3 m^2 day)	Volumetric error margin associated with rate of volume change (m^3 m^2 day)	Remark
2012-06-28 2012-08-05	-1.1	±0.41	20.3	351.7	-322.5	±127	310.6	38	-0.0273	±0.011	Net loss
2012-08-05 2012-11-15	-8.9	±0.41	26.0	2085.7	-2059.8	±99	242.6	102	-0.0832	±0.004	Net loss
2012-11-15 2013-01-30	-28.1	±0.44	0.0	9469.4	-9469.4	±153	346.8	76	-0.3593	±0.006	Net loss
2013-01-30 2013-02-28	-1.1	±0.41	18.0	382.1	-364.1	±137	334.1	29	-0.0376	±0.014	Net loss
2013-02-28 2013-04-19	-3.6	±0.44	0.0	836.1	-836.1	±104	236.1	50	-0.0708	±0.009	Net loss
2013-04-19 2013-06-05	-0.1	±0.41	24.2	48.9	-24.7	±152	371.6	47	-0.0014	±0.009	Inconclusive
2013-06-05 2013-12-11	0.0	±0.44	333.9	322.6	11.2	±157	355.8	189	0.0002	±0.002	Inconclusive
2013-12-11 2014-01-16	-37.8	±0.44	0.0	15337.3	-15337.3	±179	406.2	36	-1.0489	±0.012	Net loss
2014-01-16 2014-05-04	-2.3	±0.44	0.0	661.9	-661.9	±126	286.7	108	-0.0214	±0.004	Net loss
2014-05-04 2014-07-29	0.3	±0.44	93.0	18.1	74.8	±111	253.2	86	0.0034	±0.005	Inconclusive

Table 7.5 Summary of distance and volumetric changes for foredune at Rossbehy field site.

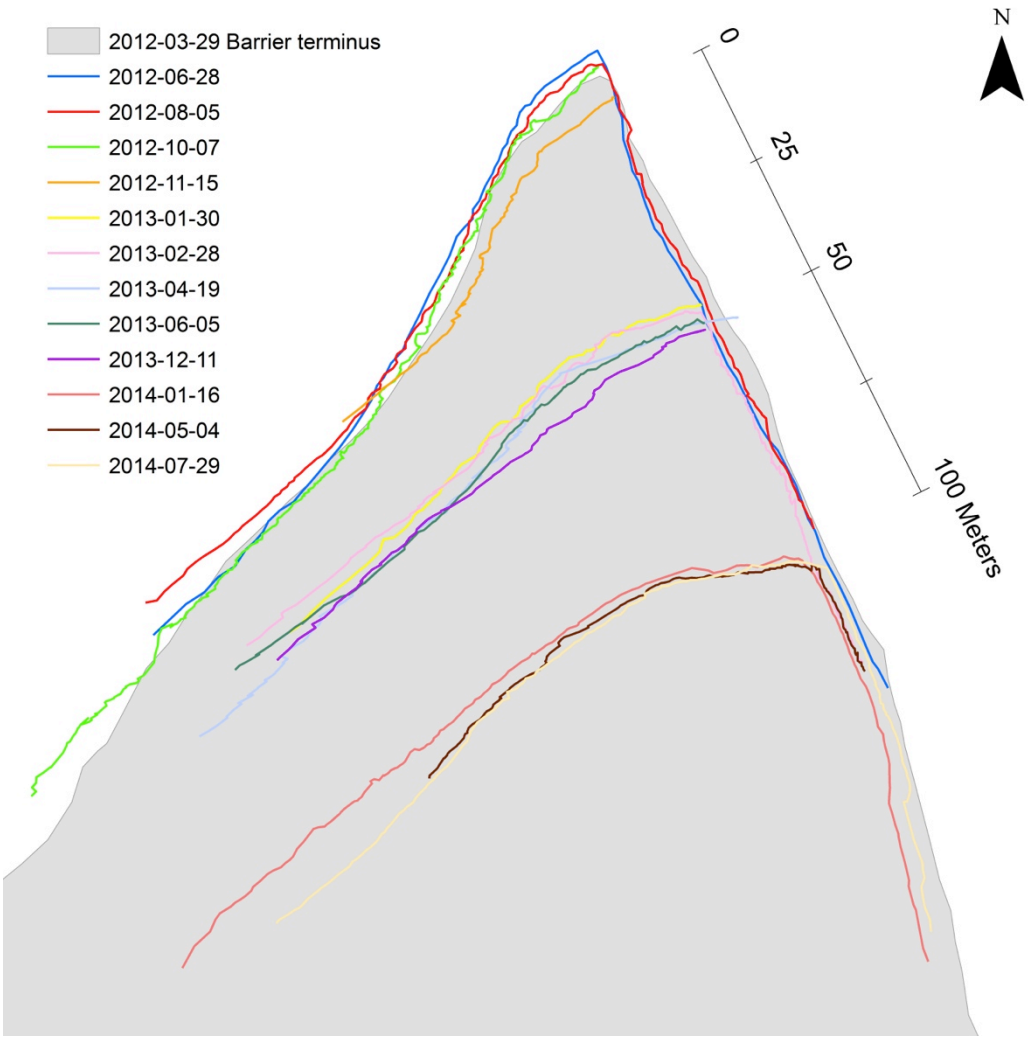

Figure 7.59 Shoreline positions at Rossbehy during TLS monitoring campaign. The shoreline is defined as position of the dune toe, or the line along which there is an abrupt change in slope, marking the boundary between the beach and dune. The March 2012 shoreline was digitized from an aerial photograph (for reference), while the others were digitized from TLS data.

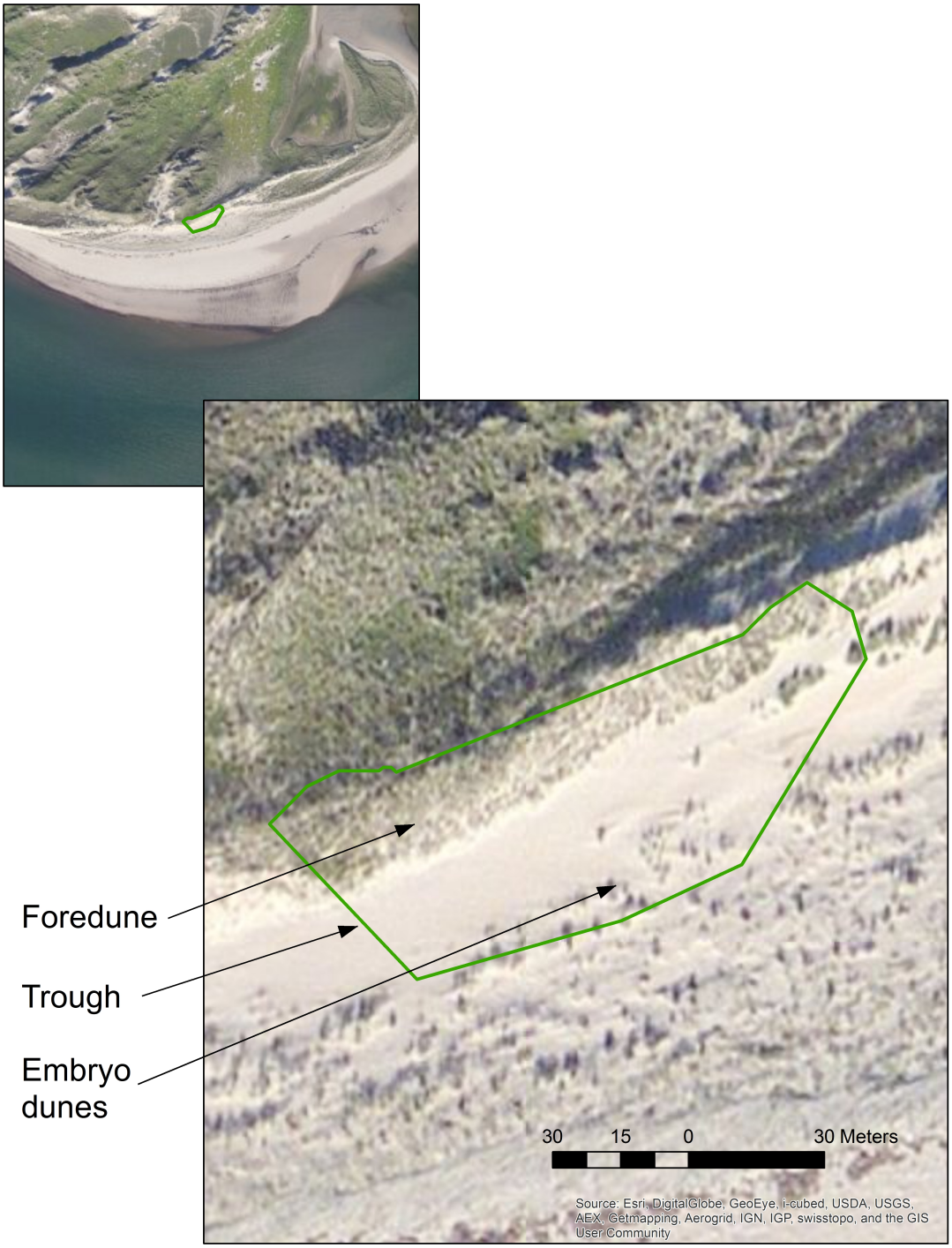

Figure 7.60 Areal photographs of Inch field site indicating location of TLS surveys. The area enclosed by the green polygon is the area over which all surveys overlap. Source of areal photography: ESRI

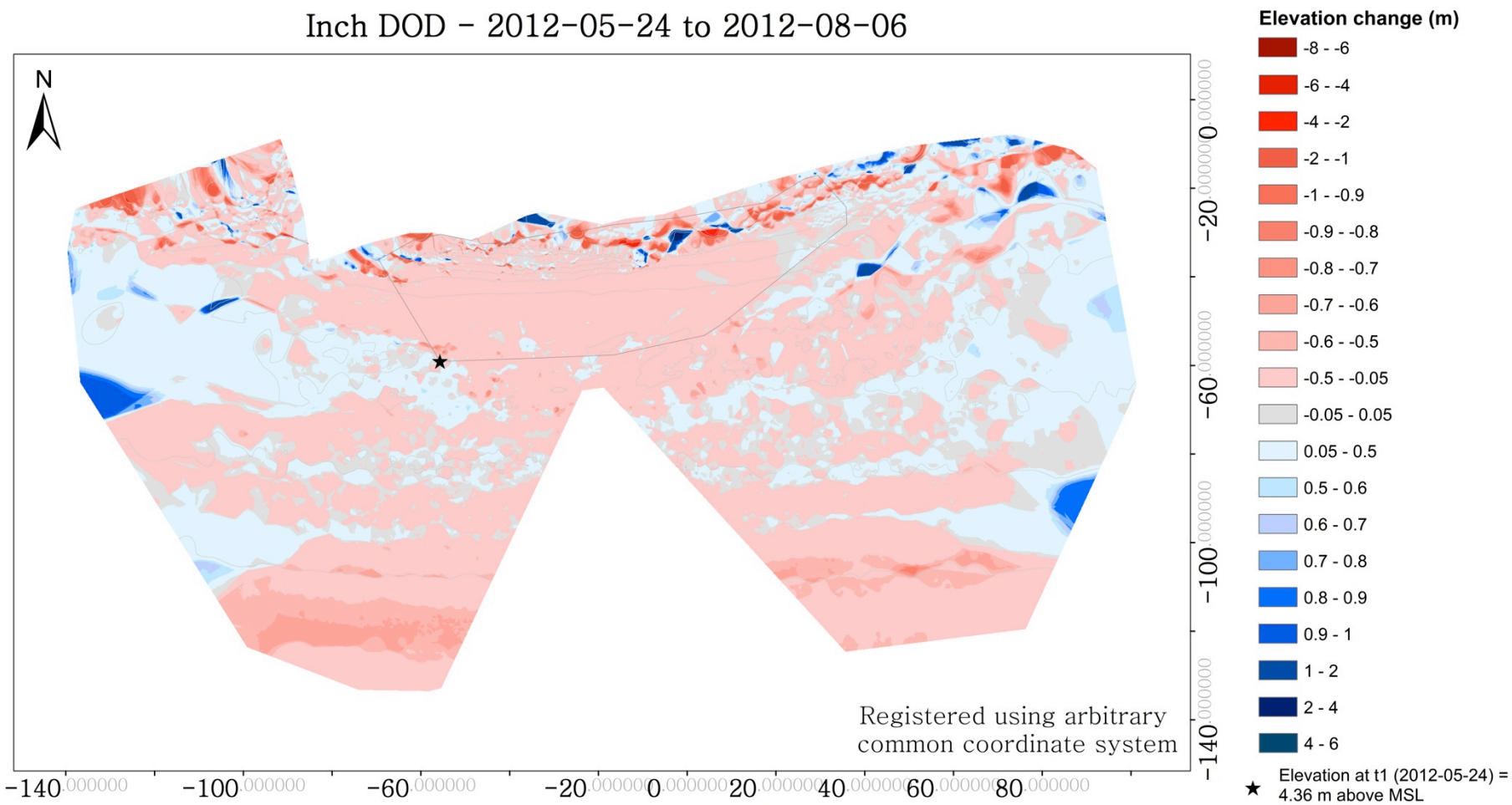

Figure 7.61 Inch beach elevation change (DOD) between 2012-05-24 and 2012-08-06. Beach erosion is shown in varying shades of red and accretion in varying shades of blue. Elevation change below the level of detectable change (±0.05 m) is shown in gray. Elevation change ranged from -3.00 m to +2.76 m. The coordinate marked with the star is at the same location as that shown in figures 7.62-7.68 (the DODs for the subsequent survey periods) for reference. The area enclosed by the gray polygon is the area across which all surveys overlap. Mean sea level (MSL) is equal to +2.3 m ODM.

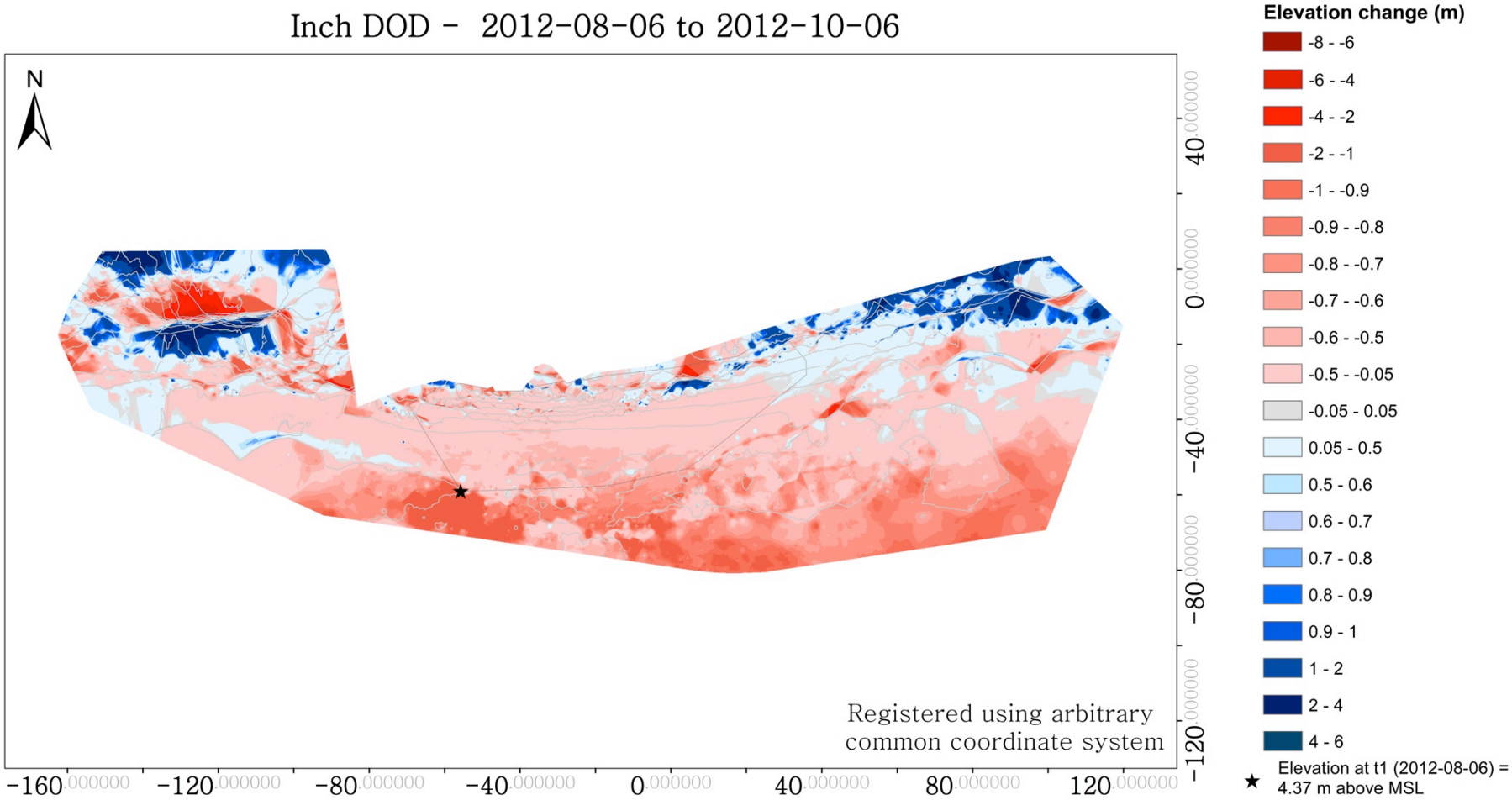

Figure 7.62 Inch beach elevation change (DOD) between 2012-08-06 and 2012-10-06. Beach erosion is shown in varying shades of red and accretion in varying shades of blue. Elevation change below the level of detectable change (±0.05 m) is shown in gray. Elevation change ranged from -5.42 m to +4.43 m. The coordinate marked with the star is at the same location as that shown in figures 7.61-7.68 (the DODs for the previous and subsequent survey periods) for reference. The area enclosed by the gray polygon is the area across which all surveys overlap. Mean sea level (MSL) is equal to +2.3 m ODM.

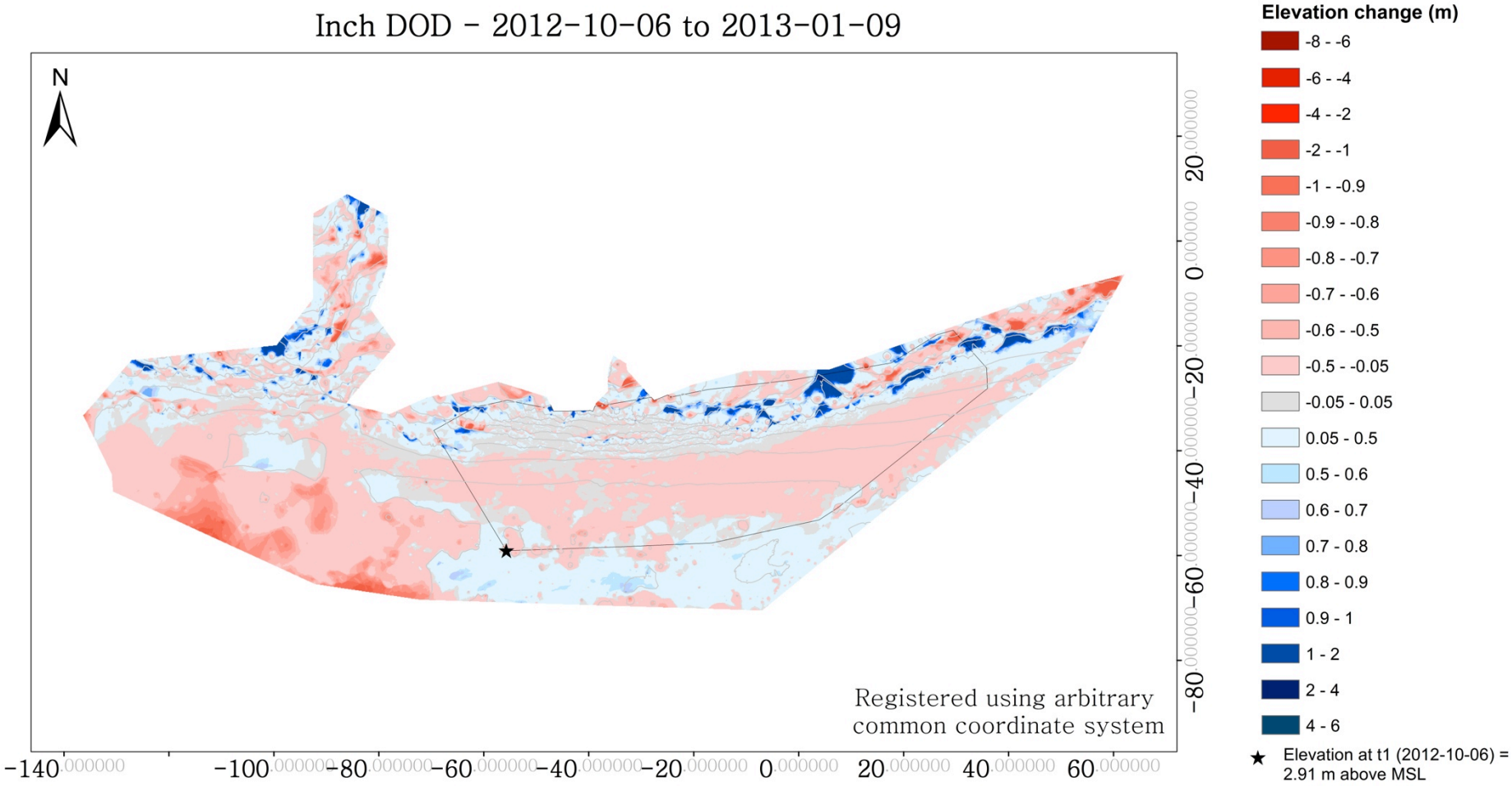

Figure 7.63 Inch beach elevation change (DOD) between 2012-10-06 and 2013-01-09. Beach erosion is shown in varying shades of red and accretion in varying shades of blue. Elevation change below the level of detectable change (±0.05 m) is shown in gray. Elevation change ranged from -1.78 m to +2.41 m. The coordinate marked with the star is at the same location as that shown in figures 7.61-7.68 (the DODs for the previous and subsequent survey periods) for reference. The area enclosed by the gray polygon is the area across which all surveys overlap. Mean sea level (MSL) is equal to +2.3 m ODM.

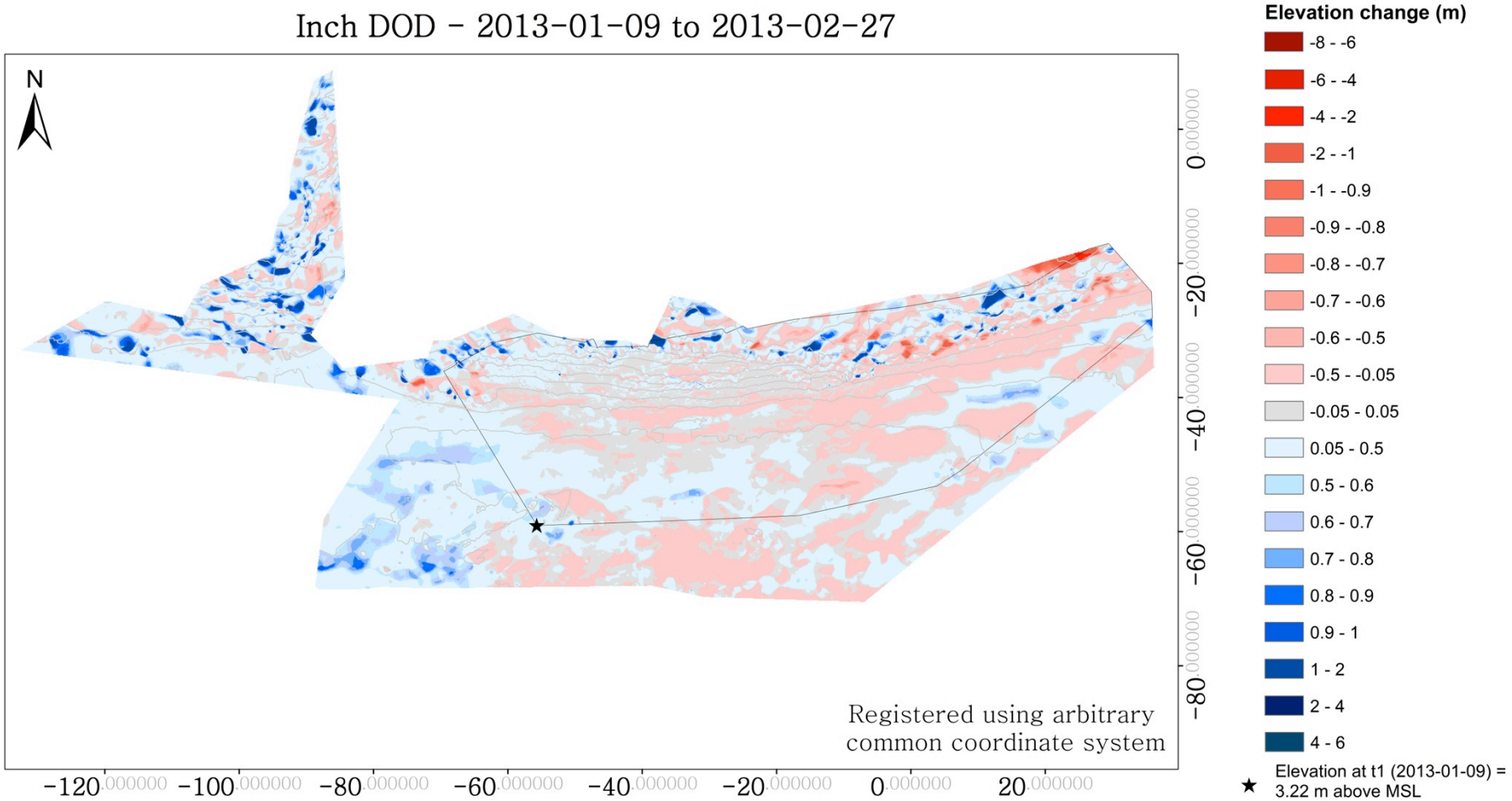

Figure 7.64 Inch beach elevation change (DOD) between 2013-01-09 and 2013-02-27. Beach erosion is shown in varying shades of red and accretion in varying shades of blue. Elevation change below the level of detectable change (±0.05 m) is shown in gray. Elevation change ranged from -2.11 m to +1.96 m. The coordinate marked with the star is at the same location as that shown in figures 7.61-7.68 (the DODs for the previous and subsequent survey periods) for reference. The area enclosed by the gray polygon is the area across which all surveys overlap. Mean sea level (MSL) is equal to +2.3 m ODM.

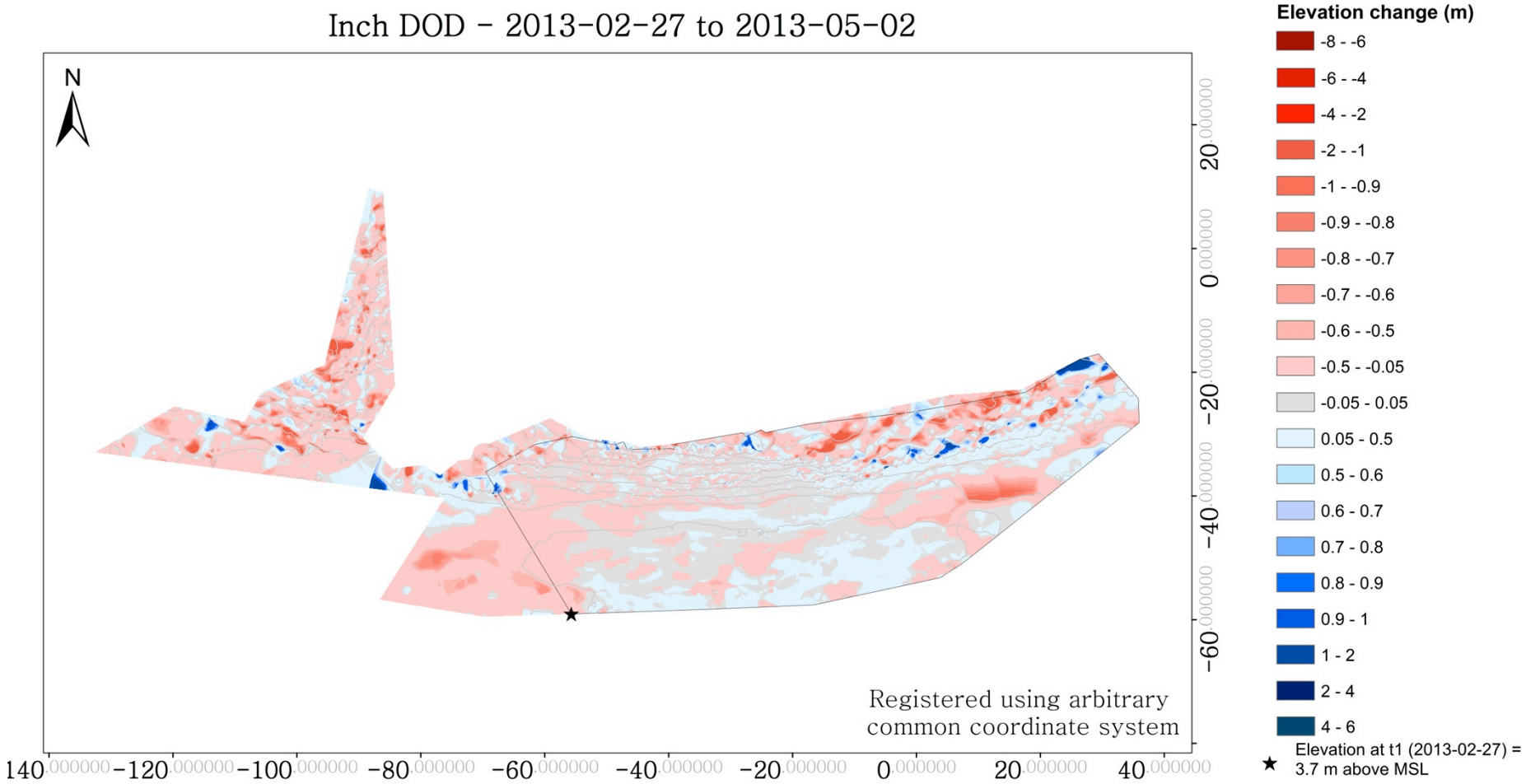

Figure 7.65 Inch beach elevation change (DOD) between 2013-02-27 and 2013-05-02. Beach erosion is shown in varying shades of red and accretion in varying shades of blue. Elevation change below the level of detectable change (±0.05 m) is shown in gray. Elevation change ranged from -2.00 m to +1.96 m. The coordinate marked with the star is at the same location as that shown in figures 7.61-7.68 (the DODs for the previous and subsequent survey periods) for reference. The area enclosed by the gray polygon is the area across which all surveys overlap. Mean sea level (MSL) is equal to +2.3 m ODM.

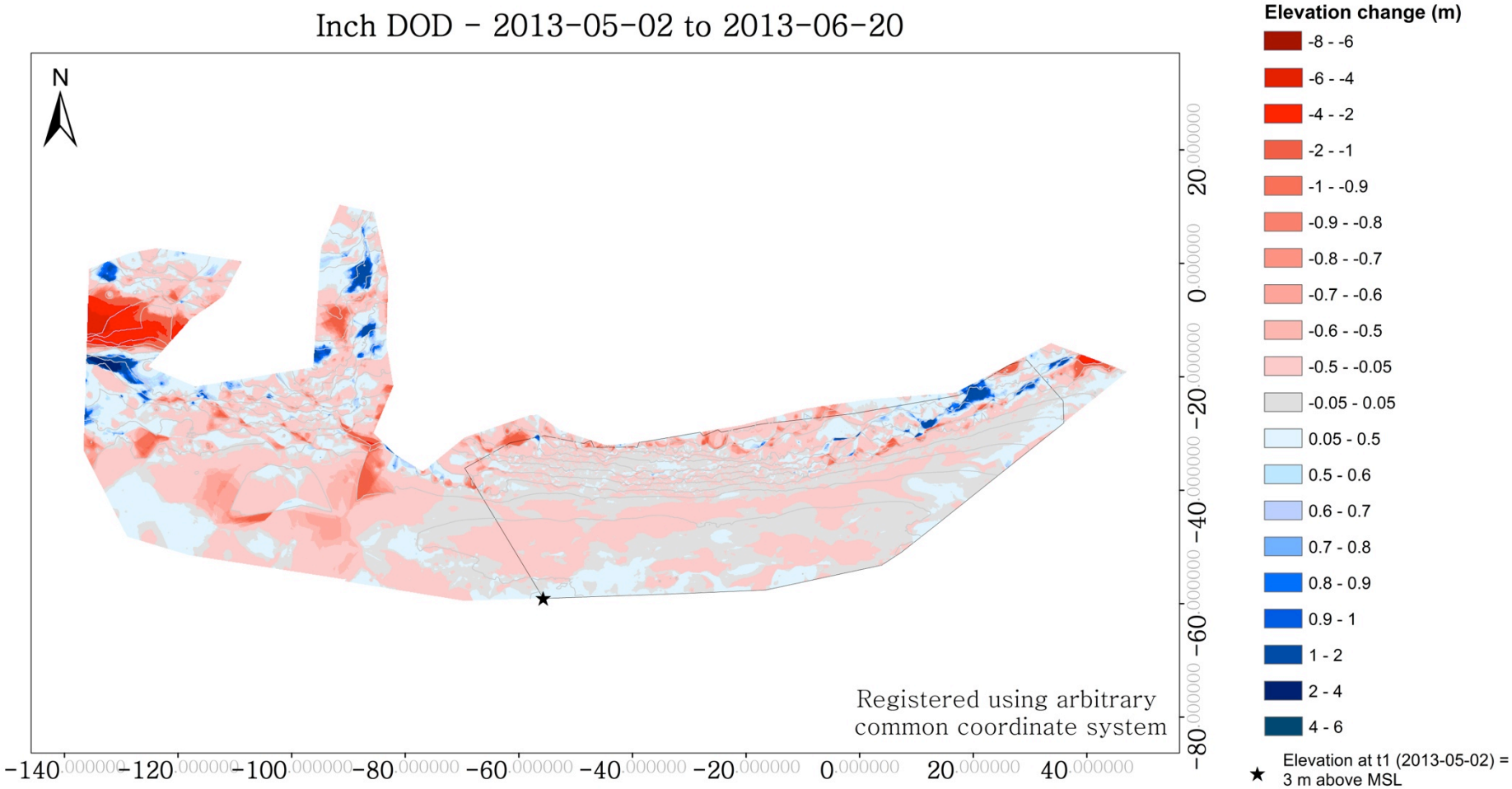

Figure 7.66 Inch beach elevation change (DOD) between 2013-05-02 and 2013-06-20. Beach erosion is shown in varying shades of red and accretion in varying shades of blue. Elevation change below the level of detectable change (±0.05 m) is shown in gray. Elevation change ranged from -5.29 m to +3.09 m. The coordinate marked with the star is at the same location as that shown in figures 7.61-7.68 (the DODs for the previous and subsequent survey periods) for reference. The area enclosed by the gray polygon is the area across which all surveys overlap. Mean sea level (MSL) is equal to +2.3 m ODM.

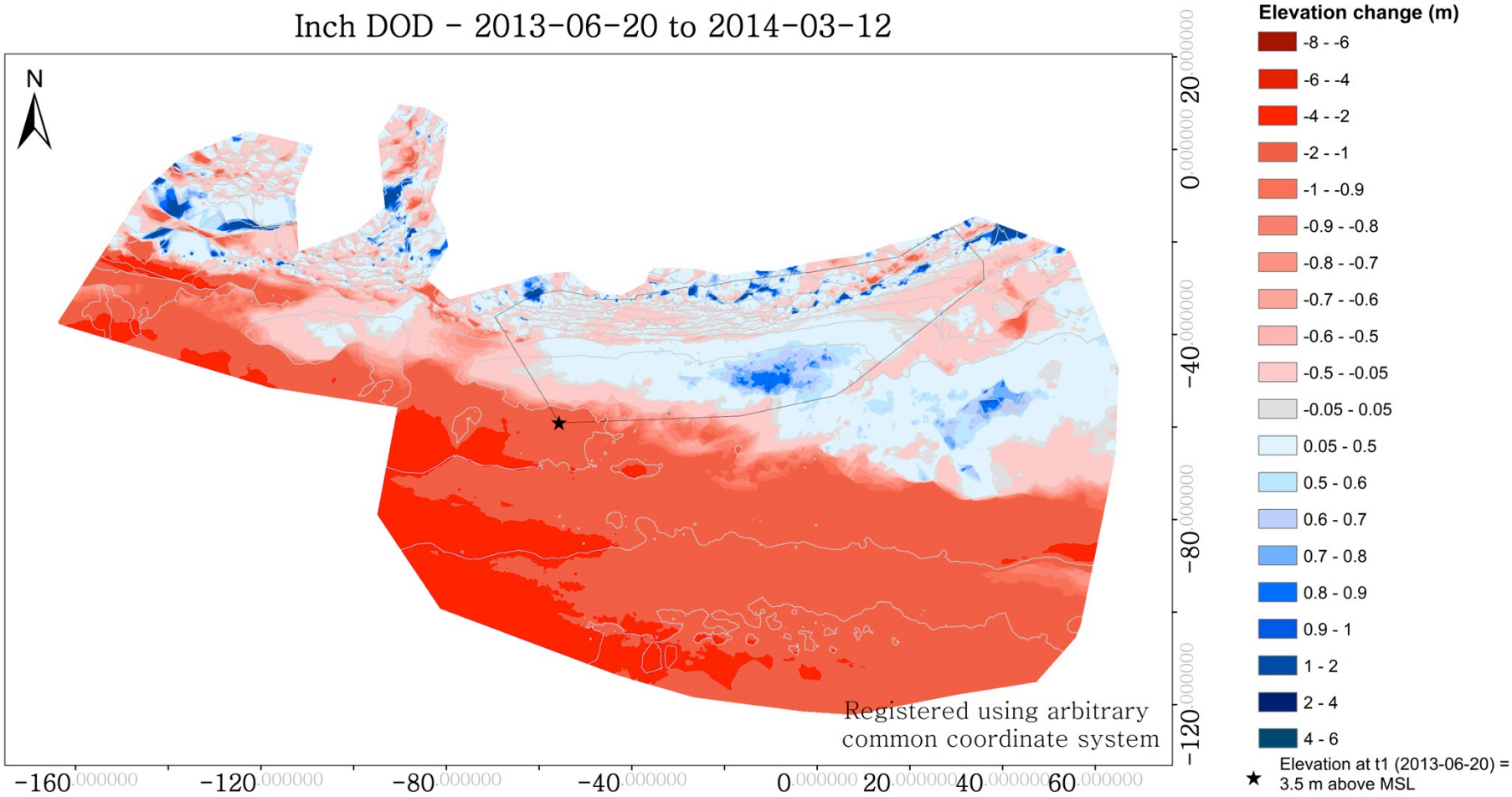

Figure 7.67 Inch beach elevation change (DOD) between 2013-06-20 and 2014-03-12. Beach erosion is shown in varying shades of red and accretion in varying shades of blue. Elevation change below the level of detectable change (±0.05 m) is shown in gray. Elevation change ranged from -3.56 m to +2.84 m. The coordinate marked with the star is at the same location as that shown in figures 7.61-7.68 (the DODs for the previous and subsequent survey periods) for reference. The area enclosed by the gray polygon is the area across which all surveys overlap. Mean sea level (MSL) is equal to +2.3 m ODM.

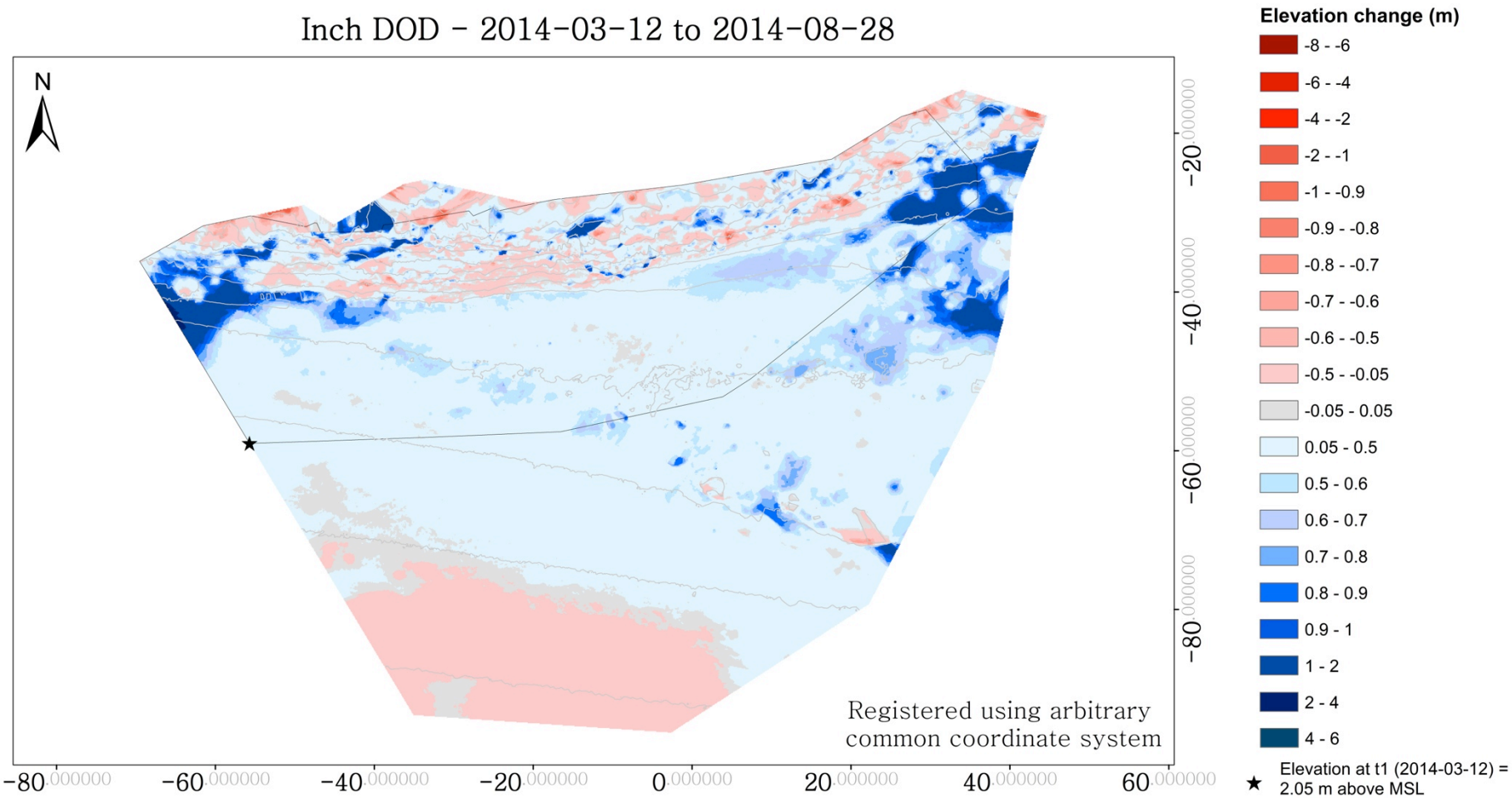

Figure 7.68 Inch beach elevation change (DOD) between 2014-03-12 and 2014-08-28. Beach erosion is shown in varying shades of red and accretion in varying shades of blue. Elevation change below the level of detectable change (±0.05 m) is shown in gray. Elevation change ranged from -1.26 m to +2.34 m. The coordinate marked with the star is at the same location as that shown in figures 7.61-7.67 (the DODs for the previous survey periods) for reference. The area enclosed by the gray polygon is the area across which all surveys overlap. Mean sea level (MSL) is equal to +2.3 m ODM.

Figure 7.69 Embryo dune field at Inch on 20 June 2013 (top) and 12 March 2014 (bottom). The embryo dune field likely shielded the foredune from extreme waves during the winter 2013/2014 storms. Source: author's own

Table 7.6 Summary of elevation and volume changes at Inch field site.

Survey start/end dates	Mean elevation change between DEMs (m)	Elevation change error margin (m)	Volume Gain (m^3)	Volume Loss (m^3)	Net volume change (V_s) (m^3)	Volumetric error margin (m^3)	Area of Survey (A) (m^2)	Time between surveys (days)	Rate of volume change (R_{vs}) (m^3 m^2 day)	Volumetric error margin associated with rate of volume change (m^3 m^2 day)	Remark
2012-05-24 2012-08-06	-0.16	±0.05	86.9	494.1	-407.2	±124	2472.04	74	-0.0022	±0.0007	Net loss
2012-08-06 2012-10-06	-0.29	±0.05	137.5	856.4	-718.9	±124	2472.04	61	-0.0048	±0.0008	Net loss
2012-10-06 2013-01-09	-0.02	±0.05	231.6	278.1	-46.5	±124	2472.04	95	-0.0002	±0.0005	Inconclusive
2013-01-09 2013-02-27	-0.03	±0.05	249.2	178.6	70.7	±124	2472.04	49	0.0006	±0.001	Inconclusive
2013-02-27 2013-05-02	-0.05	±0.05	153.5	283.0	-129.6	±124	2472.04	64	-0.0008	±0.0008	Net loss
2013-05-02 2013-06-20	-0.03	±0.05	118.4	199.4	-81.0	±124	2472.04	49	-0.0007	±0.001	Inconclusive
2013-06-20 2014-03-12	0.11	±0.05	509.9	232.2	277.7	±124	2472.04	265	0.0004	±0.0002	Net gain
2014-03-12 2014-08-28	0.33	±0.05	865.4	62.2	803.2	±124	2472.04	169	0.0019	±0.0003	Net gain

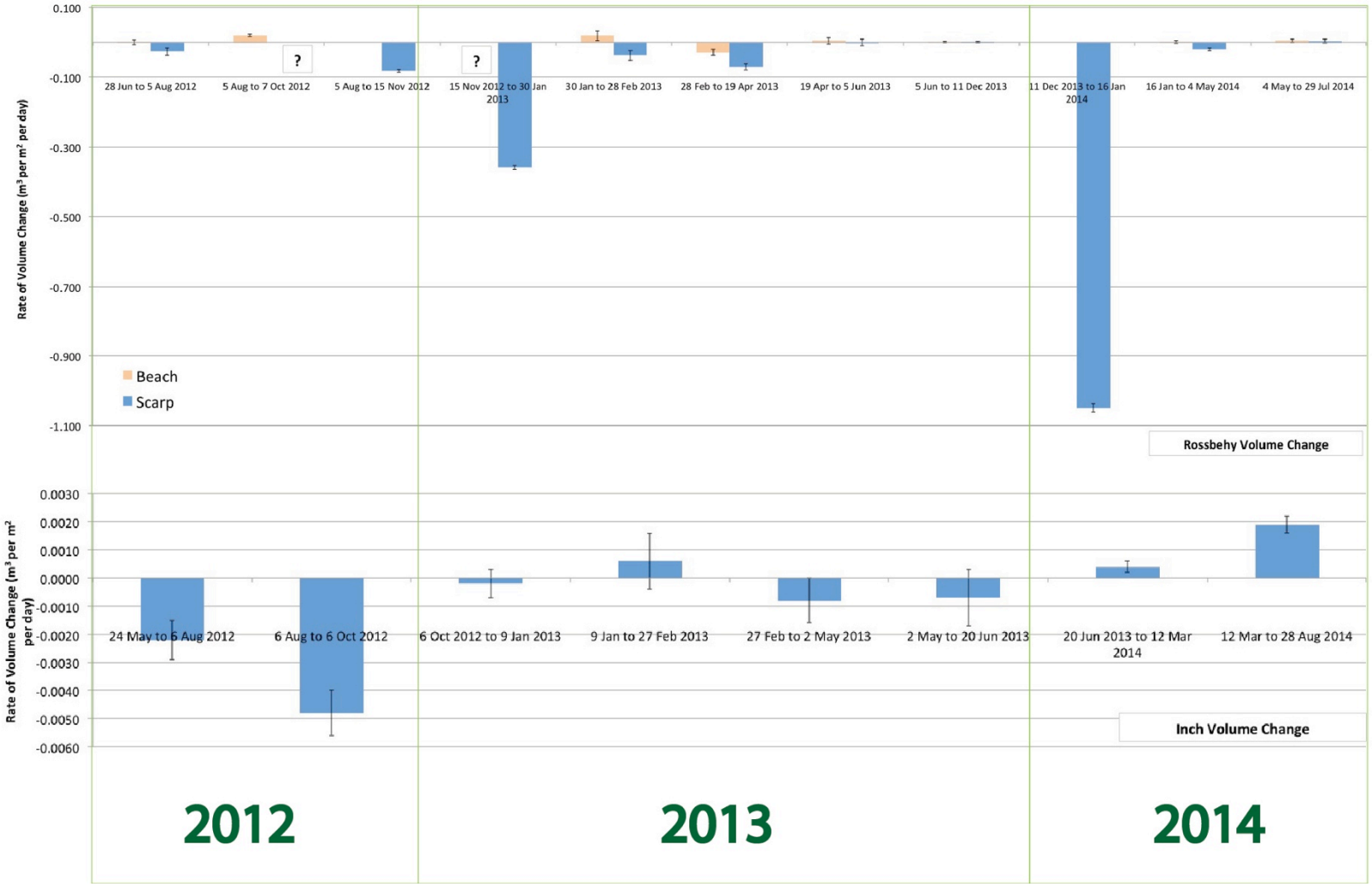

Figure 7.70 Rates of volume change for Rossbehy (top) and Inch (bottom) for TLS monitoring periods. Note the large difference in scale between rates of volume change for Rossbehy beach and scarp and between Rossbehy and Inch generally.

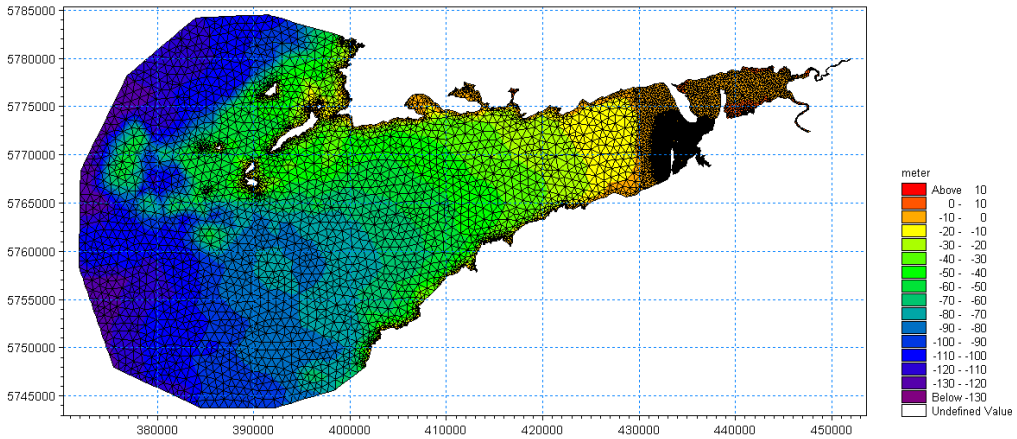

Figure 8.1 Model domain and flexible mesh on which WAM was run. Extracted from O'Shea *et al*. (2011)

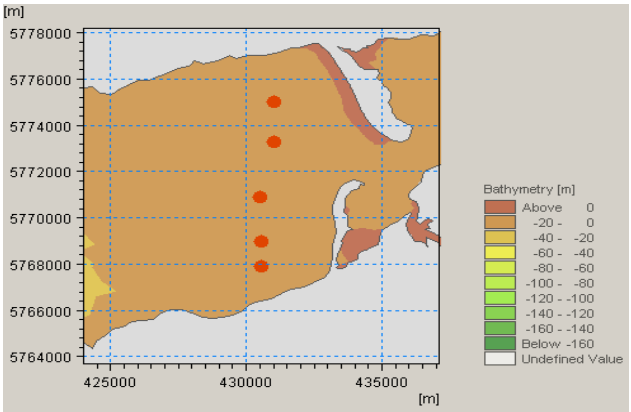

Figure 8.2 Five points in WAM model domain for which outputs (significant wave height, wave period, and wave direction) were extracted.

Event ID	Start date	End date	Event Duration	Lag time	Mean H_s	Max H_s	Peak period	Mean dxn
55	2012-05-22 14:00:00	2012-05-23 08:00:00	18:00:00	814:00:00	1.11	1.17	7	258
56	2012-06-15 06:00:00	2012-06-16 06:00:00	24:00:00	550:00:00	1.29	1.40	7	258
57	2012-07-16 01:00:00	2012-07-16 18:00:00	17:00:00	715:00:00	1.17	1.24	6	257
58	2012-07-31 13:00:00	2012-08-02 08:00:00	43:00:00	355:00:00	1.26	1.56	7	258
59	2012-08-02 11:00:00	2012-08-03 21:00:00	34:00:00	03:00:00	1.39	1.60	7	259
60	2012-08-15 20:00:00	2012-08-16 19:00:00	23:00:00	287:00:00	1.40	1.74	6	258
61	2012-08-27 08:00:00	2012-08-28 04:00:00	20:00:00	253:00:00	1.09	1.16	6	258
62	2012-08-28 10:00:00	2012-08-29 20:00:00	34:00:00	06:00:00	1.44	1.70	7	258
63	2012-09-09 12:00:00	2012-09-10 01:00:00	13:00:00	256:00:00	1.08	1.10	7	259
64	2012-09-30 03:00:00	2012-09-30 17:00:00	14:00:00	482:00:00	1.12	1.29	7	259
65	2012-10-02 01:00:00	2012-10-03 07:00:00	30:00:00	32:00:00	1.22	1.45	8	260
66	2012-10-17 01:00:00	2012-10-17 20:00:00	19:00:00	330:00:00	1.54	1.92	8	259
67	2012-10-20 18:00:00	2012-10-22 11:00:00	41:00:00	70:00:00	1.37	1.54	11	260
68	2012-11-12 12:00:00	2012-11-14 19:00:00	55:00:00	505:00:00	1.35	1.71	10	260
69	2012-11-18 13:00:00	2012-11-23 18:00:00	125:00:00	90:00:00	1.55	2.11	9	259
70	2012-11-25 02:00:00	2012-11-25 19:00:00	17:00:00	32:00:00	1.25	1.49	7	259
71	2012-12-02 15:00:00	2012-12-03 09:00:00	18:00:00	164:00:00	1.13	1.20	9	260
72	2012-12-03 17:00:00	2012-12-04 12:00:00	19:00:00	08:00:00	1.09	1.17	9	261
73	2012-12-13 05:00:00	2012-12-13 19:00:00	14:00:00	209:00:00	1.25	1.37	9	260
74	2012-12-14 02:00:00	2012-12-18 05:00:00	99:00:00	07:00:00	1.69	2.48	9	260
75	2012-12-19 10:00:00	2013-01-01 06:00:00	308:00:00	29:00:00	1.60	2.40	9	259
76	2013-01-03 03:00:00	2013-01-09 05:00:00	146:00:00	45:00:00	1.32	1.77	9	259
77	2013-01-09 21:00:00	2013-01-12 18:00:00	69:00:00	16:00:00	1.48	1.82	9	260
78	2013-01-17 21:00:00	2013-01-18 21:00:00	24:00:00	123:00:00	1.22	1.36	8	258
79	2013-01-20 17:00:00	2013-01-23 06:00:00	61:00:00	44:00:00	1.41	1.67	9	260
80	2013-01-24 22:00:00	2013-01-25 19:00:00	21:00:00	40:00:00	1.22	1.33	9	260
81	2013-01-26 01:00:00	2013-02-01 11:00:00	154:00:00	06:00:00	1.84	2.60	9	260
82	2013-02-04 13:00:00	2013-02-06 03:00:00	38:00:00	74:00:00	1.37	1.59	9	262
83	2013-02-10 12:00:00	2013-02-11 08:00:00	20:00:00	105:00:00	1.30	1.54	8	261
84	2013-02-13 05:00:00	2013-02-14 12:00:00	31:00:00	45:00:00	1.30	1.69	8	260
85	2013-02-18 22:00:00	2013-02-19 16:00:00	18:00:00	106:00:00	1.24	1.37	9	259

Event ID	Start date	End date	Event Duration	Lag time	Mean H_s	Max H_s	Peak period	Mean dxn
86	2013-02-22 18:00:00	2013-02-23 17:00:00	23:00:00	74:00:00	1.18	1.33	9	260
87	2013-02-26 01:00:00	2013-02-26 21:00:00	20:00:00	56:00:00	1.19	1.28	10	260
88	2013-03-22 22:00:00	2013-03-23 13:00:00	15:00:00	577:00:00	1.31	1.52	8	259
89	2013-03-29 14:00:00	2013-03-31 15:00:00	49:00:00	145:00:00	1.44	1.71	10	260
90	2013-04-09 09:00:00	2013-04-10 19:00:00	34:00:00	210:00:00	1.27	1.52	9	260
91	2013-04-13 23:00:00	2013-04-18 21:00:00	118:00:00	76:00:00	1.72	2.53	8	259
92	2013-05-03 13:00:00	2013-05-04 03:00:00	14:00:00	352:00:00	1.15	1.26	6	258
93	2013-05-08 08:00:00	2013-05-09 19:00:00	35:00:00	101:00:00	1.42	1.73	8	260
94	2013-06-12 19:00:00	2013-06-13 21:00:00	26:00:00	816:00:00	1.22	1.48	7	258
95	2013-06-14 03:00:00	2013-06-15 21:00:00	42:00:00	06:00:00	1.34	1.57	7	258
96	2013-06-21 16:00:00	2013-06-23 05:00:00	37:00:00	139:00:00	1.40	1.95	8	260
97	2013-08-17 03:00:00	2013-08-17 17:00:00	14:00:00	1318:00:00	1.18	1.31	6	258
98	2013-10-16 10:00:00	2013-10-18 06:00:00	44:00:00	1433:00:00	1.31	1.54	7	259
99	2013-10-19 23:00:00	2013-10-20 21:00:00	22:00:00	41:00:00	1.29	1.60	7	258
100	2013-10-22 20:00:00	2013-10-23 20:00:00	24:00:00	47:00:00	1.17	1.35	8	259
101	2013-10-26 05:00:00	2013-11-01 06:00:00	145:00:00	57:00:00	1.41	2.42	10	260
102	2013-11-02 01:00:00	2013-11-03 07:00:00	30:00:00	19:00:00	1.53	2.07	8	260
103	2013-11-03 13:00:00	2013-11-05 22:00:00	57:00:00	06:00:00	1.40	1.87	8	260
104	2013-11-06 01:00:00	2013-11-08 10:00:00	57:00:00	03:00:00	1.22	1.58	10	261
105	2013-11-09 16:00:00	2013-11-12 03:00:00	59:00:00	30:00:00	1.34	1.55	8	260
106	2013-12-09 18:00:00	2013-12-10 15:00:00	21:00:00	663:00:00	1.10	1.15	7	258
107	2013-12-11 20:00:00	2013-12-12 17:00:00	21:00:00	29:00:00	1.25	1.35	8	259
108	2013-12-13 06:00:00	2014-01-08 15:00:00	633:00:00	13:00:00	1.85	2.97	9	260
109	2014-01-10 01:00:00	2014-01-10 15:00:00	14:00:00	34:00:00	1.20	1.28	6	257
110	2014-01-12 13:00:00	2014-01-17 08:00:00	115:00:00	46:00:00	1.61	2.07	9	260
111	2014-01-17 14:00:00	2014-01-18 09:00:00	19:00:00	06:00:00	1.18	1.29	9	260
112	2014-01-21 15:00:00	2014-01-22 21:00:00	30:00:00	78:00:00	1.32	1.56	9	261
113	2014-01-23 22:00:00	2014-01-28 11:00:00	109:00:00	25:00:00	1.59	2.25	9	261
114	2014-01-31 04:00:00	2014-02-04 17:00:00	109:00:00	65:00:00	1.74	2.71	9	260
115	2014-02-04 19:00:00	2014-02-06 14:00:00	43:00:00	02:00:00	1.77	2.64	9	259
116	2014-02-07 04:00:00	2014-02-10 10:00:00	78:00:00	14:00:00	1.86	2.57	8	259

Event ID	Start date	End date	Event Duration	Lag time	Mean H_s	Max H_s	Peak period	Mean dxn
117	2014-02-10 16:00:00	2014-02-16 07:00:00	135:00:00	06:00:00	1.65	2.48	9	260
118	2014-02-16 12:00:00	2014-02-18 22:00:00	58:00:00	05:00:00	1.43	1.89	10	259
119	2014-02-19 15:00:00	2014-03-01 06:00:00	231:00:00	17:00:00	1.67	2.43	9	260
120	2014-03-02 04:00:00	2014-03-06 00:00:00	92:00:00	22:00:00	1.49	2.84	9	260
121	2014-03-06 03:00:00	2014-03-07 06:00:00	27:00:00	03:00:00	1.16	1.36	8	260
122	2014-03-07 23:00:00	2014-03-09 19:00:00	44:00:00	17:00:00	1.43	1.67	8	260
123	2014-03-19 13:00:00	2014-03-22 22:00:00	81:00:00	234:00:00	1.41	2.03	8	260
124	2014-03-24 10:00:00	2014-03-25 21:00:00	35:00:00	36:00:00	1.64	2.24	8	260
125	2014-04-05 19:00:00	2014-04-08 02:00:00	55:00:00	262:00:00	1.32	1.62	7	259
126	2014-04-23 06:00:00	2014-04-24 04:00:00	22:00:00	364:00:00	1.17	1.25	9	260
127	2014-04-25 21:00:00	2014-04-26 14:00:00	17:00:00	41:00:00	1.43	1.93	7	259

Table 8.1 Summary of event information extracted from WAM data. Events are described as times when the significant wave height, H_s, exceeded the critical wave height, h_{crit} (see text for explanation), for a minimum duration of 12 hours.

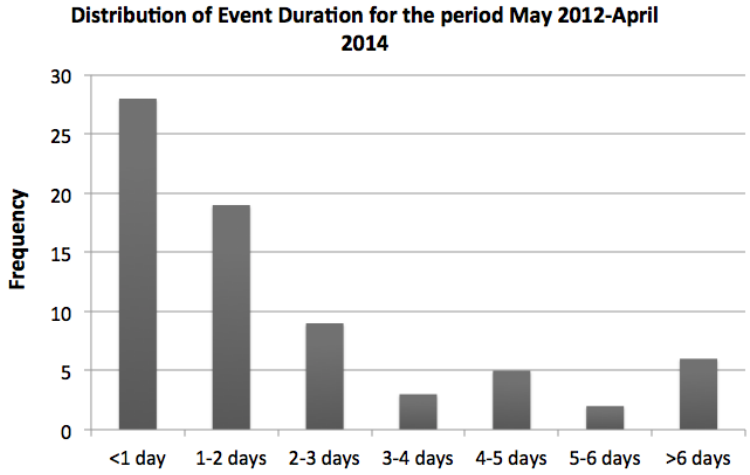

Figure 8.3 Breakdown of storm events identified using WAM data by event duration.

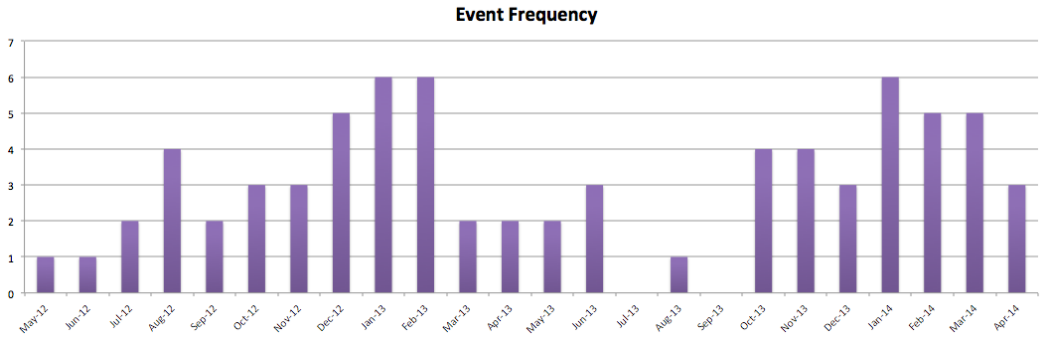

Figure 8.4 Modelled event frequency by month during morphologic monitoring period.

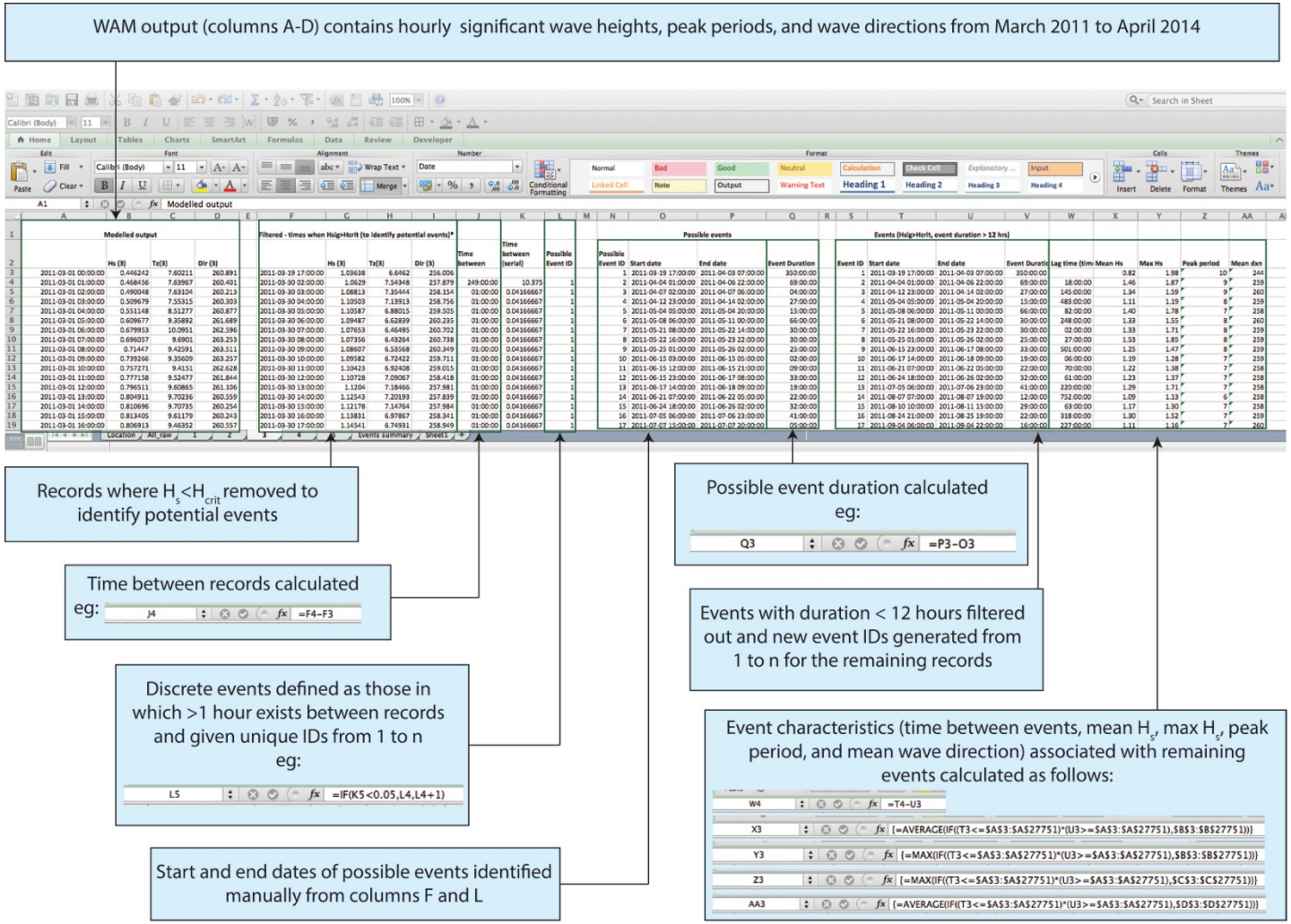

Figure 8.5 Excel spreadsheet and formulae used to identify storm events and extract storm characteristics from simulated WAM data. Records (rows) extend below the window shown. Formulae examples are for the first entry and were applied to each subsequent entry (*eg.* the cells below).

Worksheet contains information about wind direction, wind speed, and gust speed from Ventry at approximately 40 minute intervals from January 2011 to June 2014

2015-11 Weather Station Events.xlsx

Date/Time	Mean wind direction	Mean gust speed (km/hr)	Mean wind speed (km/hr)	Mean gust speed (m/s)	Mean wind speed (m/s)	N	NE	E	SE	S	SW	W	NW
2011-01-01 00:42:54	40	0.00	0	0.00	0.00	0	1	0	0	0	0	0	0
2011-01-01 01:27:32	40	0.00	0	0.00	0.00	0	1	0	0	0	0	0	0
2011-01-01 02:10:46	39	0.00	0	0.00	0.00	0	1	0	0	0	0	0	0
2011-01-01 02:54:06	40	0.00	0	0.00	0.00	0	1	0	0	0	0	0	0
2011-01-01 03:38:16	40	0.00	0	0.00	0.00	0	1	0	0	0	0	0	0
2011-01-01 04:20:46	40	0.00	0	0.00	0.00	0	1	0	0	0	0	0	0
2011-01-01 05:05:06	40	0.00	0	0.00	0.00	0	1	0	0	0	0	0	0
2011-01-01 05:50:48	40	0.00	0	0.00	0.00	0	1	0	0	0	0	0	0
2011-01-01 06:34:56	40	0.00	0	0.00	0.00	0	1	0	0	0	0	0	0
2011-01-01 07:45:02	39	1.00	0	0.28	0.00	0	1	0	0	0	0	0	0
2011-01-01 08:39:54	72	5.00	4	1.39	1.11	0	0	1	0	0	0	0	0
2011-01-01 09:28:32	123	2.00	2	0.56	0.56	0	0	0	1	0	0	0	0
2011-01-01 10:10:34	92	0.00	0	0.00	0.00	0	0	1	0	0	0	0	0
2011-01-01 10:55:47	92	0.00	0	0.00	0.00	0	0	1	0	0	0	0	0
2011-01-01 11:38:02	92	0.00	0	0.00	0.00	0	0	1	0	0	0	0	0
2011-01-01 12:21:24	91	0.00	0	0.00	0.00	0	0	1	0	0	0	0	0
2011-01-01 13:05:58	92	0.00	0	0.00	0.00	0	0	1	0	0	0	0	0
2011-01-01 13:50:18	92	0.00	0	0.00	0.00	0	0	1	0	0	0	0	0

The dominant wind direction, indicated in columns G-N by a value of 1, was determined as follows (example shown for cell G2):

G2 =IF(OR(B2<=22.5,B2>=337.5),1,0)

Date/Time	Mean wind direction	Mean gust speed (km/hr)	Mean wind speed (km/hr)	Mean gust speed (m/s)	Mean wind speed (m/s)	N	NE	E	SE	S	SW	W	NW
2011-01-01 00:42:54	40	0.00	0	0.00	0.00	0	1	0	0	0	0	0	0
2011-01-01 01:27:32	40	0.00	0	0.00	0.00	0	1	0	0	0	0	0	0
2011-01-01 02:10:46	39	0.00	0	0.00	0.00	0	1	0	0	0	0	0	0

In a second worksheet, information associated with events (whose start and end dates were defined previously based on simulated wave data) was extracted based on the information contained in the above worksheet. Columns B and C show the event start and end dates.

2015-11 Weather Station Events.xlsx

Event ID	Start date	End date	Mean wind speed (m/s)	Max Gust Speed (m/s)	Wind directions recorded during event N	NE	E	SE	S	SW	W	NW	Prevailing Wind Direction
55	2012-05-22 14:00:00	2012-05-23 08:00:00	3.82	5.22	0	0	0	0	48	0	0	0	S
56	2012-06-15 06:00:00	2012-06-16 06:00:00	3.51	9.07	0	3	13	7	1	2	26	1	W
57	2012-07-16 01:00:00	2012-07-16 18:00:00	9.16	11.54	0	0	0	0	0	11	35	0	W
58	2012-07-31 13:00:00	2012-08-02 08:00:00	4.75	10.01	0	0	0	0	9	73	29	0	SW
59	2012-08-02 11:00:00	2012-08-03 21:00:00	2.71	5.60	0	4	1	0	11	65	0	0	SW
60	2012-08-15 20:00:00	2012-08-16 19:00:00	5.18	12.13	0	0	0	0	11	45	2	0	SW
61	2012-08-27 08:00:00	2012-08-28 04:00:00	5.82	8.43	0	0	0	0	0	10	41	0	W
62	2012-08-28 10:00:00	2012-08-29 20:00:00	5.94	12.12	0	0	0	1	4	66	20	0	SW
63	2012-09-09 12:00:00	2012-09-10 01:00:00	4.75	6.84	0	0	0	0	0	12	20	0	W
64	2012-09-30 03:00:00	2012-09-30 17:00:00	7.00	10.19	0	0	0	0	0	21	16	0	SW
65	2012-10-02 01:00:00	2012-10-03 07:00:00	7.43	10.70	0	0	0	0	0	26	54	0	W
66	2012-10-17 01:00:00	2012-10-17 20:00:00	5.41	10.65	0	30	14	1	0	0	0	0	NE
67	2012-10-20 18:00:00	2012-10-22 11:00:00	2.06	2.87	0	0	1	7	90	0	0	0	S
68	2012-11-12 12:00:00	2012-11-14 19:00:00	3.98	9.29	0	2	1	0	4	90	3	0	SW
69	2012-11-18 13:00:00	2012-11-23 18:00:00	0.78	2.20	0	0	0	0	1	0	0	0	S

Examples of the formulae used to derive the information shown above are given below for row 3, columns D to N. These were applied to all subsequent rows in the worksheet.

D3 {=AVERAGE(IF((Ventry_ALL!$A$2:$A$52936>=Events!B3)*(Ventry_ALL!$A$2:$A$52936<=Events!C3),Ventry_ALL!$F$2:$F$52936)}

E3 {=MAX(IF((Ventry_ALL!$A$2:$A$52936>=Events!B3)*(Ventry_ALL!$A$2:$A$52936<=Events!C3),Ventry_ALL!$E$2:$E$52936)}

F3 {=SUM(IF((Ventry_ALL!$A$2:$A$52936>=Events!$B3)*(Ventry_ALL!$A$2:$A$52936<=Events!$C3),Ventry_ALL!G$2:G$52936)}

G3 {=SUM(IF((Ventry_ALL!$A$2:$A$52936>=Events!$B3)*(Ventry_ALL!$A$2:$A$52936<=Events!$C3),Ventry_ALL!H$2:H$52936)}

H3 {=SUM(IF((Ventry_ALL!$A$2:$A$52936>=Events!$B3)*(Ventry_ALL!$A$2:$A$52936<=Events!$C3),Ventry_ALL!I$2:I$52936)}

I3 {=SUM(IF((Ventry_ALL!$A$2:$A$52936>=Events!$B3)*(Ventry_ALL!$A$2:$A$52936<=Events!$C3),Ventry_ALL!J$2:J$52936)}

J3 {=SUM(IF((Ventry_ALL!$A$2:$A$52936>=Events!$B3)*(Ventry_ALL!$A$2:$A$52936<=Events!$C3),Ventry_ALL!K$2:K$52936)}

K3 {=SUM(IF((Ventry_ALL!$A$2:$A$52936>=Events!$B3)*(Ventry_ALL!$A$2:$A$52936<=Events!$C3),Ventry_ALL!L$2:L$52936)}

L3 {=SUM(IF((Ventry_ALL!$A$2:$A$52936>=Events!$B3)*(Ventry_ALL!$A$2:$A$52936<=Events!$C3),Ventry_ALL!M$2:M$52936)}

M3 {=SUM(IF((Ventry_ALL!$A$2:$A$52936>=Events!$B3)*(Ventry_ALL!$A$2:$A$52936<=Events!$C3),Ventry_ALL!N$2:N$52936)}

N3 =INDEX($F$2:$M$2,MATCH(MAX($F3:$M3),$F3:$M3,0))

Figure 8.6 Excel worksheets and formulae used to extract storm characteristics from Ventry weather station data. Records (rows) extend below the windows shown. Formulae examples are for the first entry and were applied to each subsequent entry (*eg.* the cells below).

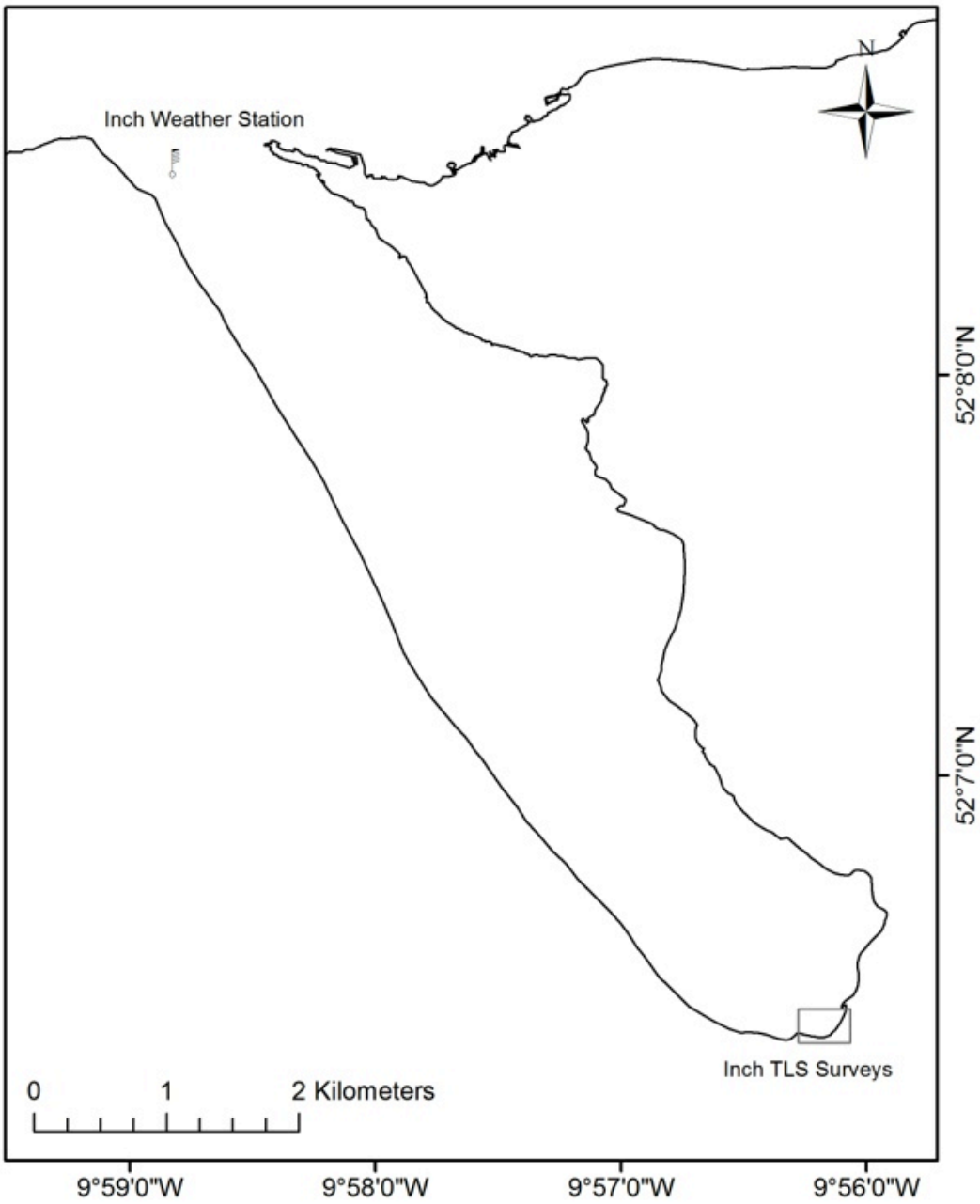

Figure 8.7 Location of weather station set up near Inch field site.

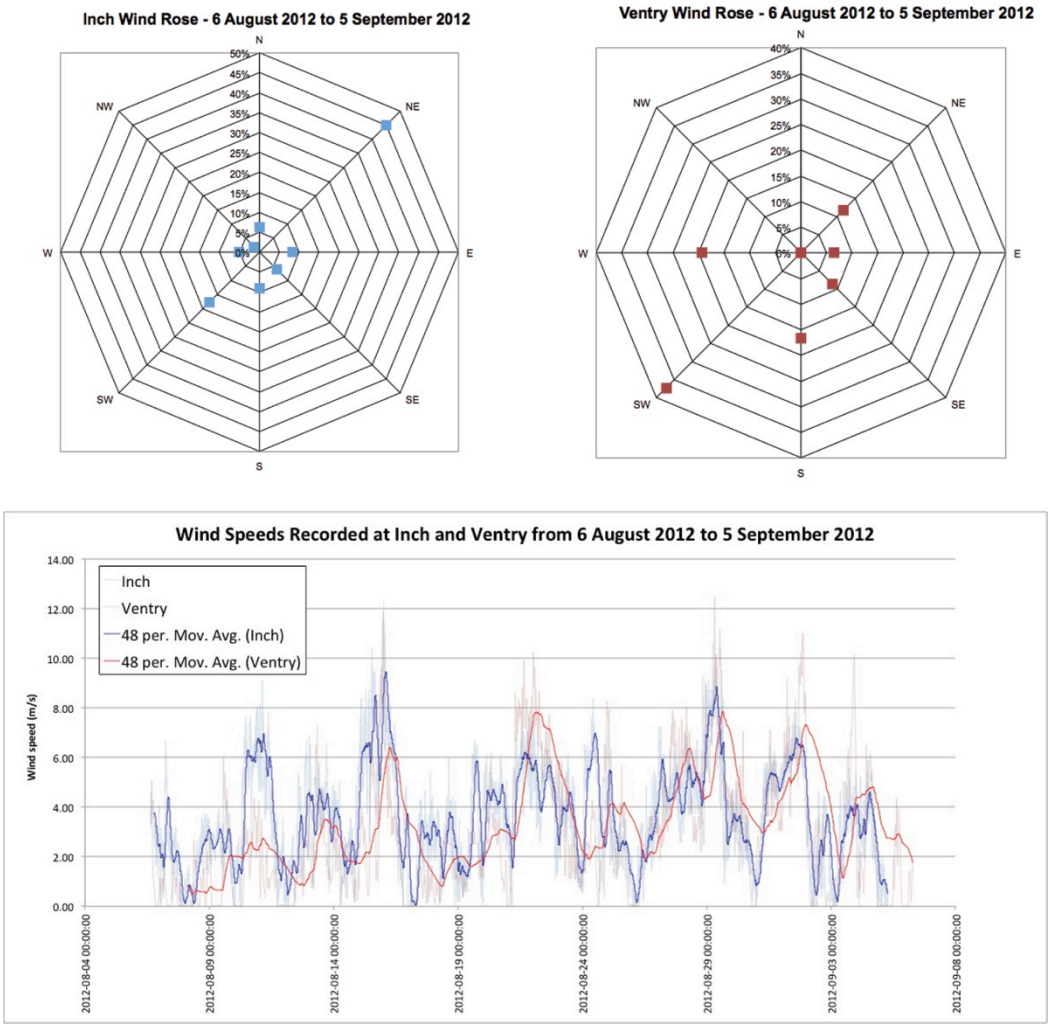

Figure 8.8 Wind roses and wind speeds for Inch and Ventry from 6 August 2012 to 5 September 2012. Wind speeds were derived from instantaneous wind speeds averaged at half hourly (or approximately half hourly) intervals. Running means (with 48 hour periods) have been superimposed on the wind speed graph for visual clarity.

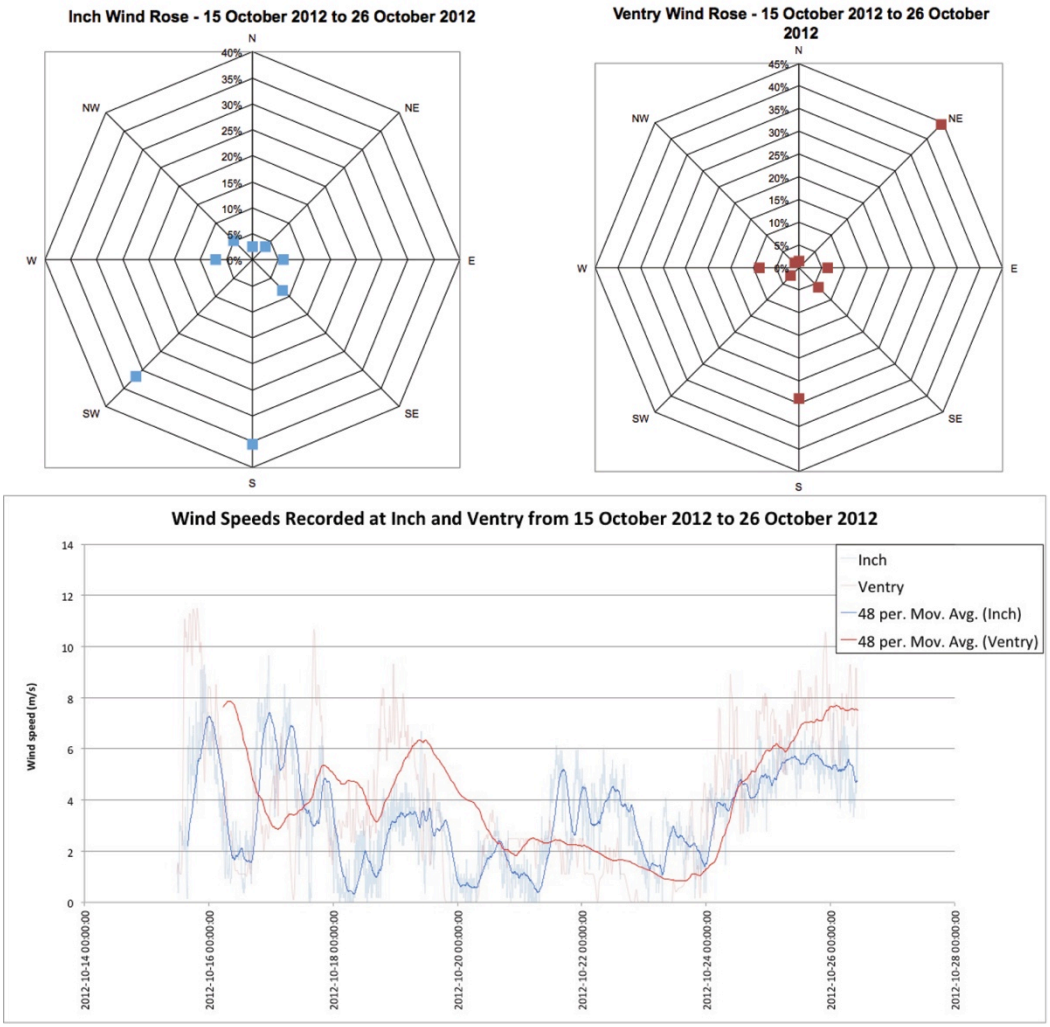

Figure 8.9 Wind roses and wind speeds for Inch and Ventry from 15 October 2012 to 26 October 2012. Wind speeds were derived from instantaneous wind speeds averaged at half hourly (or approximately half hourly) intervals. Running means (with 48 hour periods) have been superimposed on the wind speed graph for visual clarity.

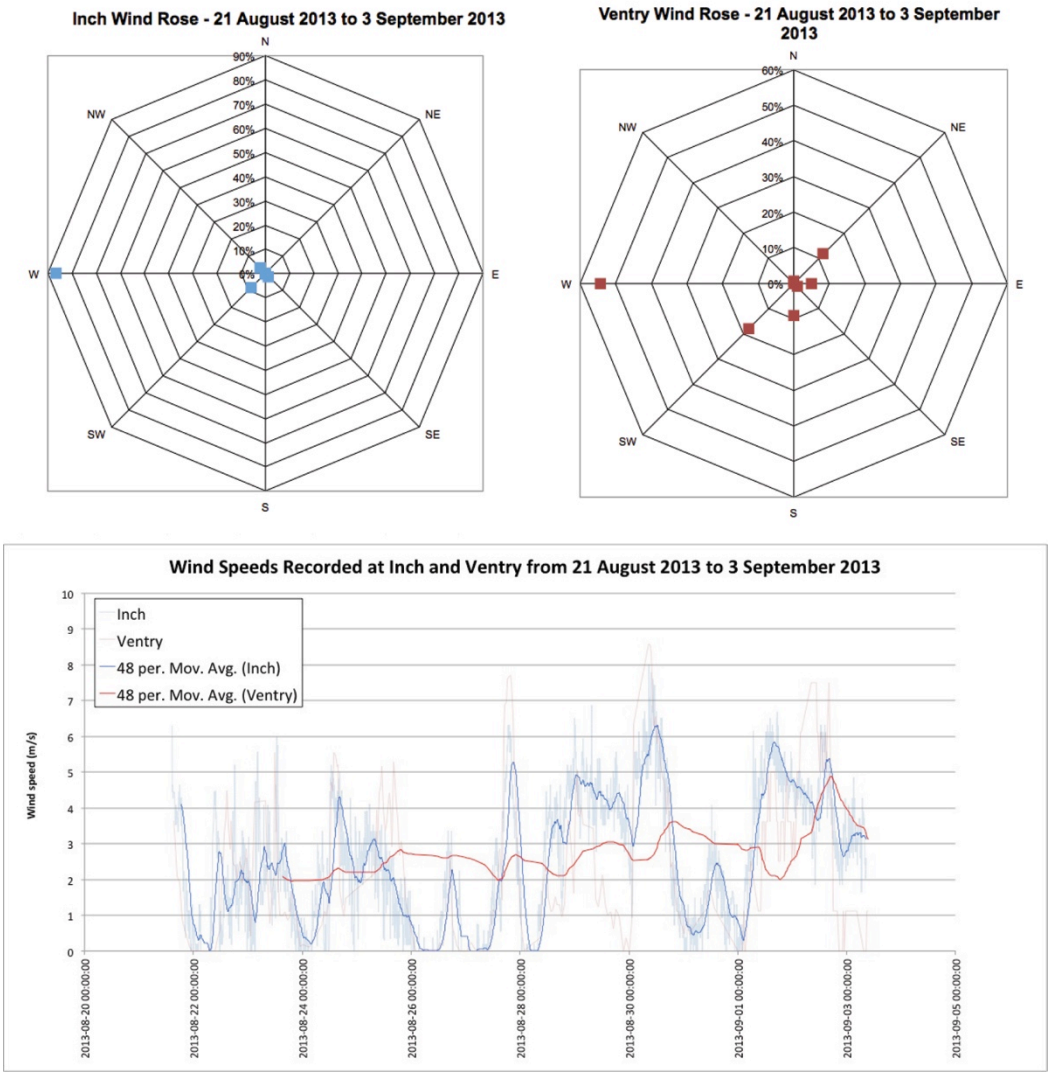

Figure 8.10 Wind roses and wind speeds for Inch and Ventry from 21 August 2013 to 3 September 2013. Wind speeds were derived from instantaneous wind speeds averaged at half hourly (or approximately half hourly) intervals. Running means (with 48 hour periods) have been superimposed on the wind speed graph for visual clarity.

Table 8.2 Summary of event information extracted from Ventry weather station data.

Event ID	Start date	End date	Mean wind speed (m/s)	Max Gust Speed (m/s)	Wind directions recorded during event								Prevailing Wind Direction
					N	NE	E	SE	S	SW	W	NW	
55	2012-05-22 14:00:00	2012-05-23 08:00:00	3.82	5.22	0	0	0	0	48	0	0	0	S
56	2012-06-15 06:00:00	2012-06-16 06:00:00	3.51	9.07	0	3	13	7	1	2	26	1	W
57	2012-07-16 01:00:00	2012-07-16 18:00:00	9.16	11.54	0	0	0	0	0	11	35	0	W
58	2012-07-31 13:00:00	2012-08-02 08:00:00	4.75	10.01	0	0	0	0	9	73	29	0	SW
59	2012-08-02 11:00:00	2012-08-03 21:00:00	2.71	5.60	0	4	1	0	11	65	0	0	SW
60	2012-08-15 20:00:00	2012-08-16 19:00:00	5.18	12.13	0	0	0	0	11	45	2	0	SW
61	2012-08-27 08:00:00	2012-08-28 04:00:00	5.82	8.43	0	0	0	0	0	10	41	0	W
62	2012-08-28 10:00:00	2012-08-29 20:00:00	5.94	12.12	0	0	0	1	4	66	20	0	SW
63	2012-09-09 12:00:00	2012-09-10 01:00:00	4.75	6.84	0	0	0	0	0	12	20	0	W
64	2012-09-30 03:00:00	2012-09-30 17:00:00	7.00	10.19	0	0	0	0	0	21	16	0	SW
65	2012-10-02 01:00:00	2012-10-03 07:00:00	7.43	10.70	0	0	0	0	0	26	54	0	W
66	2012-10-17 01:00:00	2012-10-17 20:00:00	5.41	10.65	0	30	14	1	0	0	0	0	NE
67	2012-10-20 18:00:00	2012-10-22 11:00:00	2.06	2.87	0	0	1	7	90	0	0	0	S
68	2012-11-12 12:00:00	2012-11-14 19:00:00	3.98	9.29	0	2	1	0	4	90	3	0	SW
69	2012-11-18 13:00:00	2012-11-23 18:00:00	0.78	2.20	0	0	0	0	1	0	0	0	S
70	2012-11-25 02:00:00	2012-11-25 19:00:00	n/a										
71	2012-12-02 15:00:00	2012-12-03 09:00:00	5.25	7.61	0	0	0	0	0	10	34	2	W
72	2012-12-03 17:00:00	2012-12-04 12:00:00	5.20	6.45	0	0	0	0	3	15	31	2	W
73	2012-12-13 05:00:00	2012-12-13 19:00:00	6.66	8.07	0	0	0	0	28	0	0	0	S
74	2012-12-14 02:00:00	2012-12-18 05:00:00	5.18	9.30	0	0	0	1	3	90	78	9	SW
75	2012-12-19 10:00:00	2013-01-01 06:00:00	4.92	11.43	0	0	0	2	57	232	140	0	SW
76	2013-01-03 03:00:00	2013-01-09 05:00:00	3.77	6.45	0	0	2	0	24	43	19	0	SW
77	2013-01-09 21:00:00	2013-01-12 18:00:00	4.50	7.81	0	15	2	4	39	8	20	0	S
78	2013-01-17 21:00:00	2013-01-18 21:00:00	2.94	4.89	0	2	4	1	4	0	13	0	W
79	2013-01-20 17:00:00	2013-01-23 06:00:00	1.92	5.97	0	6	2	5	10	7	18	0	W
80	2013-01-24 22:00:00	2013-01-25 19:00:00	4.96	6.71	0	0	1	3	17	12	4	0	S
81	2013-01-26 01:00:00	2013-02-01 11:00:00	7.36	18.79	0	0	0	1	3	132	116	1	SW
82	2013-02-04 13:00:00	2013-02-06 03:00:00	8.10	11.02	0	1	6	13	24	12	31	0	W
83	2013-02-10 12:00:00	2013-02-11 08:00:00	5.35	10.11	0	0	2	12	13	5	9	0	S
84	2013-02-13 05:00:00	2013-02-14 12:00:00	6.47	11.23	0	0	0	0	0	20	32	1	W
85	2013-02-18 22:00:00	2013-02-19 16:00:00	4.60	6.23	0	0	0	0	30	0	0	0	S
86	2013-02-22 18:00:00	2013-02-23 17:00:00	2.16	4.03	0	2	15	6	11	0	0	0	E
87	2013-02-26 01:00:00	2013-02-26 21:00:00	1.17	3.14	5	3	4	0	10	1	0	0	S
88	2013-03-22 22:00:00	2013-03-23 13:00:00	5.31	6.55	0	0	0	0	34	0	0	0	S

Event ID	Start date	End date	Mean wind speed (m/s)	Max Gust Speed (m/s)	Wind directions recorded during event								Prevailing Wind Direction
					N	NE	E	SE	S	SW	W	NW	
90	2013-04-09 09:00:00	2013-04-10 19:00:00	2.87	5.86	0	0	0	4	56	2	0	0	S
91	2013-04-13 23:00:00	2013-04-18 21:00:00	6.65	18.96	0	0	0	0	35	185	66	1	SW
92	2013-05-03 13:00:00	2013-05-04 03:00:00	6.58	10.27	0	0	0	0	0	25	11	1	SW
93	2013-05-08 08:00:00	2013-05-09 19:00:00	9.09	15.53	0	0	0	0	1	36	48	0	W
94	2013-06-12 19:00:00	2013-06-13 21:00:00	3.42	8.09	0	2	4	3	3	18	21	0	W
95	2013-06-14 03:00:00	2013-06-15 21:00:00	5.74	8.66	0	0	0	0	5	24	77	0	W
96	2013-06-21 16:00:00	2013-06-23 05:00:00	6.44	11.62	0	0	0	0	8	28	57	0	W
97	2013-08-17 03:00:00	2013-08-17 17:00:00	7.10	8.22	0	0	0	0	0	3	14	0	W
98	2013-10-16 10:00:00	2013-10-18 06:00:00	3.75	7.00	0	0	0	0	7	32	11	0	SW
99	2013-10-19 23:00:00	2013-10-20 21:00:00	3.05	4.78	0	0	2	2	2	4	12	0	W
100	2013-10-22 20:00:00	2013-10-23 20:00:00	2.06	3.90	0	1	4	1	2	2	8	0	W
101	2013-10-26 05:00:00	2013-11-01 06:00:00	4.77	11.68	0	0	0	0	3	71	133	14	W
102	2013-11-02 01:00:00	2013-11-03 07:00:00	5.41	11.93	0	0	0	0	5	9	35	3	W
103	2013-11-03 13:00:00	2013-11-05 22:00:00	2.78	5.39	0	16	3	2	5	0	41	8	W
104	2013-11-06 01:00:00	2013-11-08 10:00:00	3.23	6.77	0	0	0	1	3	5	61	3	W
105	2013-11-09 16:00:00	2013-11-12 03:00:00	3.37	7.10	0	12	1	1	7	11	21	1	W
106	2013-12-09 18:00:00	2013-12-10 15:00:00	5.11	6.03	0	0	0	0	16	21	0	0	SW
107	2013-12-11 20:00:00	2013-12-12 17:00:00	4.97	6.27	0	0	0	0	0	38	0	0	SW
108	2013-12-13 06:00:00	2014-01-08 15:00:00	6.14	20.38	0	9	12	8	62	586	319	1	SW
109	2014-01-10 01:00:00	2014-01-10 15:00:00	3.84	5.88	0	0	0	0	0	8	14	0	W
110	2014-01-12 13:00:00	2014-01-17 08:00:00	5.54	11.03	0	0	1	1	6	113	53	3	SW
111	2014-01-17 14:00:00	2014-01-18 09:00:00	1.96	4.26	0	0	2	2	5	3	8	0	W
112	2014-01-21 15:00:00	2014-01-22 21:00:00	6.63	10.86	0	0	0	0	0	14	38	0	W
113	2014-01-23 22:00:00	2014-01-28 11:00:00	10.68	18.24	0	0	0	1	2	36	152	0	W
114	2014-01-31 04:00:00	2014-02-04 17:00:00	9.64	23.46	0	0	0	2	38	59	84	0	W
115	2014-02-04 19:00:00	2014-02-06 14:00:00	7.09	16.02	0	0	2	2	13	2	43	1	W
116	2014-02-07 04:00:00	2014-02-10 10:00:00	10.30	18.89	0	1	1	4	14	49	63	0	W
117	2014-02-10 16:00:00	2014-02-16 07:00:00	8.10	28.35	0	0	0	10	31	34	67	0	W
118	2014-02-16 12:00:00	2014-02-18 22:00:00	3.15	7.50	0	4	0	1	25	12	20	3	S
119	2014-02-19 15:00:00	2014-03-01 06:00:00	7.65	15.10	0	0	1	5	31	172	189	1	W
120	2014-03-02 04:00:00	2014-03-06 00:00:00	5.11	10.56	0	4	3	6	12	65	49	0	SW
121	2014-03-06 03:00:00	2014-03-07 06:00:00	5.18	8.13	0	0	0	0	8	24	11	0	SW
122	2014-03-07 23:00:00	2014-03-09 19:00:00	5.28	10.90	0	21	2	0	20	19	7	0	NE
123	2014-03-19 13:00:00	2014-03-22 22:00:00	7.61	13.77	0	0	0	0	3	58	81	0	W

Event ID	Start date	End date	Mean wind speed (m/s)	Max Gust Speed (m/s)	Wind directions recorded during event								Prevailing Wind Direction
					N	NE	E	SE	S	SW	W	NW	
90	2013-04-09 09:00:00	2013-04-10 19:00:00	2.87	5.86	0	0	0	4	56	2	0	0	S
125	2014-04-05 19:00:00	2014-04-08 02:00:00	6.41	11.48	0	0	0	0	6	52	24	0	SW
126	2014-04-23 06:00:00	2014-04-24 04:00:00	3.36	6.07	0	0	0	0	11	23	0	0	SW
127	2014-04-25 21:00:00	2014-04-26 14:00:00	8.24	15.16	0	14	8	7	0	0	0	0	NE

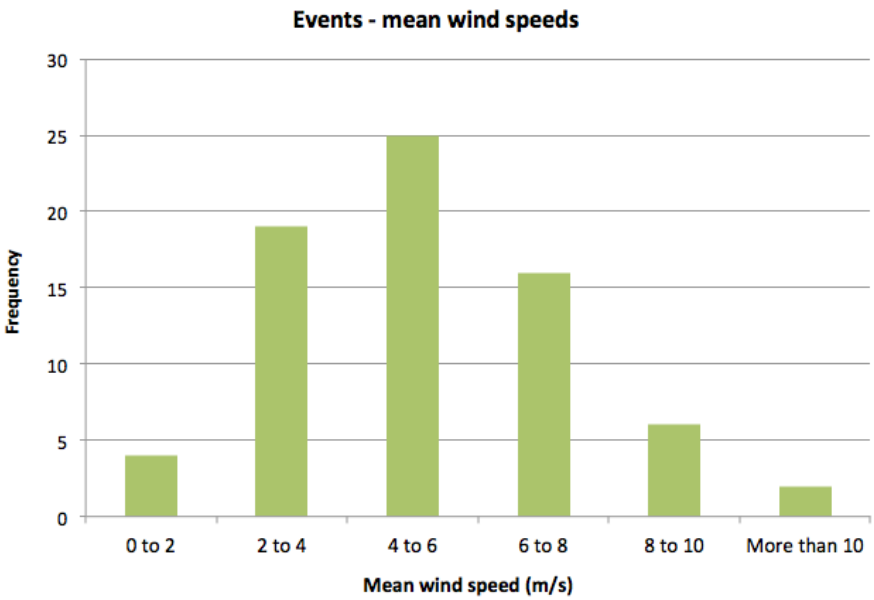

Figure 8.11 Histogram showing frequency of storm events with a range of mean wind speeds.

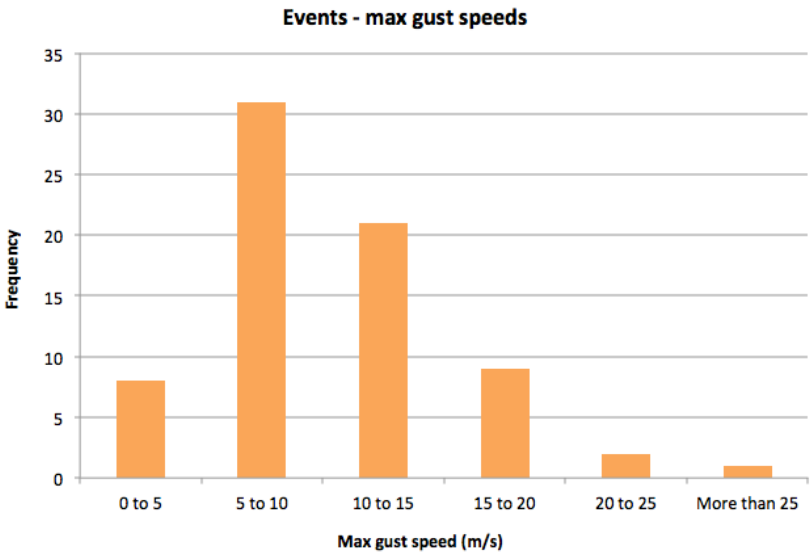

Figure 8.12 Histogram showing frequency of storm events with a range of maximum gust speeds.

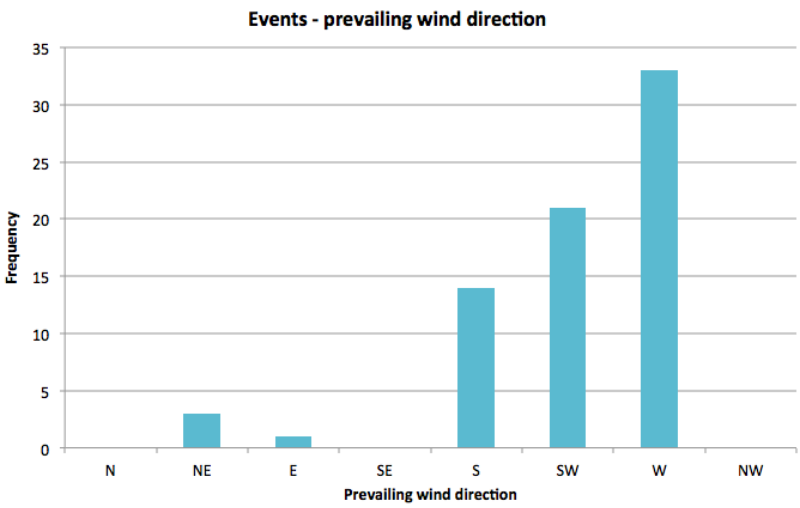

Figure 8.13 Frequency of events with prevailing wind directions from the north, northeast, east, southeast, south, southwest, west, and northwest.

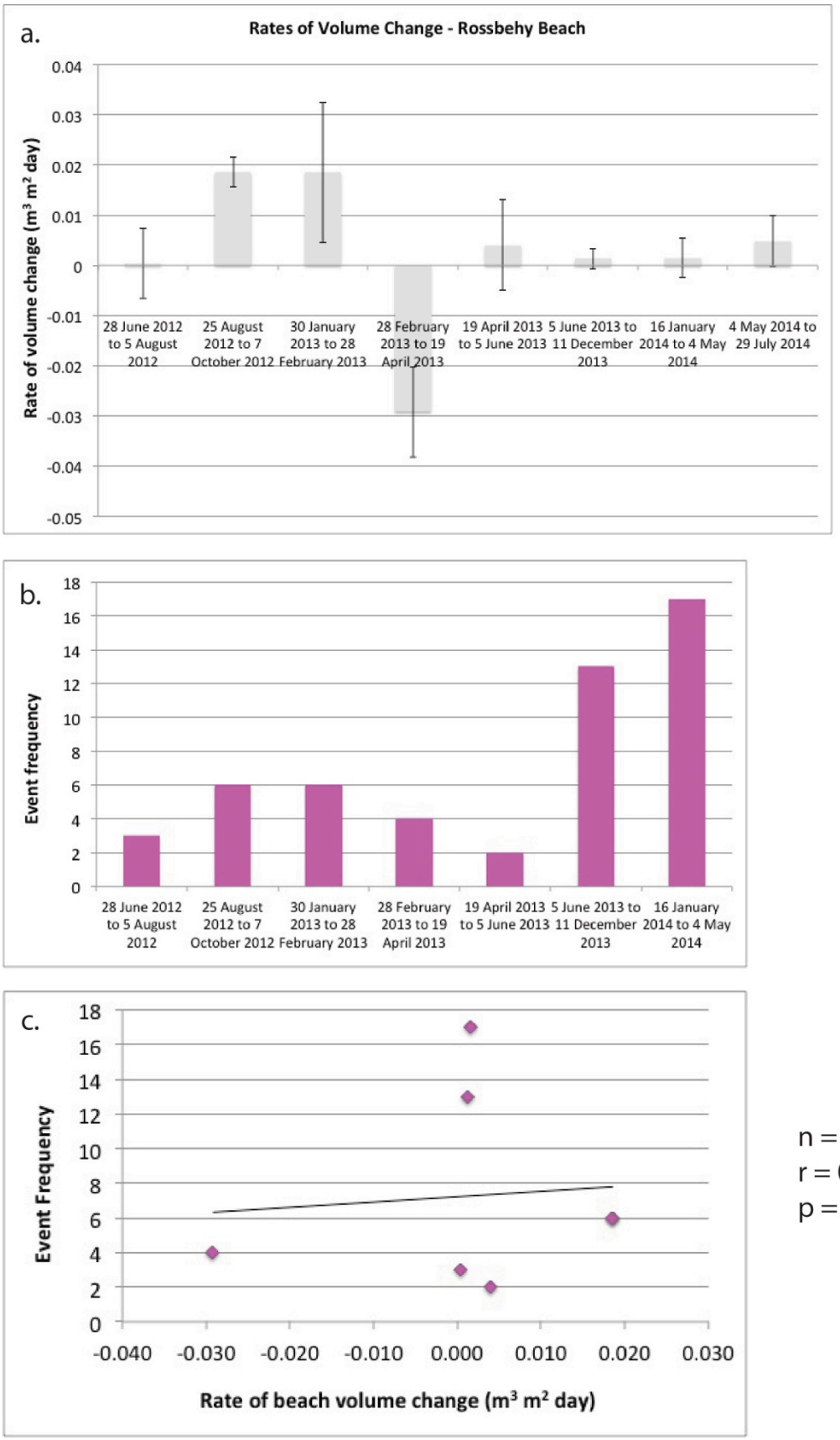

Figure 8.14 (a.) Rates of volume change at Rossbehy beach broken down by morphological monitoring period. (b.) Event frequency for storm events occurring during corresponding morphological monitoring periods. (c.) There was a very weak positive relationship between rate of beach volume change and event frequency (n=7, r=0.09). This relationship was not statistically significant (p=0.85). Negative rates of beach volume change are associated with net volume losses; positive rates of beach volume change are associated with net volume gains.

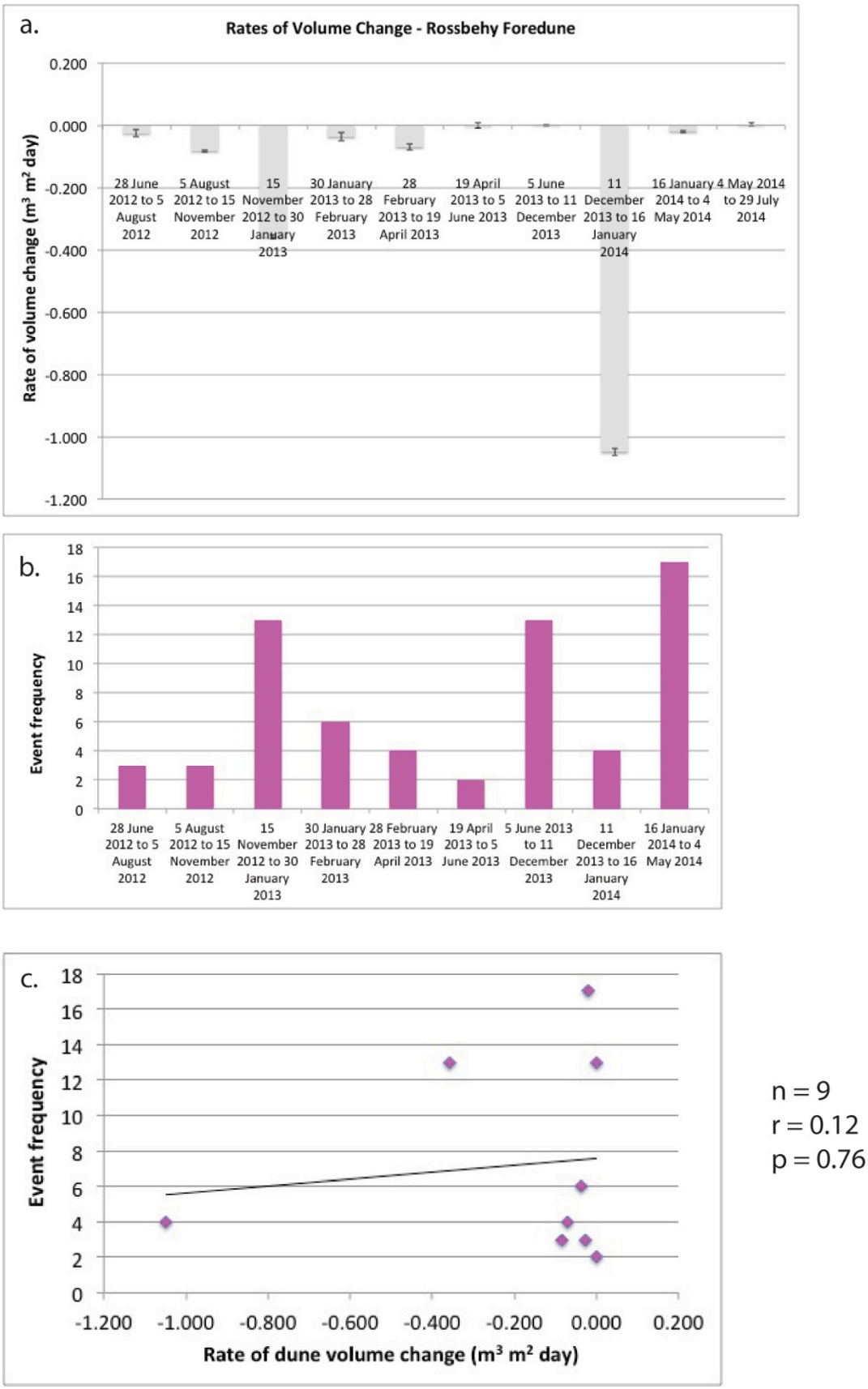

Figure 8.15 (a.) Rates of foredune volume change at Rossbehy broken down by morphological monitoring period. (b.) Event frequency for storm events occurring during corresponding morphological monitoring periods. (c.) There was a very weak positive relationship between rate of foredune volume change and event frequency (n=9, r=0.12). This relationship was not statistically significant (p=0.76). Negative rates of dune volume change are associated with net volume losses; positive rates of dune volume change are associated with net volume gains.

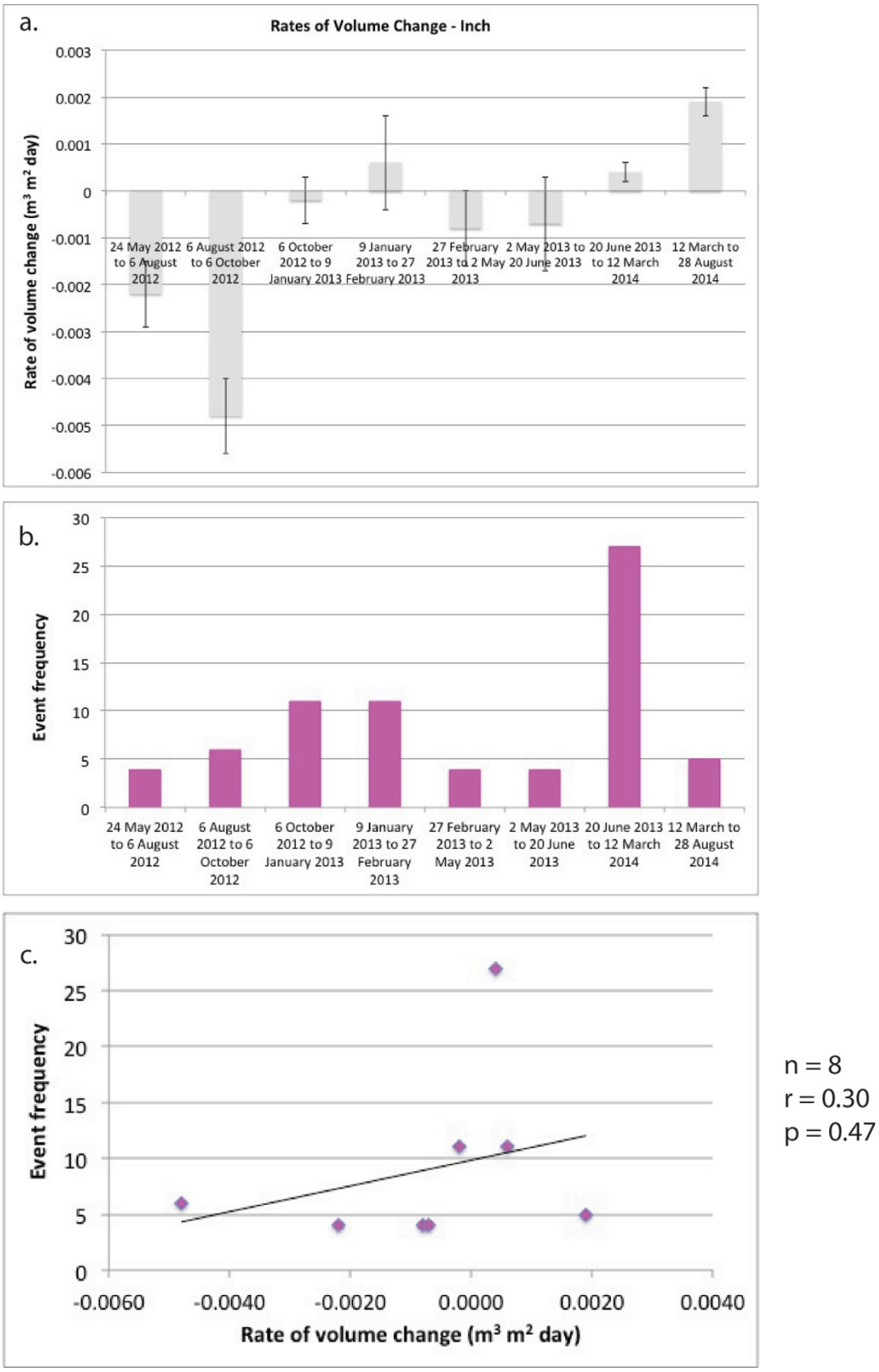

Figure 8.16 (a.) Rates of volume change at Inch broken down by morphological monitoring period. (b.) Event frequency for storm events occurring during corresponding morphological monitoring periods. (c.) There was a weak positive relationship between rate of volume change and event frequency (n=8, r=0.3). This relationship was not statistically significant (p=0.47). Negative rates of volume change are associated with net volume losses; positive rates of volume change are associated with net volume gains.

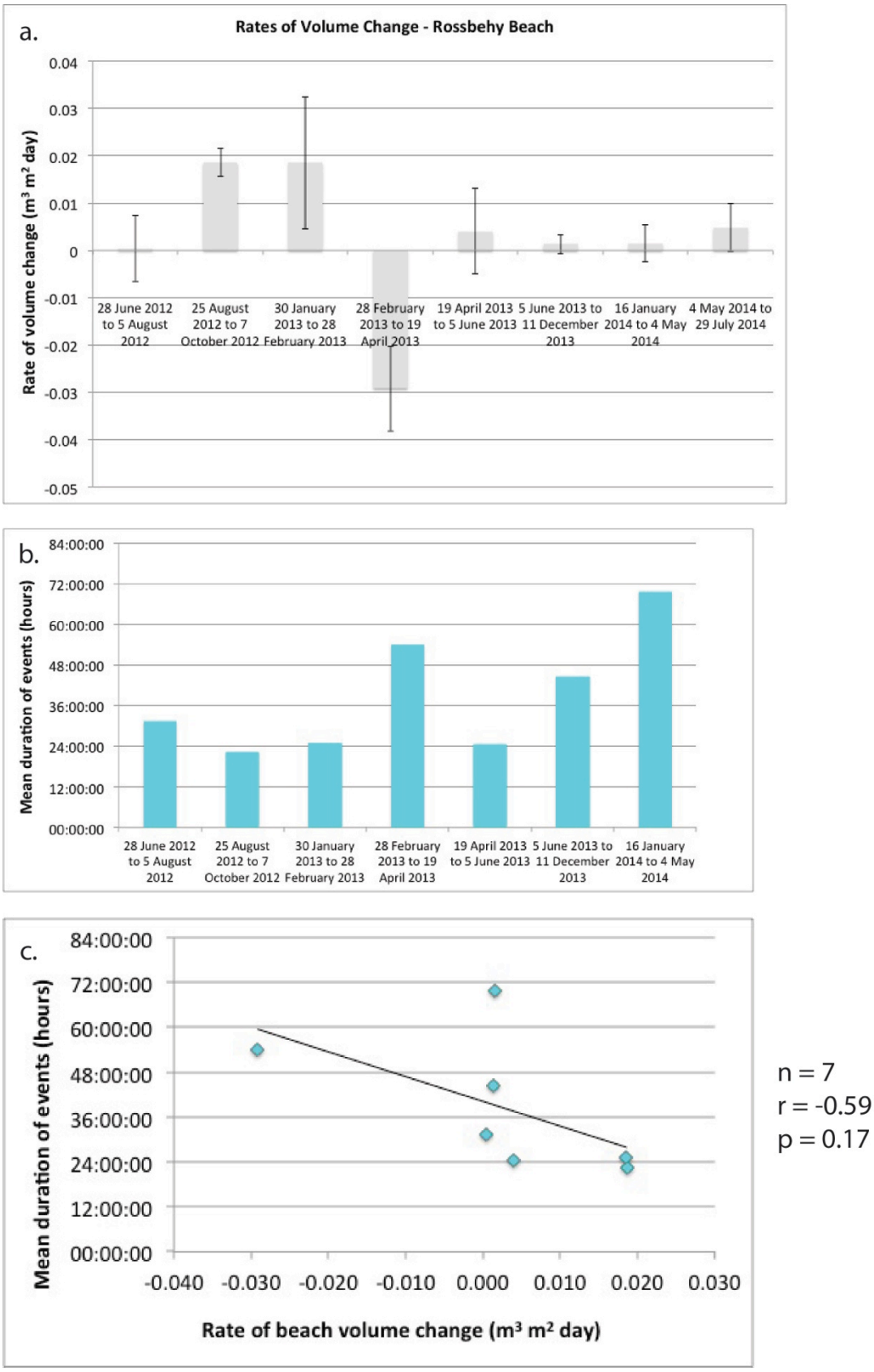

Figure 8.17 (a.) Rates of volume change at Rossbehy beach broken down by morphological monitoring period. (b.) Mean duration of storm events that occurred during corresponding morphological monitoring periods. (c.) There was a moderate negative relationship between rate of beach volume change and mean duration of events (n=7, r=-0.59). This relationship was not statistically significant (p=0.17). Negative rates of beach volume change are associated with net volume losses; positive rates of beach volume change are associated with net volume gains.

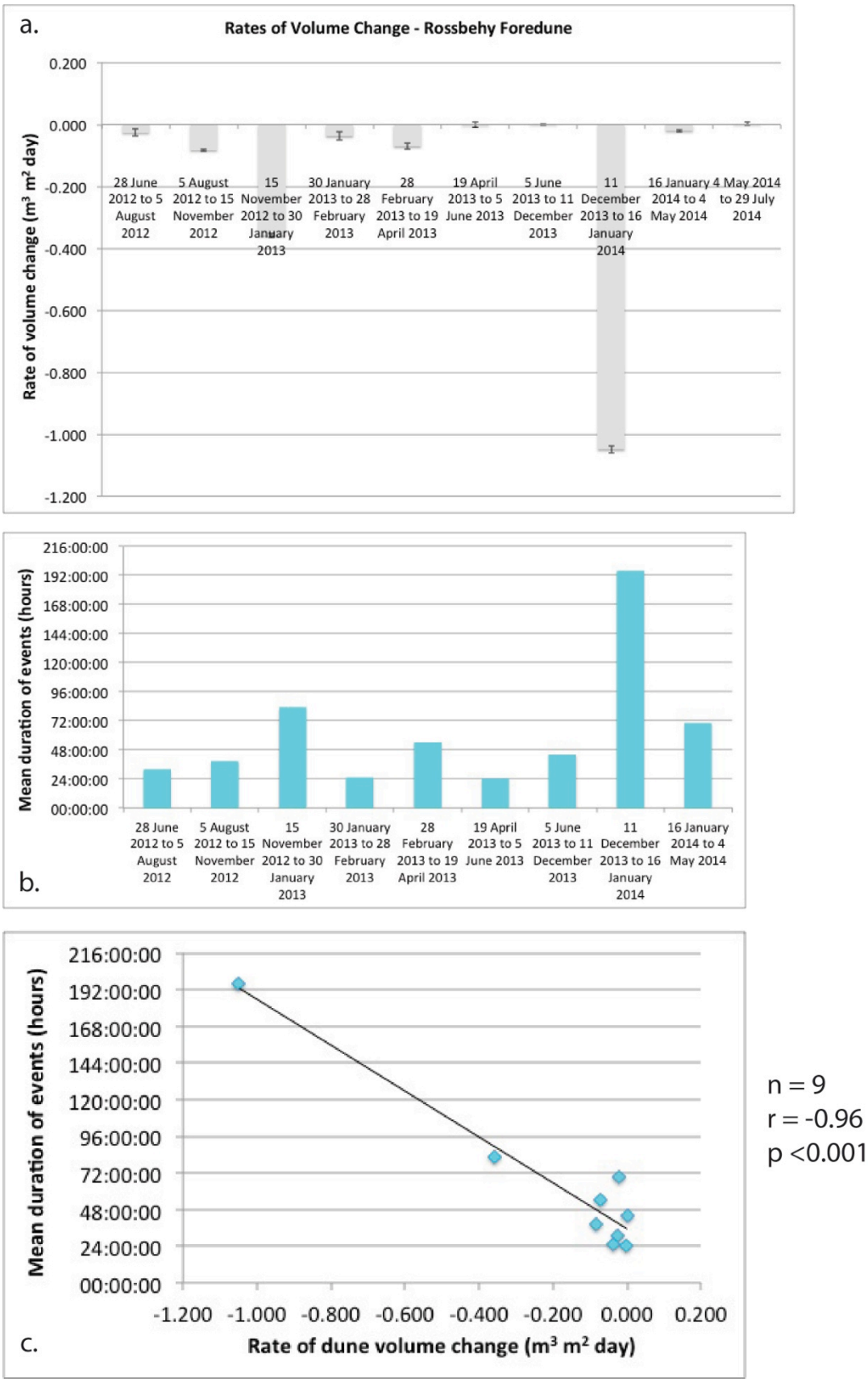

Figure 8.18 (a.) Rates of foredune volume change at Rossbehy broken down by morphological monitoring period. (b.) Mean duration of storm events occurring during corresponding morphological monitoring periods. (c.) There was a very strong negative relationship between rate of foredune volume change and mean duration of events (n=9, r=-0.96). This relationship was statistically significant (p<0.001). Negative rates of dune volume change are associated with net volume losses; positive rates of dune volume change are associated with net volume gains. This result indicates longer duration events are associated with higher rates of dune volume loss.

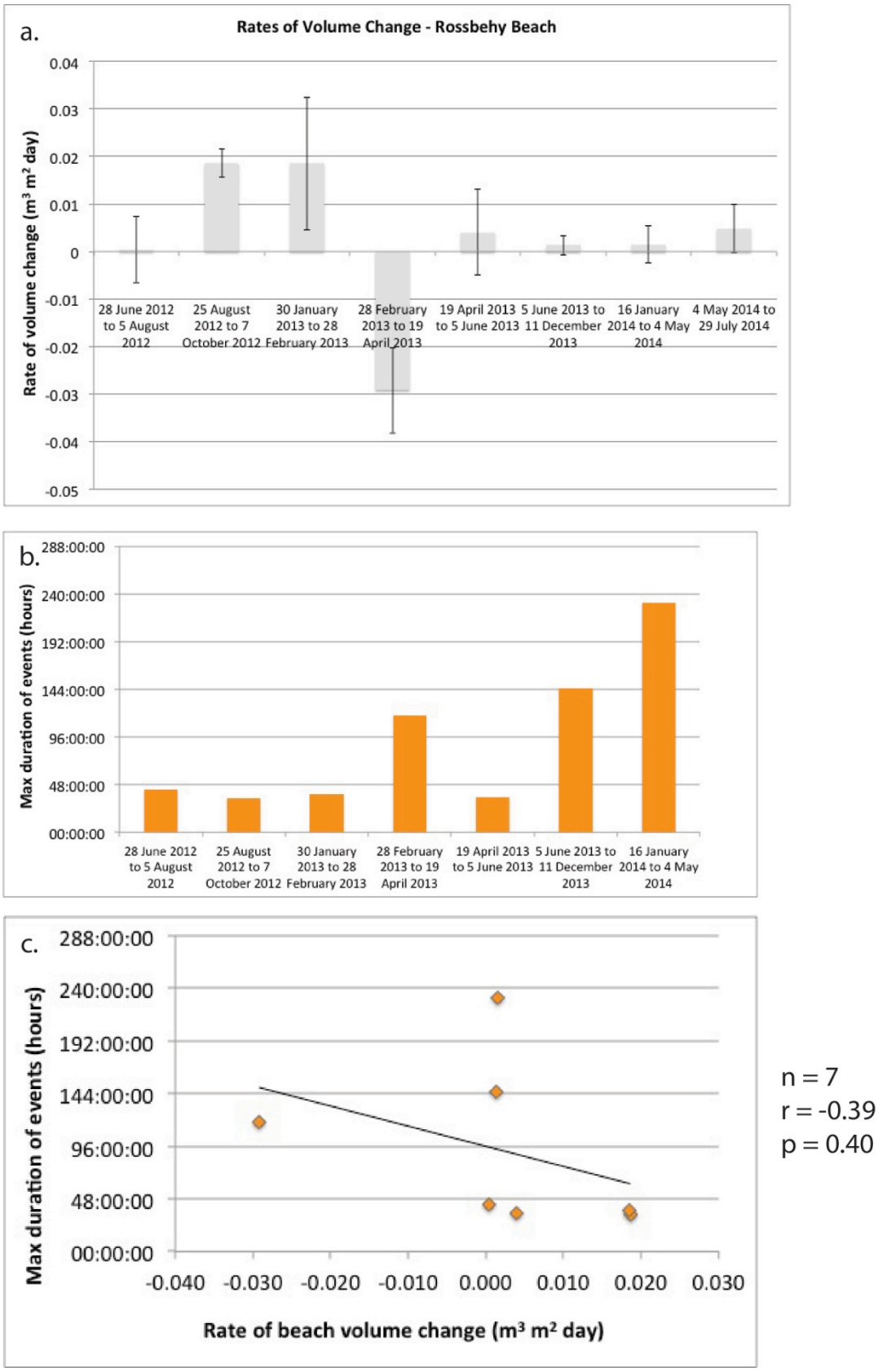

Figure 8.19 (a.) Rates of volume change at Rossbehy beach broken down by morphological monitoring period. (b.) Maximum duration of storm events that occurred during corresponding morphological monitoring periods. (c.) There was a weak negative relationship between rate of beach volume change and max duration of events (n=7, r=-0.39). This relationship was not statistically significant (p=0.40). Negative rates of beach volume change are associated with net volume losses; positive rates of beach volume change are associated with net volume gains.

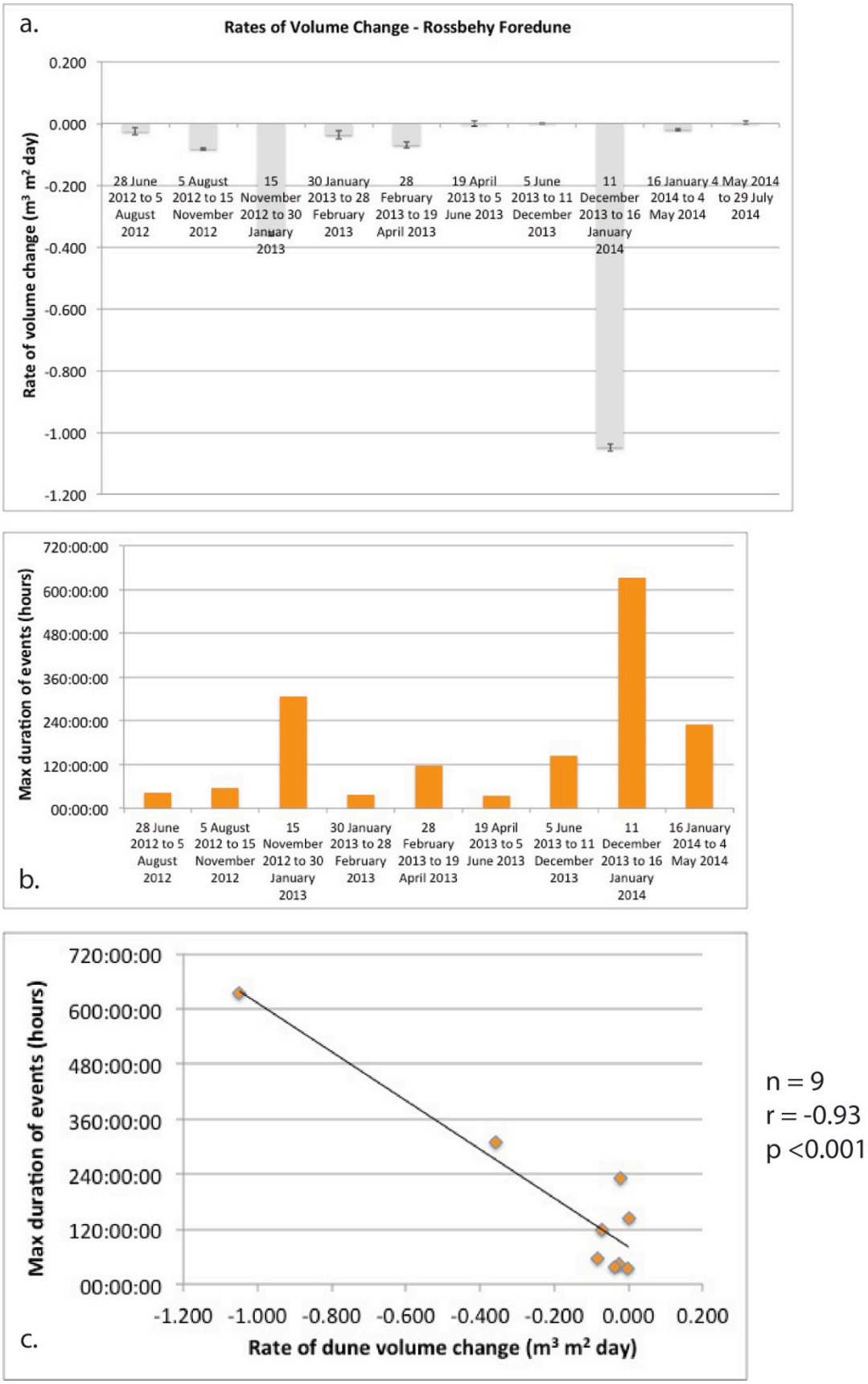

Figure 8.20 (a.) Rates of foredune volume change at Rossbehy broken down by morphological monitoring period. (b.) Maximum durations of storm events occurring during corresponding morphological monitoring periods. (c.) There was a very strong negative relationship between rate of foredune volume change and maximum duration of events (n=9, r=-0.93). This relationship was statistically significant (p<0.001). Negative rates of dune volume change are associated with net volume losses; positive rates of dune volume change are associated with net volume gains. This result indicates longer duration events are associated with higher rates of dune volume loss.

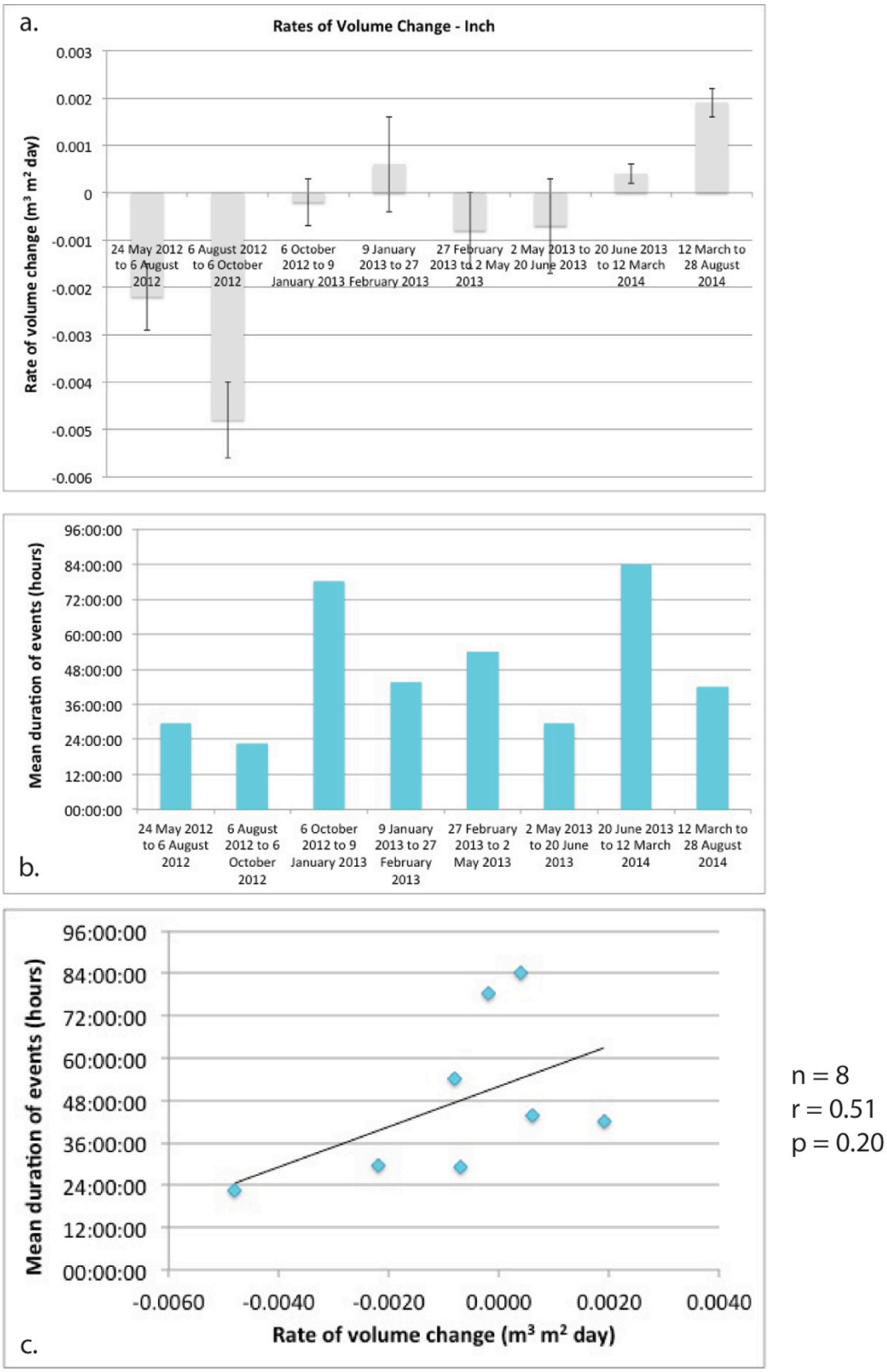

Figure 8.21 (a.) Rates of volume change at Inch broken down by morphological monitoring period. (b.) Mean duration of storm events which occurred during corresponding morphological monitoring periods. (c.) There was a moderate positive relationship between rate of beach volume change and mean duration of events (n=8, r=0.51). This relationship was not statistically significant (p=0.20). Negative rates of volume change are associated with net volume losses; positive rates of volume change are associated with net volume gains.

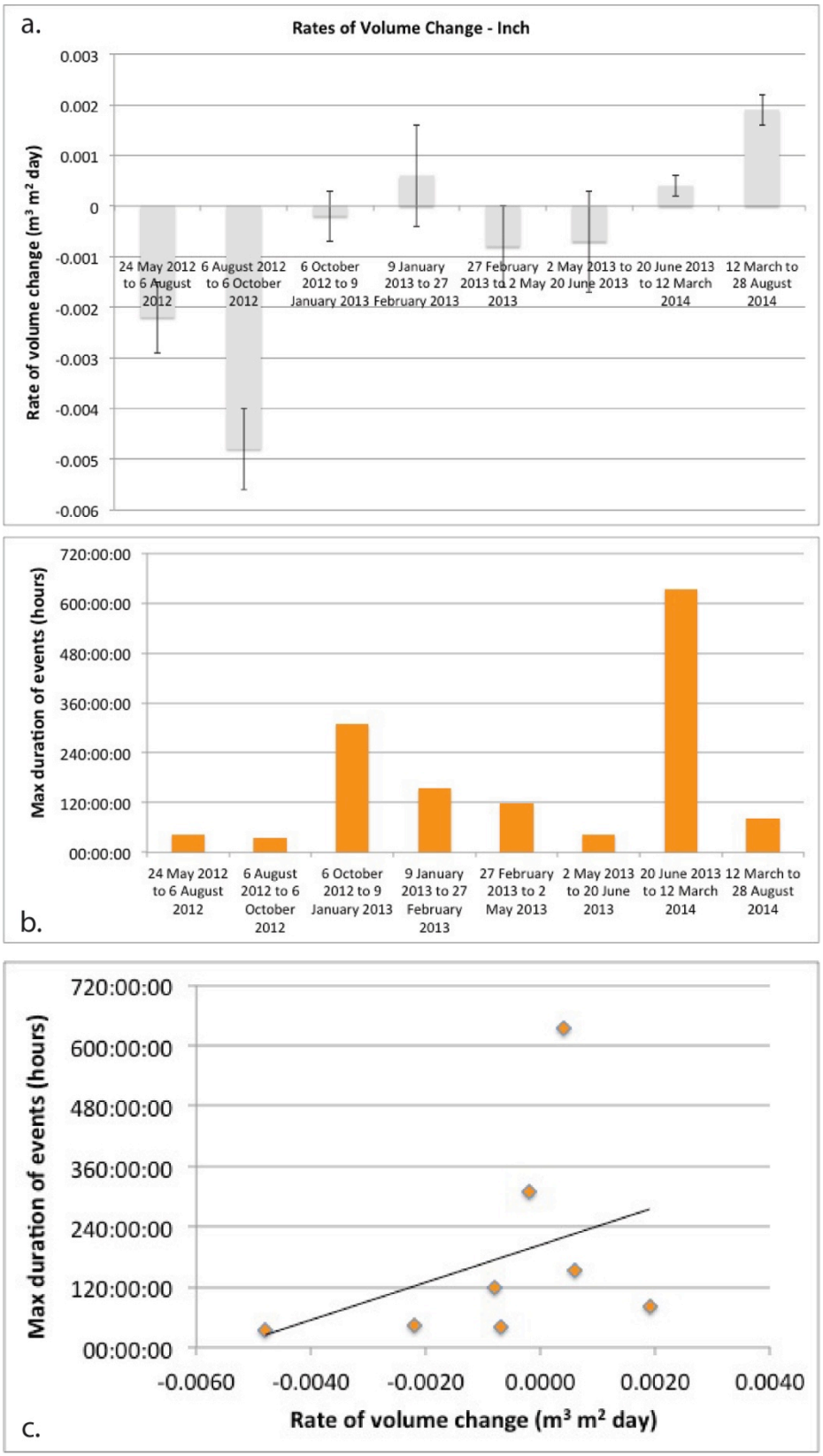

Figure 8.22 (a.) Rates of volume change at Inch broken down by morphological monitoring period. (b.) Maximum duration of storm events which occurred during corresponding morphological monitoring periods. (c.) There was a weak positive relationship between rate of beach volume change and max duration of events (n=8, r=0.37). This relationship was not statistically significant (p=0.37). Negative rates of volume change are associated with net volume losses; positive rates of volume change are associated with net volume gains.

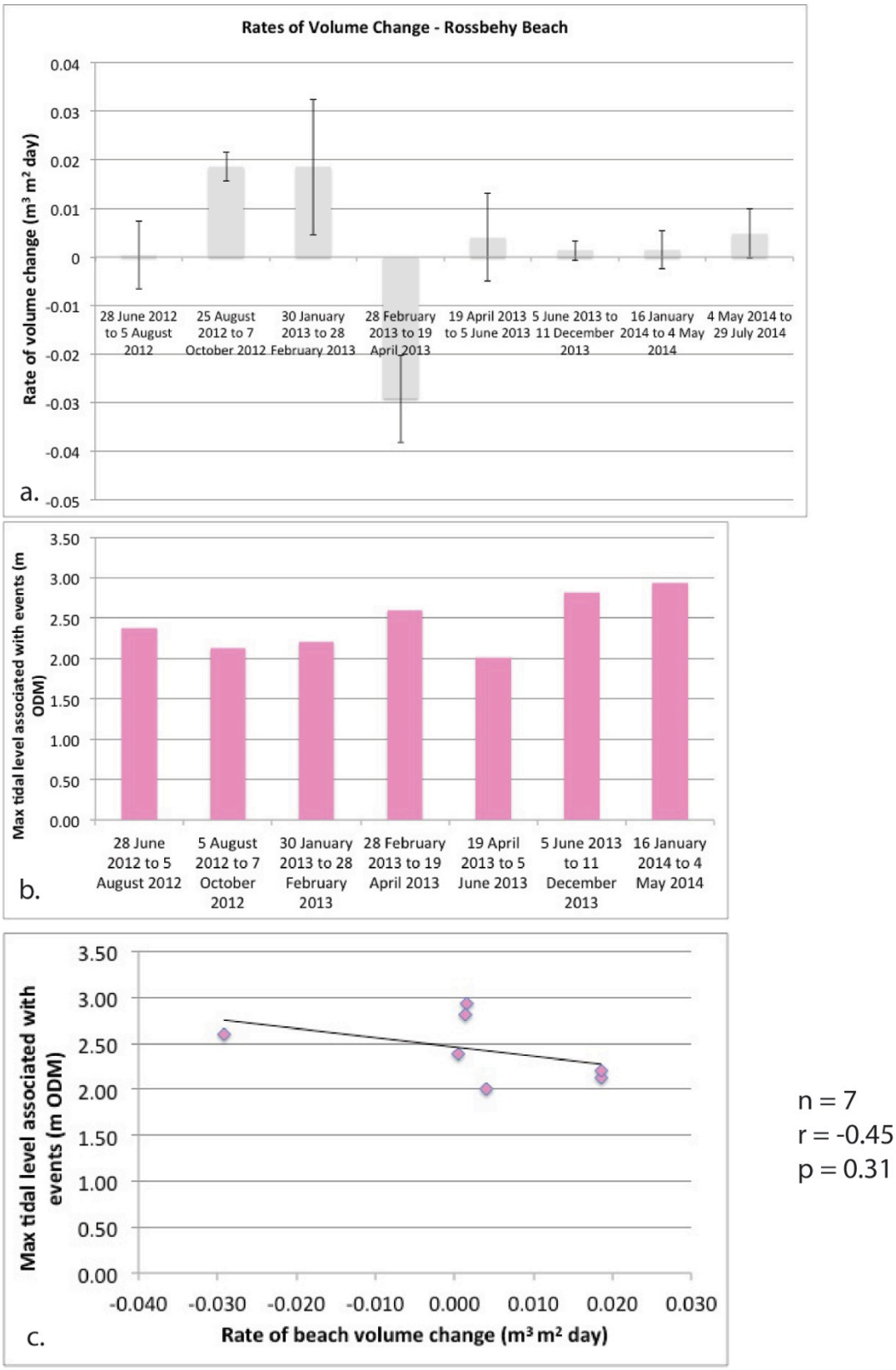

Figure 8.23 (a.) Rates of volume change at Rossbehy beach broken down by morphological monitoring period. (b.) Max tidal level for events that occurred during corresponding morphological monitoring periods. (c.) There was a moderate negative relationship between rate of beach volume change and max tidal levels associated with events (n=7, r=-0.45). This relationship was not statistically significant (p=0.31). Negative rates of beach volume change are associated with net volume losses; positive rates of beach volume change are associated with net volume gains.

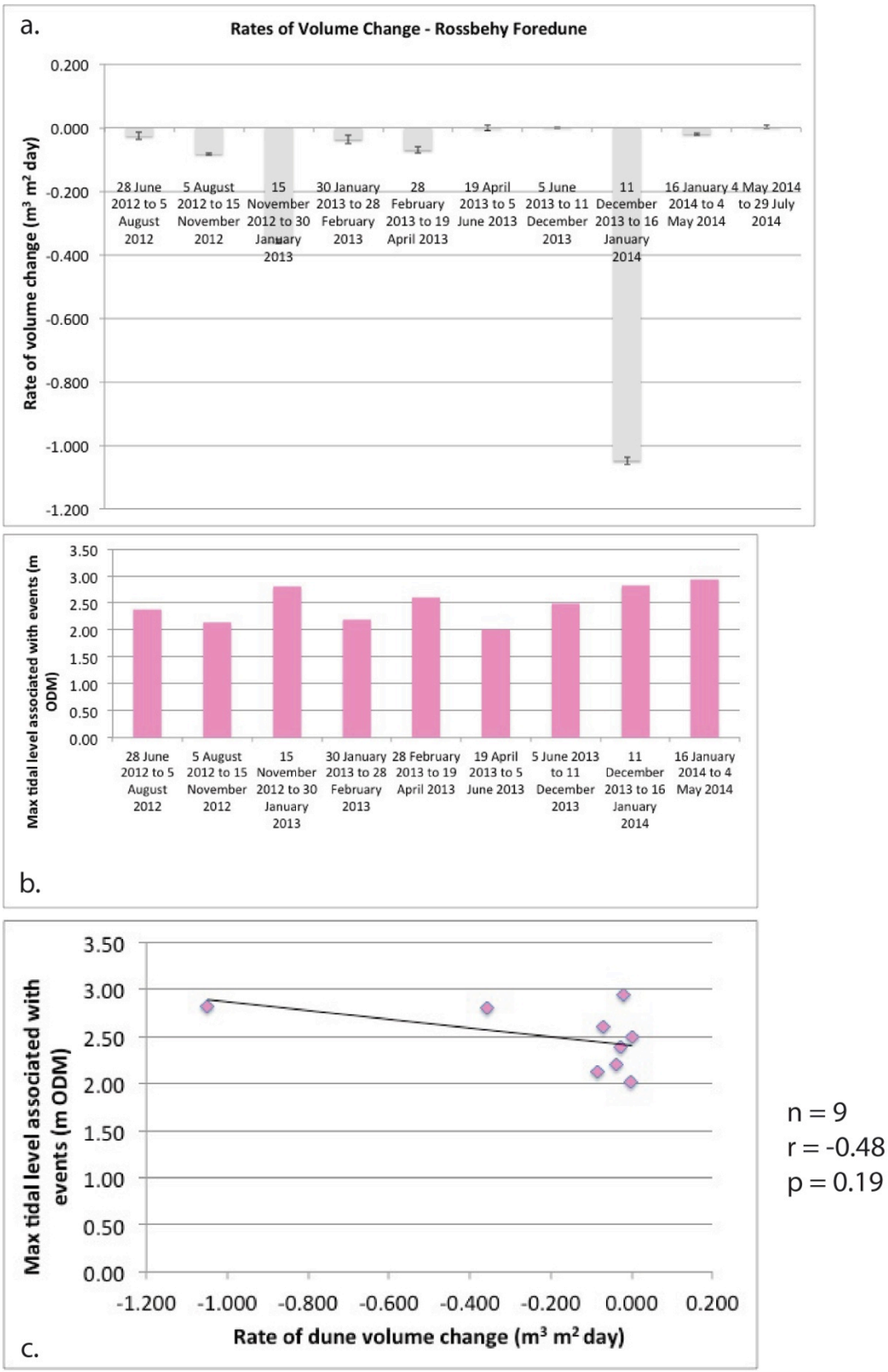

Figure 8.24 (a.) Rates of foredune volume change at Rossbehy broken down by morphological monitoring period. (b.) Maximum tidal levels associated with events that occurred during corresponding morphological monitoring periods. (c.) There was a moderate negative relationship between rate of foredune volume change and max tidal levels associated with events (n=9, r=-0.48). This relationship was not statistically significant (p=0.19). Negative rates of dune volume change are associated with net volume losses; positive rates of dune volume change are associated with net volume gains.

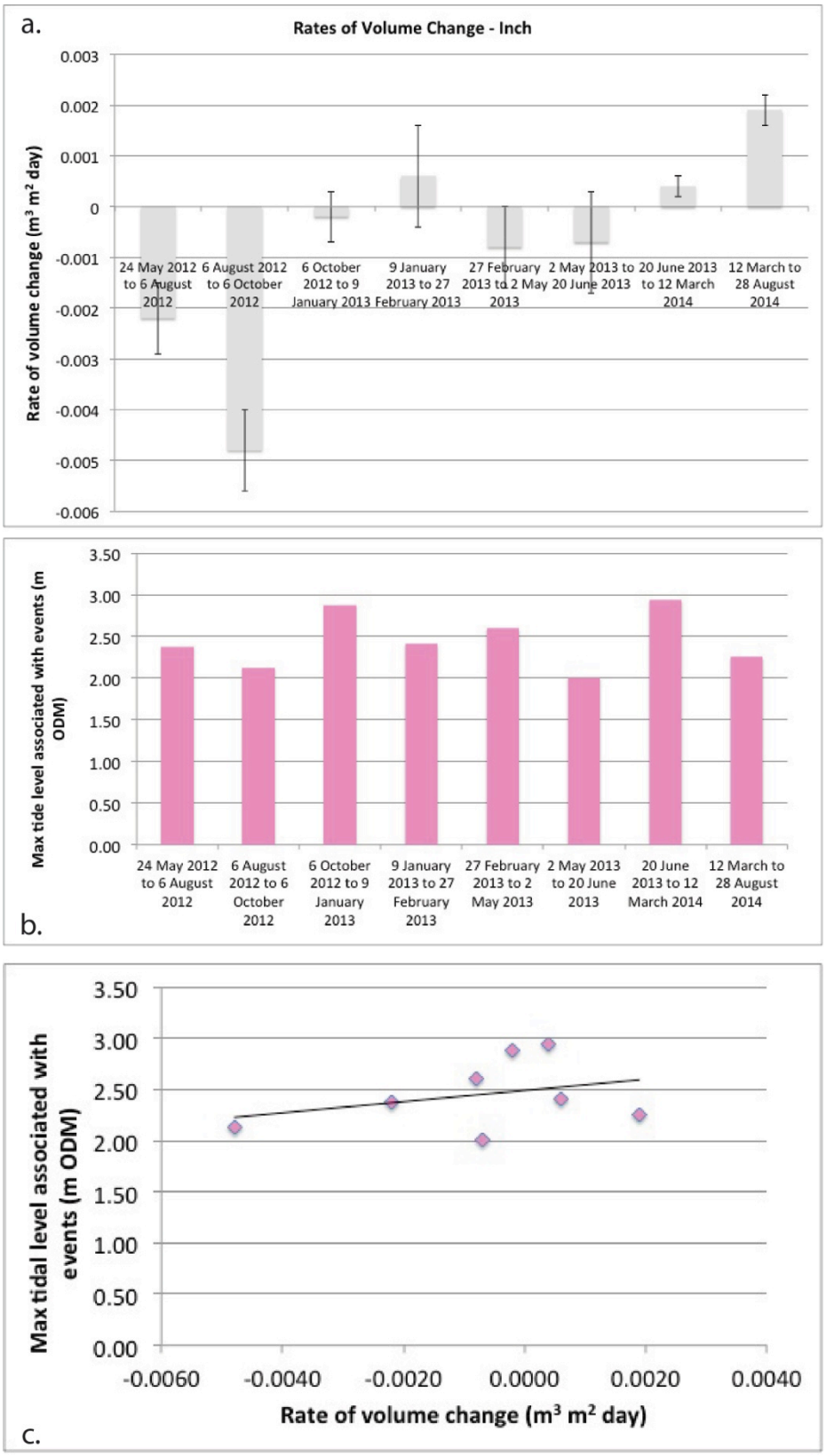

Figure 8.25 (a.) Rates of volume change at Inch broken down by morphological monitoring period. (b.) Max tidal levels associated with storm events that occurred during corresponding morphological monitoring periods. (c.) There was a weak positive relationship between rate of volume change and mean time between events (n=8, r=0.33). This relationship was not statistically significant (p=0.42). Negative rates of volume change are associated with net volume losses; positive rates of volume change are associated with net volume gains.

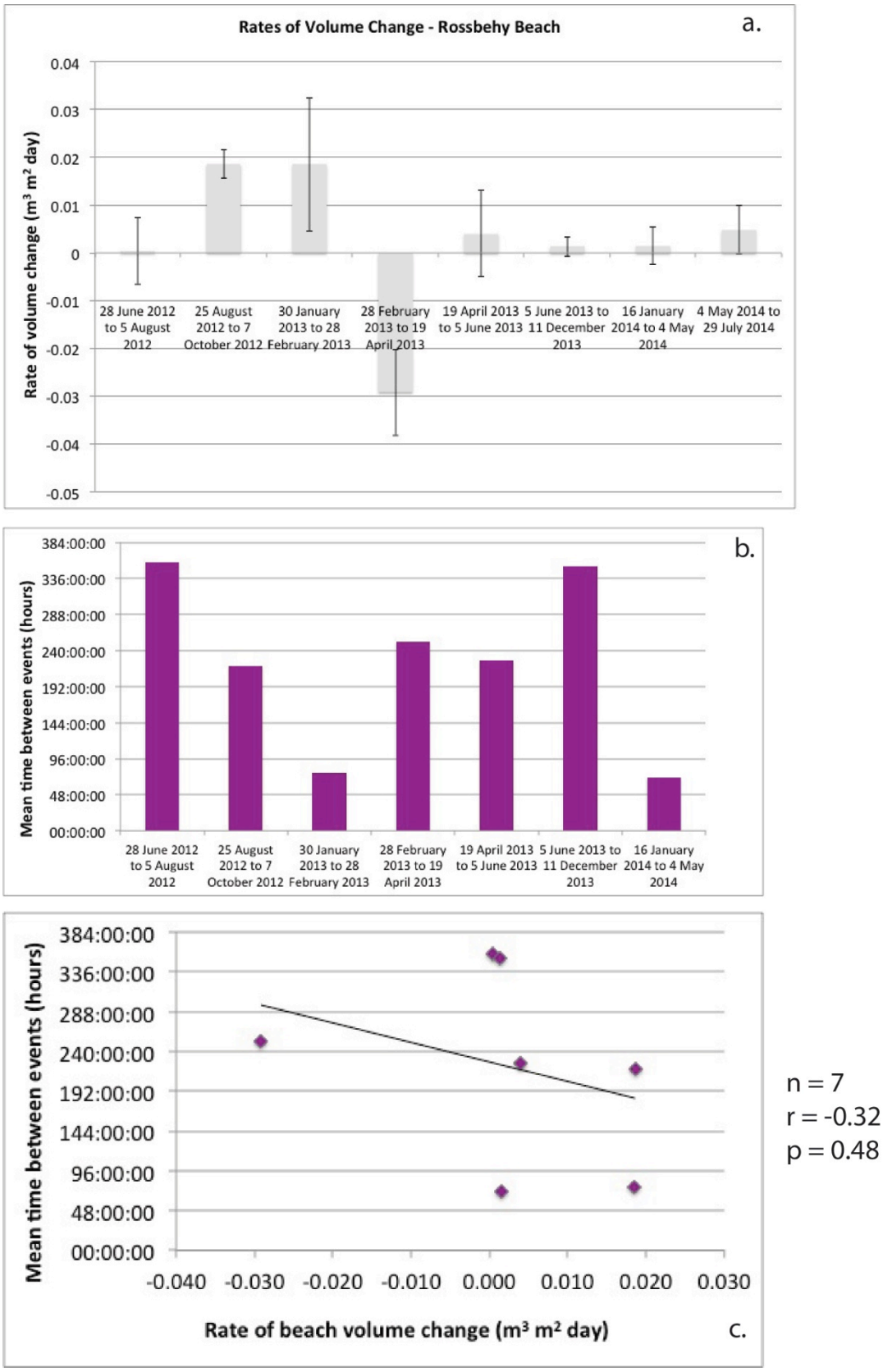

Figure 8.26 (a.) Rates of volume change at Rossbehy beach broken down by morphological monitoring period. (b.) Mean time betwen storm events that occurred during corresponding morphological monitoring periods. (c.) There was a weak negative relationship between rate of beach volume change and mean time between events (n=7, r=-0.32). This relationship was not statistically significant (p=0.48). Negative rates of beach volume change are associated with net volume losses; positive rates of beach volume change are associated with net volume gains.

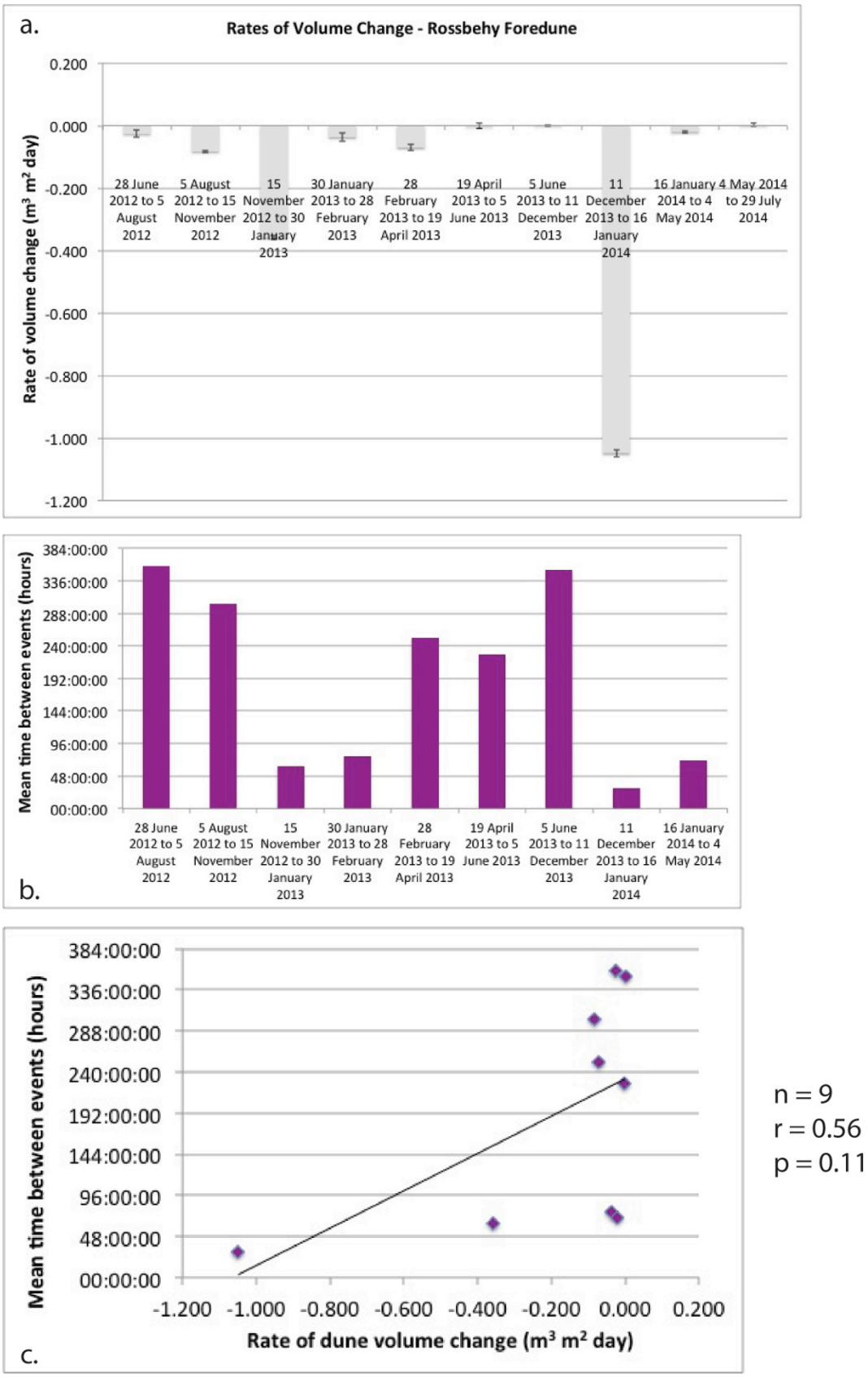

Figure 8.27 (a.) Rates of foredune volume change at Rossbehy broken down by morphological monitoring period. (b.) Mean time between storm events that occurred during corresponding morphological monitoring periods. (c.) There was a moderate positive relationship between rate of foredune volume change and mean time between events (n=9, r=0.56). This relationship was not statistically significant (p=0.11). Negative rates of dune volume change are associated with net volume losses; positive rates of dune volume change are associated with net volume gains.

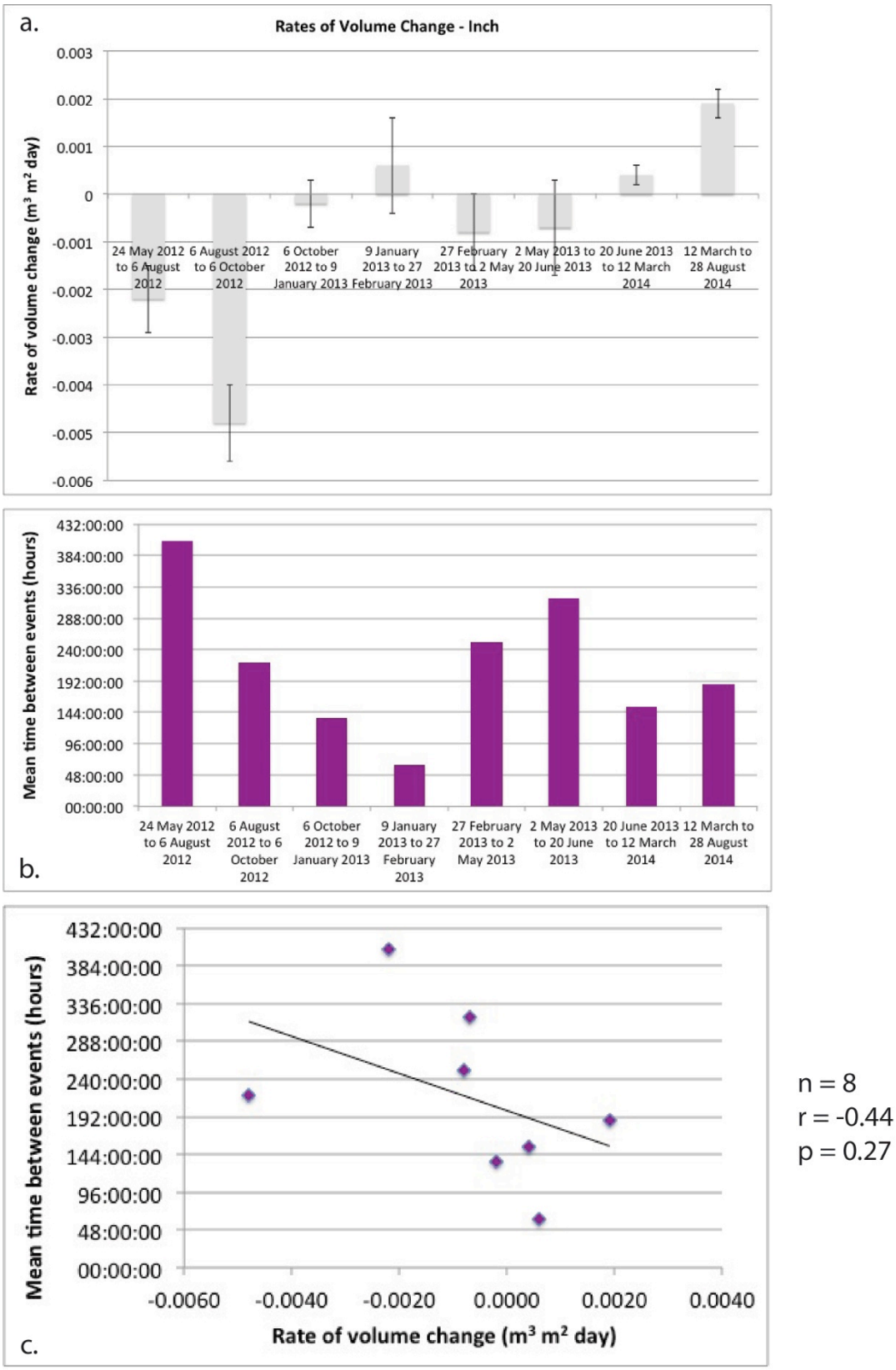

Figure 8.28 (a.) Rates of volume change at Inch broken down by morphological monitoring period. (b.) Mean time between storm events that occurred during corresponding morphological monitoring periods. (c.) There was a moderate negative relationship between rate of volume change and mean time between events (n=8, r=-0.44). This relationship was not statistically significant (p=0.27). Negative rates of volume change are associated with net volume losses; positive rates of volume change are associated with net volume gains.

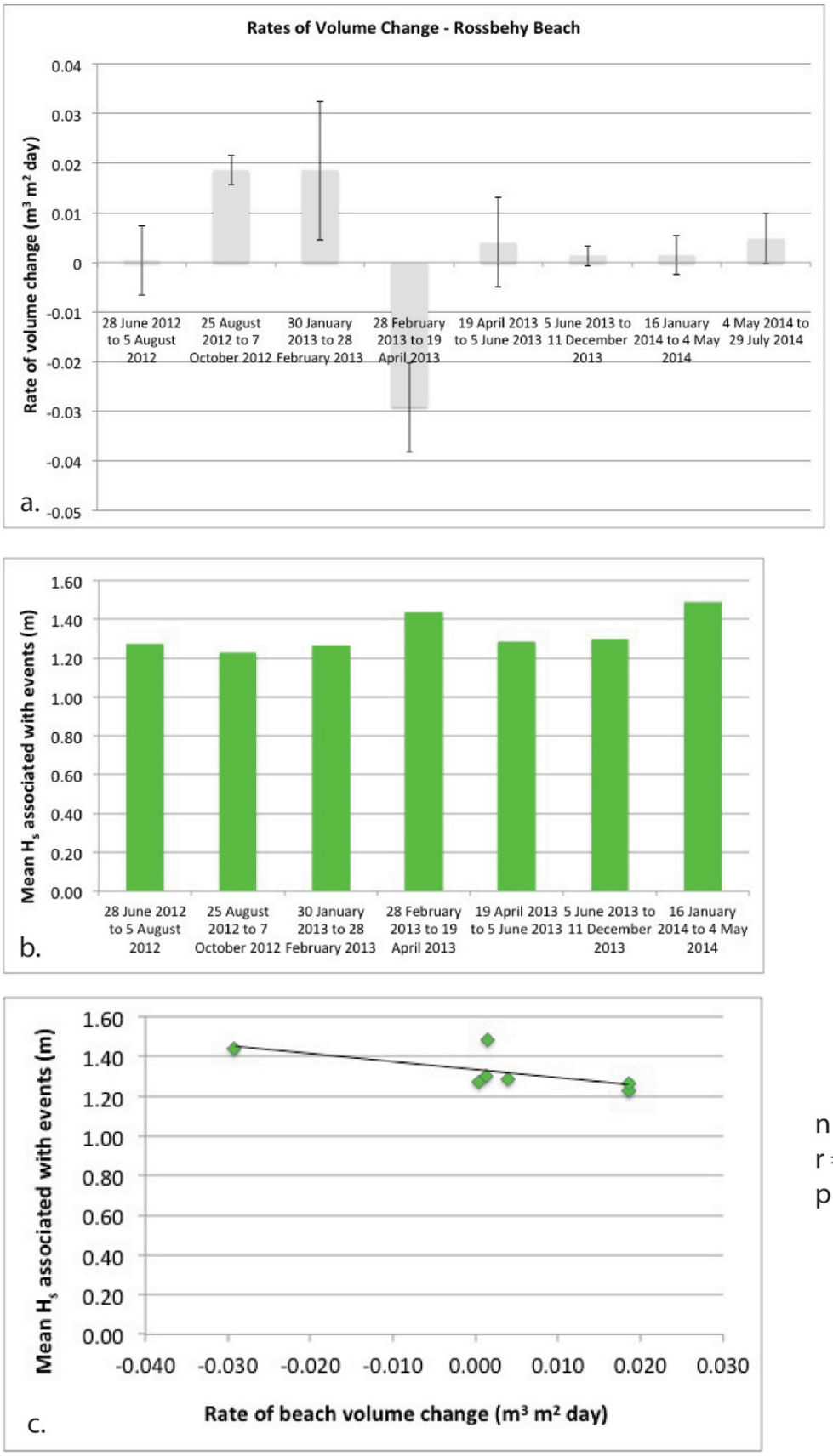

Figure 8.29 (a.) Rates of volume change at Rossbehy beach broken down by morphological monitoring period. (b.) Mean significant wave height associated with storm events that occurred during corresponding morphological monitoring periods. (c.) There was a strong negative relationship between rate of beach volume change and mean H_s associated with events (n=7, r=-0.67). This relationship was not statistically significant (p=0.10). Negative rates of beach volume change are associated with net volume losses; positive rates of beach volume change are associated with net volume gains.

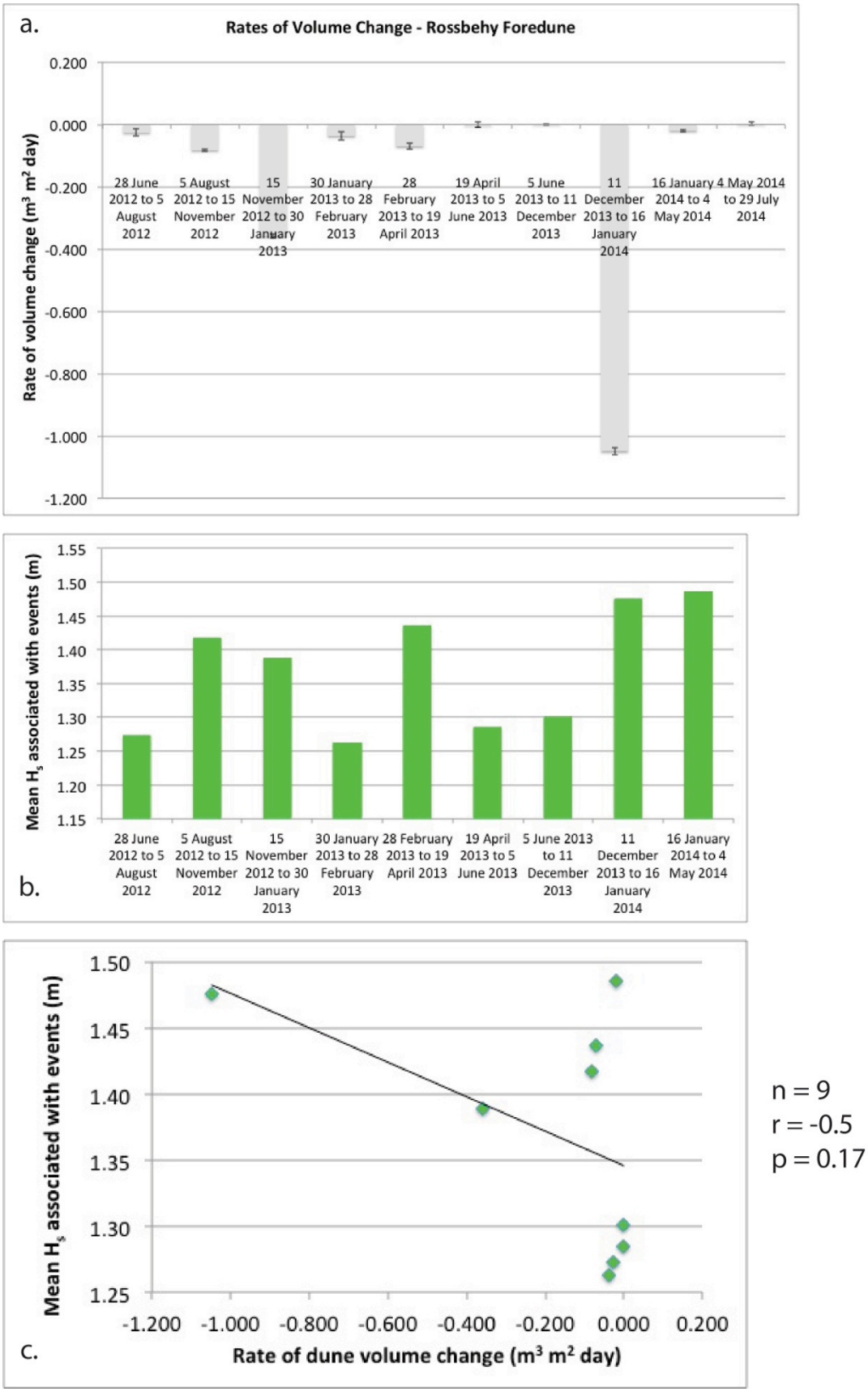

Figure 8.30 (a.) Rates of foredune volume change at Rossbehy broken down by morphological monitoring period. (b.) Mean significant wave height associated with storm events that occurred during corresponding morphological monitoring periods. (c.) There was a moderate negative relationship between rate of foredune volume change and mean H_s associated with events (n=9, r=-0.5). This relationship was not statistically significant (p=0.17). Negative rates of dune volume change are associated with net volume losses; positive rates of dune volume change are associated with net volume gains.

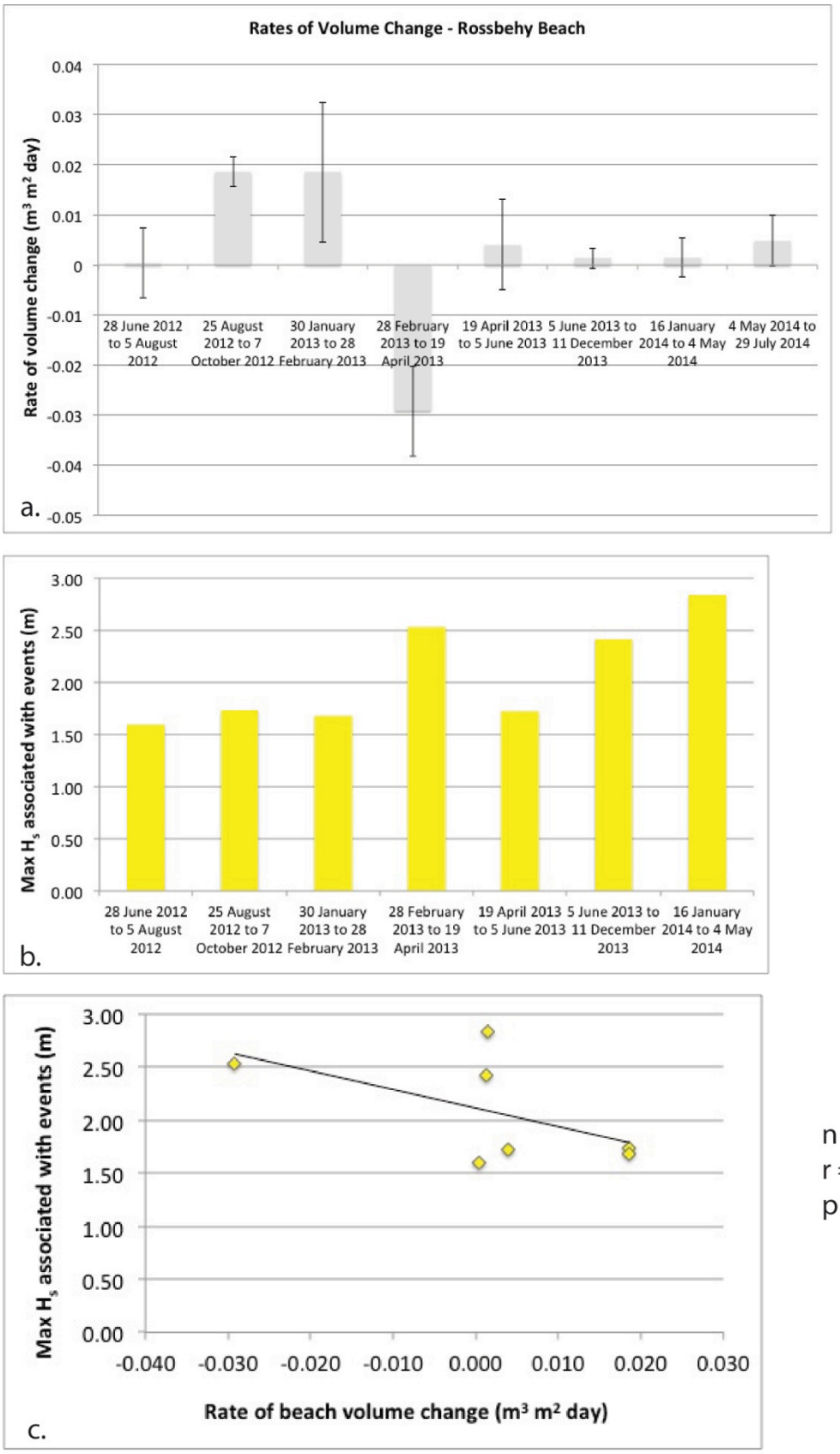

Figure 8.31 (a.) Rates of volume change at Rossbehy beach broken down by morphological monitoring period. (b.) Maximum significant wave height associated with storm events that occurred during corresponding morphological monitoring periods. (c.) There was a moderate negative relationship between rate of beach volume change and max H_s associated with events (n=7, r=-0.56). This relationship was not statistically significant (p=0.20). Negative rates of beach volume change are associated with net volume losses; positive rates of beach volume change are associated with net volume gains.

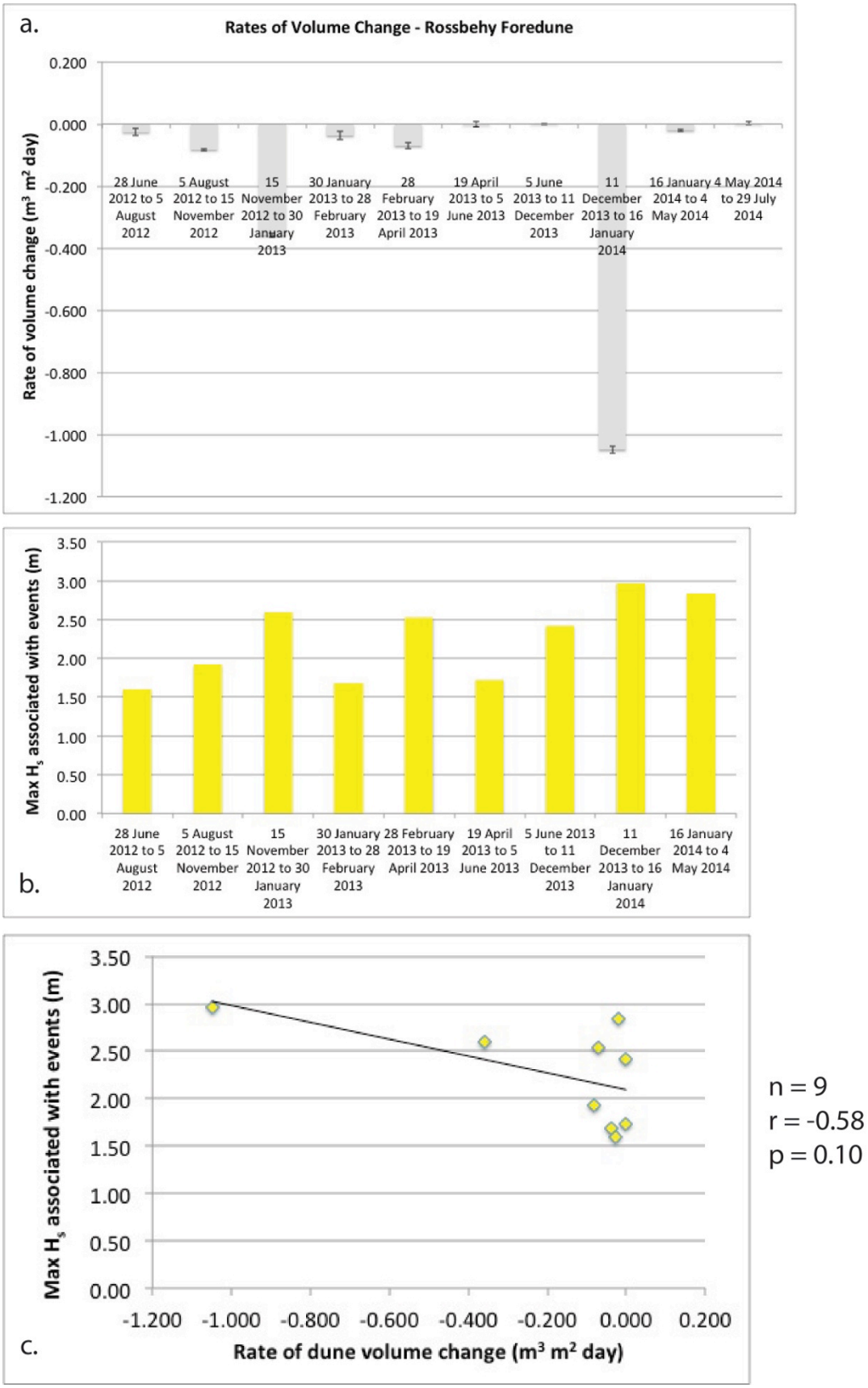

Figure 8.32 (a.) Rates of foredune volume change at Rossbehy broken down by morphological monitoring period. (b.) Maximum significant wave height associated with storm events that occurred during corresponding morphological monitoring periods. (c.) There was a moderate negative relationship between rate of foredune volume change and max H_s associated with events (n=9, r=-0.58). This relationship was not statistically significant (p=0.10). Negative rates of dune volume change are associated with net volume losses; positive rates of dune volume change are associated with net volume gains.

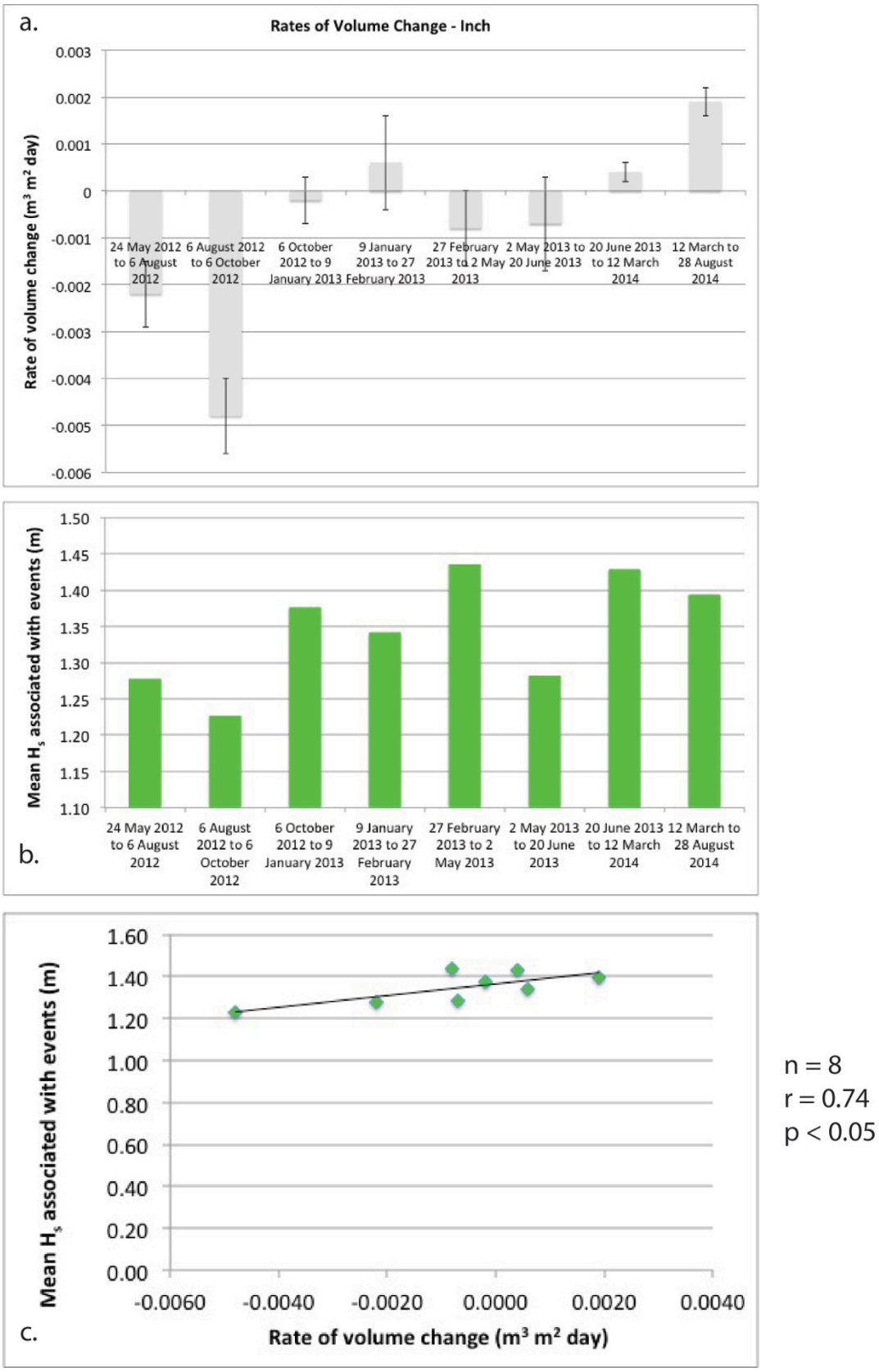

Figure 8.33 (a.) Rates of volume change at Inch broken down by morphological monitoring period. (b.) Mean significant wave height associated with storm events that occurred during corresponding morphological monitoring periods. (c.) There was a strong positive relationship between rate of volume change and mean H_s associated with events (n=8, r=0.74). This relationship was statistically significant ($p<0.05$). Negative rates of volume change are associated with net volume losses; positive rates of volume change are associated with net volume gains. This result indicates higher significant wave heights during storms are associated with higher rates of volume gain at the site.

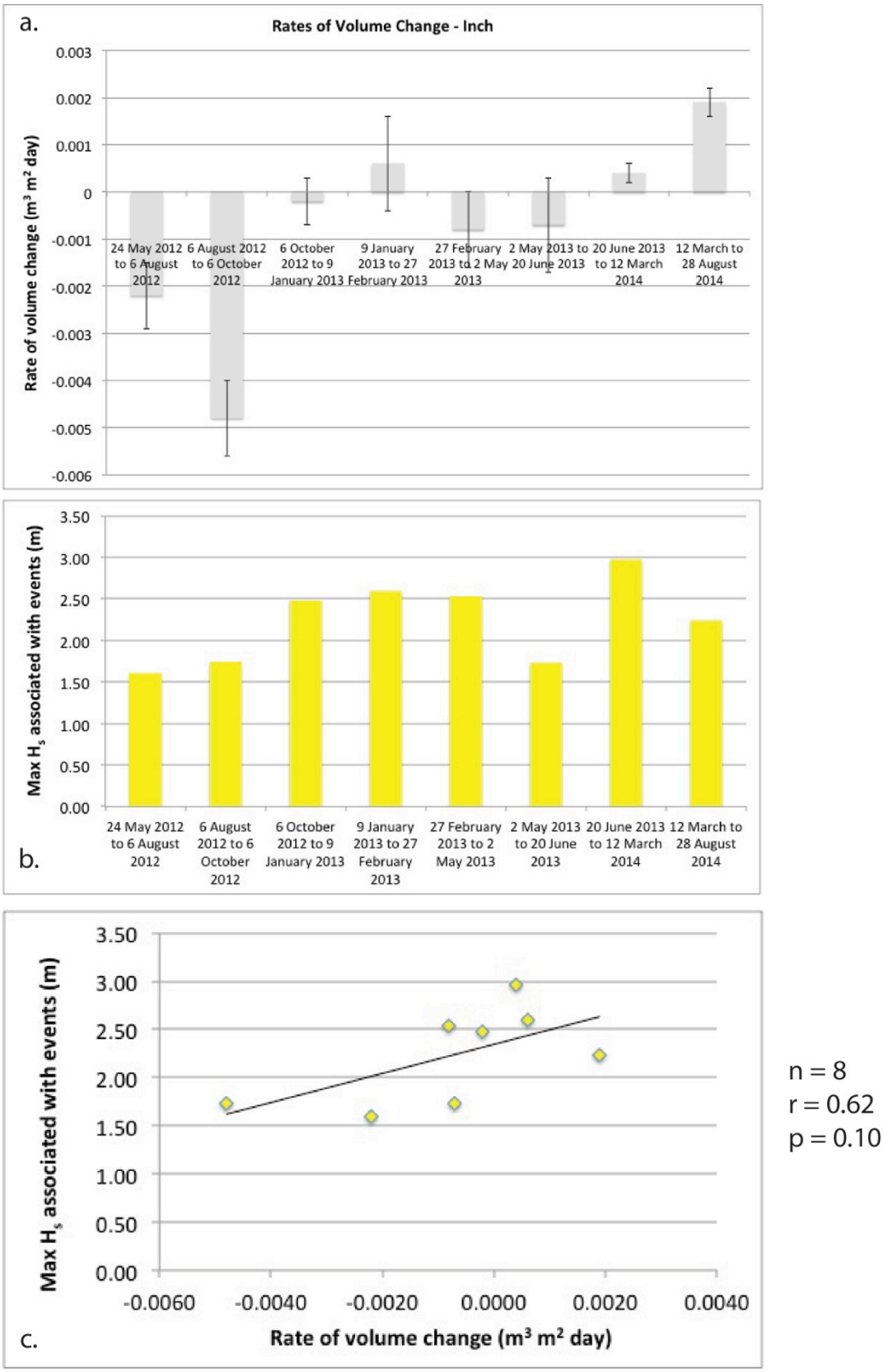

Figure 8.34 (a.) Rates of volume change at Inch broken down by morphological monitoring period. (b.) Maximum significant wave height associated with storm events that occurred during corresponding morphological monitoring periods. (c.) There was a strong positive relationship between rate of volume change and max H_s associated with events (n=8, r=0.62). This relationship was not statistically significant (p=0.10). Negative rates of volume change are associated with net volume losses; positive rates of volume change are associated with net volume gains.

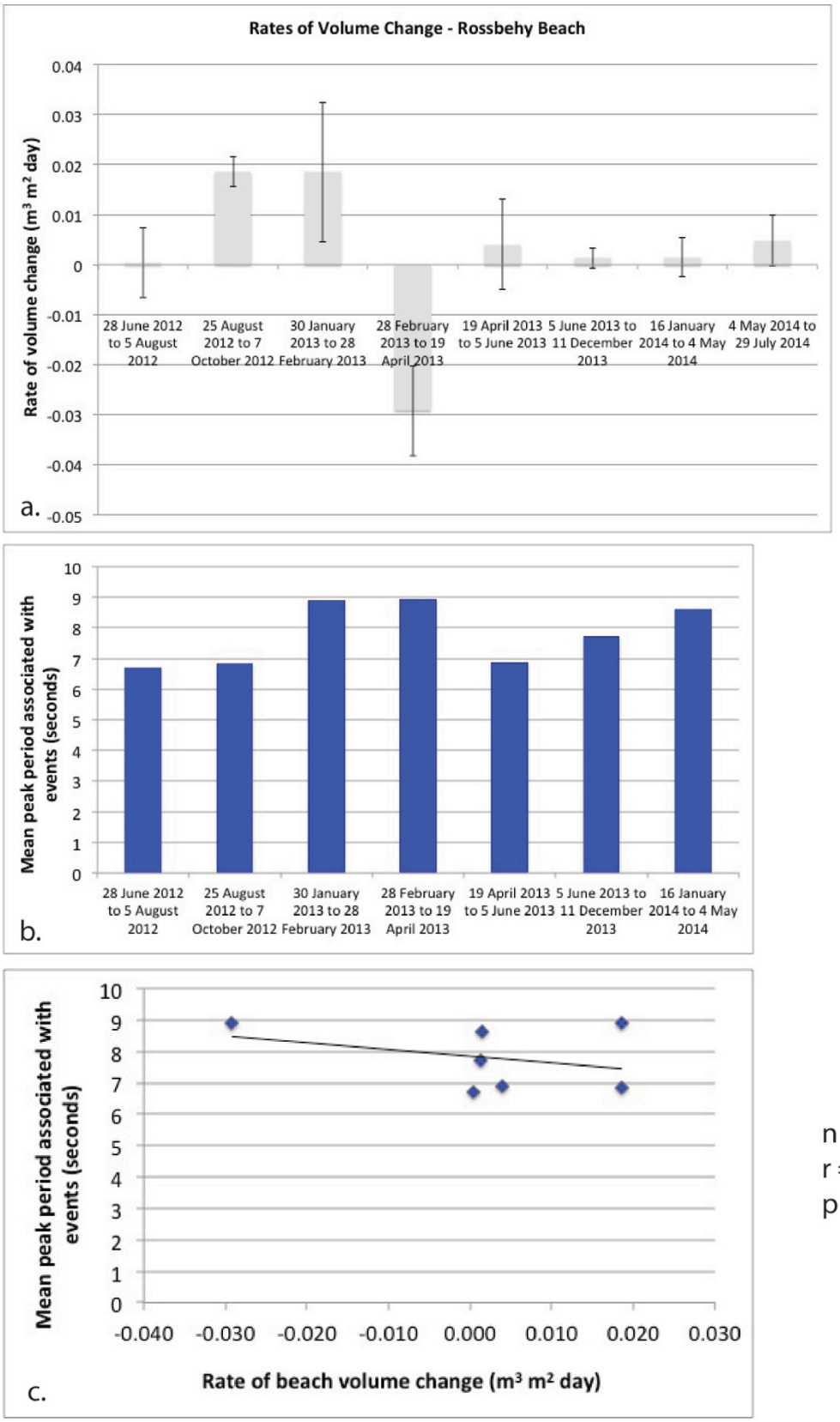

Figure 8.35 (a.) Rates of volume change at Rossbehy beach broken down by morphological monitoring period. (b.) Mean peak wave period associated with storm events that occurred during corresponding morphological monitoring periods. (c.) There was a weak negative relationship between rate of beach volume change and mean peak period associated with events (n=7, r=-0.34). This relationship was not statistically significant (p=0.46). Negative rates of beach volume change are associated with net volume losses; positive rates of beach volume change are associated with net volume gains.

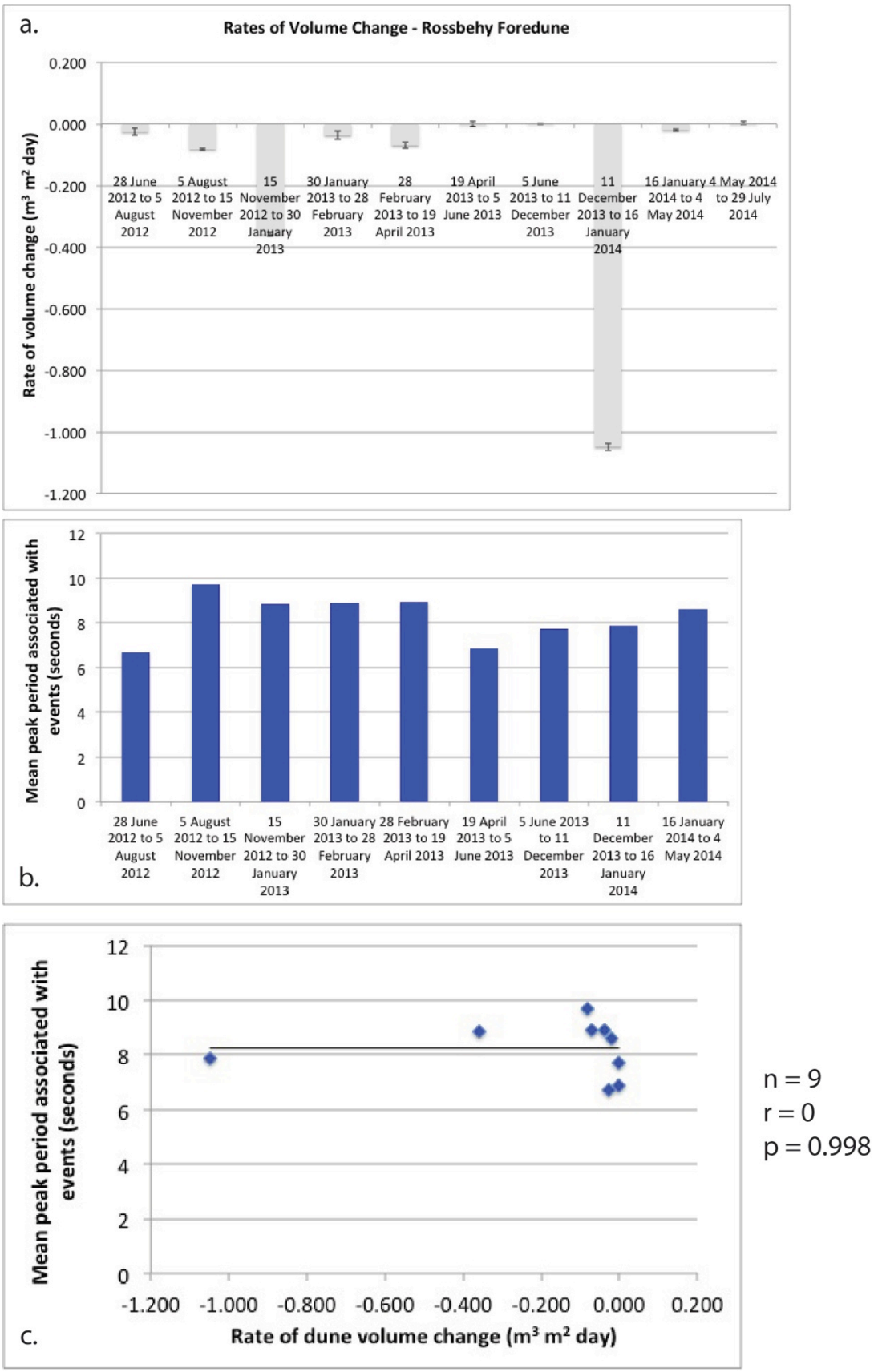

Figure 8.36 (a.) Rates of foredune volume change at Rossbehy broken down by morphological monitoring period. (b.) Mean peak wave period associated with storm events that occurred during corresponding morphological monitoring periods. (c.) There was a very weak relationship (neither positive or negative) between rate of foredune volume change and mean peak period associated with events (n=9, r=0). This relationship was not statistically significant (p=0.998). Negative rates of dune volume change are associated with net volume losses; positive rates of dune volume change are associated with net volume gains.

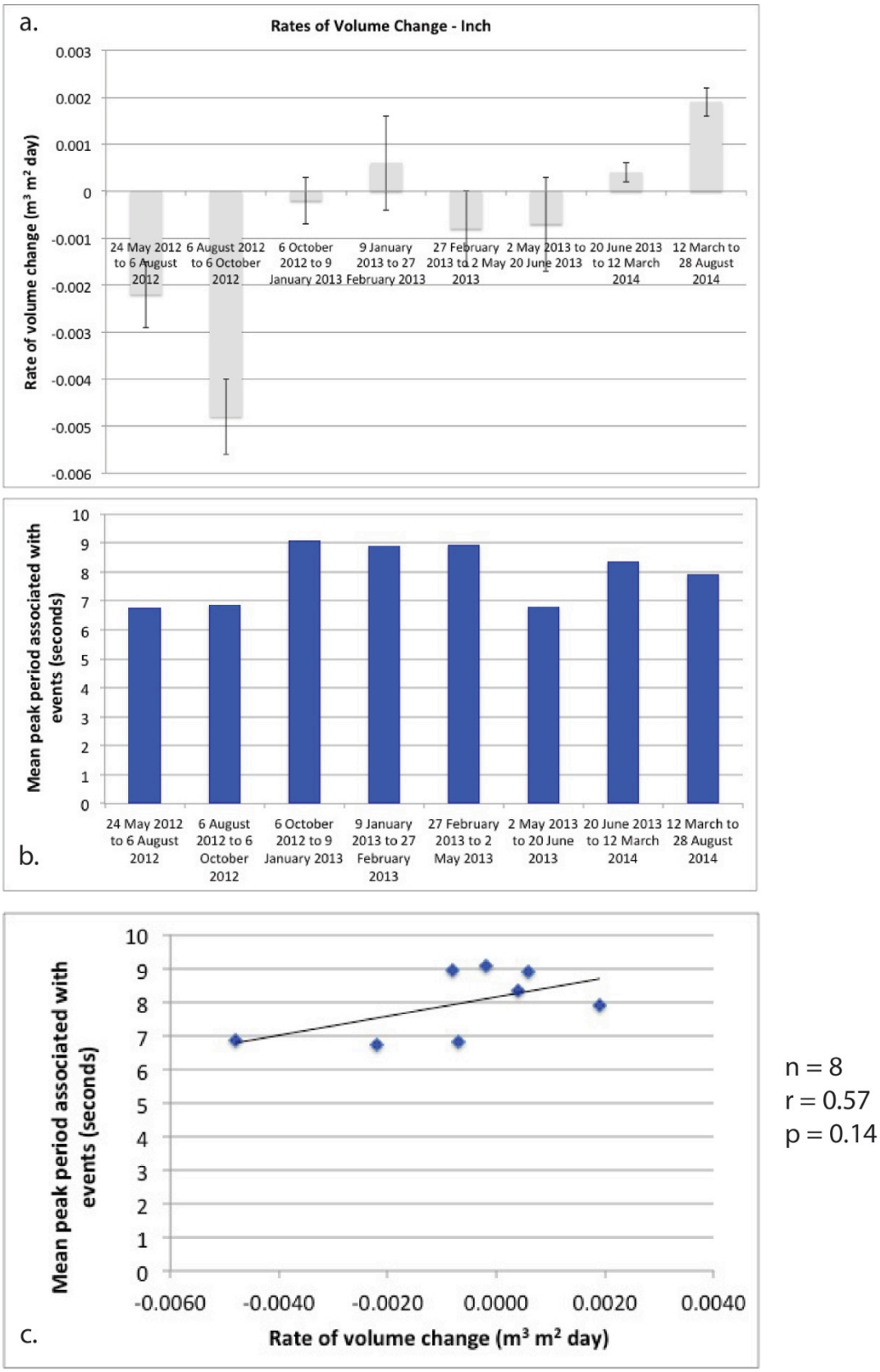

Figure 8.37 (a.) Rates of volume change at Inch broken down by morphological monitoring period. (b.) Mean peak wave period associated with storm events that occurred during corresponding morphological monitoring periods. (c.) There was a moderate positive relationship between rate of volume change and mean peak period associated with events (n=8, r=0.57). This relationship was not statistically significant (p=0.14). Negative rates of volume change are associated with net volume losses; positive rates of volume change are associated with net volume gains.

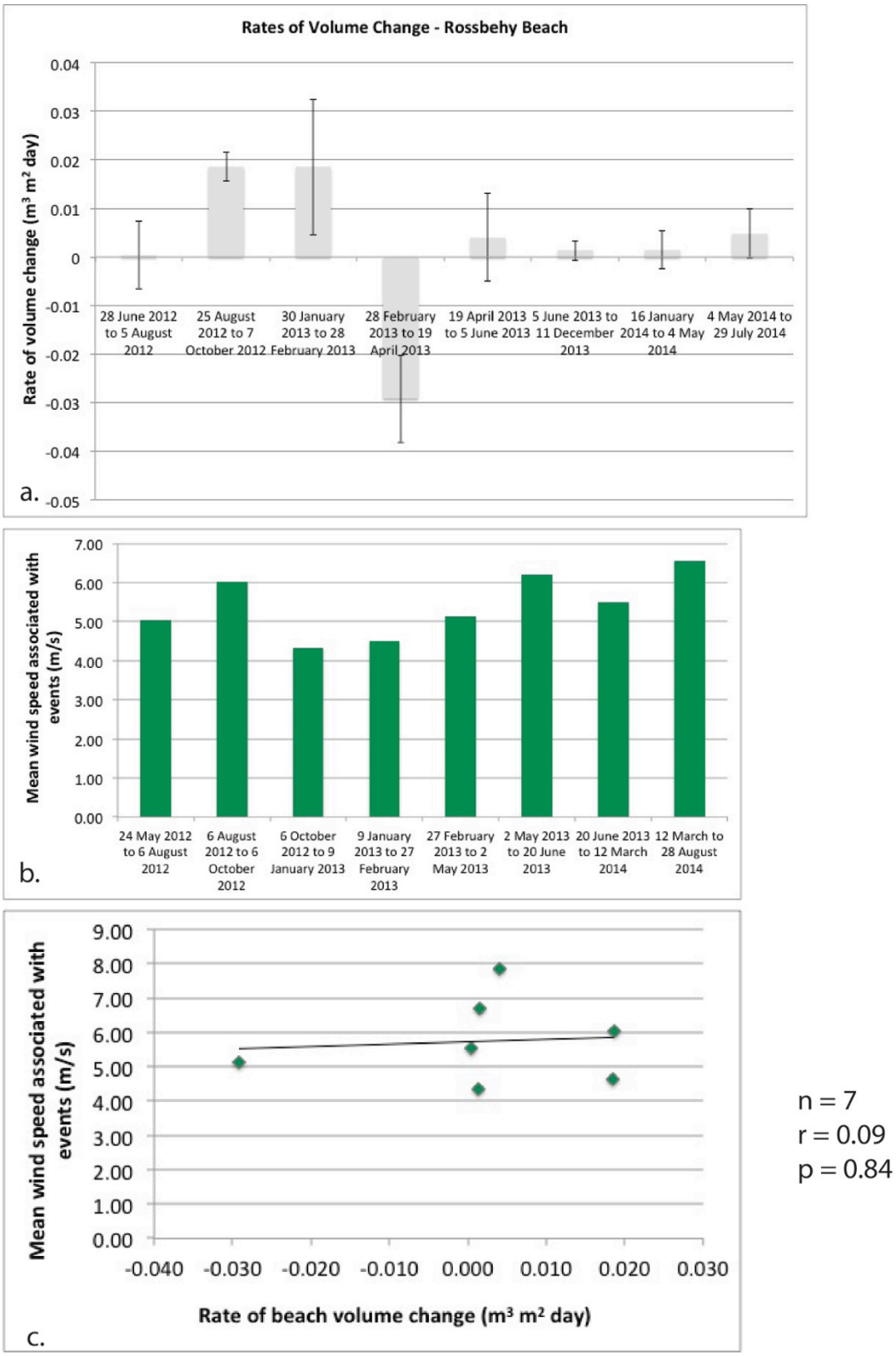

Figure 8.38 (a.) Rates of volume change at Rossbehy beach broken down by morphological monitoring period. (b.) Mean wind speed associated with storm events that occurred during corresponding morphological monitoring periods. (c.) There was a very weak positive relationship between rate of beach volume change and mean wind speed associated with events (n=7, r=0.09). This relationship was not statistically significant (p=0.84). Negative rates of beach volume change are associated with net volume losses; positive rates of beach volume change are associated with net volume gains.

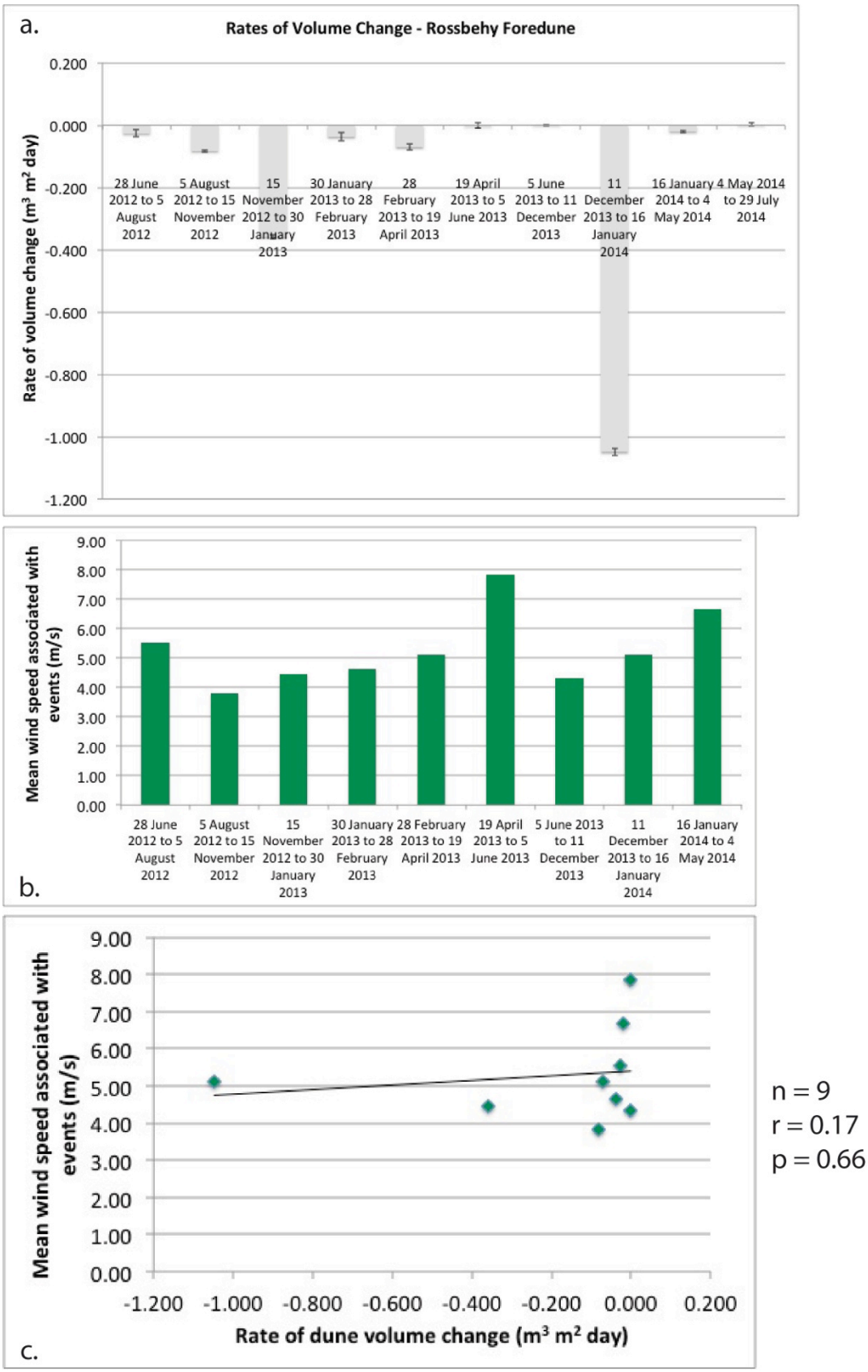

Figure 8.39 (a.) Rates of foredune volume change at Rossbehy broken down by morphological monitoring period. (b.) Mean wind speeds associated with storm events that occurred during corresponding morphological monitoring periods. (c.) There was a very weak positive relationship between rate of foredune volume change and mean wind speed associated with events (n=9, r=0.17). This relationship was not statistically significant (p=0.66). Negative rates of dune volume change are associated with net volume losses; positive rates of dune volume change are associated with net volume gains.

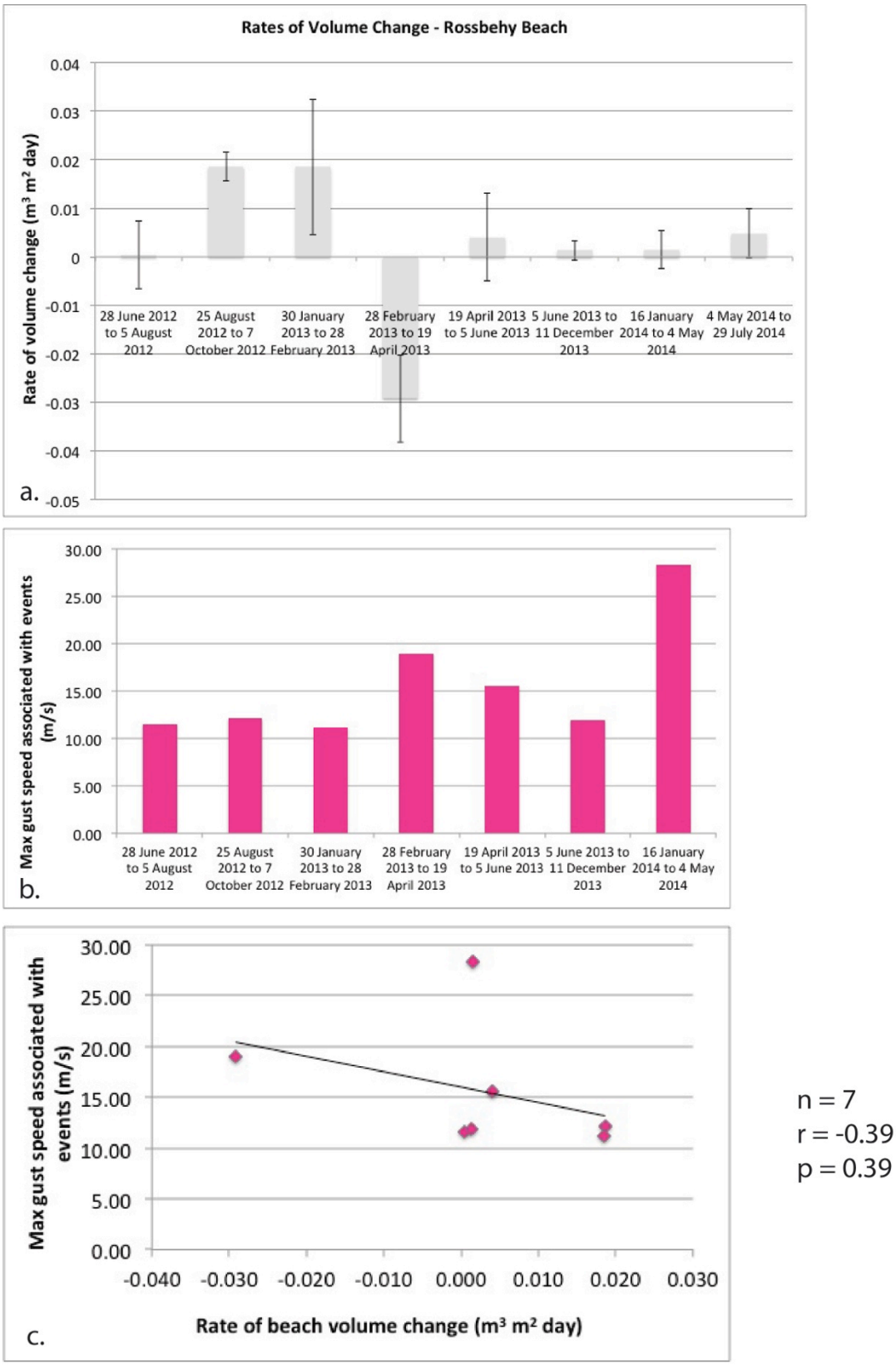

Figure 8.40 (a.) Rates of volume change at Rossbehy beach broken down by morphological monitoring period. (b.) Max gust speed associated with storm events that occurred during corresponding morphological monitoring periods. (c.) There was a weak negative relationship between rate of beach volume change and mean wind speed associated with events (n=7, r=-0.39). This relationship was not statistically significant (p=0.39). Negative rates of beach volume change are associated with net volume losses; positive rates of beach volume change are associated with net volume gains.

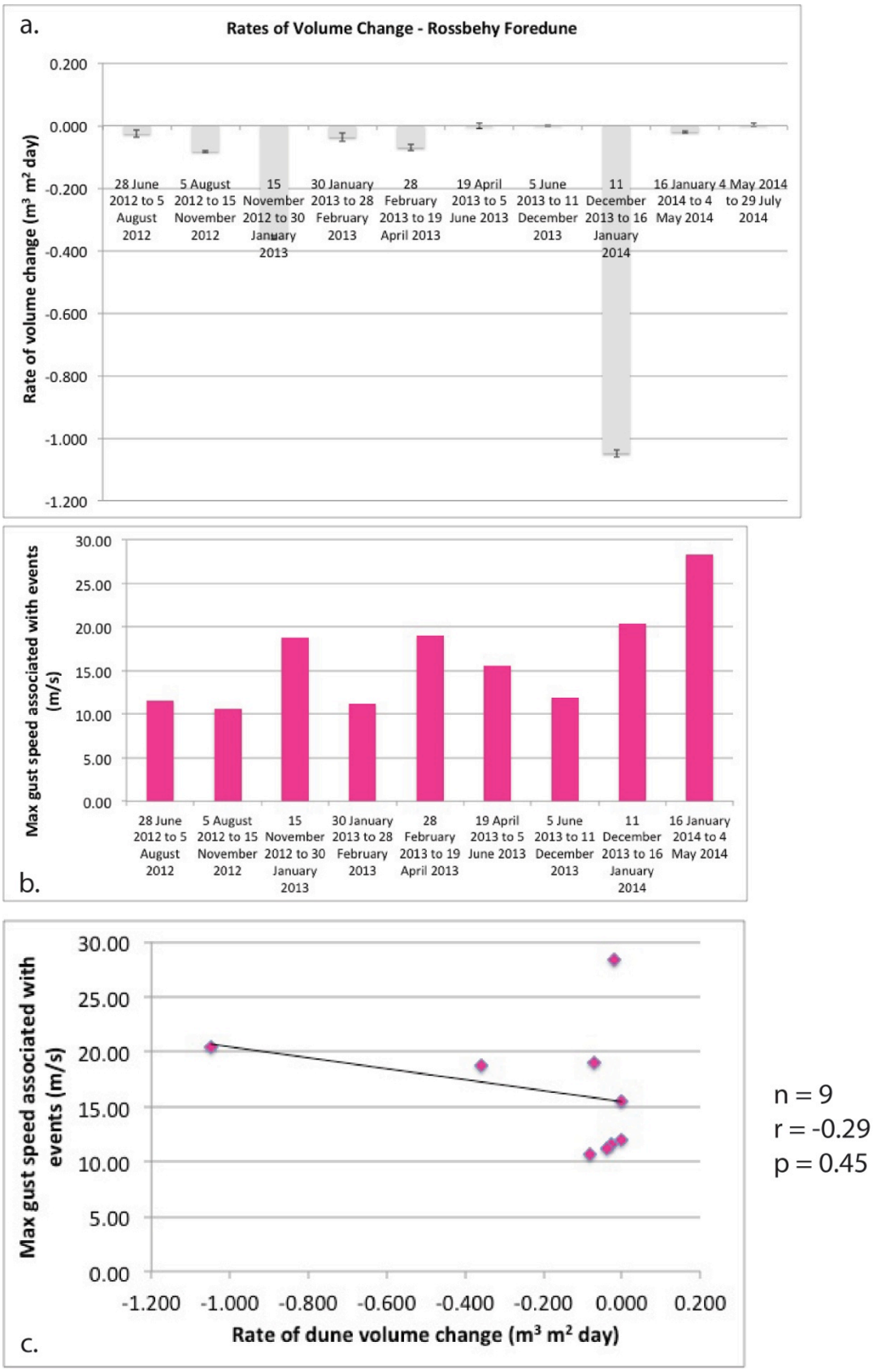

Figure 8.41 (a.) Rates of foredune volume change at Rossbehy broken down by morphological monitoring period. (b.) Maximum gust speeds associated with storm events that occurred during corresponding morphological monitoring periods. (c.) There was a weak negative relationship between rate of foredune volume change and max gust speed associated with events (n=9, r=-0.29). This relationship was not statistically significant (p=0.45). Negative rates of dune volume change are associated with net volume losses; positive rates of dune volume change are associated with net volume gains.

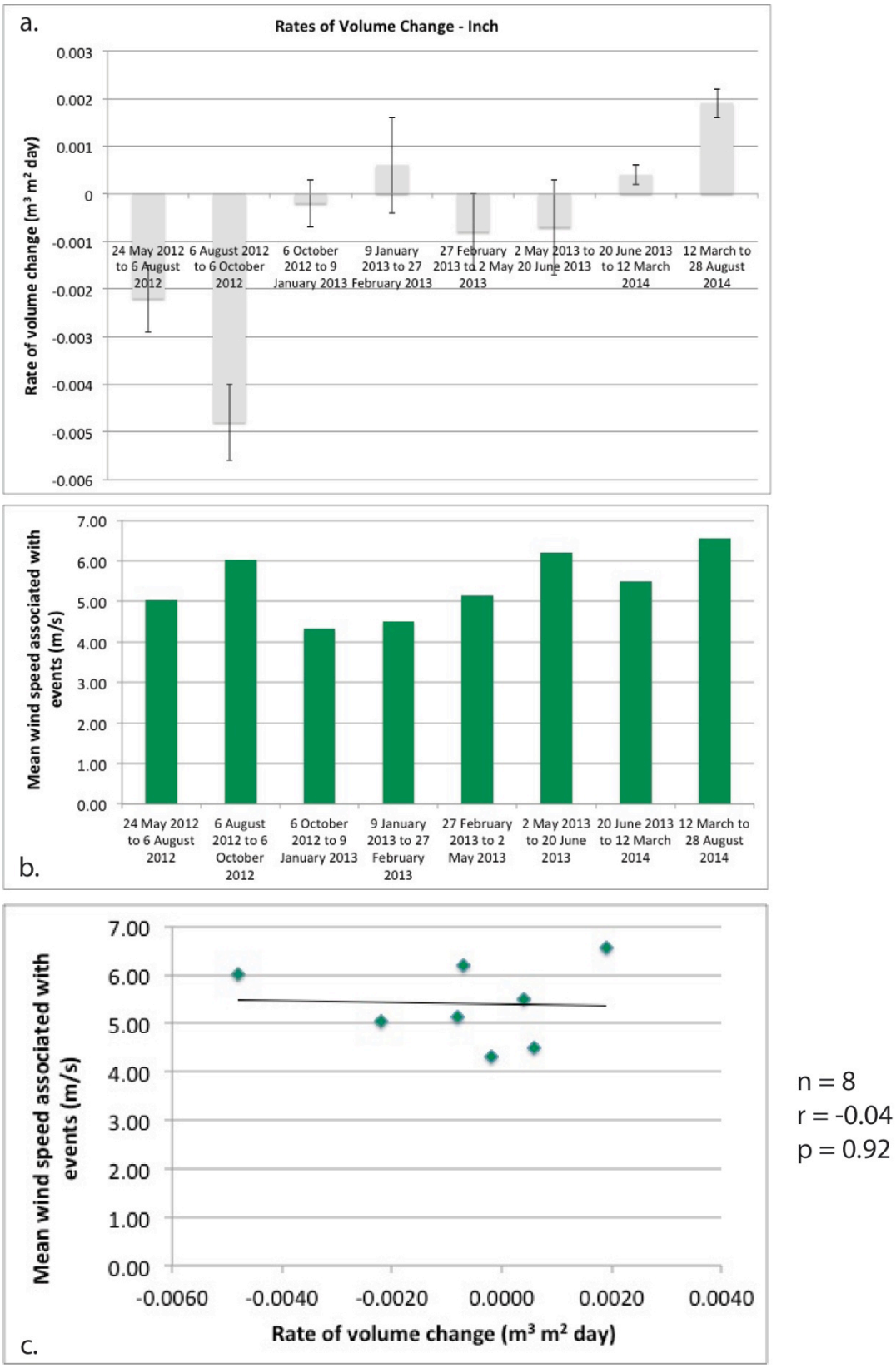

Figure 8.42 (a.) Rates of volume change at Inch broken down by morphological monitoring period. (b.) Mean wind speed associated with storm events that occurred during corresponding morphological monitoring periods. (c.) There was a very weak negative relationship between rate of beach volume change and mean wind speeds associated with events (n=8, r=-0.04). This relationship was not statistically significant (p=0.92). Negative rates of volume change are associated with net volume losses; positive rates of volume change are associated with net volume gains.

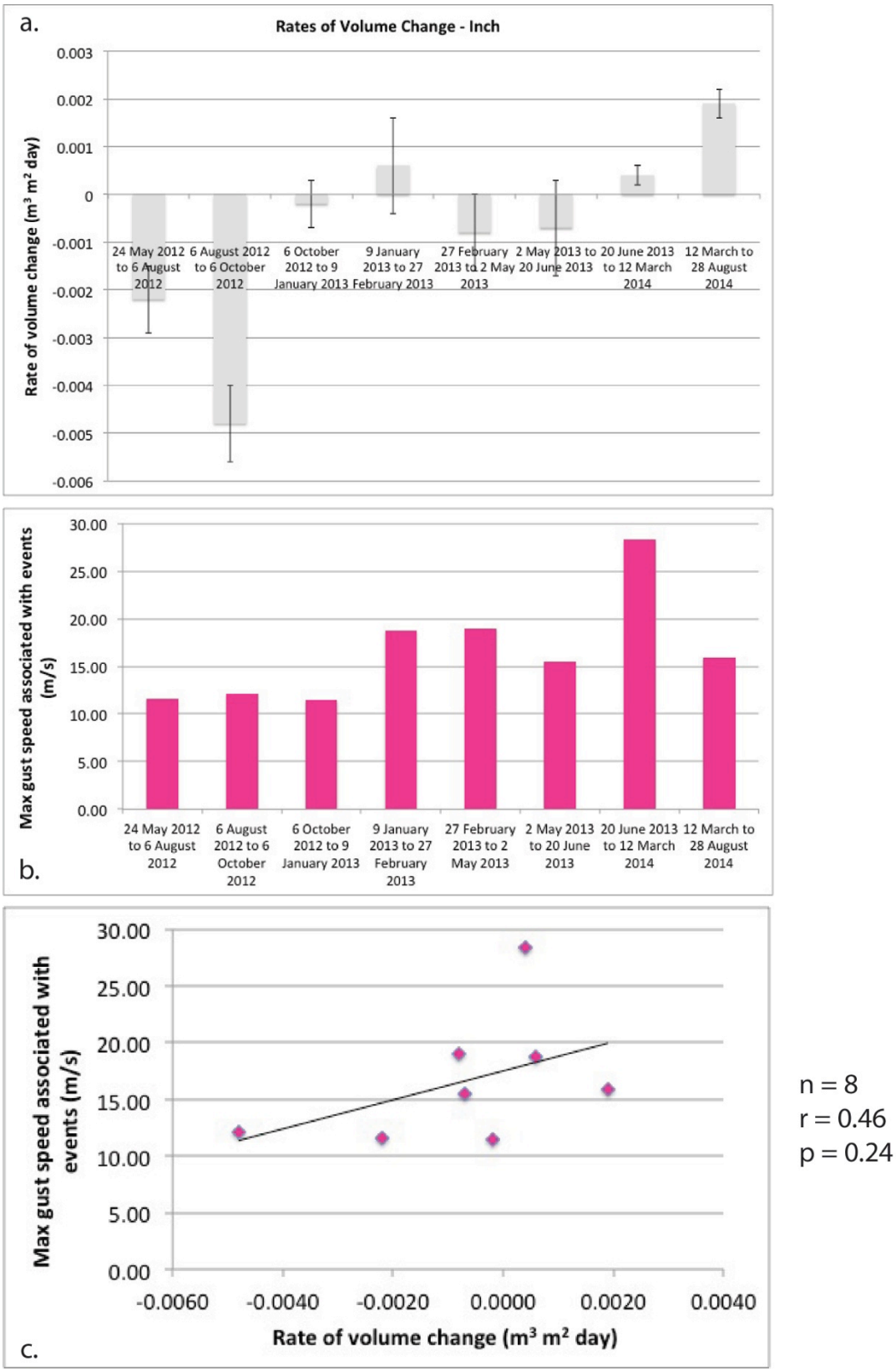

Figure 8.43 (a.) Rates of volume change at Inch broken down by morphological monitoring period. (b.) Maximum gust speed associated with storm events that occurred during corresponding morphological monitoring periods. (c.) There was a moderate positive relationship between rate of beach volume change and max gust speeds associated with events (n=8, r=0.46). This relationship was not statistically significant (p=0.24). Negative rates of volume change are associated with net volume losses; positive rates of volume change are associated with net volume gains.

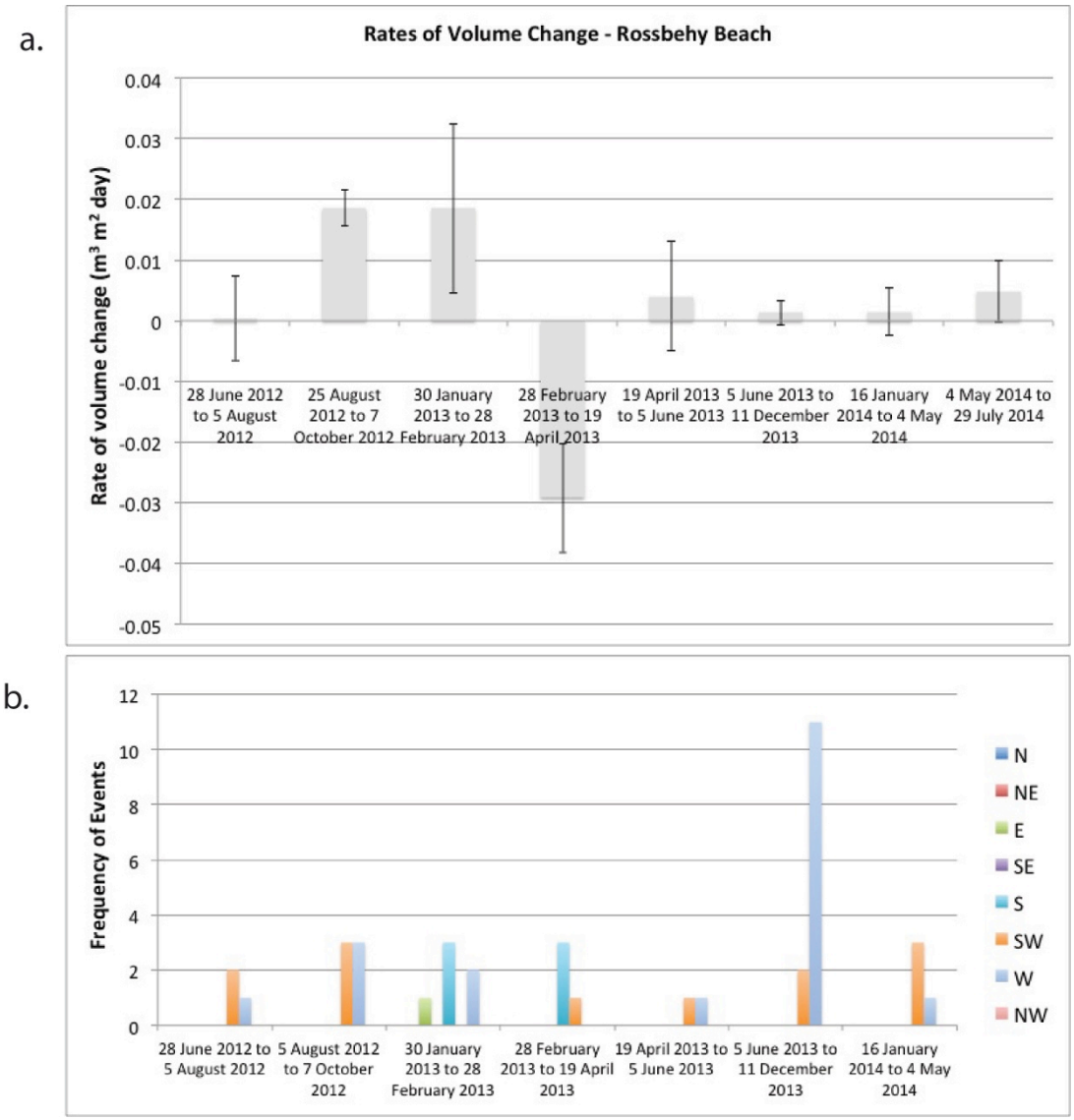

Figure 8.44 (a.) Rates of volume change at Rossbehy beach broken down by morphological monitoring period. (b.) Prevailing wind directions for events occurring during each corresponding morphological monitoring period.

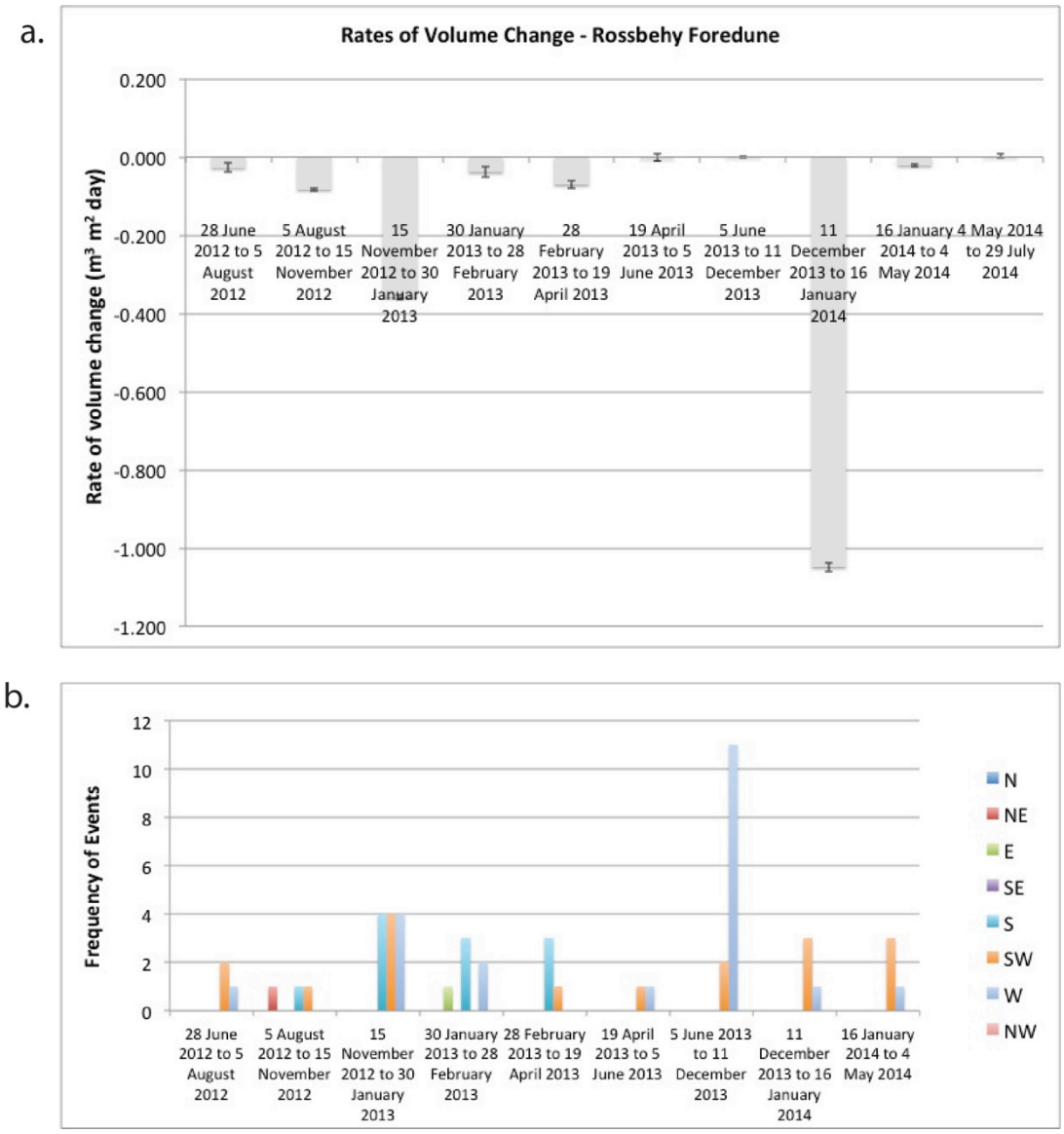

Figure 8.45 (a.) Rates of foredune volume change at Rossbehy broken down by morphological monitoring period. (b.) Prevailing wind directions for events occurring during each corresponding morphological monitoring period.

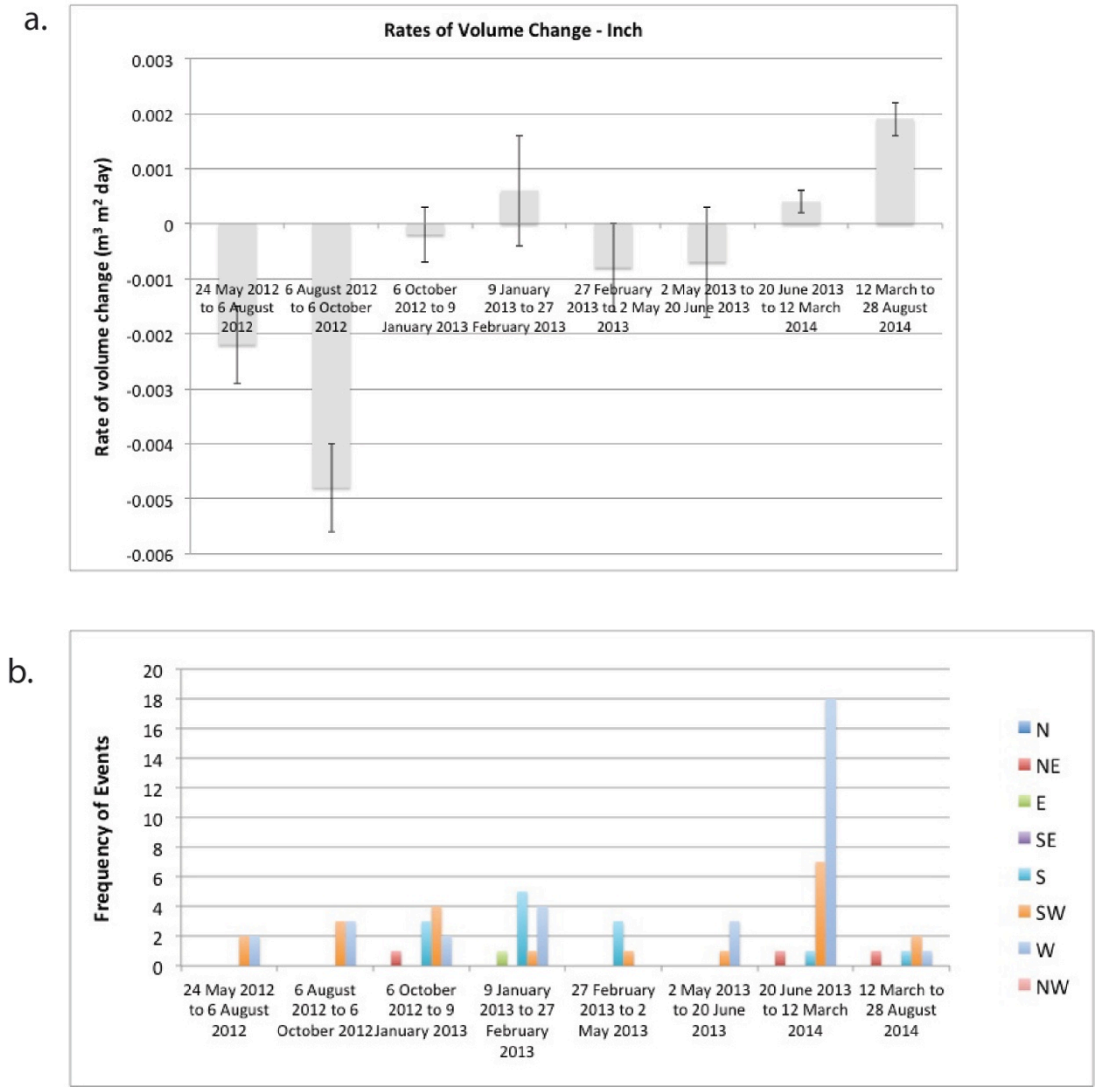

Figure 8.46 (a.) Rates of volume change at Inch broken down by morphological monitoring period. (b.) Prevailing wind directions for events occurring during each corresponding morphological monitoring period.

Rossbehy Beach												
Start	**End**	**Rate of beach volume change (R_{vs}) ($m^3/m^2/day$)**	**Frequency of Events**	**Mean Duration of Events (hours)**	**Maximum Duration of Events (hours)**	**Max tidal level associated with Events (m ODM)**	**Mean lag time between events (hours)**	**Mean H_s associated with events (m)**	**Maximum H_s associated with events (m)**	**Mean peak period associated with events (sec)**	**Mean wind speed associated with events (m/s)**	**Maximum gust speed associated with events (m/s)**
2012-06-28	2012-08-05	0.0005	3	31	43	2.38	357	1.27	1.60	7	5.54	11.54
2012-08-05	2012-10-07	0.019	6	22	34	2.13	219	1.23	1.74	7	6.02	12.13
2013-01-30	2013-02-28	0.019	6	25	38	2.20	76	1.26	1.69	9	4.64	11.23
2013-02-28	2013-04-19	-0.029	4	54	118	2.60	252	1.44	2.53	9	5.13	18.96
2013-04-19	2013-06-05	0.004	2	24	35	2.01	226	1.29	1.73	7	7.83	15.53
2013-06-05	2013-12-11	0.001	13	44	145	2.82	352	1.30	2.42	8	4.33	11.93
2014-01-16	2014-05-04	0.002	17	69	231	2.94	70	1.49	2.84	9	6.68	28.35
		r	0.09	-0.59	-0.39	-0.45	-0.32	-0.67	-0.56	-0.34	0.09	-0.39
		N	7	7	7	7	7	7	7	7	7	7
		t (abs. value)	0.199	1.623	0.934	1.129	0.768	1.992	1.494	0.804	0.201	0.940
		p	0.85029	0.16561	0.39338	0.31032	0.47698	0.10300	0.19551	0.45790	0.84886	0.39029

Table 8.3 Rates of beach volume change for each of the morphological monitoring periods at Rossbehy and event characteristics used to test for the existence of simple linear relationships. No statistically significant correlations were observed between rate of beach volume change and any of these variables.

Rossbehy Foredune												
Start	**End**	**Rate of scarp volume change (R_{vs}) ($m^3/m^2/day$)**	**Frequency of Events**	**Mean Duration of Events (hours)**	**Maximum Duration of Events (hours)**	**Max tidal level associated with Events (m ODM)**	**Mean lag time between events (hours)**	**Mean H_s associated with events (m)**	**Maximum H_s associated with events (m)**	**Mean peak period associated with events (sec)**	**Mean wind speed associated with events (m/s)**	**Maximum gust speed associated with events (m/s)**
2012-06-28	2012-08-05	-0.027	3	31	43	2.38	357	1.27	1.60	7	5.54	11.54
2012-10-07	2012-11-15	-0.083	3	38	55	2.13	301	1.42	1.92	10	3.82	10.65
2012-11-15	2013-01-30	-0.359	13	82	308	2.80	62	1.39	2.60	9	4.45	18.79
2013-01-30	2013-02-28	-0.038	6	25	38	2.20	76	1.26	1.69	9	4.64	11.23
2013-02-28	2013-04-19	-0.071	4	54	118	2.60	252	1.44	2.53	9	5.13	18.96
2013-04-19	2013-06-05	-0.001	2	24	35	2.01	226	1.29	1.73	7	7.83	15.53
2013-06-05	2013-12-11	0.000	13	44	145	2.49	352	1.30	2.42	8	4.33	11.93
2013-12-11	2014-01-16	-1.049	4	195	633	2.82	30	1.48	2.97	8	5.12	20.38
2014-01-16	2014-05-04	-0.021	17	69	231	2.94	70	1.49	2.84	9	6.68	28.35
		r	0.12	-0.96	-0.93	-0.48	0.56	-0.50	-0.58	0.00	0.17	-0.29
		N	9	9	9	9	9	9	9	9	9	9
		t (abs. value)	0.322	9.351	6.954	1.455	1.807	1.521	1.886	0.003	0.453	0.809
		p	0.75663	0.00003	0.00022	0.18887	0.11378	0.17211	0.10127	0.99787	0.66419	0.44523

Table 8.4 Rates of scarp volume change for each of the morphological monitoring periods at Rossbehy and event characteristics used to test for the existence of simple linear relationships. Strong negative statistically significant correlations were observed between mean duration of events and rate of scarp volume change and maximum duration of events and rate of scarp volume change (p-values highlighted in blue).

Inch												
Start	**End**	**Rate of volume change (R_{vs}) ($m^3/m^2/day$)**	**Frequency of Events**	**Mean Duration of Events (hours)**	**Maximum Duration of Events (hours)**	**Max tidal level associated with events (m ODM)**	**Mean lag time between events (hours)**	**Mean H_s associated with events (m)**	**Maximum H_s associated with events (m)**	**Mean peak period associated with events (sec)**	**Mean wind speed associated with events (m/s)**	**Maximum gust speed associated with events (m/s)**
2012-05-24	2012-08-06	-0.0022	4	29	43	2.38	405	1.28	1.60	7	5.03	11.54
2012-08-06	2012-10-06	-0.0048	6	22	34	2.13	219	1.23	1.74	7	6.02	12.13
2012-10-06	2013-01-09	-0.0002	11	78	308	2.88	135	1.38	2.48	9	4.32	11.43
2013-01-09	2013-02-27	0.0006	11	43	154	2.41	62	1.34	2.60	9	4.50	18.79
2013-02-27	2013-05-02	-0.0008	4	54	118	2.60	252	1.44	2.53	9	5.13	18.96
2013-05-02	2013-06-20	-0.0007	4	29	42	2.01	318	1.28	1.73	7	6.21	15.53
2013-06-20	2014-03-12	0.0004	27	84	633	2.94	153	1.43	2.97	8	5.49	28.35
2014-03-12	2014-08-28	0.0019	5	42	81	2.25	187	1.39	2.24	8	6.57	15.93
		r	0.30	0.51	0.37	0.33	-0.44	0.74	0.62	0.57	-0.04	0.46
		N	8	8	8	8	8	8	8	8	8	8
		t (abs. value)	0.764	1.449	0.975	0.859	1.213	2.697	1.943	1.710	0.110	1.295
		p	0.47401	0.19759	0.36741	0.42310	0.27072	0.03572	0.10000	0.13816	0.91632	0.24284

Table 8.5 Rates of volume change for each of the morphological monitoring periods at Inch and event characteristics used to test for the existence of simple linear relationships. A strong positive statistically significant correlation was observed between mean H_s associated with events and rate of volume (p-value highlighted in blue).

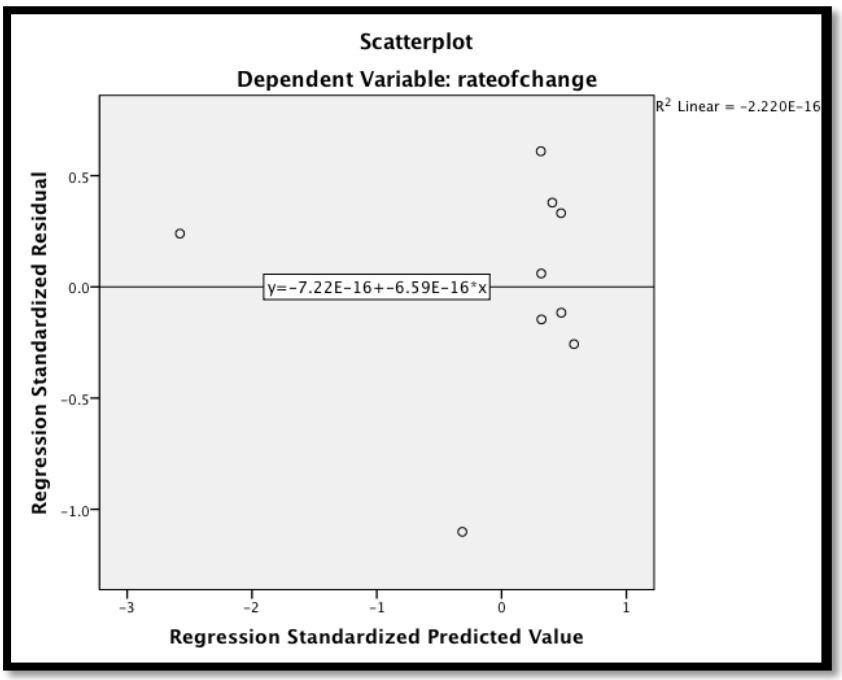

Figure 8.47 Residual scatterplot showing predicted scores against errors of prediction for Rossbehy foredune rate of change multiple regression analysis. The plot confirms that the homoscedasticity assumption is met.

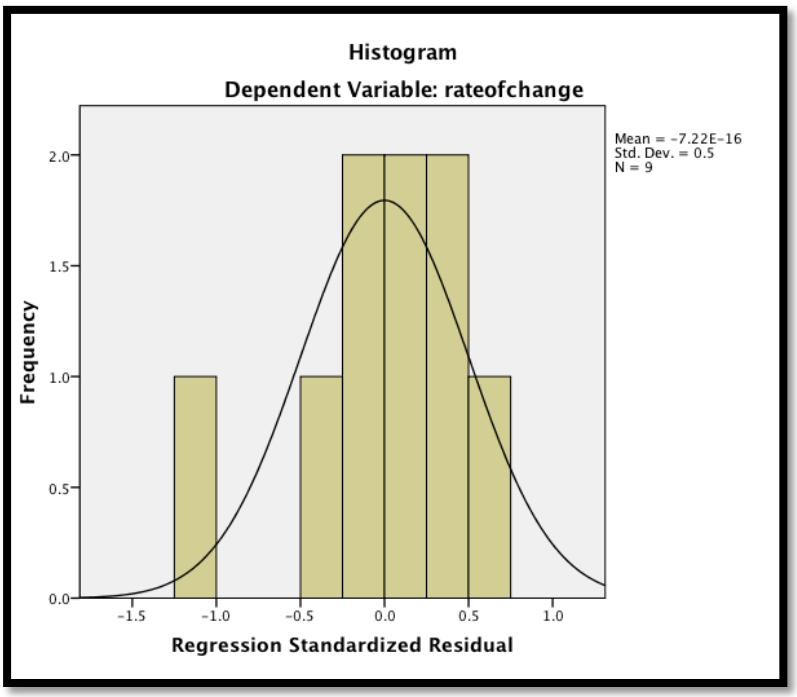

Figure 8.48 Distribution of residuals for Rossbehy scarp rate of change multiple regression analysis. The distribution is close to normal, satisfying a principal assumption for multiple regression analysis

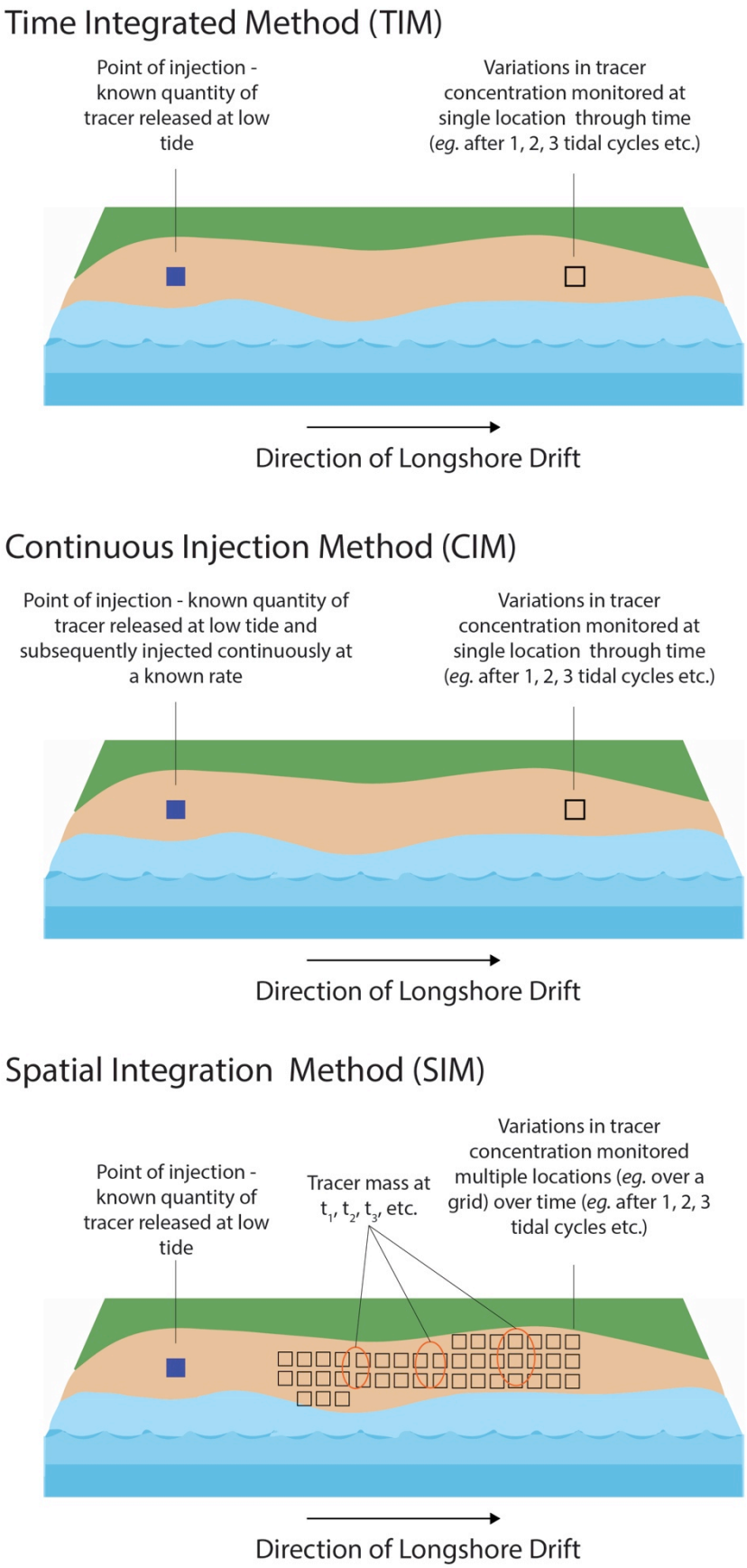

Figure 9.1 Methods of tracer injection.

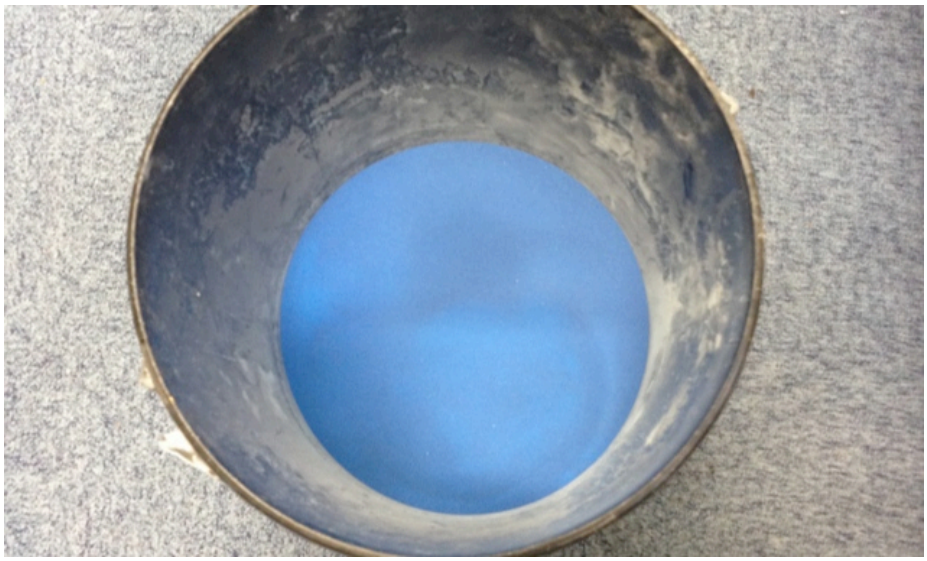

Figure 9.2 Dry tracer particles used in this experiment.

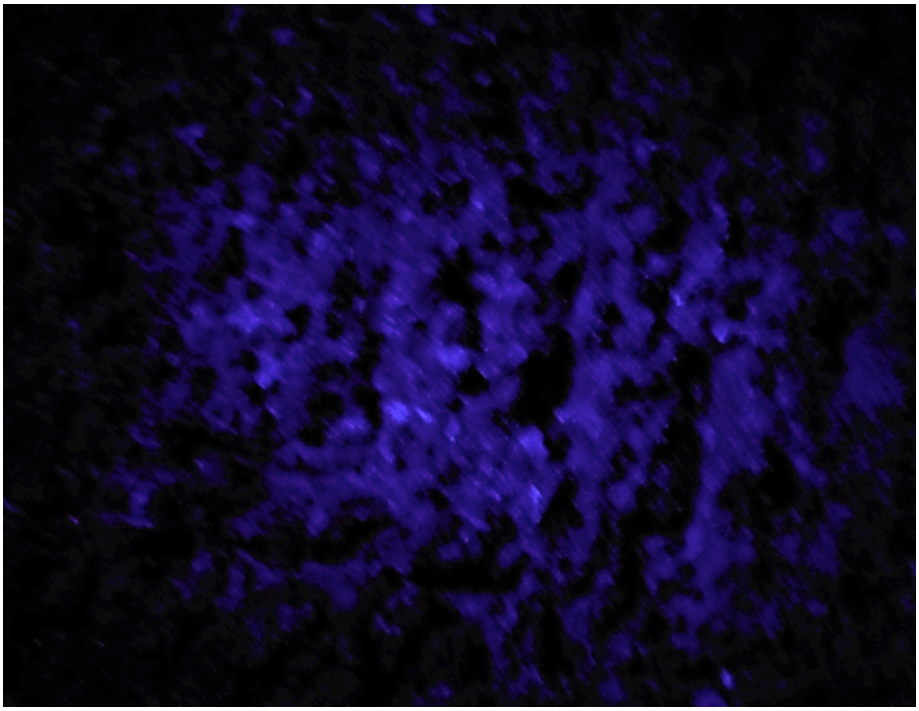

Figure 9.3 Tracer/sand mix under UV light at injection site.

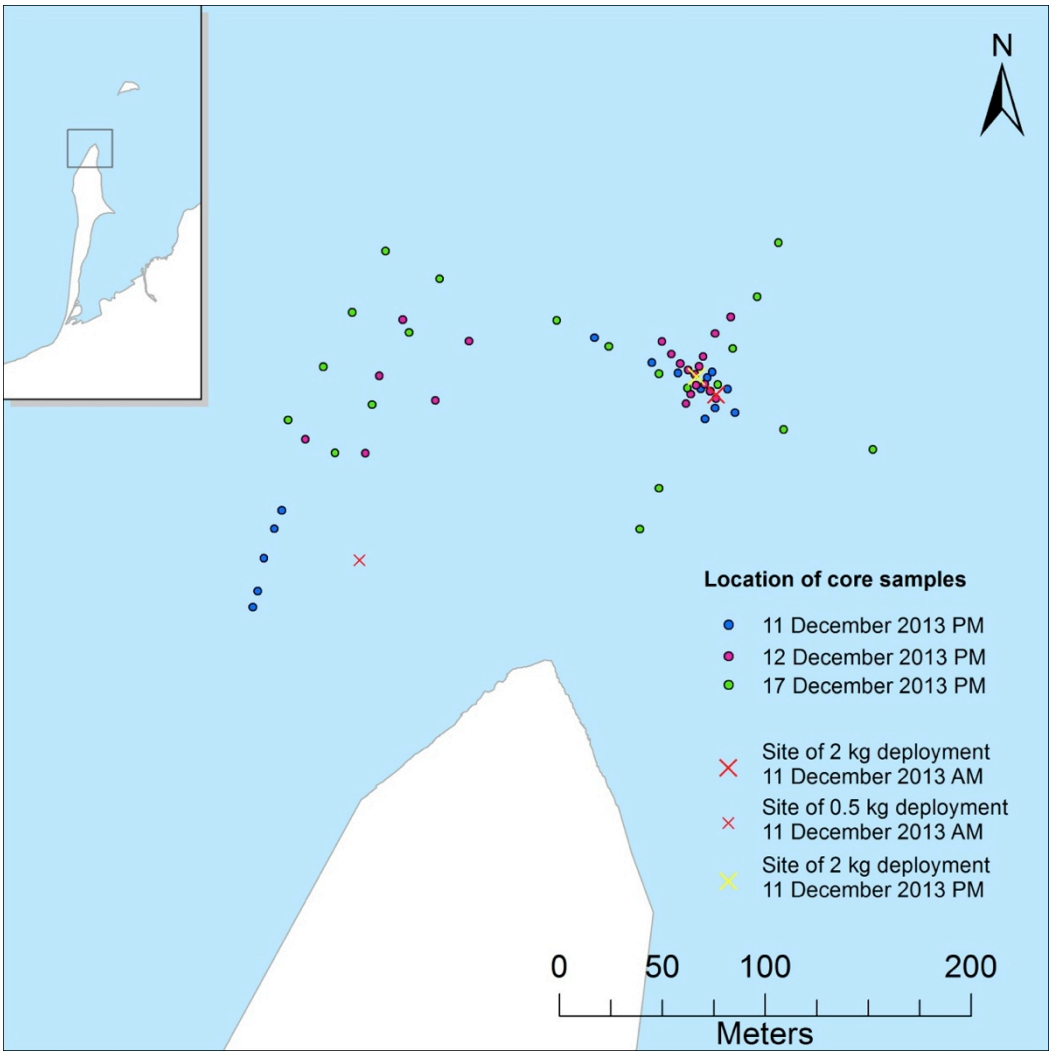

Figure 9.4 Sites of sediment tracer injection and locations of core samples for December 2013 tracer experiment. The shoreline at distal end of the barrier has been updated to reflect the dune toe position on 11 December 2013, at which time a TLS survey was also carried out. The 2 kg injection site was at an elevation of 2.91 m ODM and the 0.5 kg injection site was at an elevation of 2.50 m.

Figure 9.5 Sampling with half pipes and trowel.

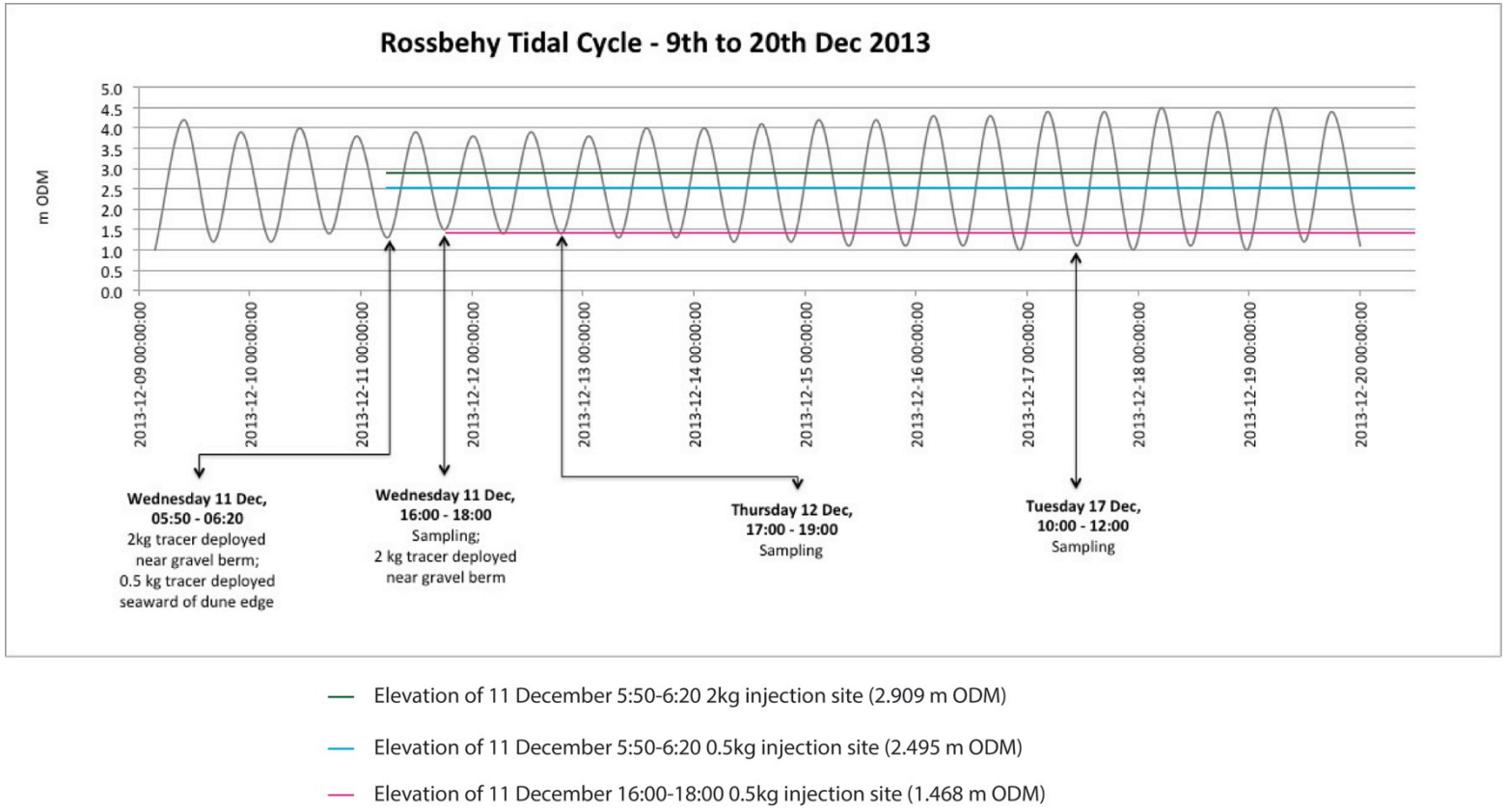

Figure 9.6 December sediment tracer experiment timeline in relation to tidal cycle. Source of tide data: Marine Institute

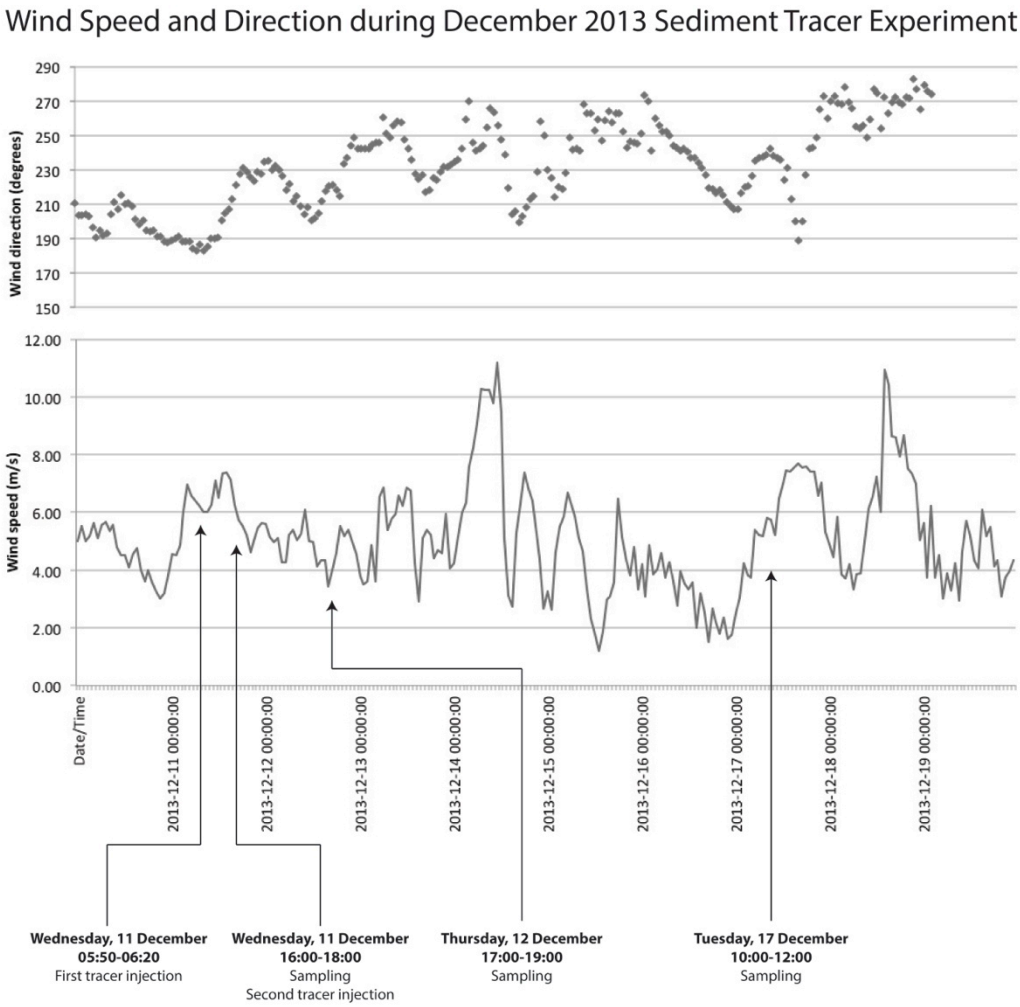

Figure 9.7 Wind speeds and directions during December 2012 tracer experiment. Winds were predominantly southwesterly, with average speeds of 5.5 m/s. Hourly data obtained from Ventry weather station.

Figure 9.8 Samples from the December tracer experiment were analysed in 1.5 cm layers, whereby each layer was carefully removed, broken, and sifted through. The presence and number of individual tracer particles was noted for each layer.

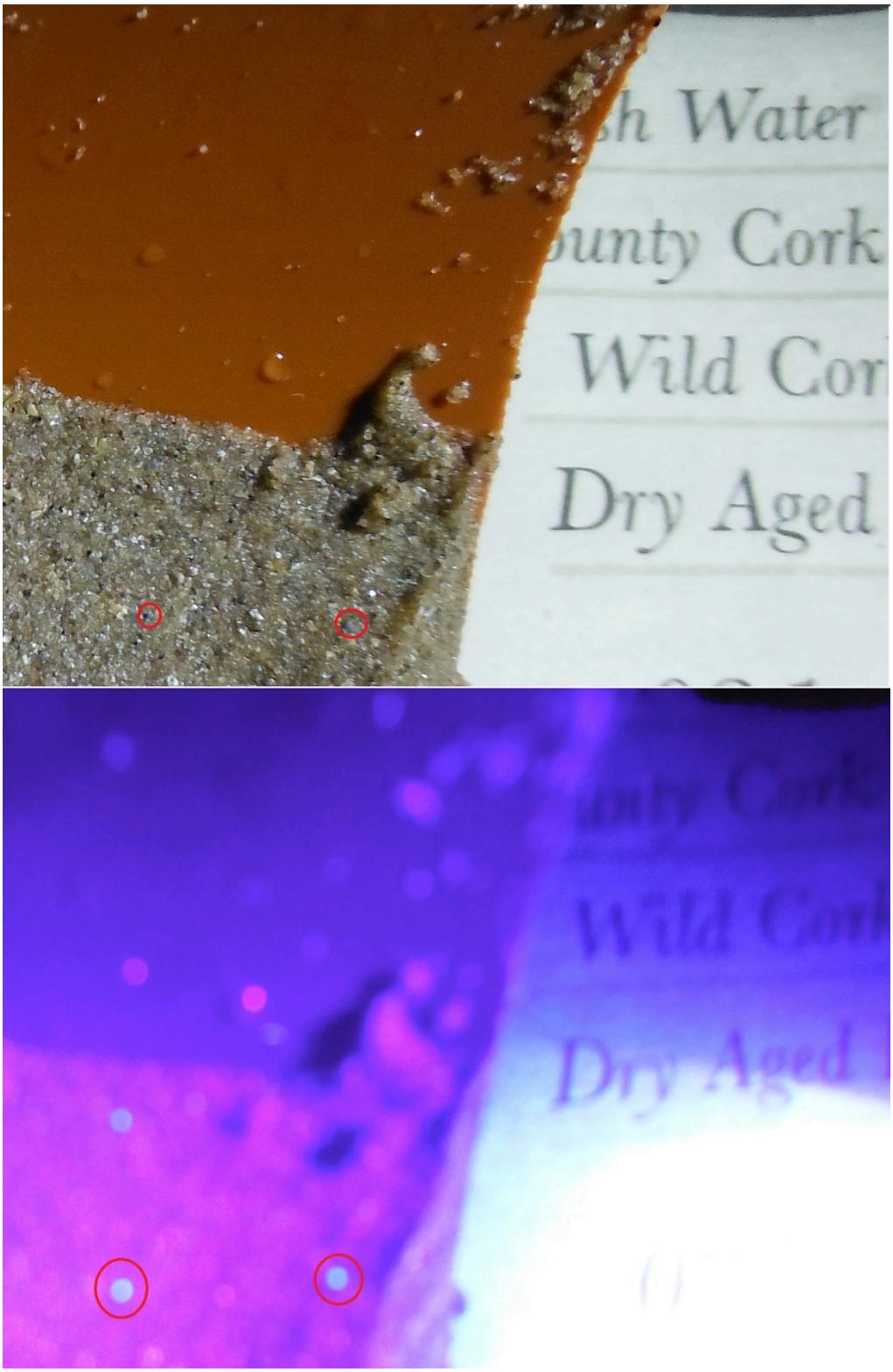

Figure 9.9 Individual tracer particles in a core sample.

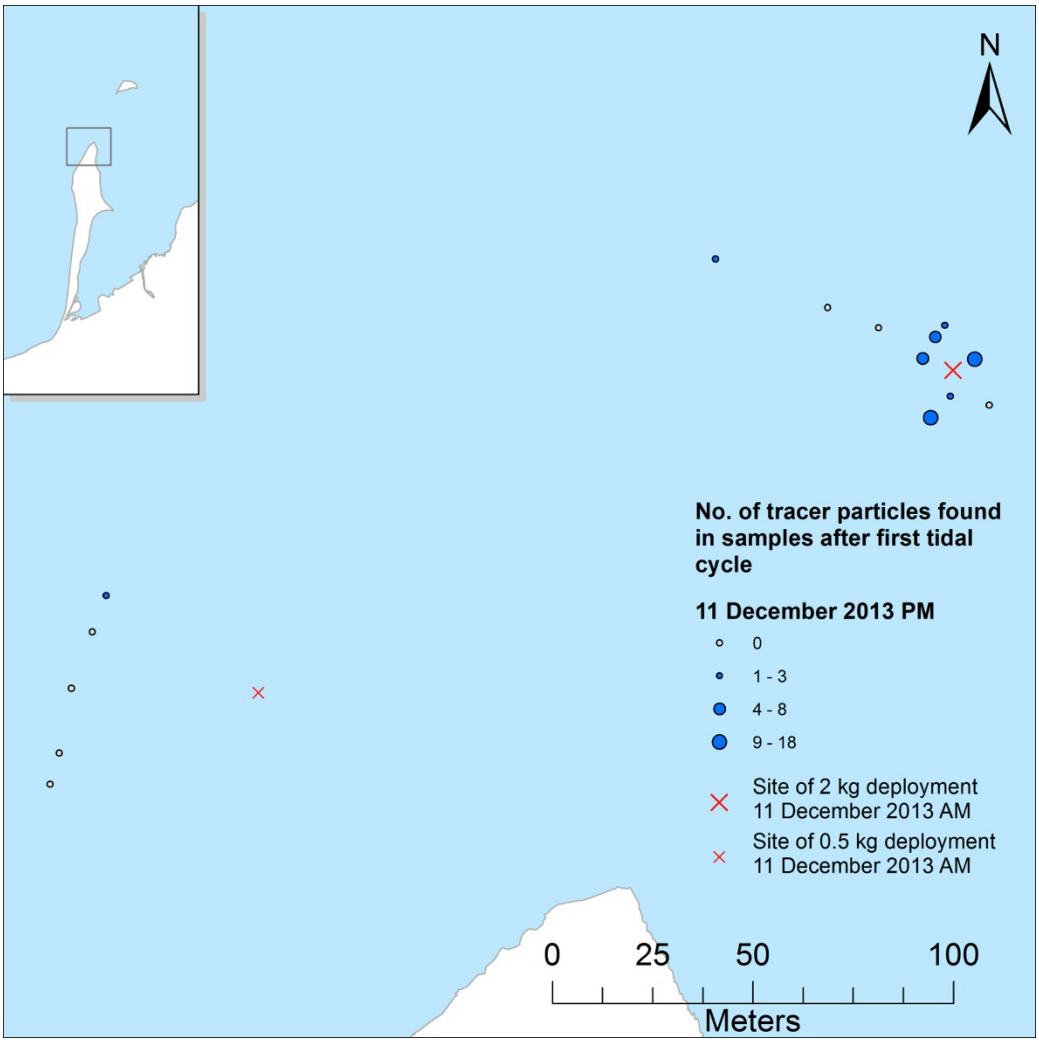

Figure 9.10 Tracer distribution after first tidal cycle following first injection.

11 December PM															
Depth (cm)	**11-1**	**11-2**	**11-3**	**11-4**	**11-5**	**11-6**	**11-7**	**11-8**	**11-9**	**11-10**	**11-11**	**11-12**	**11-13**	**11-14**	**11-15**
0-1.5	3	0	9	0	9	1	7	0	0	2	0	0	0	0	0
1.5-3	0	0	1	2	4	1	0	0	0	0	0	0	0	0	0
3-4.5	0	0	0	0	2	0	0	0	0	0	2	0	0	0	0
4-4.5	0	0	0	0	0	0	0	0	0	0	0	0	0	0	0
4.5-6	0	0	0	0	2	0	0	0	0	0	0	0	0	0	0
6-7.5	0	0	0	0	0	0	0	0	0	0	0	0	0	0	0
7.5-9	0	0	1	0	1	0	0	0	0	0	0	0	0	0	0
9-10.5	1	0	0	0	0	1	0	0	0	0	0	0	0	0	0
10.5-12	0	0	0	1	0	0	0	0	0	0	0	0	0	0	0
12-13.5	0	0	0	0	0	0	0	0	0	0	0	0	0		0
13.5-15	0	0	0	0	0	0	0	0	0	0	0	0	0		0
15-16.5	0	0	0	0	0	0	0	0	0		0	0	0		
16.5-18	0	0	0	0		0	0	0	0		0	0			
18-19.5	4	0	0	0		0	0					0			
19.5-21		0	6			0						0			
21-22.5		0													
22.5-24															
24-25.5															

Table 9.1 Tracer distribution with depth for each sample collected on 11 Dec.

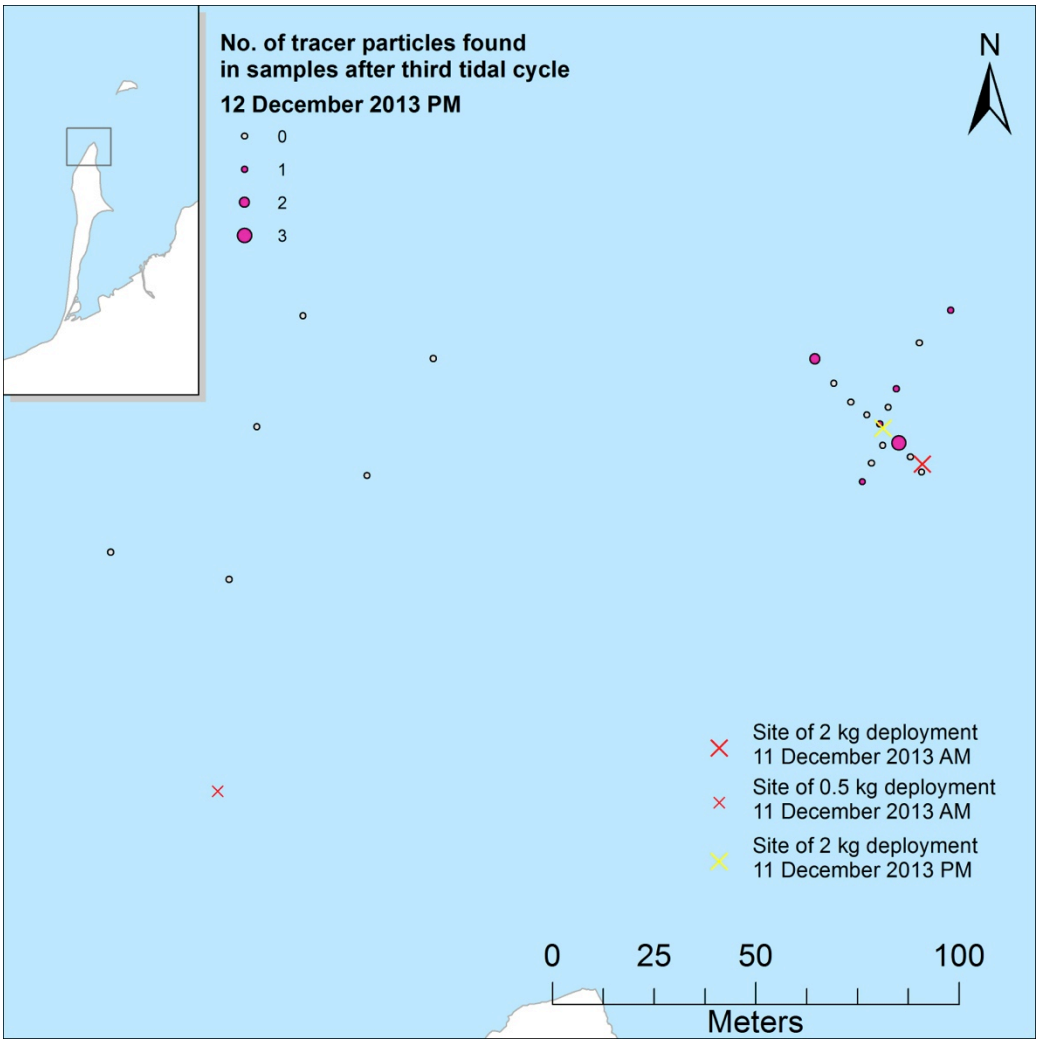

Figure 9.11 Tracer distribution after third tidal cycle following first injection and second tidal cycle following second injection.

12 December AM																					
Depth	**12-1**	**12-2**	**12-3**	**12-4**	**12-5**	**12-6**	**12-7**	**12-8**	**12-9**	**12-10**	**12-11**	**12-13**	**12-14**	**12-15**	**12-16**	**12-17**	**12-18**	**12-19**	**12-20**	**12-21**	**12-22**
0-1.5	0	0	0	0	0	0	0	3	1	0	0	0	0	0	0	0	0	0	0	0	0
1.5-3	0	0	0	0	0	0	0	0	0	0	0	0	0	0	0	0	0	0	0	0	0
3-4.5	0	0	0	0	0	0	0	0	0	0	0	0	0	0	0	0	0	0	0	0	0
4-4.5	0	0	0	0	0	0	0	0	0	0	0	0	0	0	0	0	0	0	0	0	0
4.5-6	0	0	0	0	0	0	0	0	0	0	0	0	0	0	0	0	0	0	0	0	0
6-7.5	1	0	0	0	0	0	0	0	0	0	0	0	0	0	0	0	0	0	0	0	0
7.5-9	0	0	0	1	0	0	0	0	0	0	0	0	0	0	0	0	0	0	0	0	0
9-10.5	0	0	0	0	0	0	0	0	0	0	0	1	0	0	0	0	0	0	0	0	0
10.5-12	0	1	0	0	0	0	0	0	0	0	0	0	0	0	0	0	0	0	0	0	0
12-13.5	0	0	0	0	0	0	0	0	0	0		0	0	0	0	0	0	0	0		0
13.5-15	0		0	0	0	0	0	0	0	0		1	0	0		0		0	0		0
15-16.5			0	0	0	0	0	0	0			0									0
16.5-18			0	0	0	0						0									0
18-19.5					0	0						0									
19.5-21						0															
21-22.5						0															
22.5-24						0															
24-25.5						0															

Table 9.2 Tracer distribution with depth for each sample collected on 12 Dec.

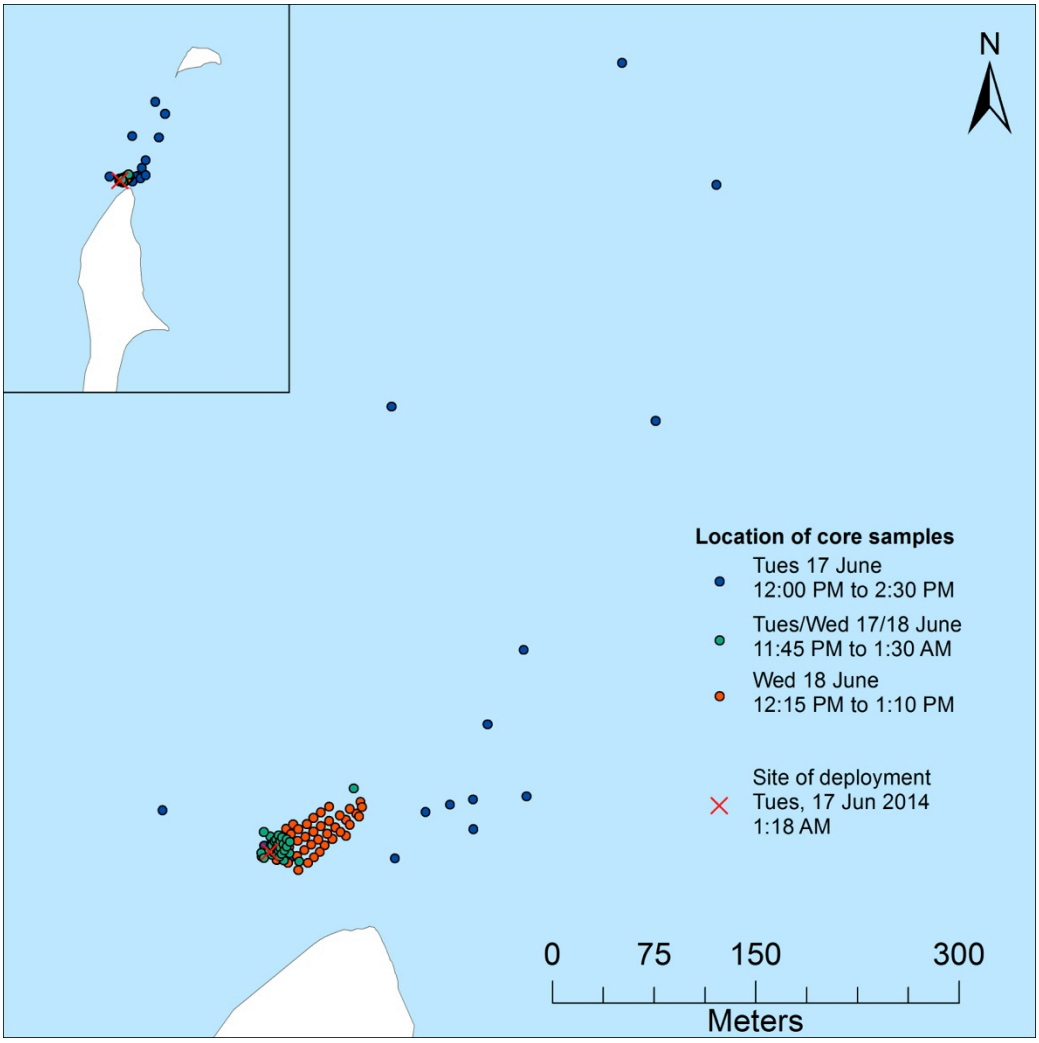

Figure 9.12 Sites of sediment tracer injection and locations of core samples for June 2014 tracer experiment. The shoreline at distal end of the barrier has been updated to reflect the dune toe position on 4 May 2014 (the last TLS survey before the experiment). It should be noted that the dune toe here had receded by approximately 50 m since the last experiment in December 2013.

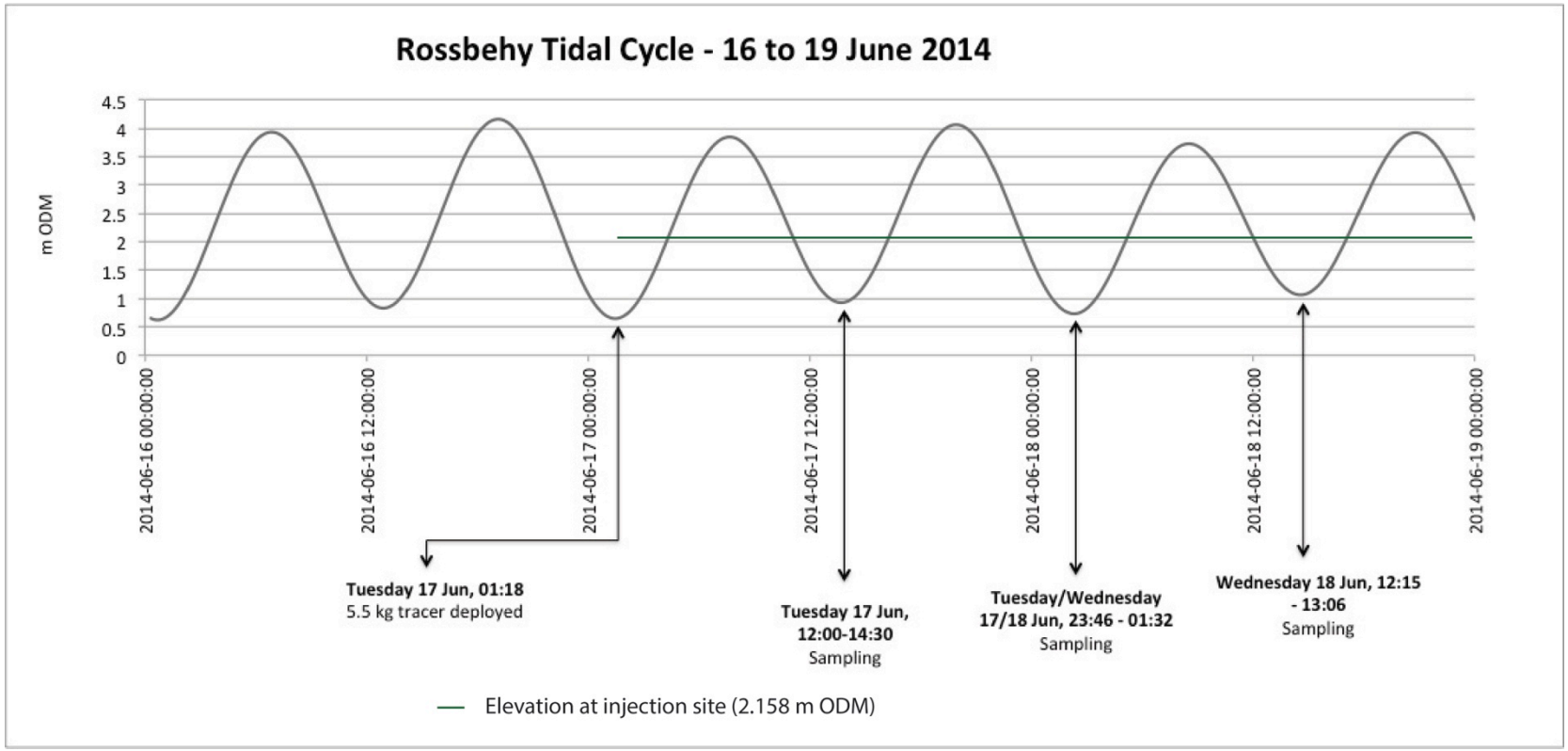

Figure 9.13 June sediment tracer experiment timeline in relation to tidal cycle. Source of tide data: Marine Institute

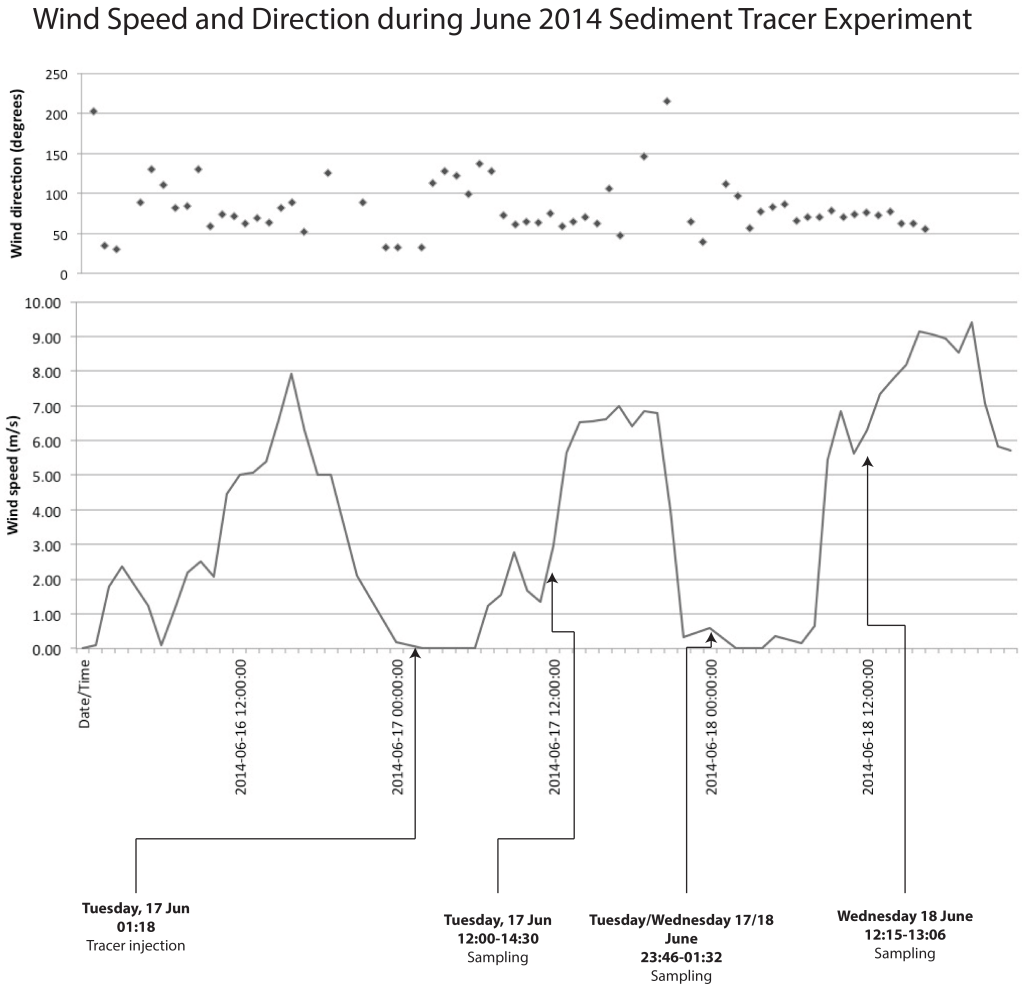

Figure 9.14 Wind speeds and directions during June 2014 tracer experiment. Winds were predominantly southeasterly, with average speeds of 8.6 m/s. Hourly data obtained from Ventry weather station.

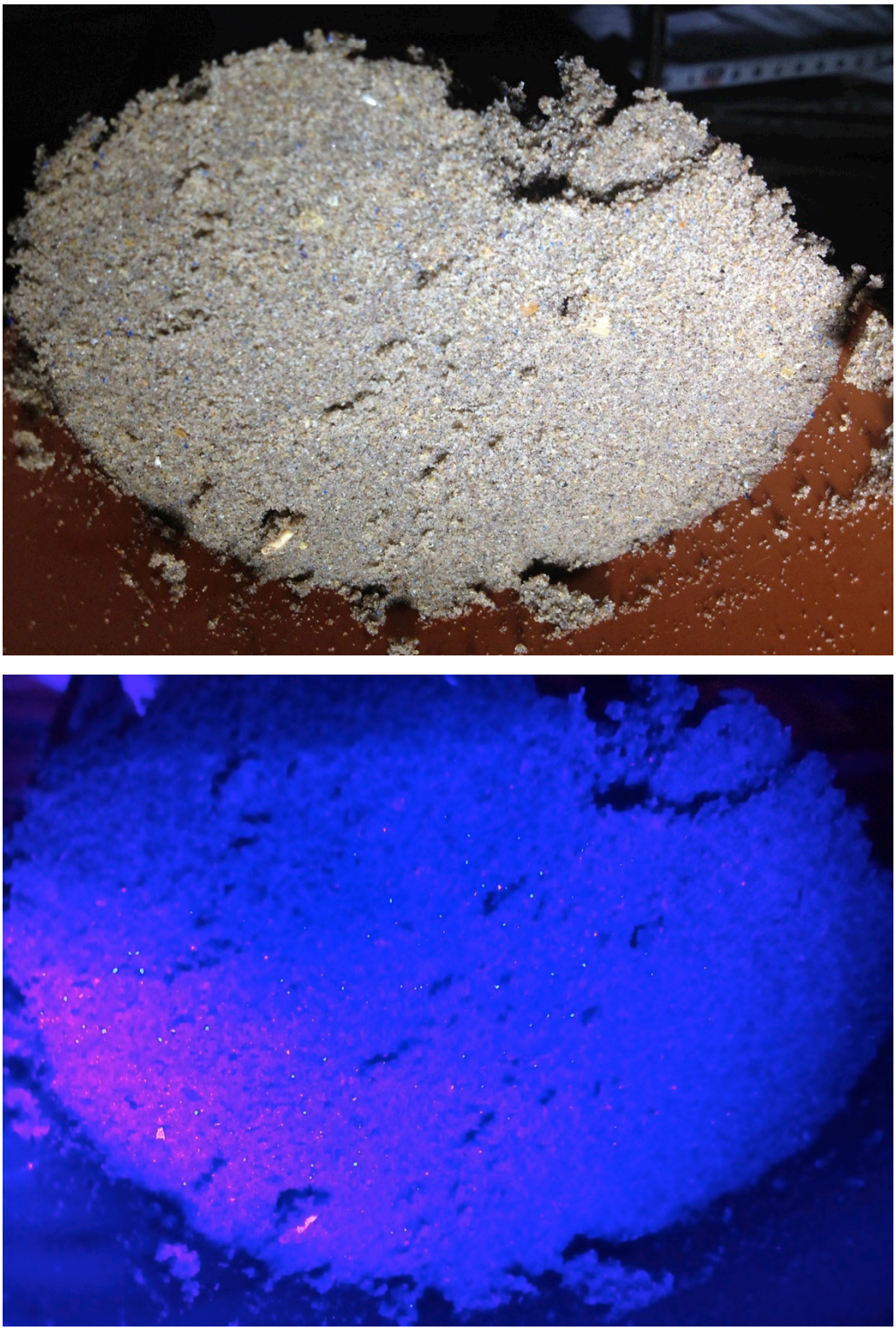

Figure 9.15 Tracer particles in a June 2013 core under ordinary and UV light.

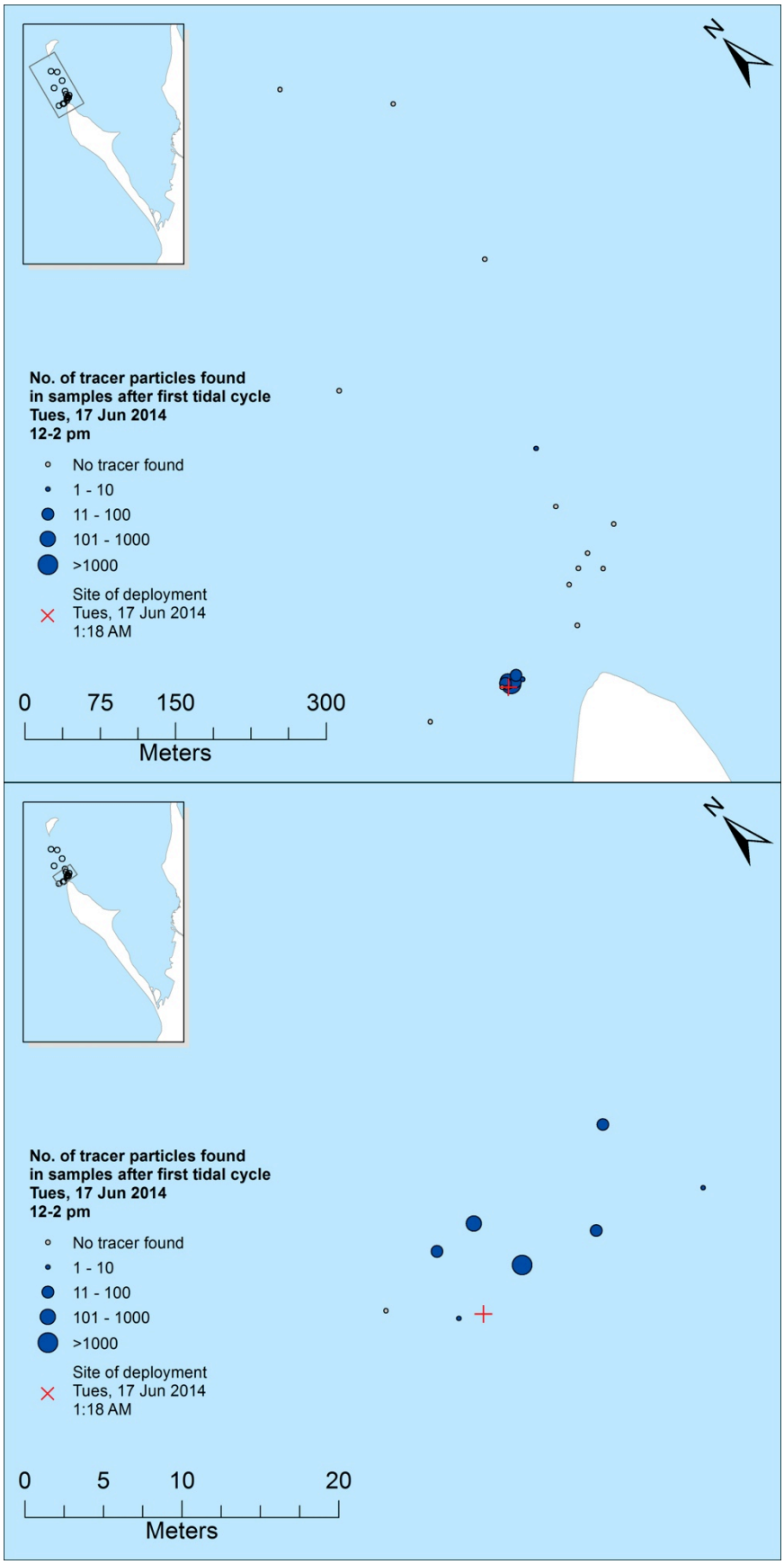

Figure 9.16 Tracer distribution after first tidal cycle following injection. Small (top) and large (bottom) scale views of the site are shown to better illustrate sample distribution.

	17 June - Midday																
Depth	**T1-1**	**T1-2**	**T1-3**	**T1-4**	**T1-5**	**T1-6**	**T1-7**	**T1-13**	**T1-14**	**T1-15**	**T1-16**	**T1-17**	**T1-18**	**T1-19**	**T1-20**	**T1-21**	**T1-22**
0-2 cm	4	0	0	0	0	0	0	0	0	0	0	15	1200	33	9	451	32
2-4 cm	0	0	0	0	0	0	1	0	0	0	0	0	1100	7	0	61	9
4-6 cm	1	0	0	0	0	0	0	0	0	0	0	0	1000	0	0	1	0
6-8 cm	0	0	0	0	0	0	0	0	0	0	0	0	900	2	0	3	0
8-10 cm	0	0	0	0	0	0	0	0	0	0	0	0	737	0	0	0	0
10-12 cm	0	0	0	0		0		0	0	0	0	0	361	0	0	0	0
12-14 cm	0	0	0	0		0		0	0	0	0	0		0		0	
14-16 cm	0	0	0	0				0	0	0				0			
16-18 cm	0	0	0	0				0	0	0							
18-20 cm	0	0		0				0									

Table 9.3 Tracer distribution with depth for each sample collected after the first tidal cycle. Maps showing the locations of samples (labeled with corresponding sample IDs) are shown in figure 9.17.

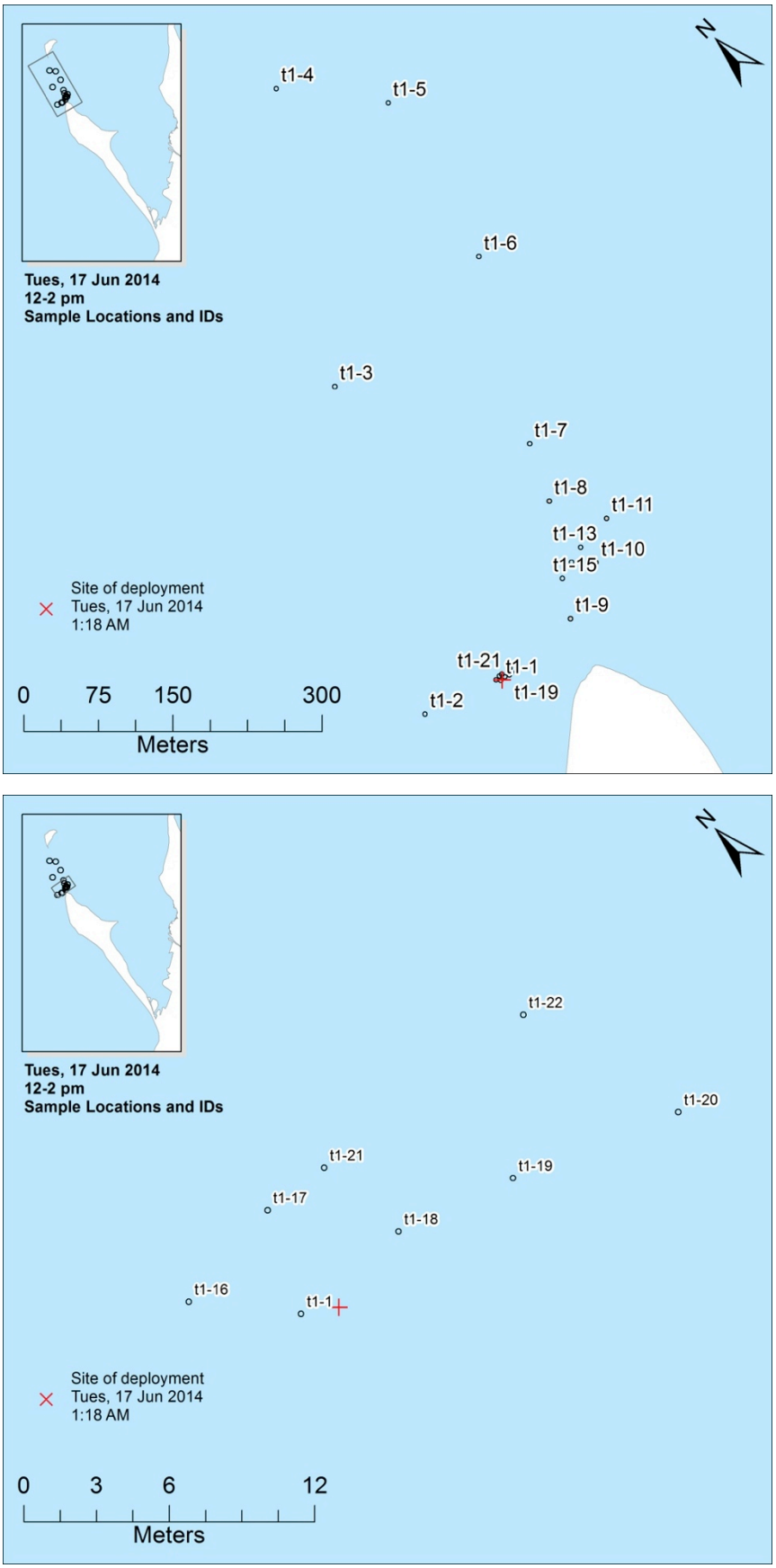

Figure 9.17 Locations of samples labeled with sample IDs, which correspond to those in table 9.3. Small (top) and large (bottom) scale views of the site are shown to better illustrate sample distribution.

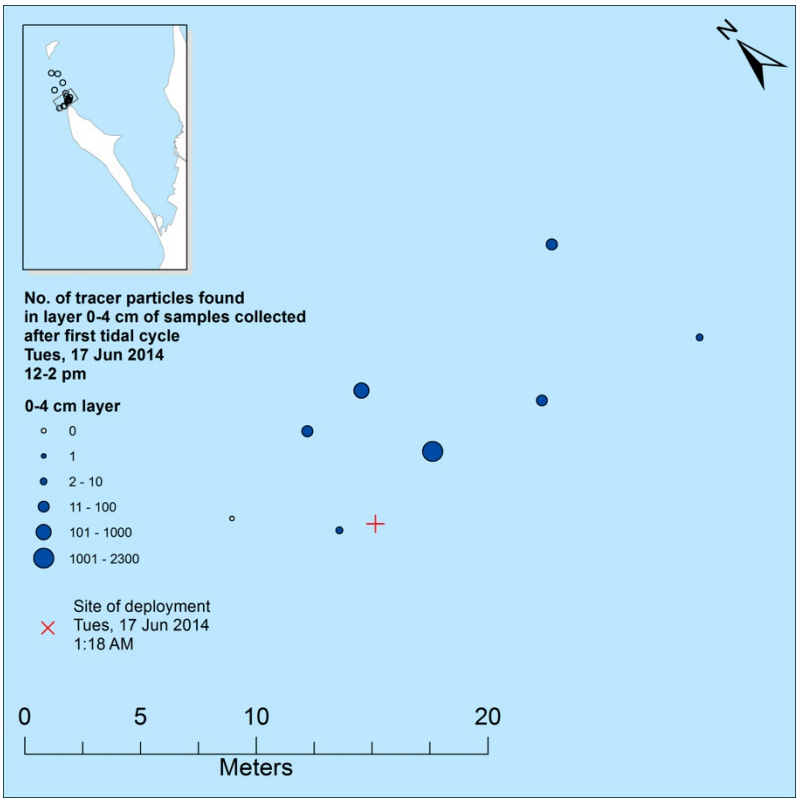

Figure 9.18 Tracer distribution in top 0-4 cm layer for samples collected after first tidal cycle following injection. Only area where samples containing positively identified tracer are shown.

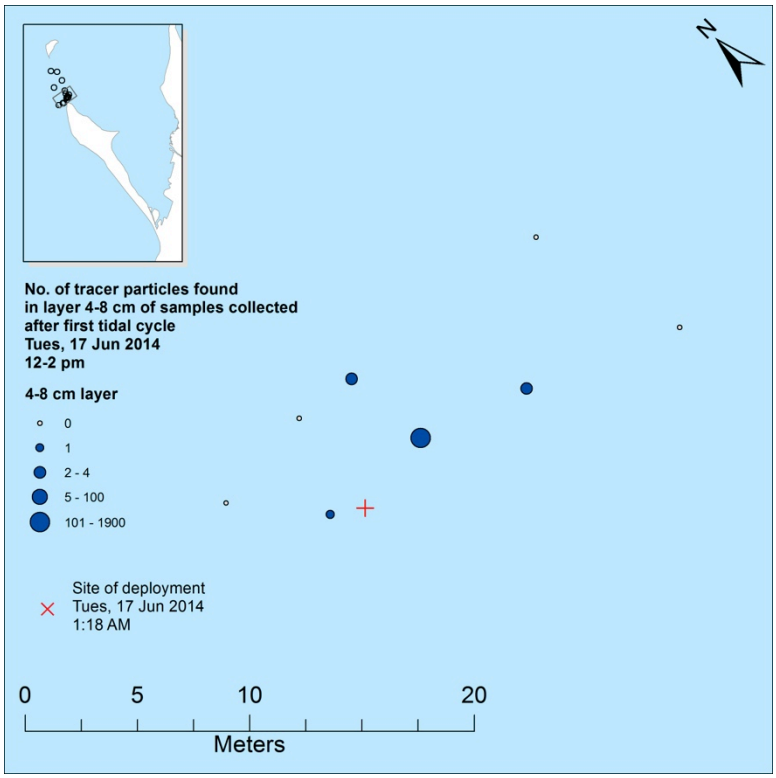

Figure 9.19 Tracer distribution in 4-8 cm depth layer for samples collected after first tidal cycle following injection.

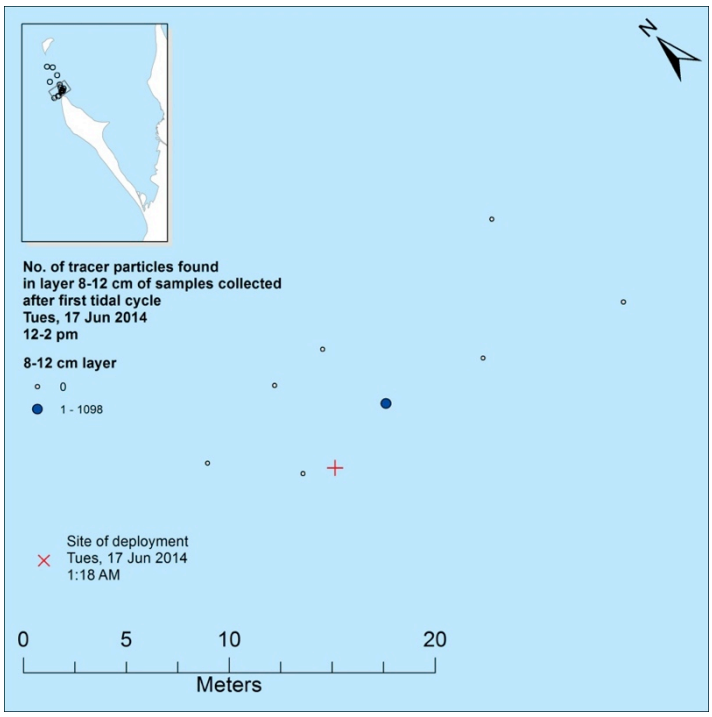

Figure 9.20 Tracer distribution in 8-12 cm depth layer for samples collected after first tidal cycle following injection.

		After 1st tidal cycle (t_1)
0-4 cm	Longshore position of tracer cloud centroid (Y) - metres from injection point	4.6
	Velocity of transport (mm/s)	0.1072
4-8 cm	Longshore position of tracer cloud centroid (Y) - metres from injection point	4.0
	Velocity of transport (mm/s)	0.0924
8-12 cm	Longshore position of tracer cloud centroid (Y) - metres from injection point	4.0
	Velocity of transport (mm/s)	0.0922

Table 9.4 Longshore position of tracer cloud centroids and velocities of transport for sample layers 0-4 cm, 4-8 cm, and 8-12 cm. (Samples collected after 1st tidal cycle)

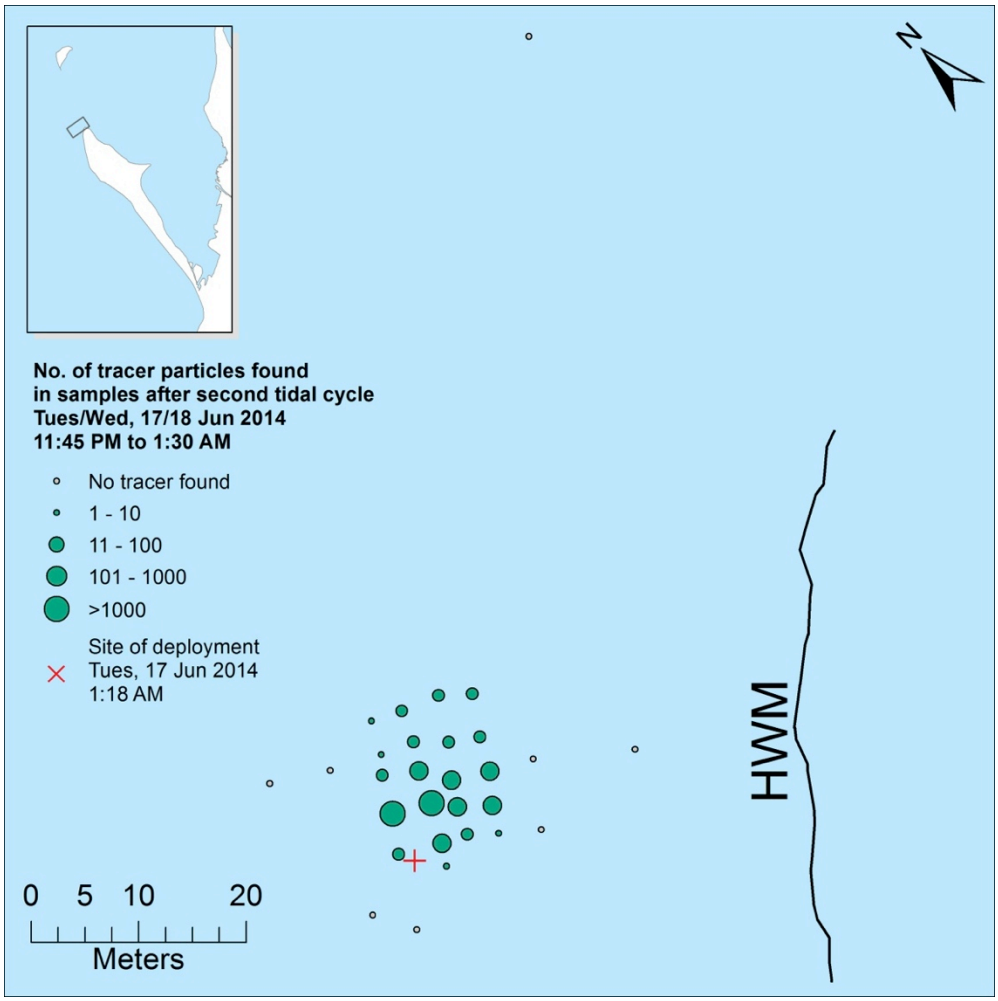

Figure 9.21 Tracer distribution after second tidal cycle following injection.

17/18 June - Midnight																					
Depth (cm)	**T2-1**	**T2-2**	**T2-3**	**T2-4**	**T2-5**	**T2-6**	**T2-7**	**T2-8**	**T2-9**	**T2-10**	**T2-11**	**T2-12**	**T2-13**	**T2-14**	**T2-15**	**T2-16**	**T2-17**	**T2-18**	**T2-19**	**T2-20**	**T2-21**
0-2	14	152	13	2	0	0	398	3344	53	23	8	45	710	164	43	13	1	166	251	87	42
2-4	18	320	5	0	1	2	210	39	17	7	4	0	9	28	0	0	0	51	1	1	0
4-6	34	450	8	0	2	0	33	2	25	0	0	0	4	0	0	1	0	0	0	0	0
6-8	18	160	12	0	0	0	1	0	13	0	0	0	1	0	0	0	0	0	0	0	1
8-10	6	99	4	0	0	0	4	4	23	0	0	0	1	1	0	0	0	0	0		
10-12	1	7	0	0	0	0	0		0	0	0	0	2	1		0	0		0		
12-14		0	0	0	0	0			0	0	0	0	0	0		0					
14-16		9	0		0	0			0		0					0					
16-18		0			0	0					0										
18-20		0			0																

Table 9.4 Tracer distribution with depth for each sample collected after the second tidal cycle. A map showing the locations of samples (labeled with corresponding sample IDs) is shown in figure 9.22.

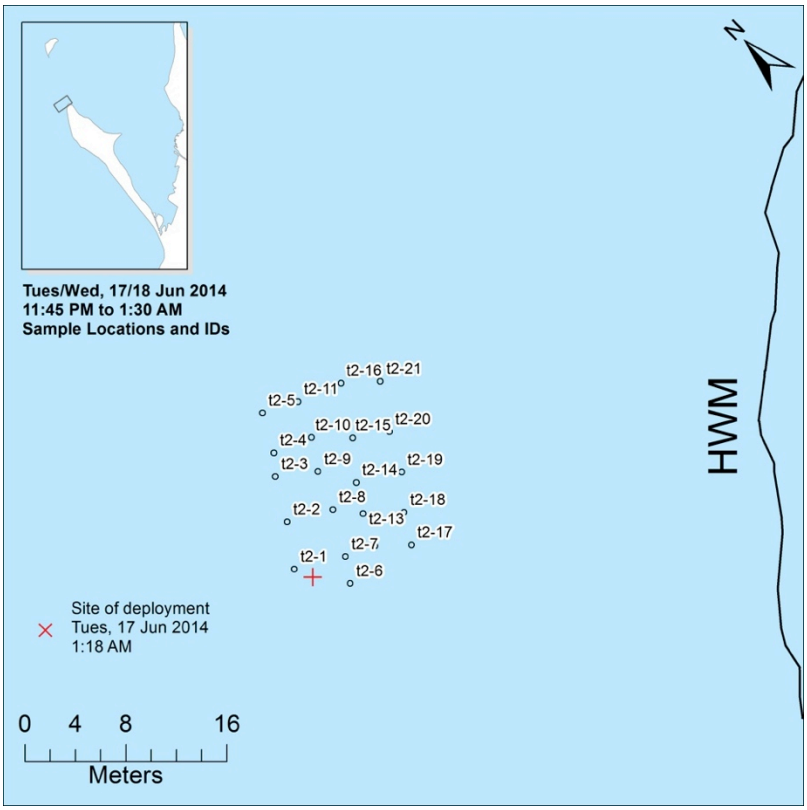

Figure 9.22 Locations of samples labeled with sample IDs, which correspond to those in table 9.4.

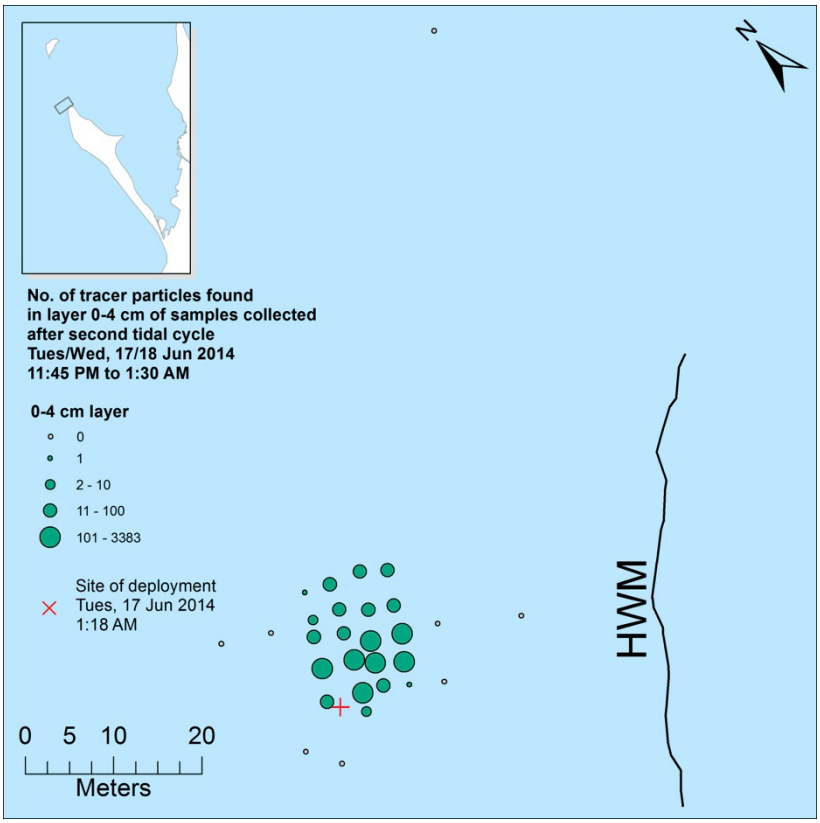

Figure 9.23 Tracer distribution in top 0-4 cm layer in samples collected after second tidal cycle following injection.

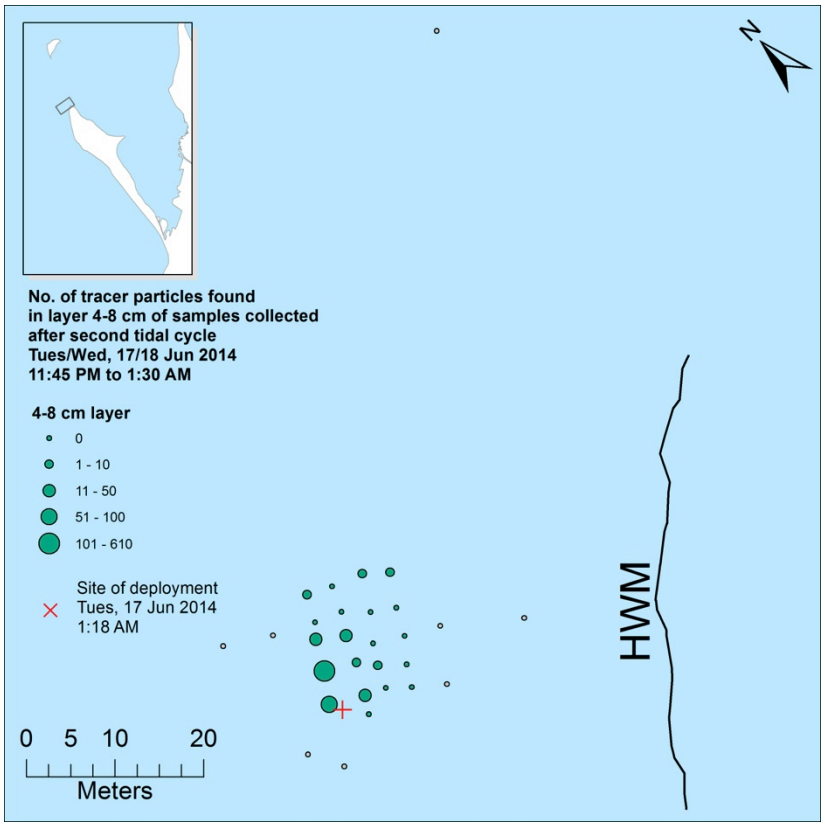

Figure 9.24 Tracer distribution in 4-8 cm layer in samples collected after second tidal cycle following injection.

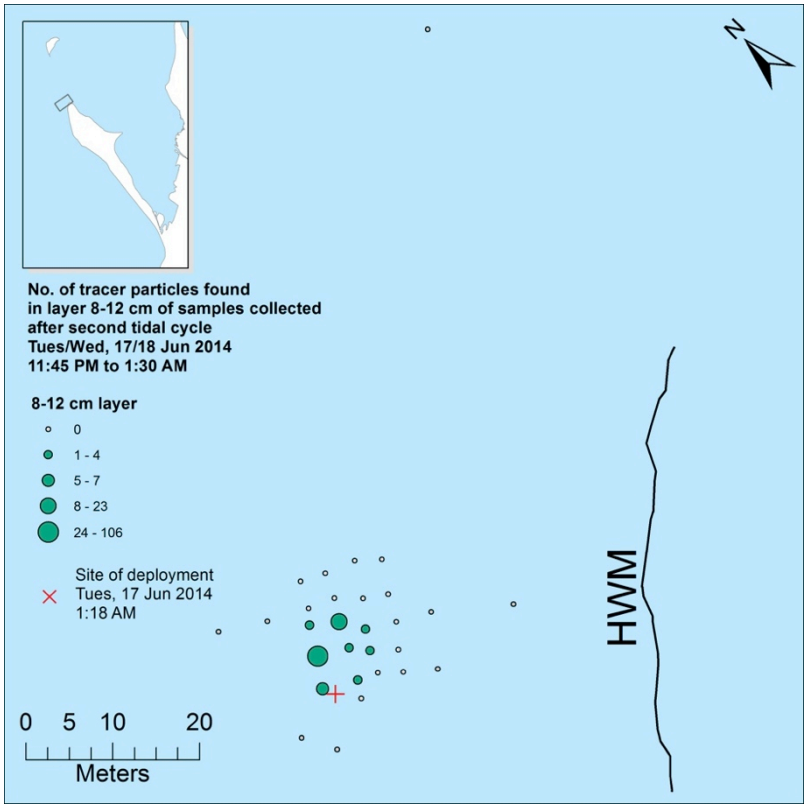

Figure 9.25 Tracer distribution in 8-12 cm layer in samples collected after second tidal cycle following injection.

		After 2nd tidal cycle (t_2)
0-4 cm	Longshore position of tracer cloud centroid (Y) - metres from injection point	6.1
	Distance from centroid at t_1 (m)	1.5
	Velocity of transport (mm/s)	0.0337
4-8 cm	Longshore position of tracer cloud (Y) relative to previous position of centroid (m)	4.9
	Distance from centroid at t_1 (m)	0.9
	Velocity of transport (mm/s)	0.0205
8-12 cm	Longshore position of tracer cloud centroid (Y) - metres from injection point	5.4
	Distance from centroid at t_1 (m)	1.4
	Velocity of transport (mm/s)	0.0320

Table 9.5 Longshore position of tracer cloud centroids and velocities of transport for sample layers 0-4 cm, 4-8 cm, and 8-12 cm. (Samples collected after 2nd tidal cycle)

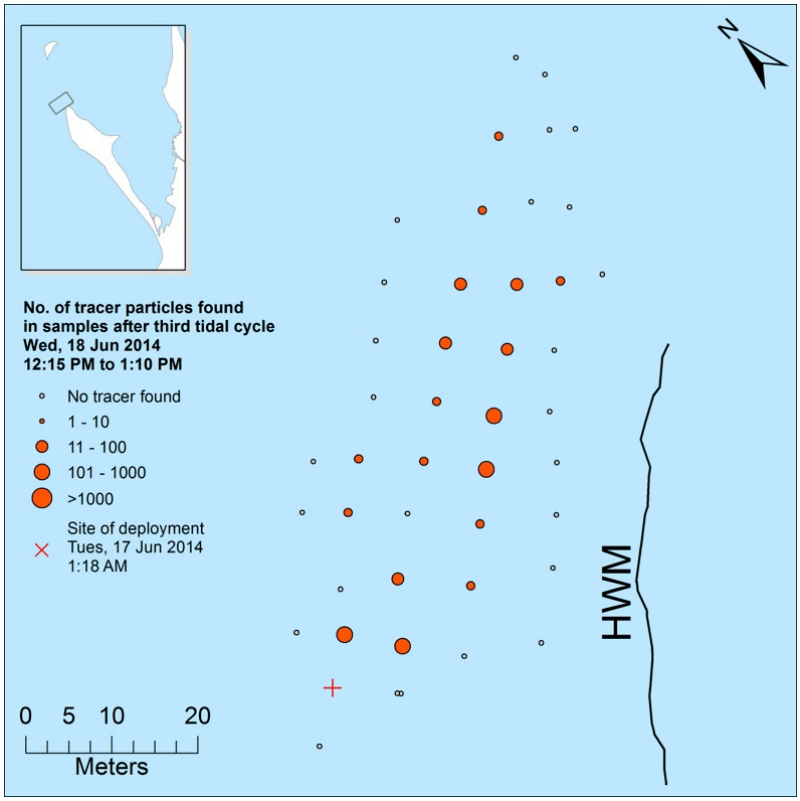

Figure 9.26 Tracer distribution after third tidal cycle following injection.

	18 June - Midday																		
Depth (cm)	**T3-1**	**T3-2**	**T3-3**	**T3-4**	**T3-5**	**T3-6**	**T3-7**	**T3-8**	**T3-9**	**T3-10**	**T3-11**	**T3-12**	**T3-13**	**T3-14**	**T3-15**	**T3-16**	**T3-17**	**T3-18**	**T3-19**
0-2	98	1	3	3	0	6	10	3	0	0	43	192	0	5	9	55	11	23	1
2-4	56	0	2	2	2	8	2	3	1	0	6	56	1	0	16	28	10	9	0
4-6	46	0	0	0	4	6	1	0	0	0	0	0	0	0	19	27	11	5	0
6-8	0	0		3	0	0	0	0	0	0	0	0	0	0	44	47	11	1	0
8-10	0	0		0	0	0	0	0			0	0	0		12	25	0	2	2
10-12		0		0	0		0				0	0	0		5		2	1	0
12-14				0	0						0	1	0				0	1	
14-16					0								0				0	0	
16-18																	0	0	
18-20																			

Table 9.6 Tracer distribution with depth for each sample collected after the third tidal cycle. A map showing the locations of samples (labeled with corresponding sample IDs) is shown in figure 9.27.

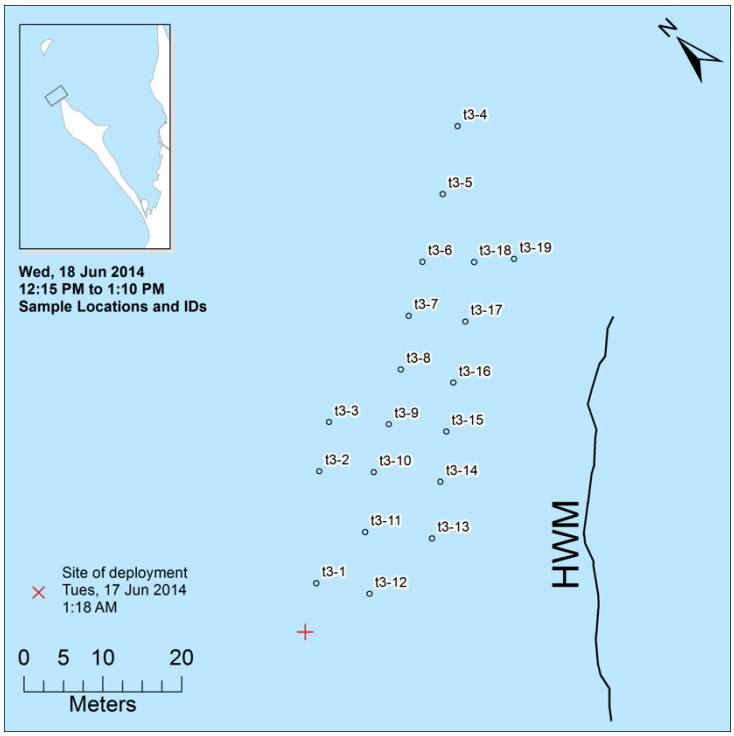

Figure 9.27 Locations of samples labeled with sample IDs, which correspond to those in table 9.6.

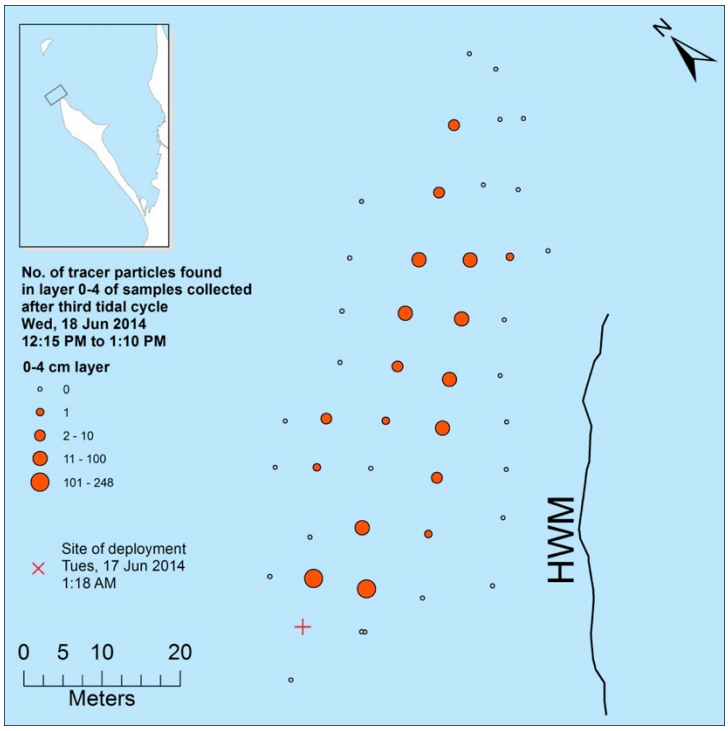

Figure 9.28 Tracer distribution in top 0-4 cm layer in samples collected after third tidal cycle following injection.

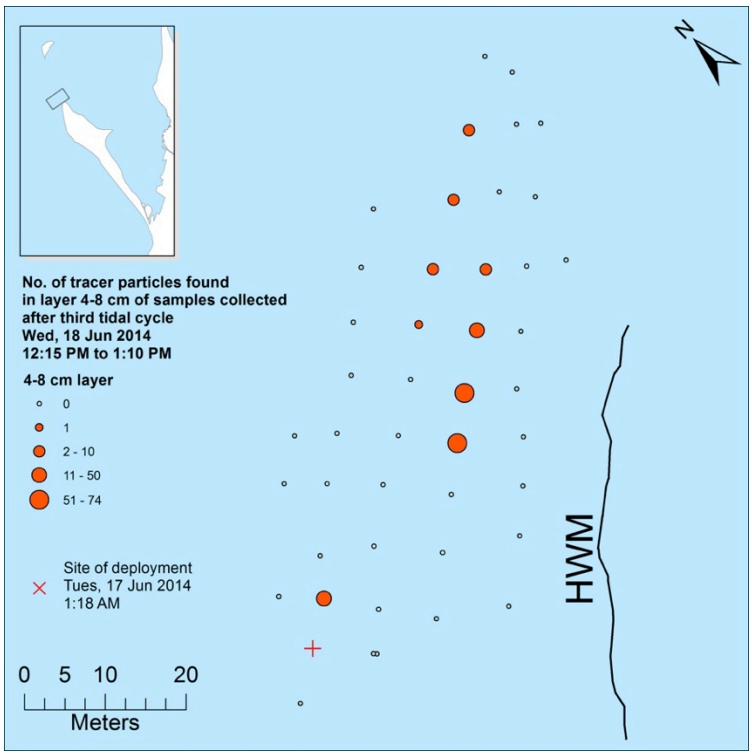

Figure 9.29 Tracer distribution in 4-6 cm layer in samples collected after third tidal cycle following injection.

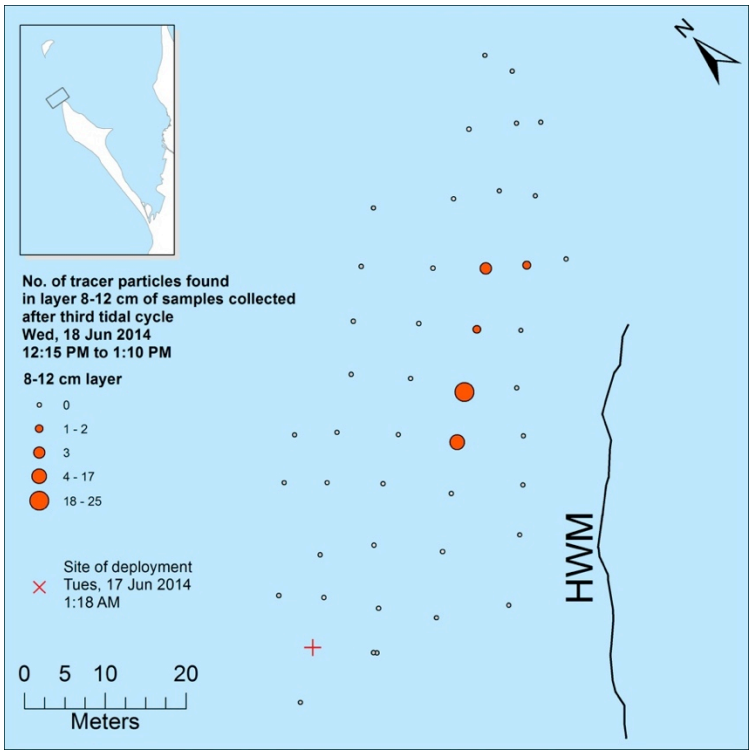

Figure 9.30 Tracer distribution in 8-12 cm layer in samples collected after third tidal cycle following injection.

		After 3rd tidal cycle (t_3)
0-4 cm	Longshore position of tracer cloud centroid (Y) - metres from injection point	19.1
	Distance from centroid at t_2 (m)	13.1
	Velocity of transport (mm/s)	0.3022
4-8 cm	Longshore position of tracer cloud centroid (Y) - metres from injection point	31.3
	Distance from centroid at t_2 (m)	26.4
	Velocity of transport (mm/s)	0.6110
8-12 cm	Longshore position of tracer cloud centroid (Y) - metres from injection point	36.8
	Distance from centroid at t_2 (m)	31.4
	Velocity of transport (mm/s)	0.7268

Table 9.7 Longshore position of tracer cloud centroids and velocities of transport for sample layers 0-4 cm, 4-8 cm, and 8-12 cm. (Samples collected after 3rd tidal cycle)

		After 1st tidal cycle	After 2nd tidal cycle	After 3rd tidal cycle
0-4 cm	Longshore position of tracer cloud centroid (Y) - metres from injection point	4.6	6.1	19.1
	Distance between tracer cloud centroids	-	1.5	13.1
	Velocity of transport (mm/s)	0.1072	0.0337	0.3022
4-8 cm	Longshore position of tracer cloud centroid (Y) - metres from injection point	4.0	4.9	31.3
	Distance between tracer cloud centroids	-	0.9	26.4
	Velocity of transport (mm/s)	0.0924	0.0205	0.6110
8-12 cm	Longshore position of tracer cloud centroid (Y) - metres from injection point	4.0	5.4	36.8
	Distance between tracer cloud centroids	-	1.4	31.4
	Velocity of transport (mm/s)	0.0922	0.0320	0.7268

Table 9.8 Longshore position of tracer cloud centroids and velocities of transport for subsample layers 0-4 cm, 4-8 cm, and 8-12 cm from samples collected after each of the three tidal cycles.

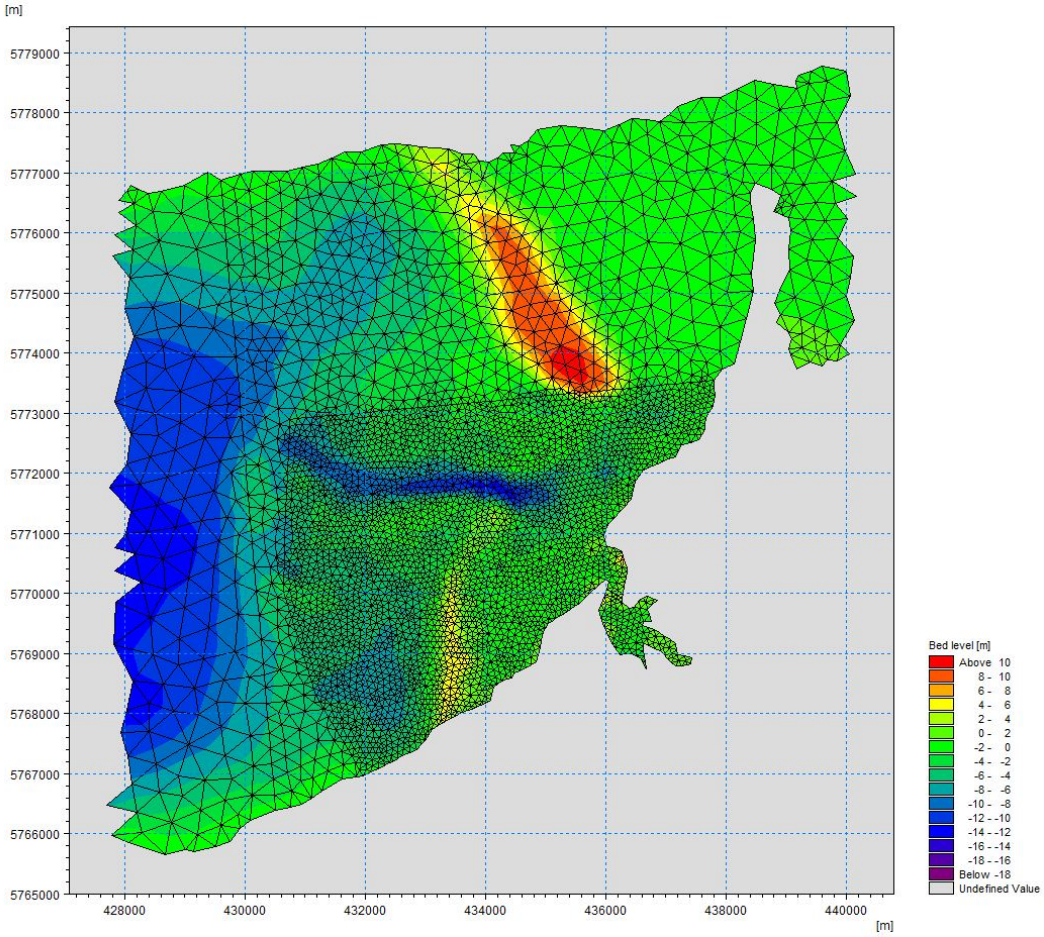

Figure 10.1 Nearshore mesh, across which equations are solved in MIKE21, at Rossbehy. Bathymetric data has been interpolated to the mesh.

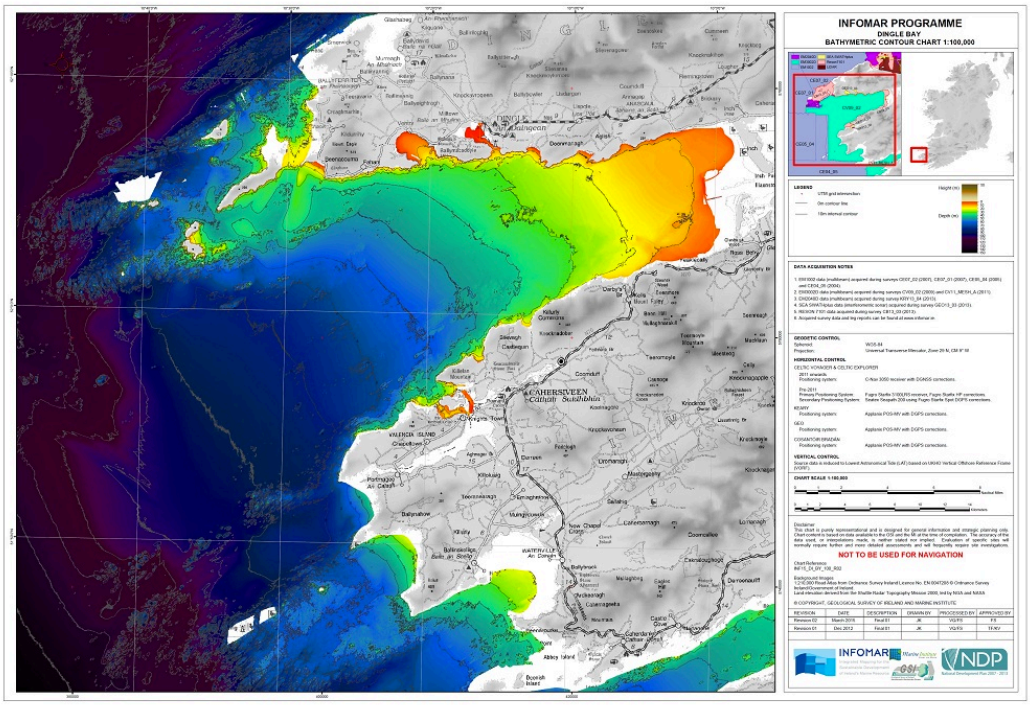

Figure 10.2 INFOMAR Bathymetry Data for Dingle Bay used in model set-up. Extracted from INFOMAR (2015b)

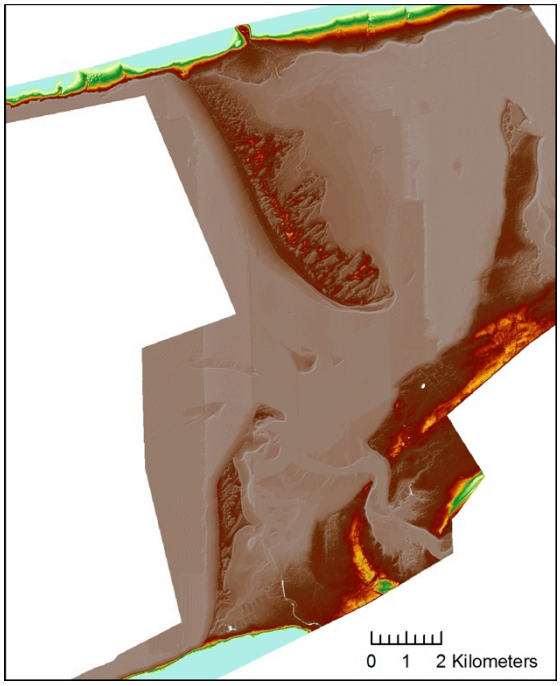

Figure 10.3 Aerial LiDAR data used in model set-up. The survey took place in April 2011. Data was provided by Kerry County Council.

Cross-shore dune recession analysis (van Rijn, 2009)			
Period	**Location**	**Calculated Dune Recession (m)**	**Measured Dune Recession (m)**
July 2009-Feb 2010	Swash	2.2–3.3	0–4
July 2009-Feb 2010	Drift	12.5–18.77	37–70
July 2009-Feb 2010	Island low	16.1–24.2	26–30
July 2009-Feb 2010	Island high	2.5–3.9	0–22
Feb 2010-June 2010	Swash	0.65–1.0	N/A
Feb 2010-June 2010	Drift	3.6–5.5	0–11
Feb 2010-June 2010	Island low	4.7-7.1	10–22
Feb 2010-June 2010	Island high	0.7–1.1	0–7
June 2010-Nov 2010	Swash	1-1.5	N/A
June 2010-Nov 2010	Drift	5.8–8.7	19–35
June 2010-Nov 2010	Island low	7.5–11.3	21–22
June 2010-Nov 2010	Island high	1.2–1.8	10–21
Nov 2010-Feb 2011	Swash	0.9-1.44	0–0.5
Nov 2010-Feb 2011	Drift	5.6–8.4	26–29
Nov 2010-Feb 2011	Island low	7.3–11	12–16
Nov 2010-Feb 2011	Island high	1.1-1.66	7–8
Feb 2011-June 2011	Swash	0.7–1.1	0
Feb 2011-June 2011	Drift	4.25–6.30	0–8
Feb 2011-June 2011	Island low	5.4–8.14	0
Feb 2011-June 2011	Island high	0.8–1.29	0–7
June 2011-Oct 2011	Swash	0.5–1.06	0–0.5
June 2011-Oct 2011	Drift	3.9–5.9	10–33
June 2011-Oct 2011	Island low	5–7.6	0.5–7.5
June 2011-Oct 2011	Island high	0.8–1.2	10–16

Table 10.1 Measured versus calculated rates of dune recession using the cross-shore formula of van Rijn (2009) from a study by O'Shea and Murphy (2013). In that study, an evaluation of the effectiveness of various transport formulae was carried out in an effort to choose the most appropriate one for the Dingle Bay model set-up used in this PhD research. There was good agreement between modeled dune recession using the cross-shore formula of van Rijn (2009) and measurements for the swash-aligned zone. Data source: O'Shea and Murphy (2013).

Alongshore dune recession analysis (van Rijn, 1998)			
Year	**Location**	**Effective Recession Rates from Alongshore Transport (Load/Length X Avg Dune Height) - calculated using formula of van Rijn (1998) (m)**	**Measured Dune Recession Approx. (m)**
2009-10	Swash	0.02	0–4
2010–11	Swash	0.2	0–1
2009–10	Drift	73	45–80
2010–11	Drift	82	30–70
2009–10	Island high	31	10–44
	Island low	138	36–100
2010–11	Island high	44	17–36
	Island low	196	20–50

Table 10.2 Measured versus calculated rates of dune recession using the alongshore formula of van Rijn (1998) from a study by O'Shea and Murphy (2013). In that study, an evaluation of the effectiveness of various transport formulae was carried out in an effort to choose the most appropriate one for the Dingle Bay model set-up used in this PhD research. There was some agreement between modeled dune recession using the alongshore formula of van Rijn (1998) and measurements for the drift-aligned zone. Data source: O'Shea and Murphy (2013).

Modal wave direction associated with events (°)	**Mean duration of events characterised by modal wave conditions (HH:MM :SS)**	**Mean wave direction associated with modal wave conditions (°)**	**Mean H_{sig} associated with modal wave conditions (m)**	**Peak period associated with modal wave conditions (seconds)**
255-260	52:47:13	259	1.34	8

Table 10.3 Characteristics associated with all storm events that occurred during the period 2011-2014 that were characterized by modal wave conditions. Data extracted from nearshore wave hindcast data.

Start date	**End date**	**Event Duration (HH:MM: SS)**	**Mean H_{sig} (m)**	**Max H_{sig} (m)**	**Peak period (seconds)**	**Mean wave direction (°)**
2012-01-24 18:00:00	2012-01-26 23:00:00	53:00:00	1.49	1.90	9	259

Table 10.4 Characteristics of event chosen to represent "typical" storm conditions. Data extracted from nearshore wave hindcast data.

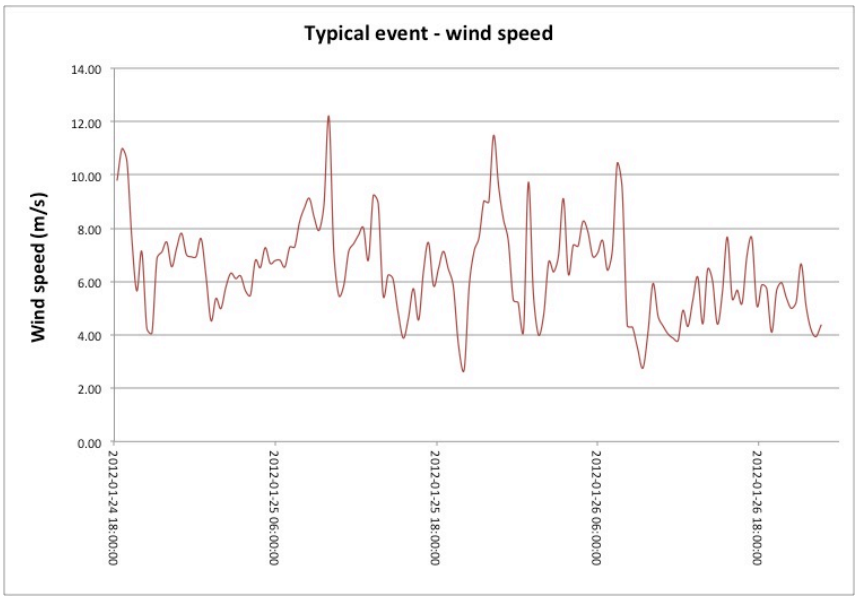

Figure 10.4 Wind speeds used to drive typical event scenario.

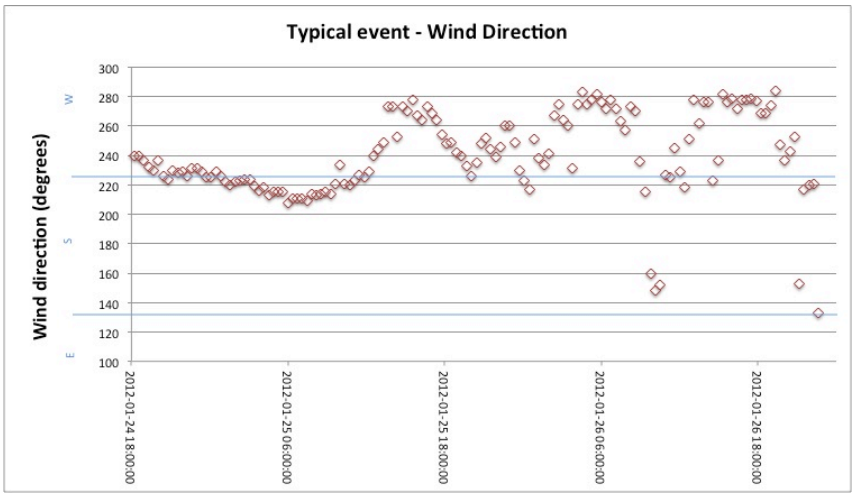

Figure 10.5 Wind directions used to drive typical event scenario.

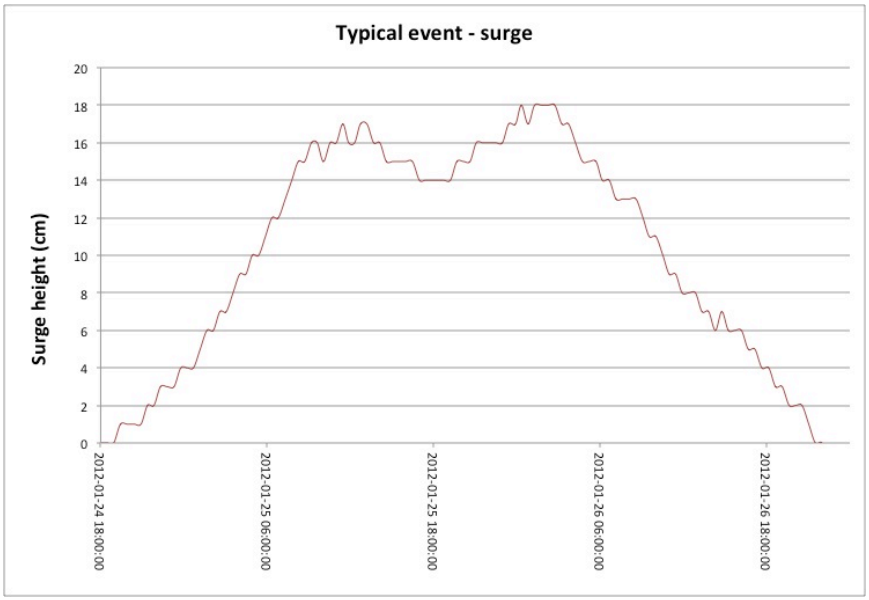

Figure 10.6 Surge heights used to drive typical event scenario.

Start date	End date	Event Duration (HH:MM: SS)	Mean H_{sig} (m)	Max H_{sig} (m)	Peak period (seconds)	Mean wave direction (°)
2013-12-13 06:00:00	2014-01-08 15:00:00	633:00:00	1.85	2.97	9	260

Table 10.5 Characteristics of most extreme event to have occurred during period over which data was available (2011-2014). Data extracted from nearshore wave hindcast data.

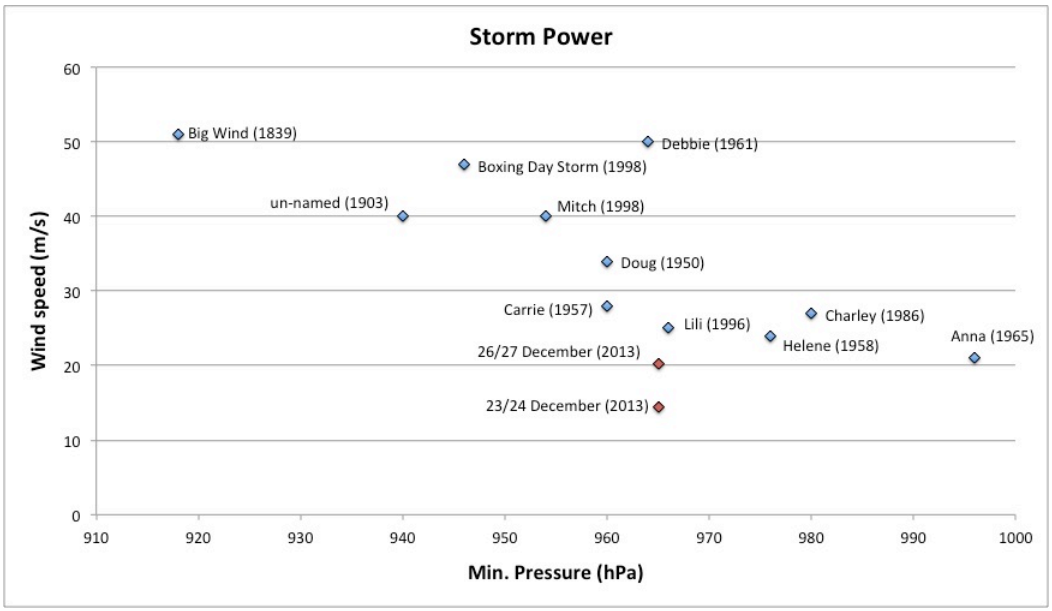

Figure 10.7 Storm power (in terms of minimum pressure and wind speed) for extreme events that have affected Ireland compared to the 26/27 December and 23/24 December 2013 events. Data for historic events compiled by Orford *et al*. (1999).

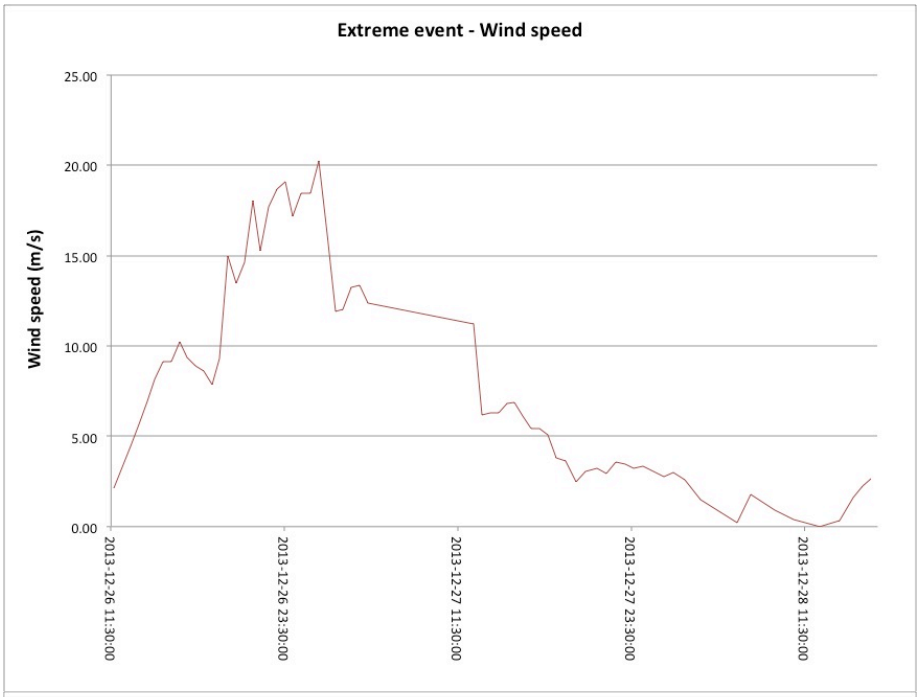

Figure 10.8 Wind speeds used to drive extreme event scenario.

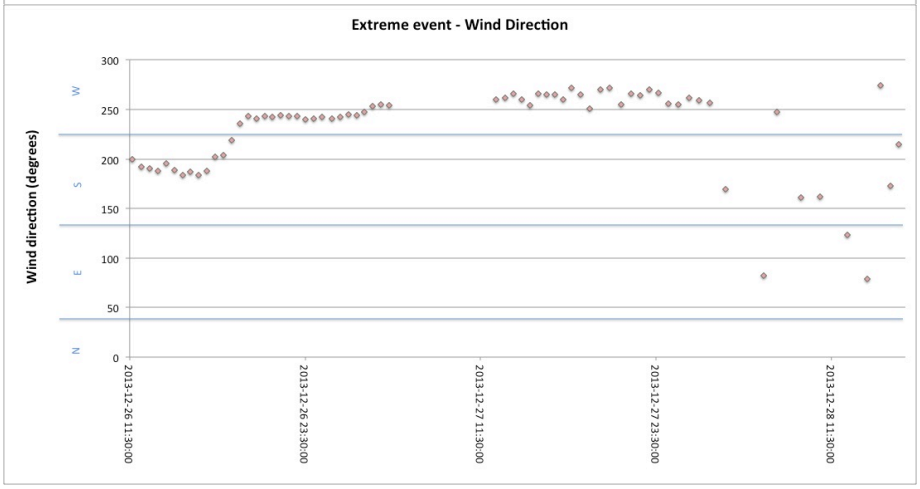

Figure 10.9 Wind directions used to drive extreme event scenario.

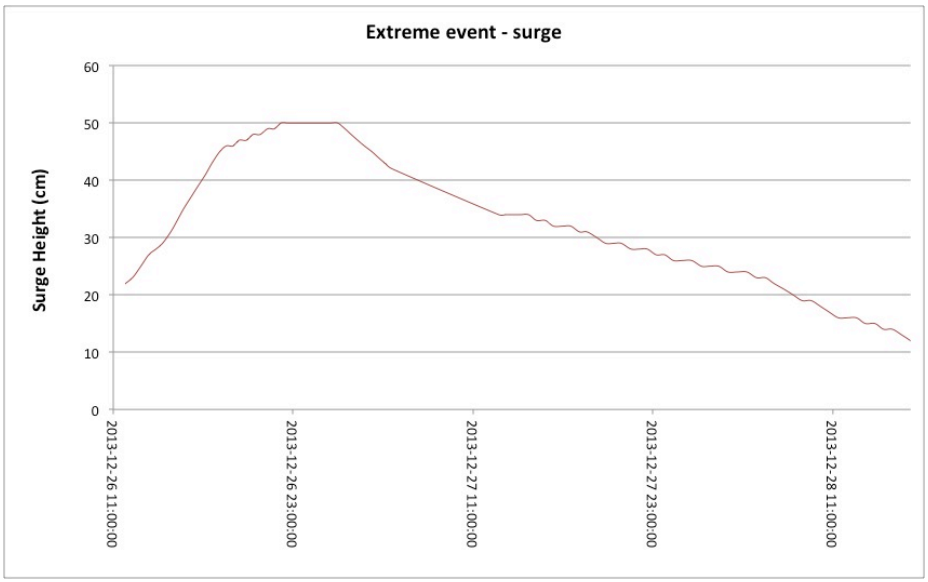

Figure 10.10 Surge heights used to drive extreme event scenario.

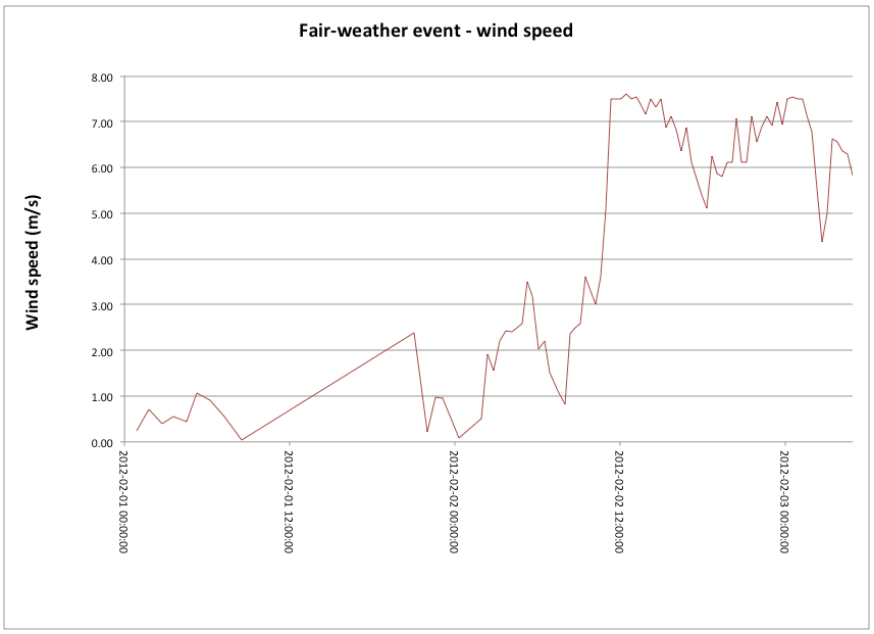

Figure 10.11 Wind speeds used to drive fair-weather scenario.

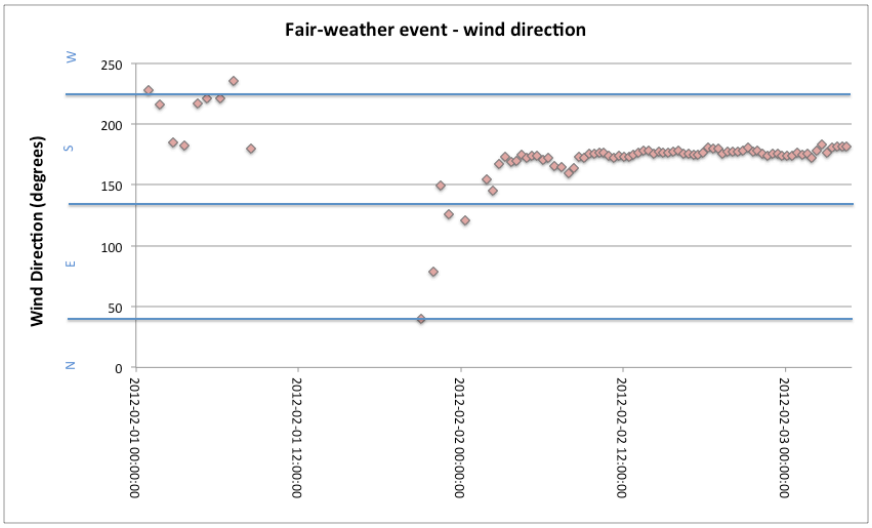

Figure 10.12 Wind directions used to drive fair-weather scenario.

	Extreme Event	Typical Event	Fair-weather Event
Start Date	26/12/2013 11:30	24/01/2012 18:00	01/02/2012 00:00
End Date	28/12/2013 16:30	26/01/2012 23:00	03/02/2012 05:00
Event Duration	53 hours	53 hours	53 hours
Mean Wind Speed	7.7 m/s	6.4 m/s	4.6 m/s
Max Wind Speed	20.3 m/s	12.2 m/s	7.6 m/s
Dominant wind direction	SW	SW	S
Max surge height	50 cm	18 cm	none

Table 10.6 Model inputs for extreme event scenario, typical event scenario, and fair-weather event scenario. Inputs were derived from simulated nearshore wave data and local weather station data. Each scenario was run under sea-levels of 0 cm, 10 cm, and 50 cm.

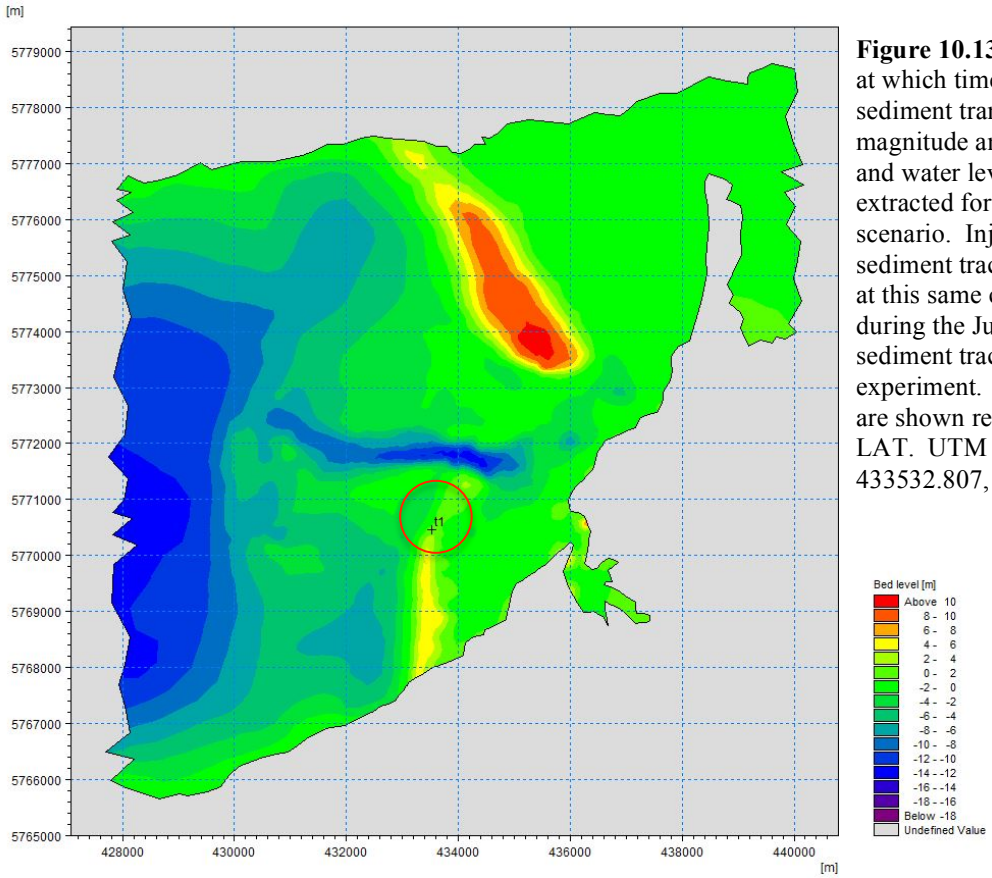

Figure 10.13 Coordinate at which time series of sediment transport magnitude and direction and water levels were extracted for each scenario. Injection of sediment tracer took place at this same coordinate during the June 2014 sediment tracer experiment. Bed levels are shown relative to LAT. UTM coordinate 433532.807, 5770466.742

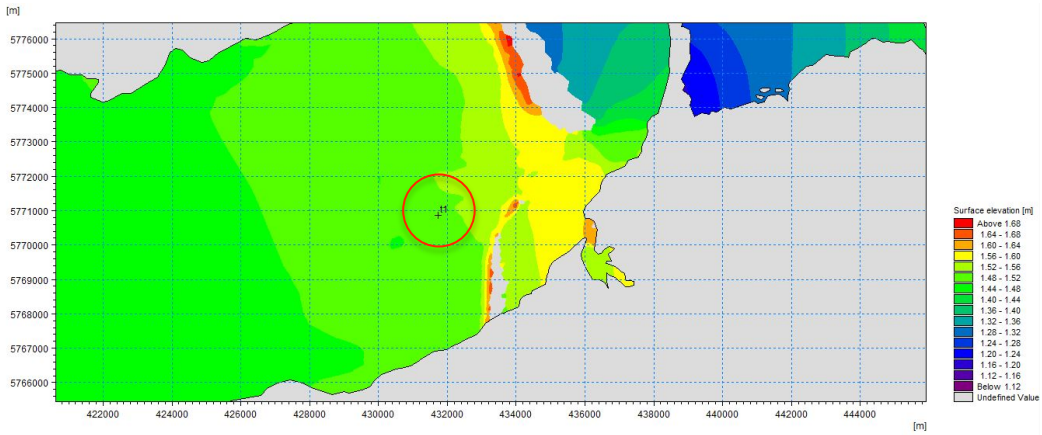

Figure 10.14 Second coordinate at which time series of water levels were extracted to give full picture of tidal state during simulations. Bed levels are shown relative to LAT.

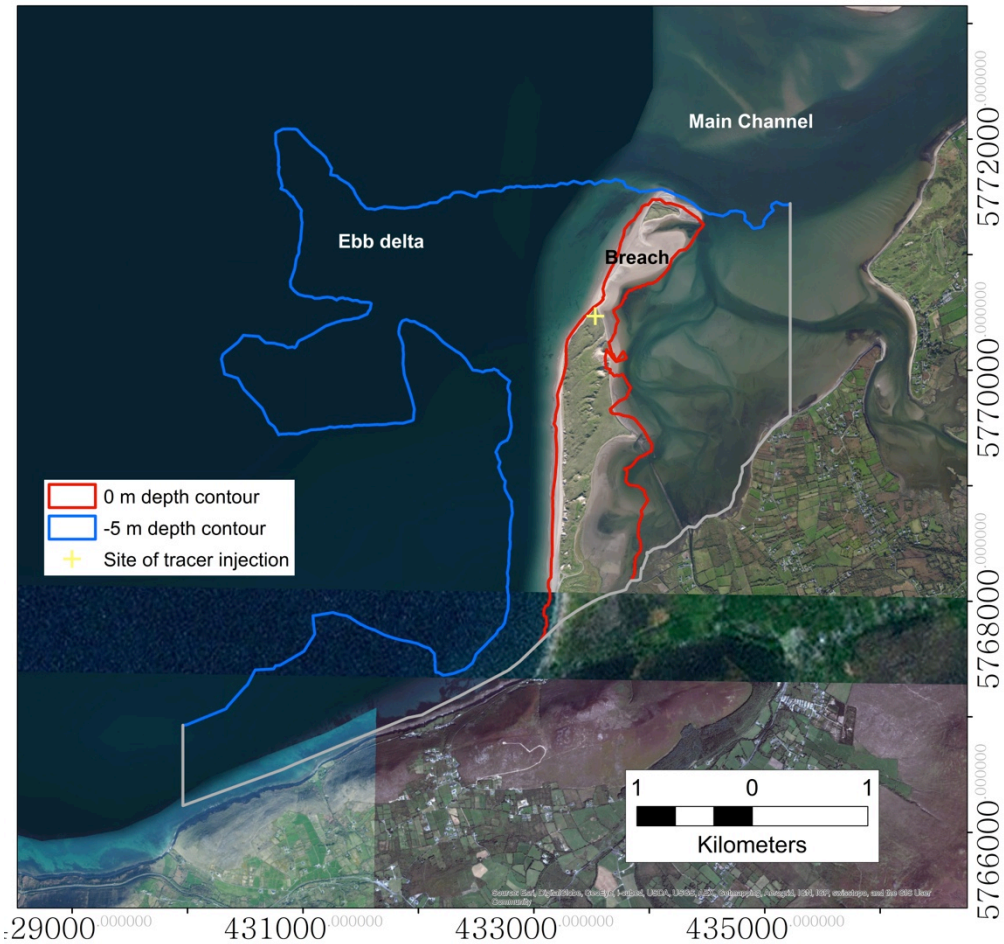

Figure 10.15 Aerial view of the area covered by the maps presented in section 10.3.1 relative to the 0 m and -5 m depth contours and the site of the sediment tracer experiment.

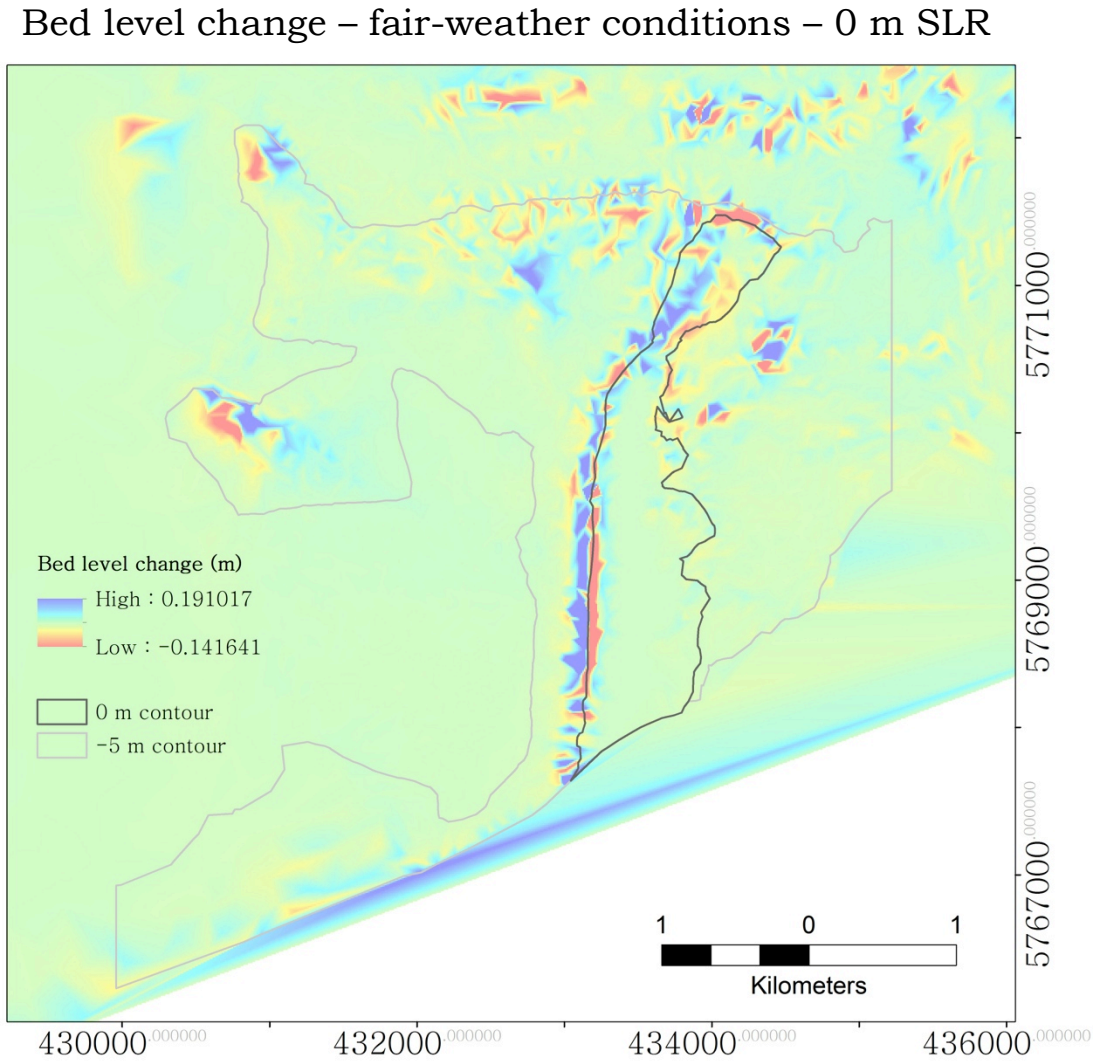

Figure 10.16 Bed level change for the fair-weather, 0 m SLR scenario. Contours are relative to LAT.

Volume gains and losses - fair-weather conditions – 0 m SLR

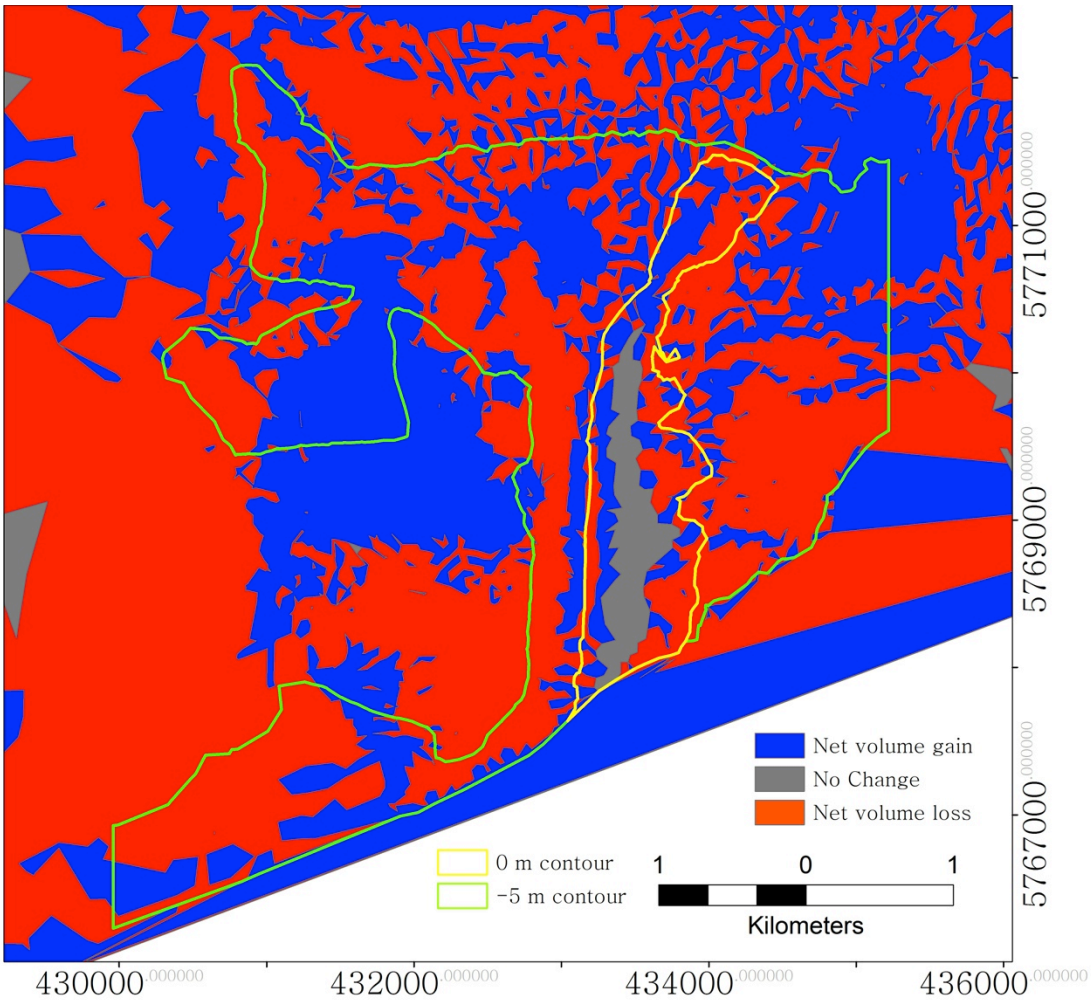

Figure 10.17 Volume gains and losses for the fair-weather, 0 m SLR scenario. Contours are relative to LAT.

Bed level change - fair-weather conditions – 0.1 m SLR

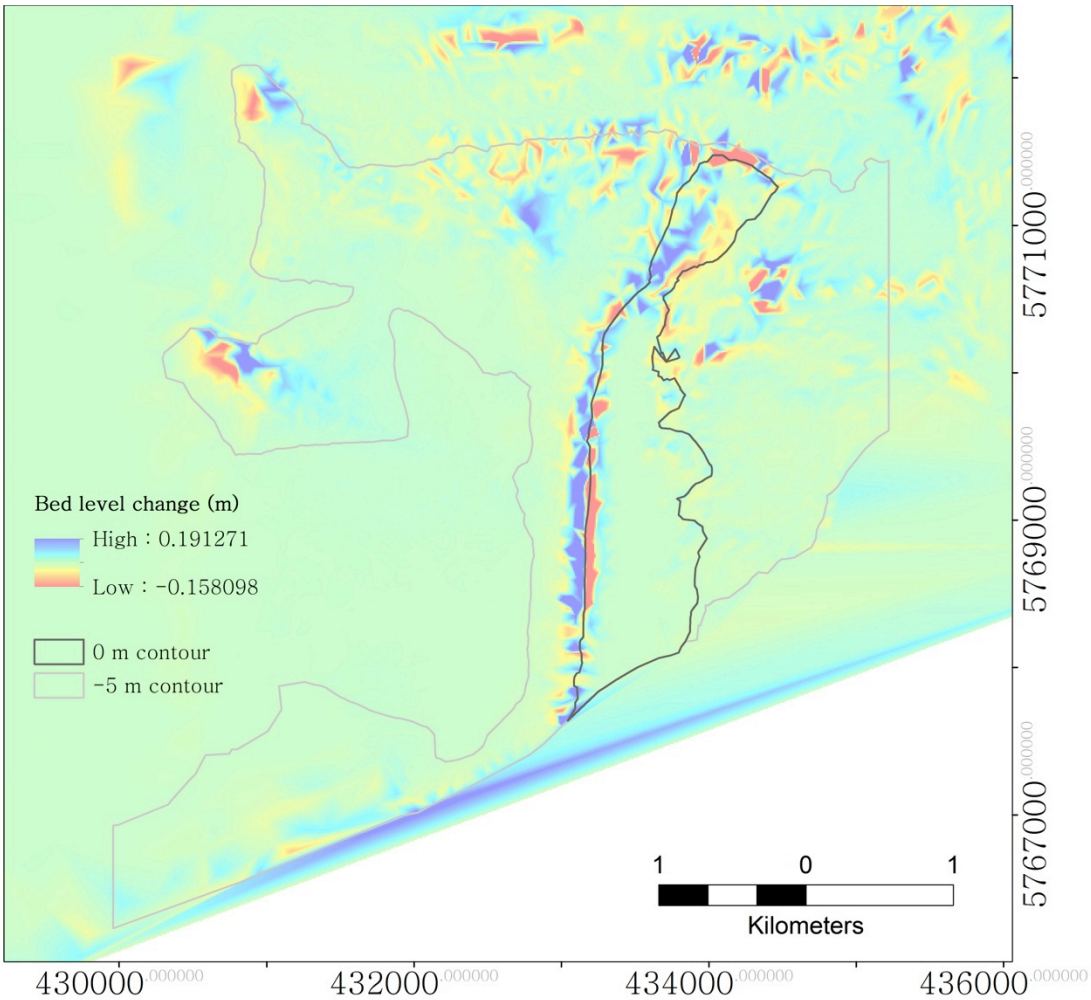

Figure 10.18 Bed level change for the fair-weather, 0.1 m SLR scenario. Contours are relative to LAT.

Volume gains and losses - fair-weather conditions – 0.1 m SLR

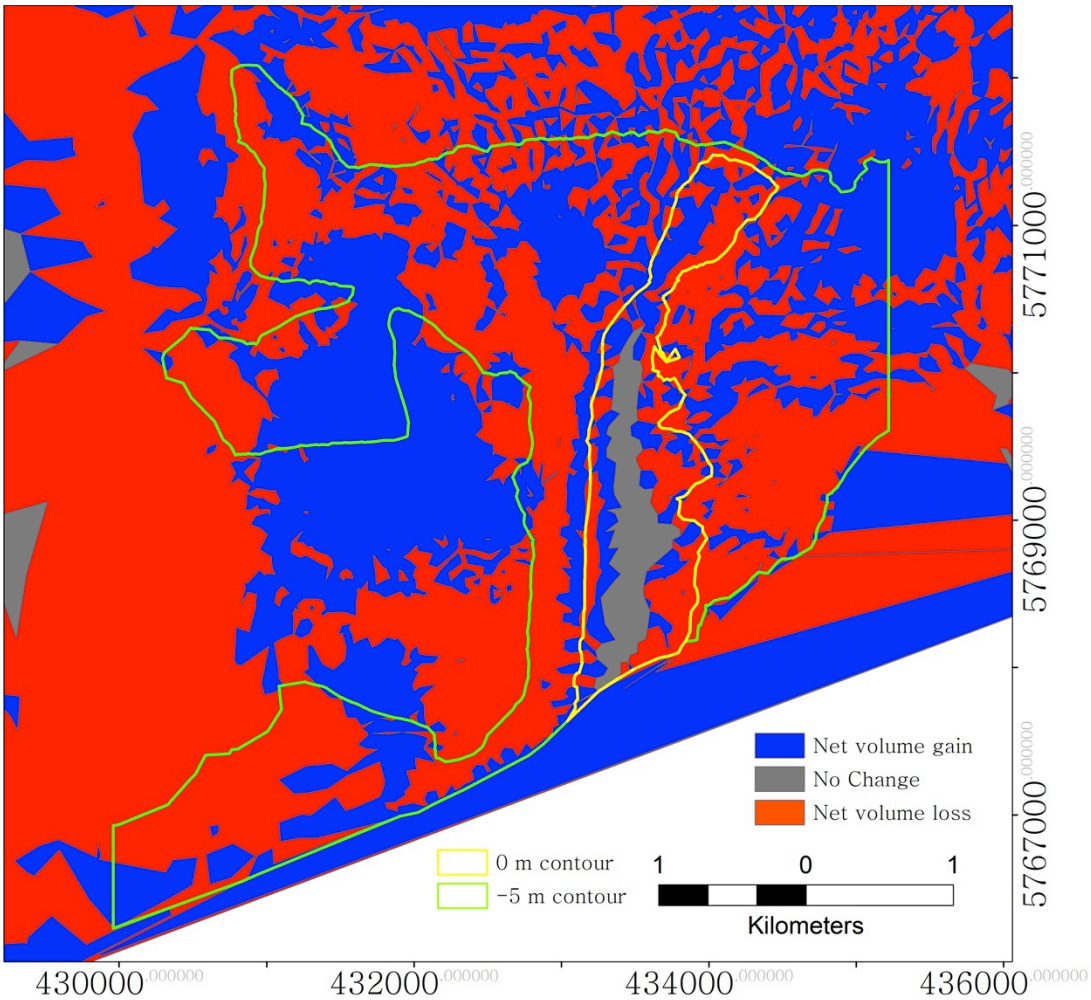

Figure 10.19 Volume gains and losses for the no event, 0.1 m SLR scenario. Contours are relative to LAT.

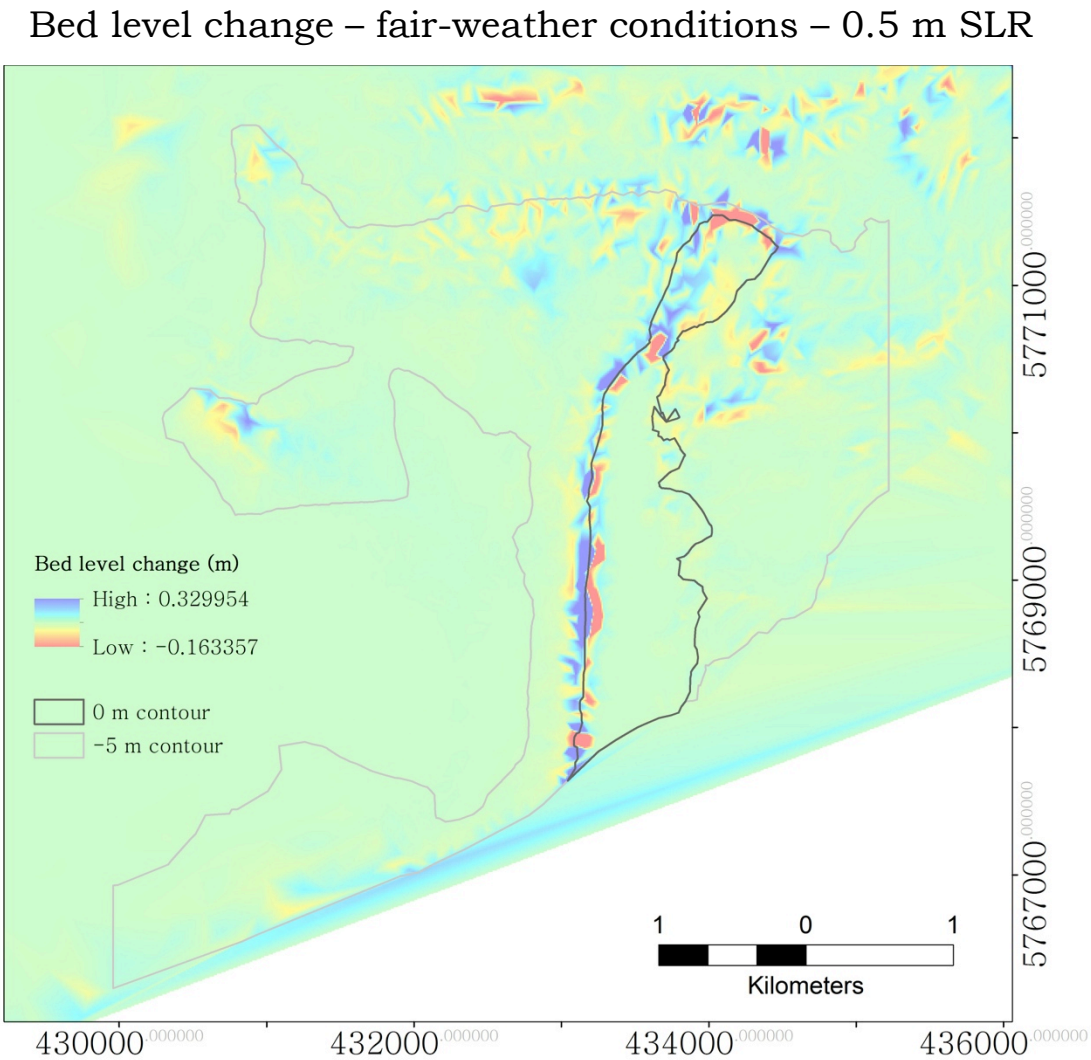

Figure 10.20 Bed level change for the no event, 0.5 m SLR scenario. Contours are relative to LAT.

Volume gains and losses - fair-weather conditions – 0.5 m SLR

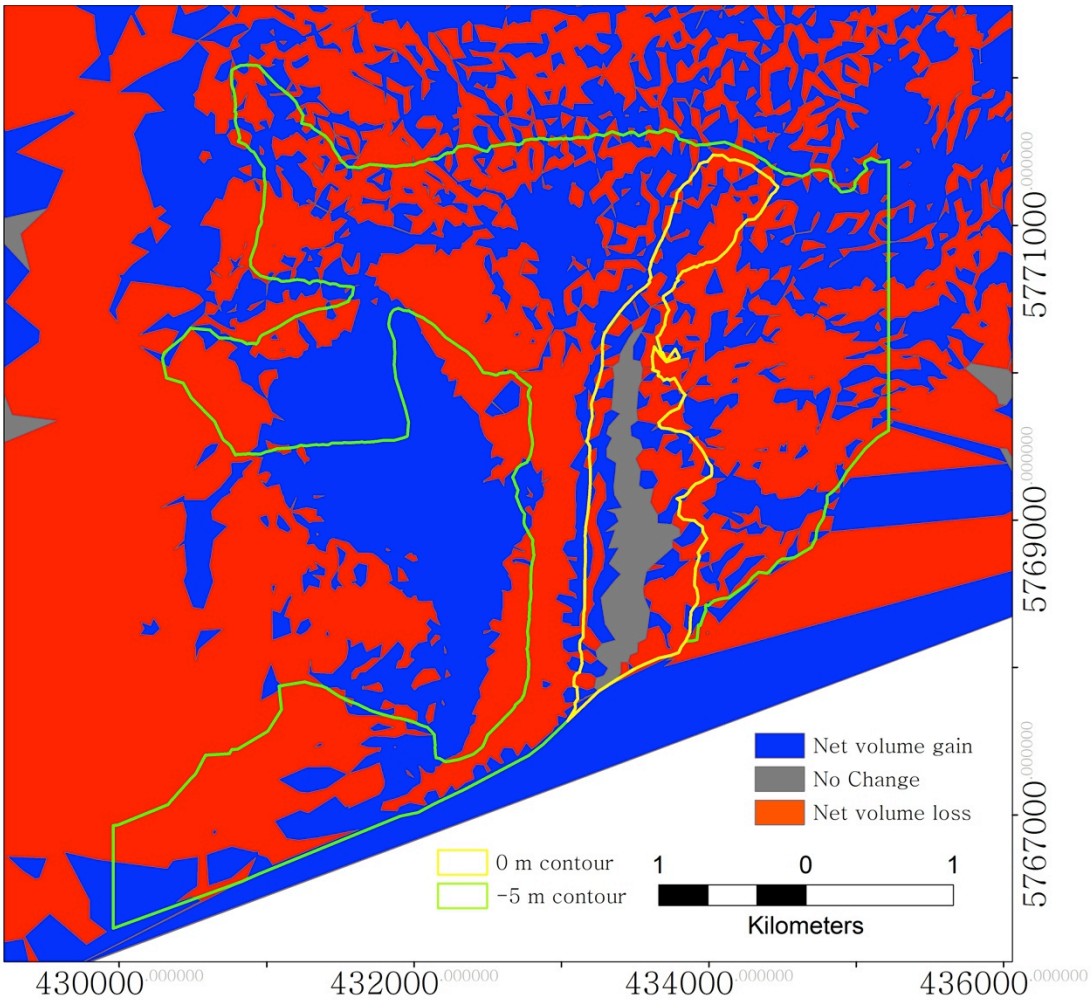

Figure 10.21 Volume gains and losses for the no event, 0.5 m SLR scenario. Contours are relative to LAT.

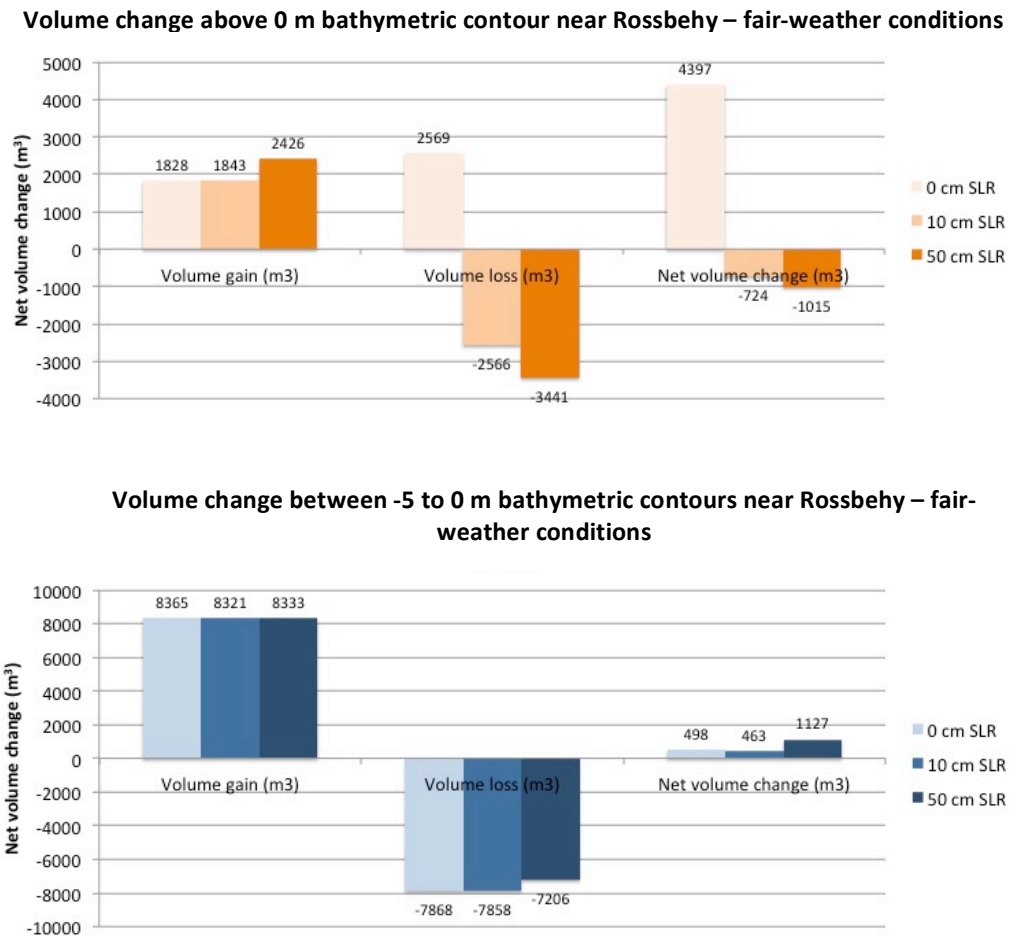

Figure 10.22 Volume change above the 0 m bathymetric contour (top) and between the -5 to 0 m bathymetric contours (bottom) for the 3 SLR scenarios run over the course of the fair-weather scenario at Rossbehy. 0 m contour is equal to LAT.

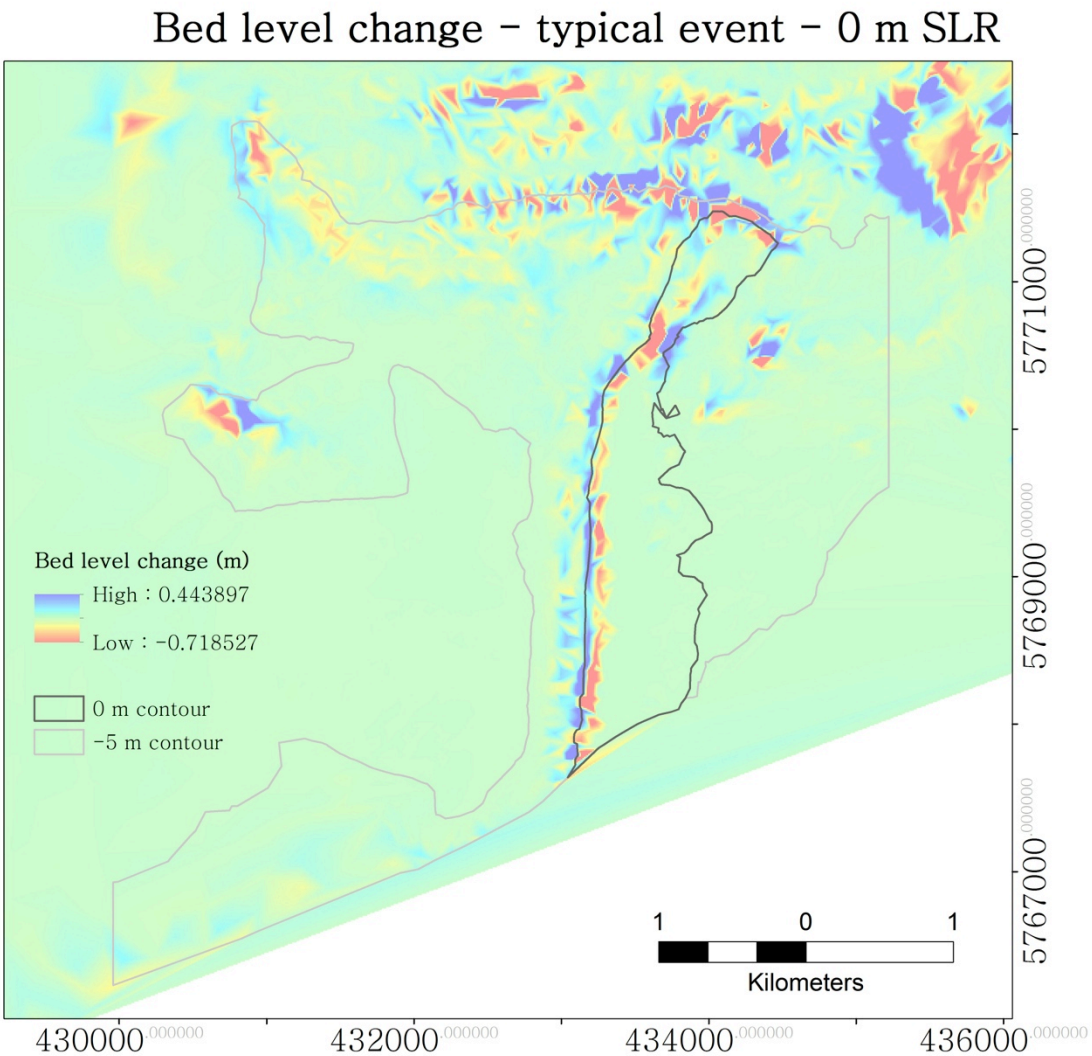

Figure 10.23 Bed level change for the typical event, 0 m SLR scenario. The polygons representing the 0 m and -5 m contours were extracted from the initial bathymmetry. Net volume change was calculated within the bounds of these polygons. Contours are relative to LAT.

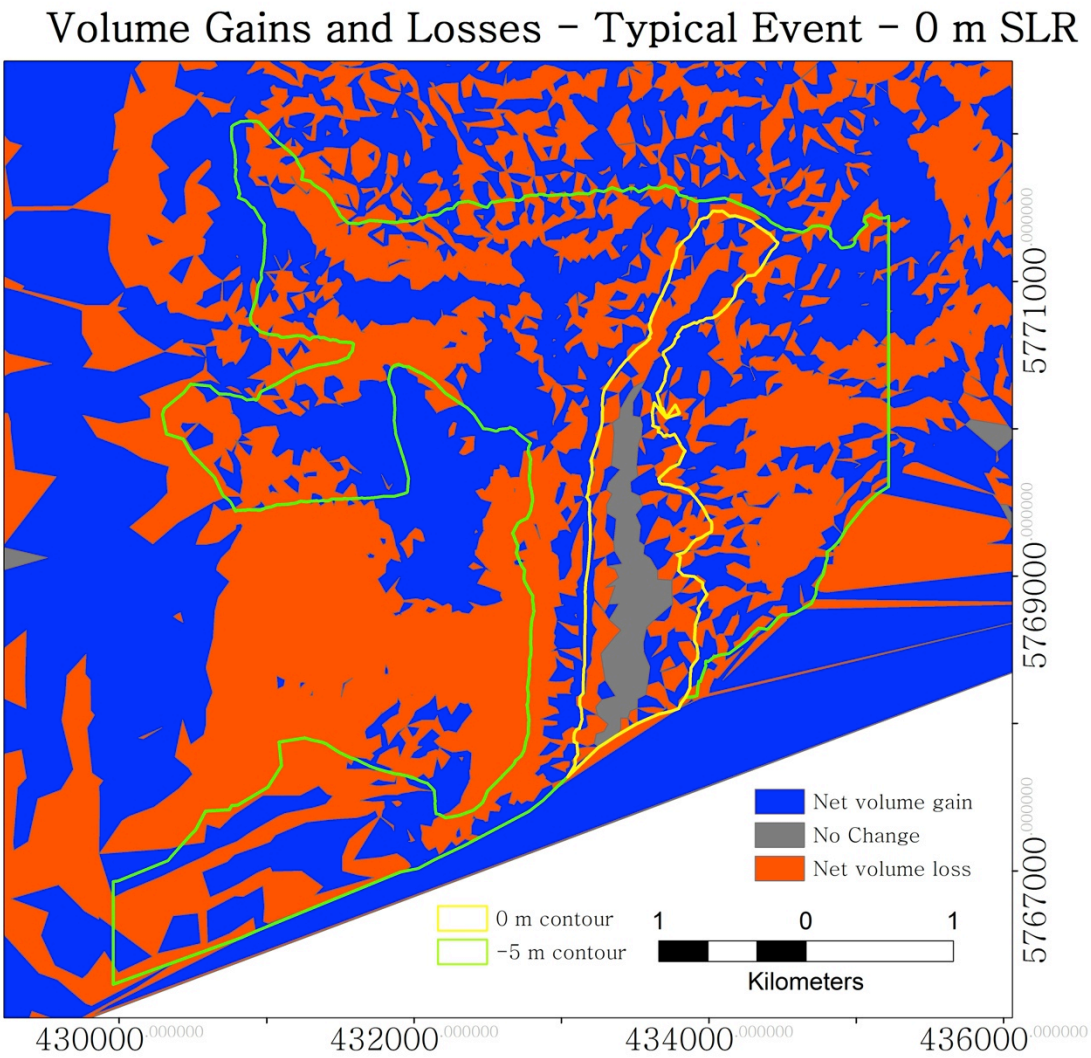

Figure 10.24 Volume gains and losses for the typical event, 0 m SLR scenario. Contours are relative to LAT.

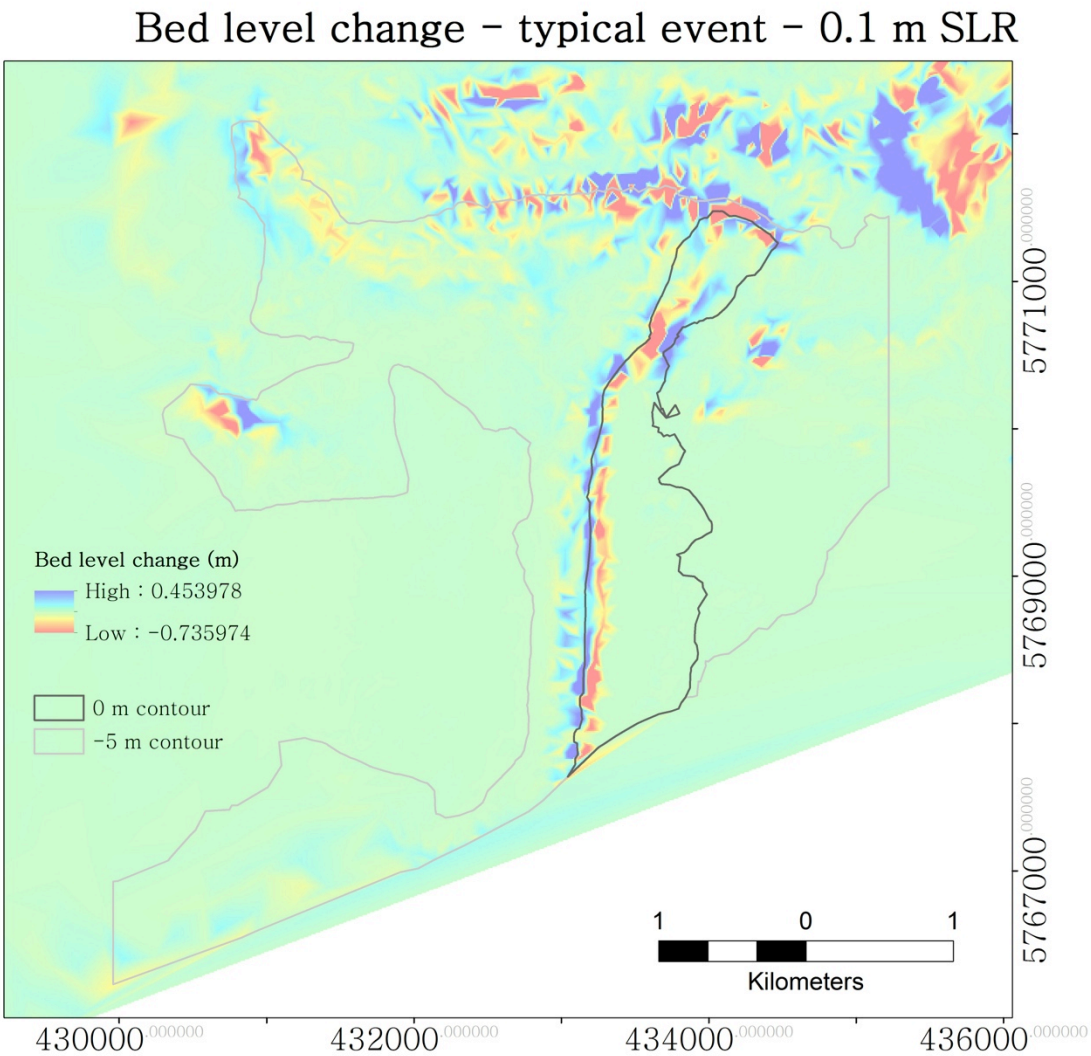

Figure 10.25 Bed level change for the typical event, 0.1 m SLR scenario. Contours are relative to LAT.

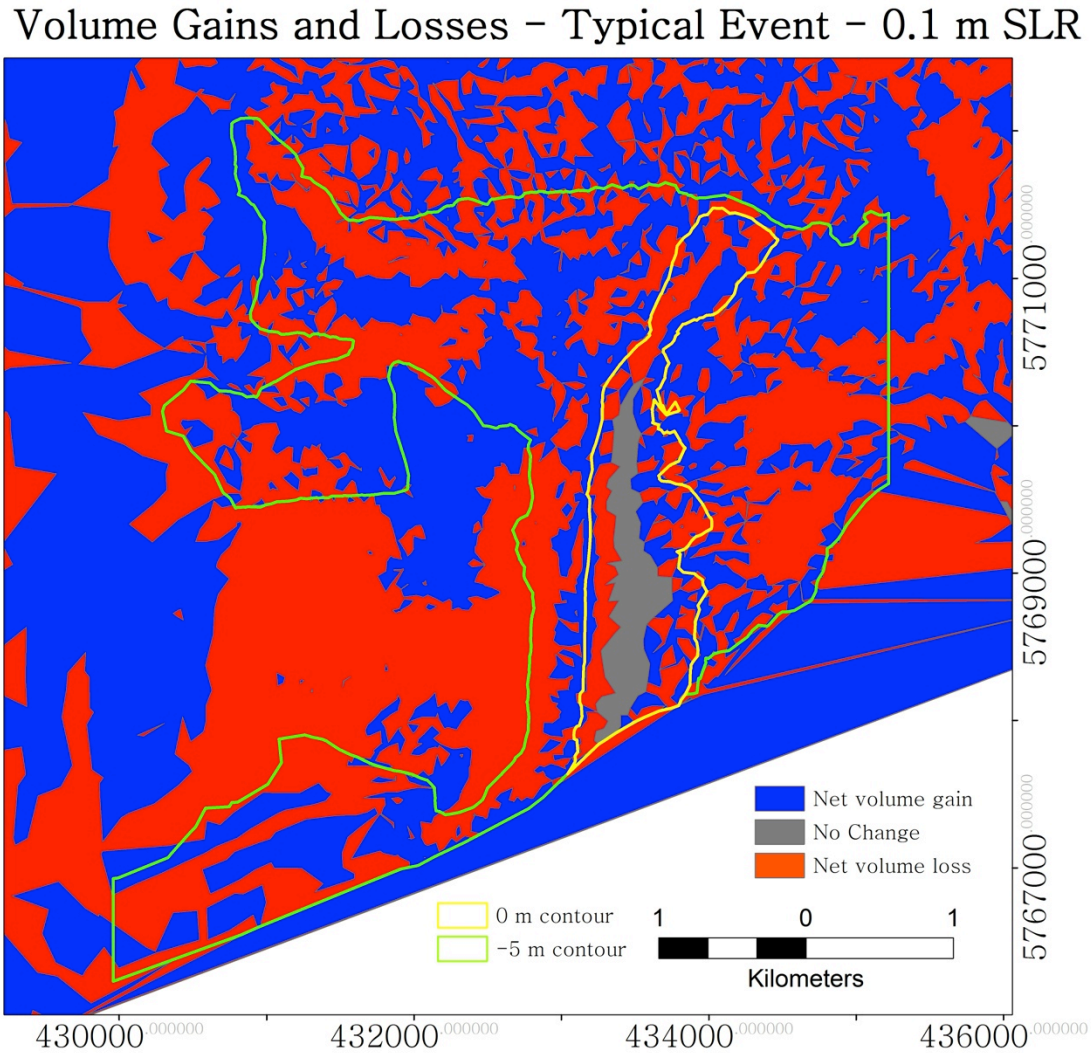

Figure 10.26 Volume gains and losses for the typical event, 0.1 m SLR scenario. Contours are relative to LAT.

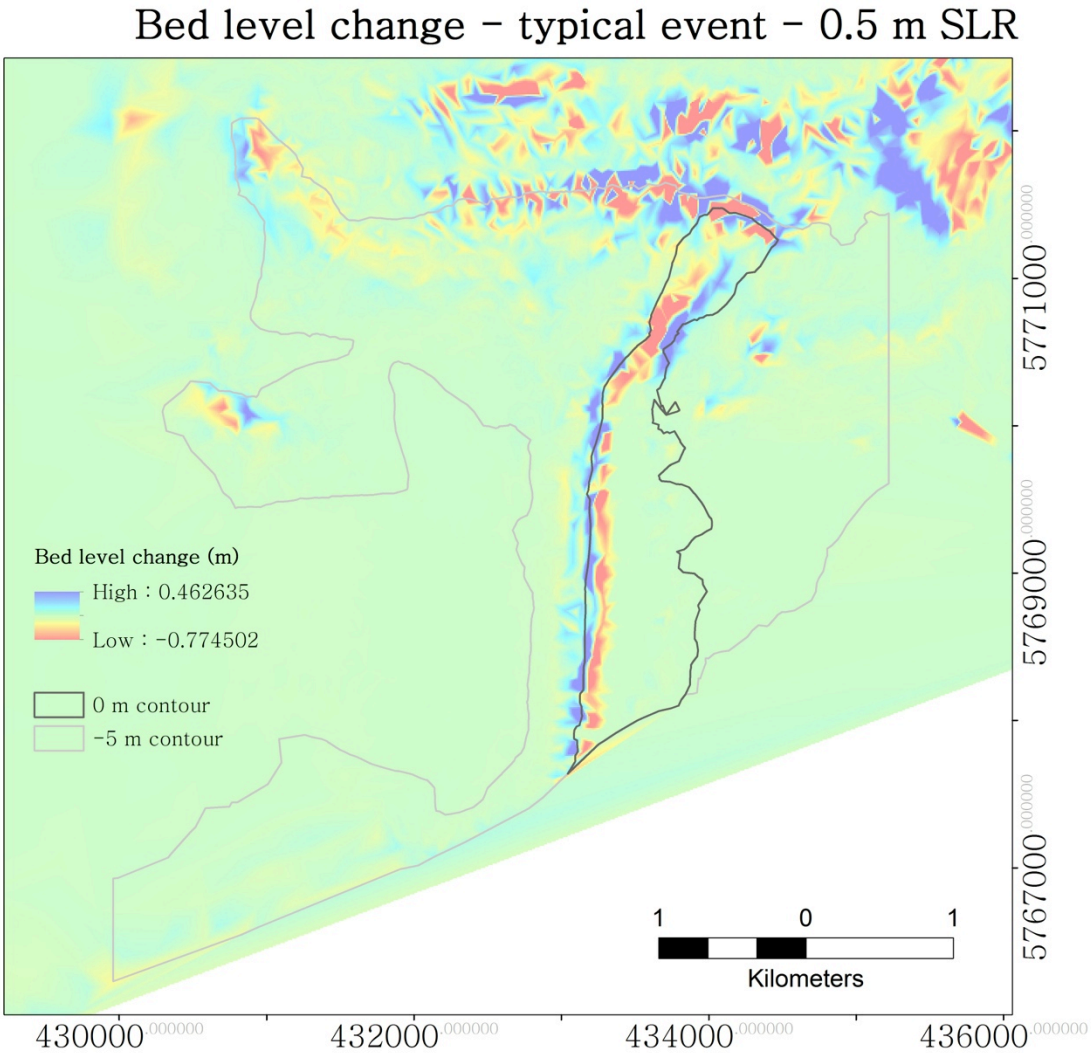

Figure 10.27 Bed level change for the typical event, 0.5 m SLR scenario. Contours are relative to LAT.

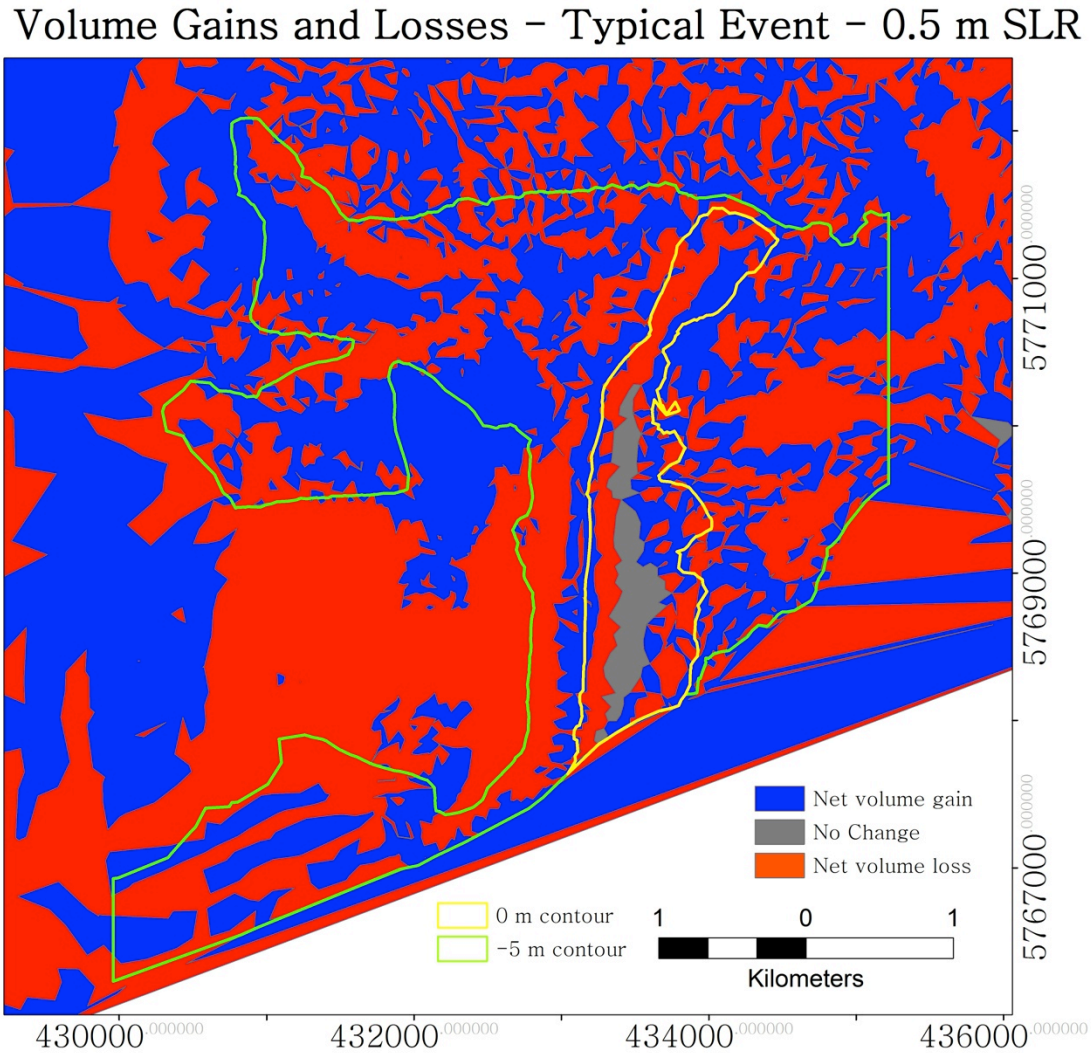

Figure 10.28 Volume gains and losses for the typical event, 0.5 m SLR scenario. Contours are relative to LAT.

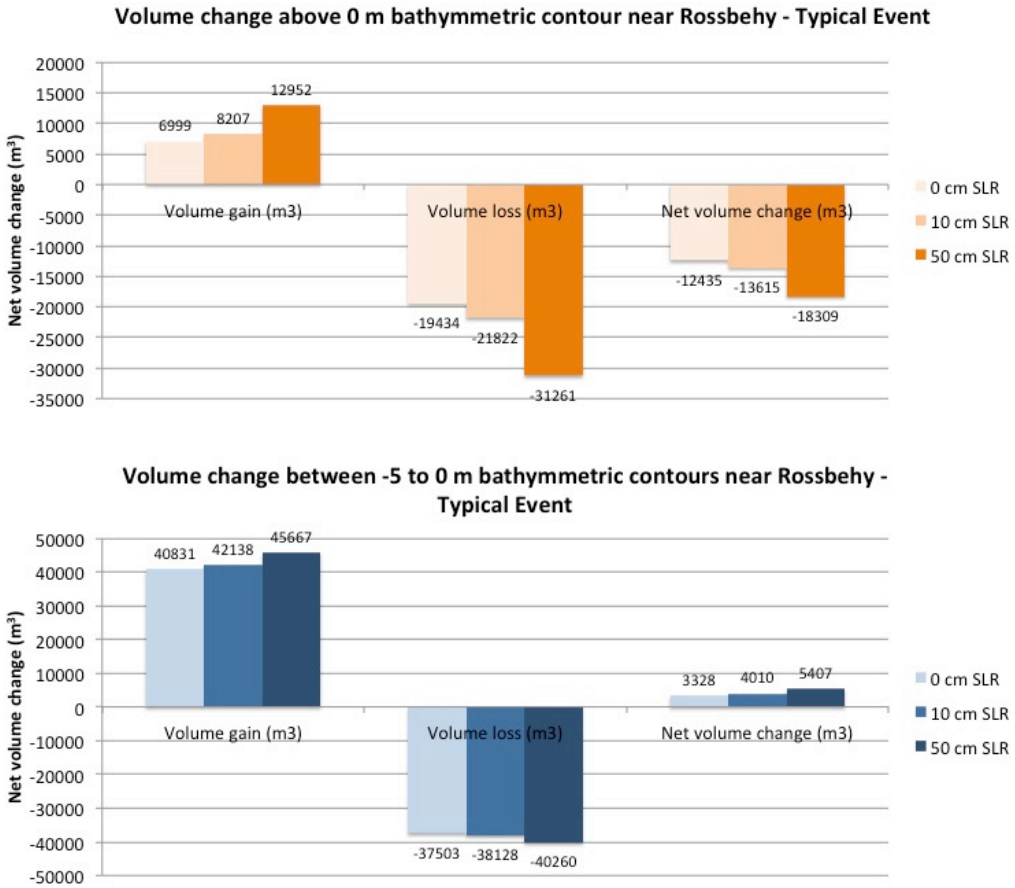

Figure 10.29 Volume change above the 0 m bathymetric contour (top) and between the -5 to 0 m bathymetric contours (bottom) for the 3 SLR scenarios run over the course of the "typical event" scenario at Rossbehy. 0 m contour is equal to LAT.

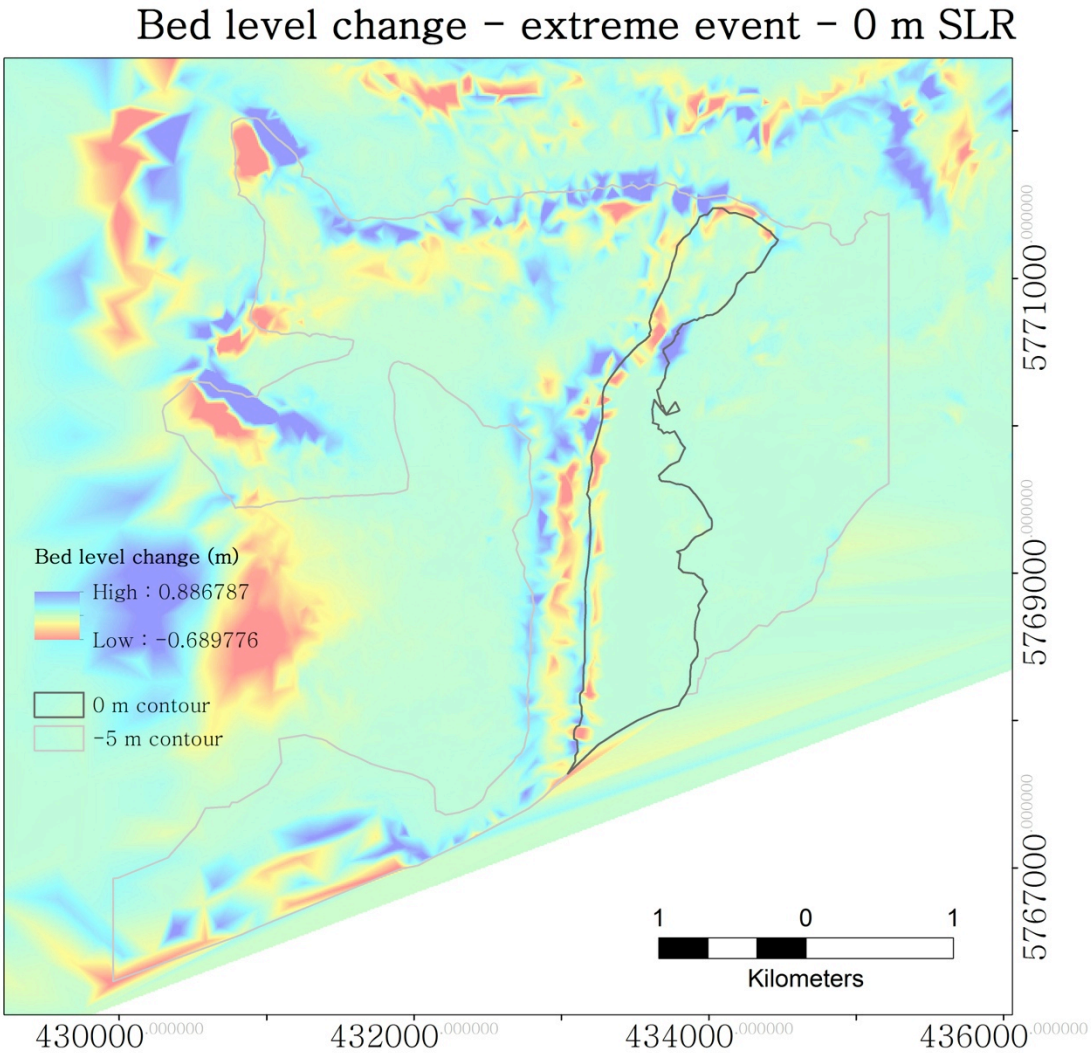

Figure 10.30 Bed level change for the extreme event, 0 m SLR scenario. Contours are relative to LAT.

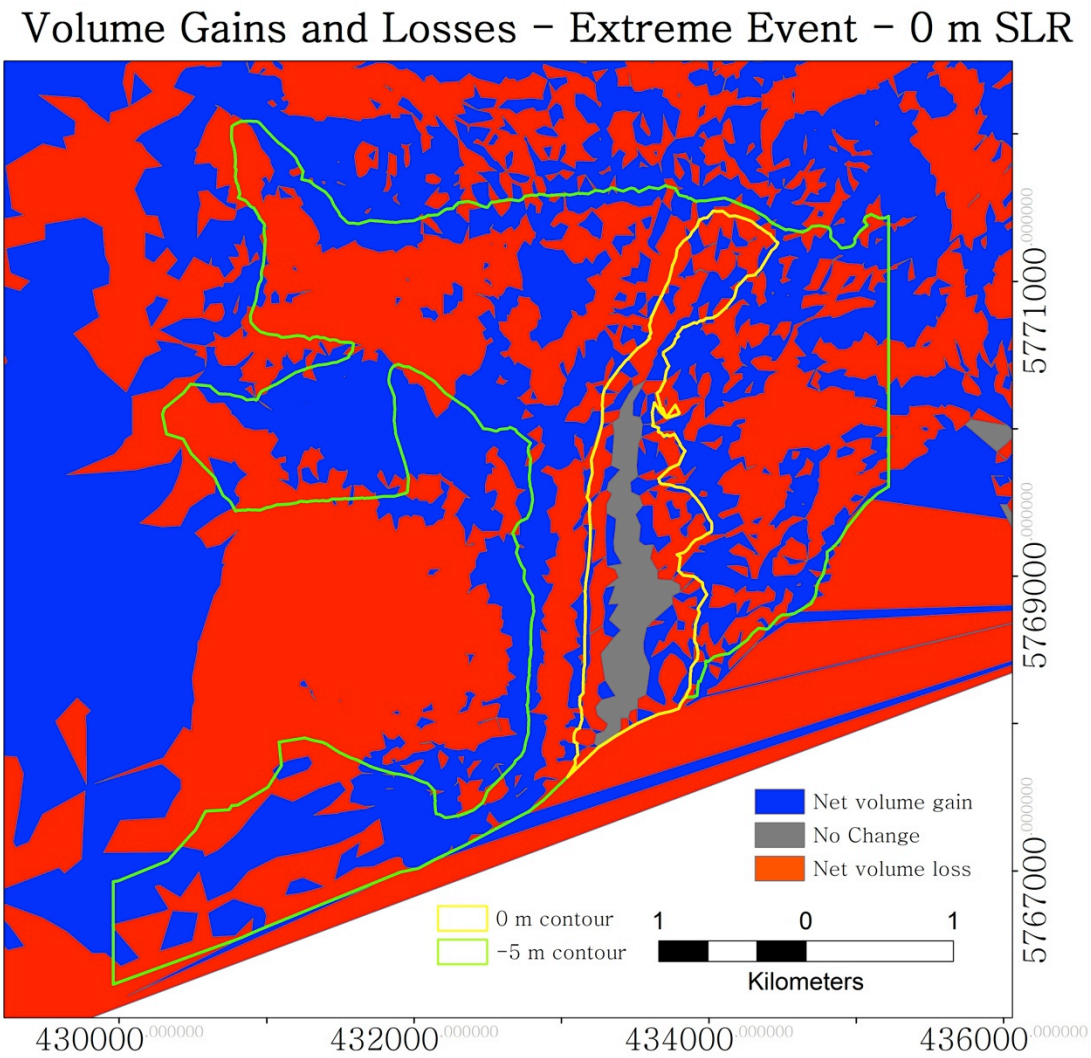

Figure 10.31 Volume gains and losses for the extreme event, 0 m SLR scenario. Contours are relative to LAT.

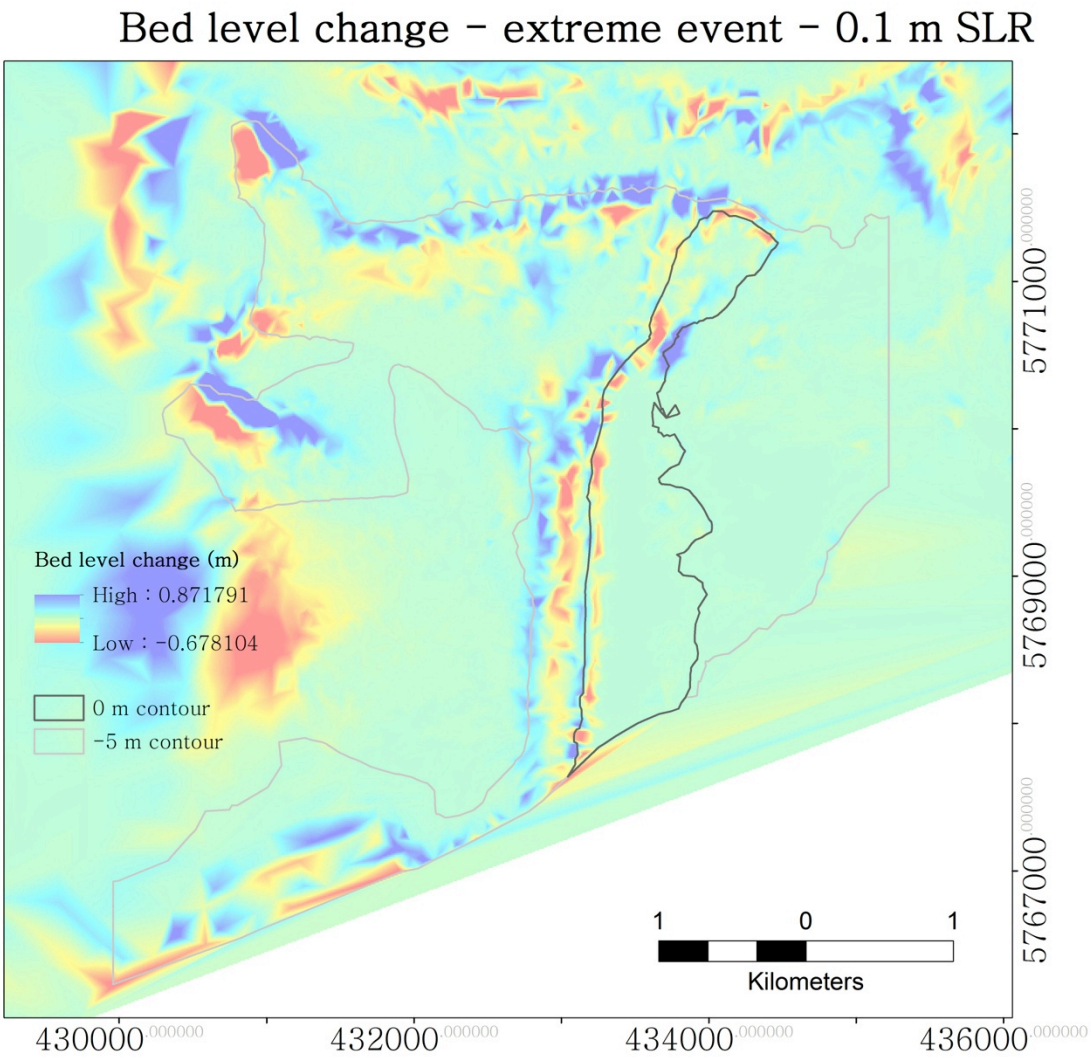

Figure 10.32 Bed level change for the extreme event, 0.1 m SLR scenario. Contours are relative to LAT.

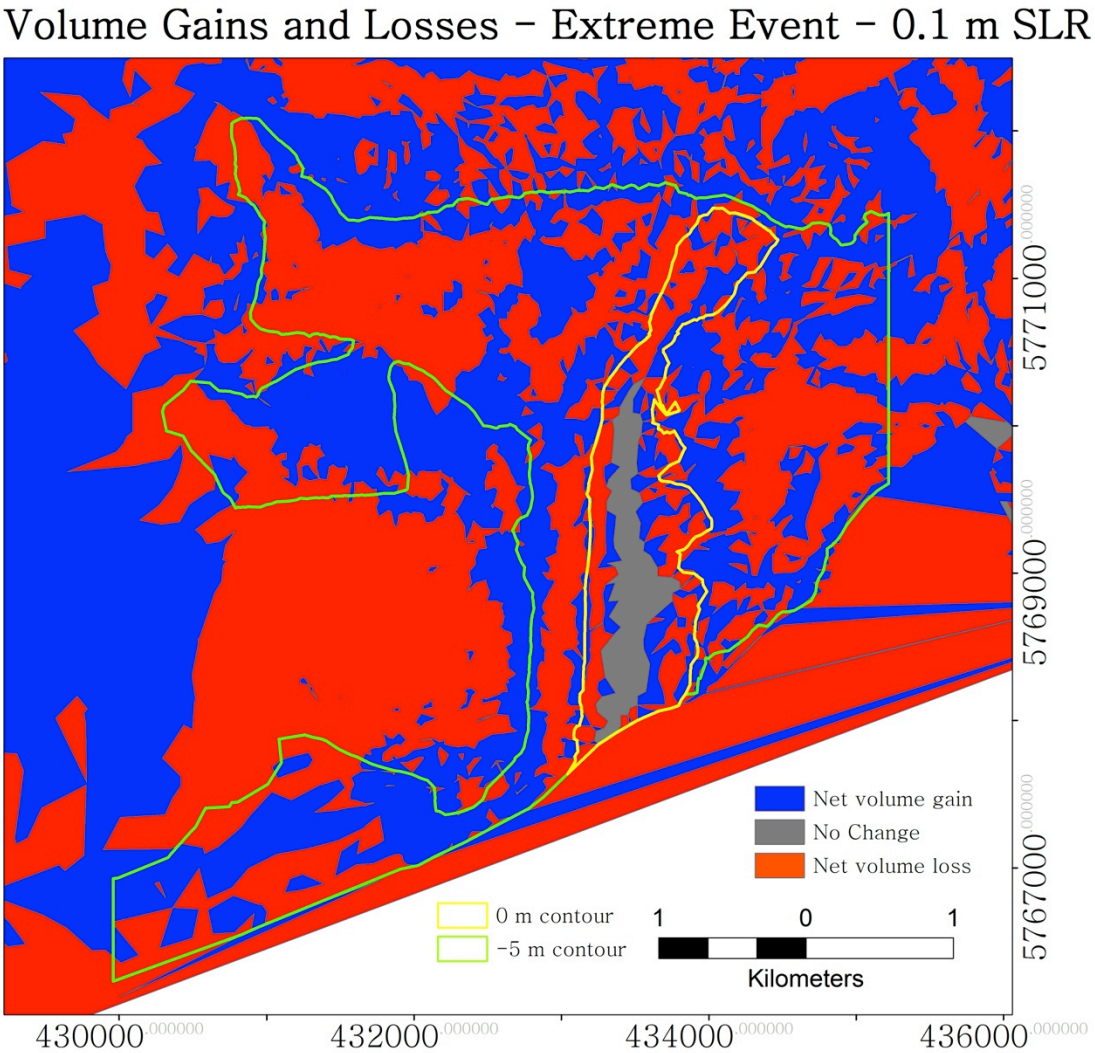

Figure 10.33 Volume gains and losses for the extreme event, 0.1 m SLR scenario. Contours are relative to LAT.

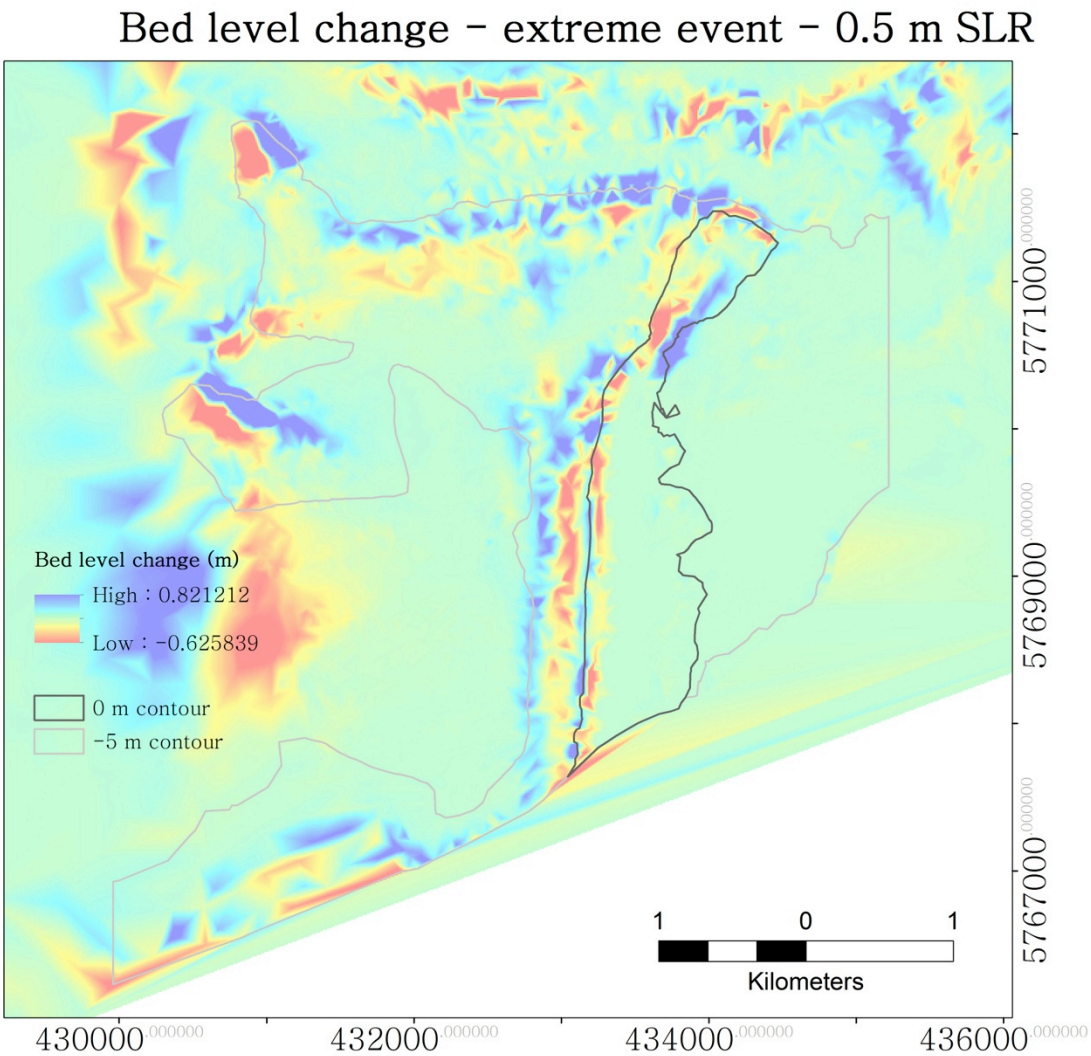

Figure 10.34 Bed level change for the extreme event, 0.5 m SLR scenario. Contours are relative to LAT.

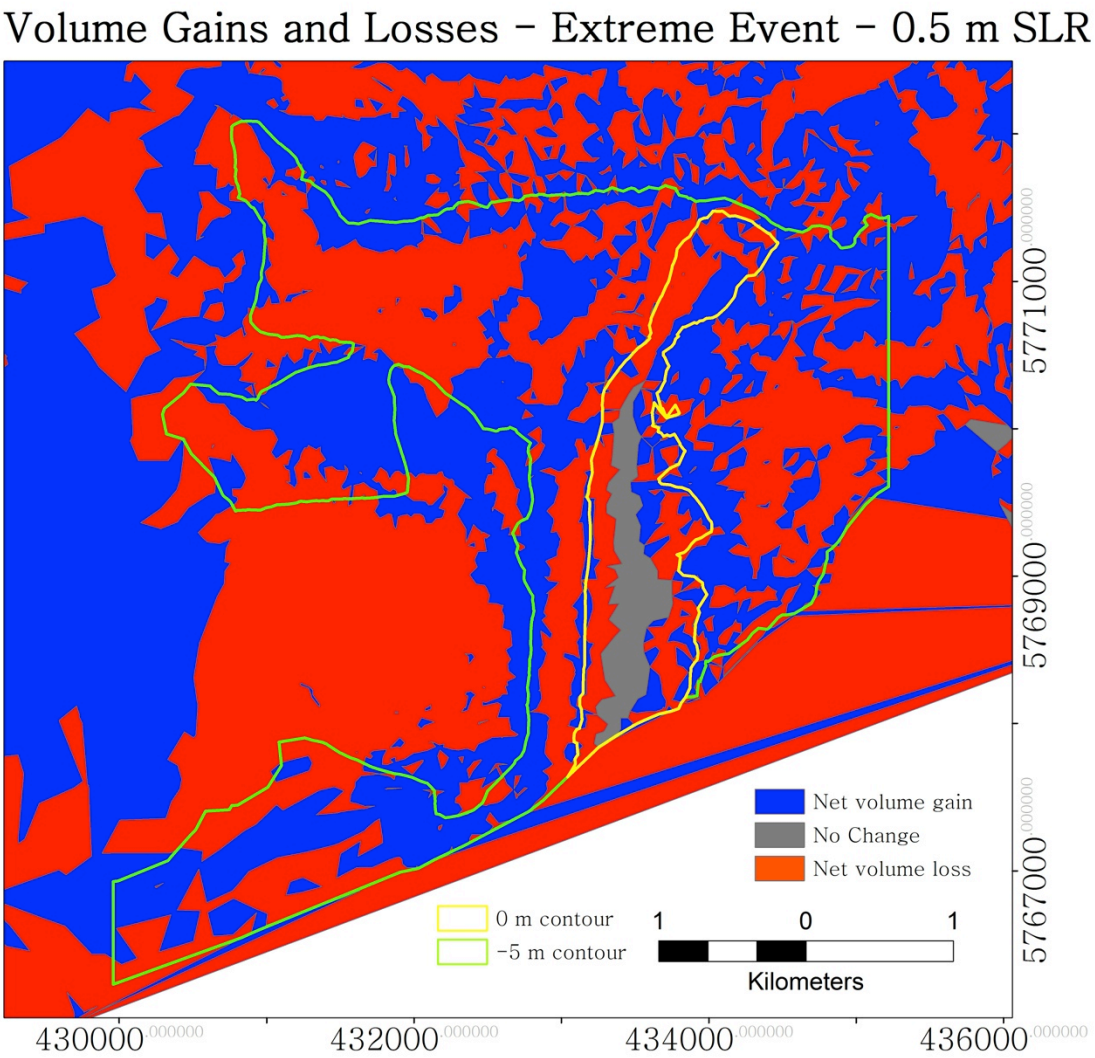

Figure 10.35 Volume gains and losses for the extreme event, 0.5 m SLR scenario. Contours are relative to LAT.

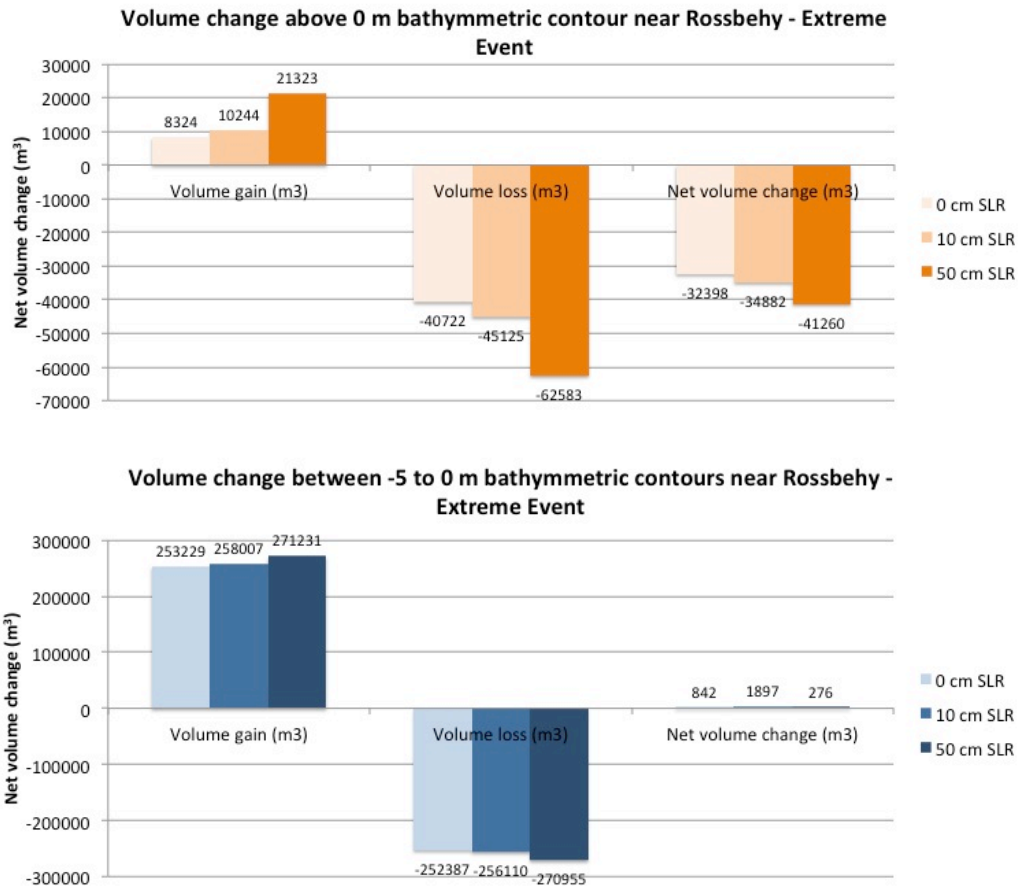

Figure 10.36 Volume change above the 0 m bathymetric contour (top) and between the -5 to 0 m bathymetric contours (bottom) for the 3 SLR scenarios run over the course of the extreme event scenario at Rossbehy. 0 m contour is equal to LAT.

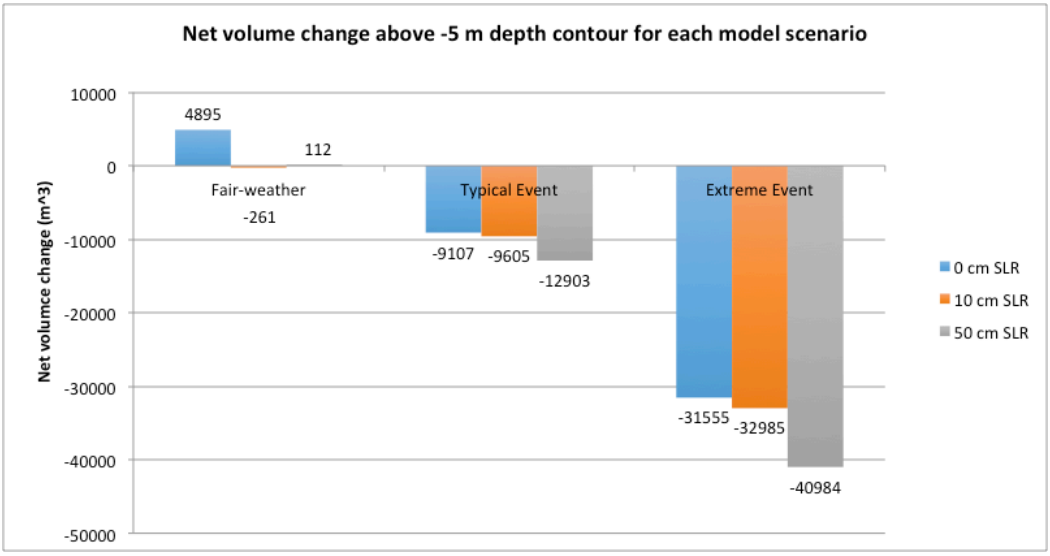

Figure 10.37 Graphic summary of net volume change above the -5 m depth contour for each model scenario. 0 m contour is equal to LAT.

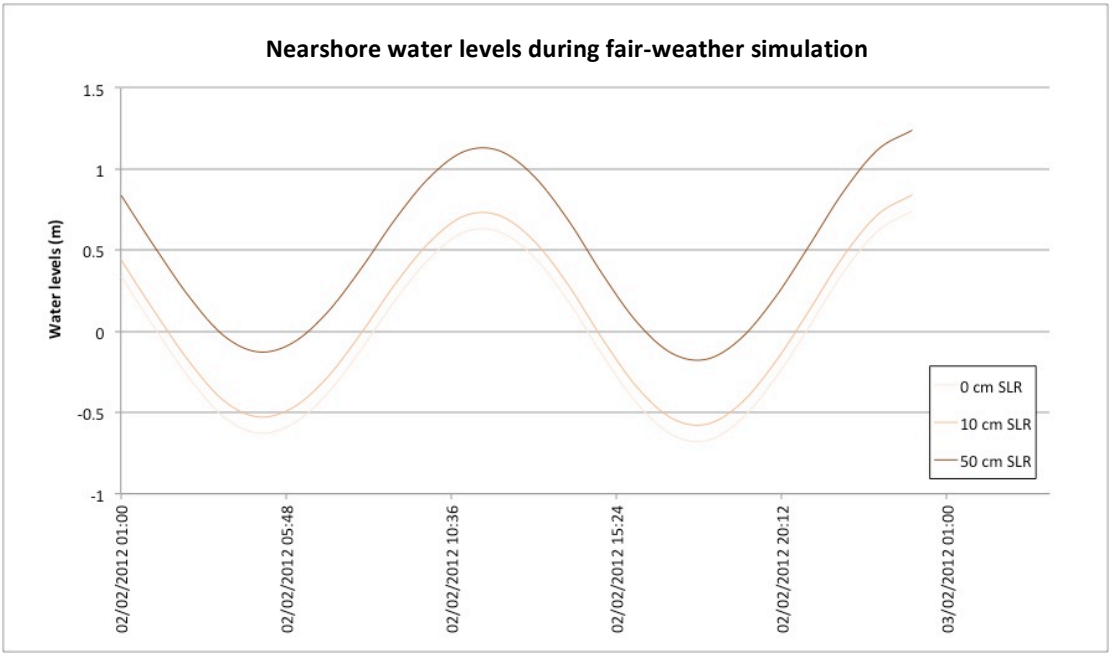

Figure 10.38 Nearshore water levels for UTM coordinate 431732.69, 5770864.57 – shown in fig. 10.14 - during the three fair-weather simulations (0 m SLR, 0.1 m SLR, and 0.5 m SLR). **NB:** While the simulation began on 1 Feb 2012 at 00:00, a 24 hour spin-up meant water levels did not reach statistical equilibrium until 2 Feb 2012 at 01:00. Water levels are relative to MSL.

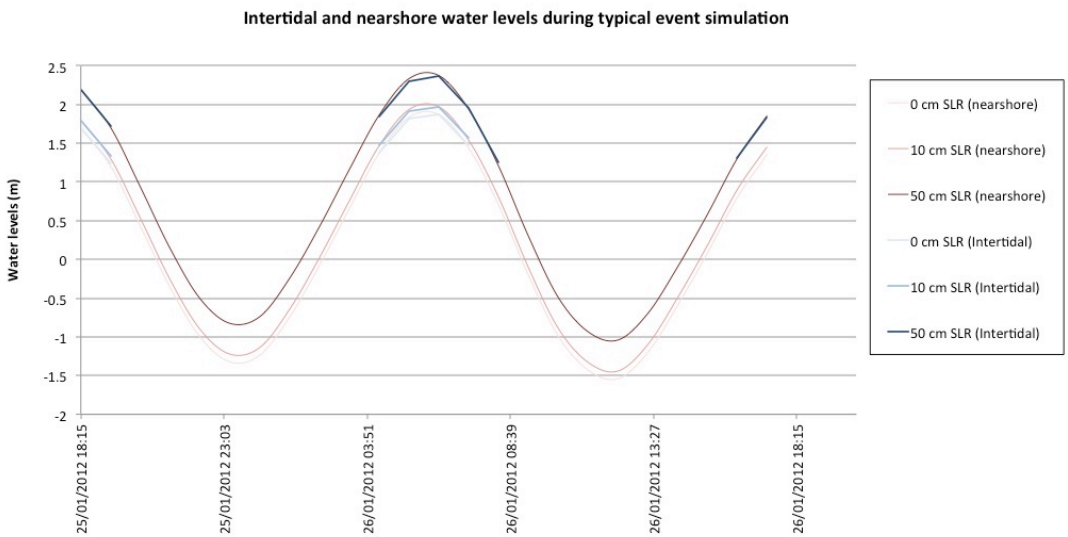

Figure 10.39 Water levels for nearshore coordinate (UTM coordinate 431732.69, 5770864.57 – shown in fig. 10.14) and sediment tracer injection point coordinate (UTM coordinate 433532.807, 5770466.742 – shown in fig. 10.13) during the three typical event simulations (0 m SLR, 0.1 m SLR, and 0.5 m SLR). NB: While the simulation began on 24 Jan 2012 at 18:00, a 24 hour spin-up meant water levels did not reach statistical equilibrium until 25 Jan 2012 at 18:15. Water levels are relative to MSL.

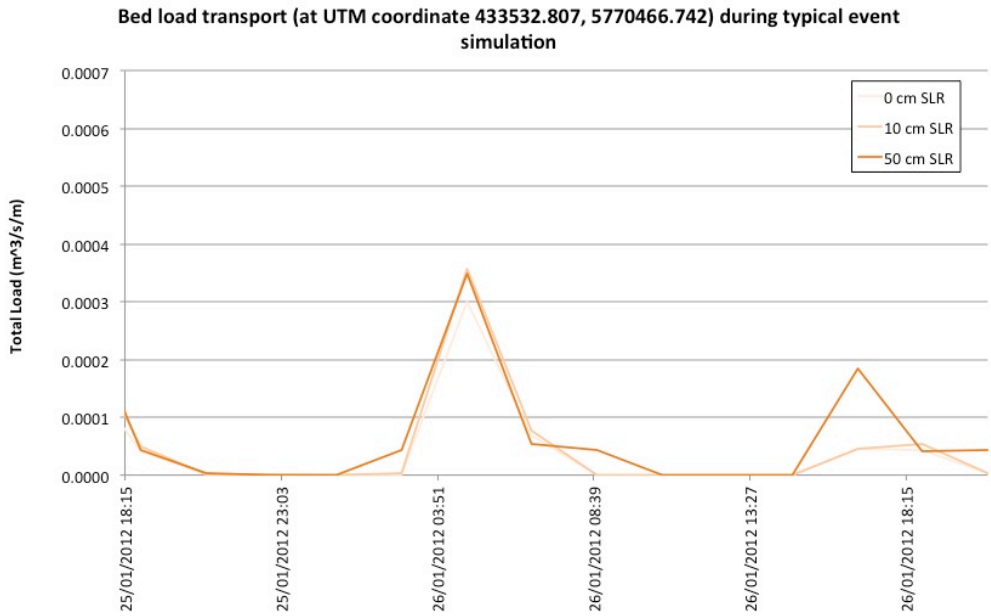

Figure 10.40 Time series showing transport magnitude at the sediment tracer injection point during the typical event simulation for all three SLR scenarios.

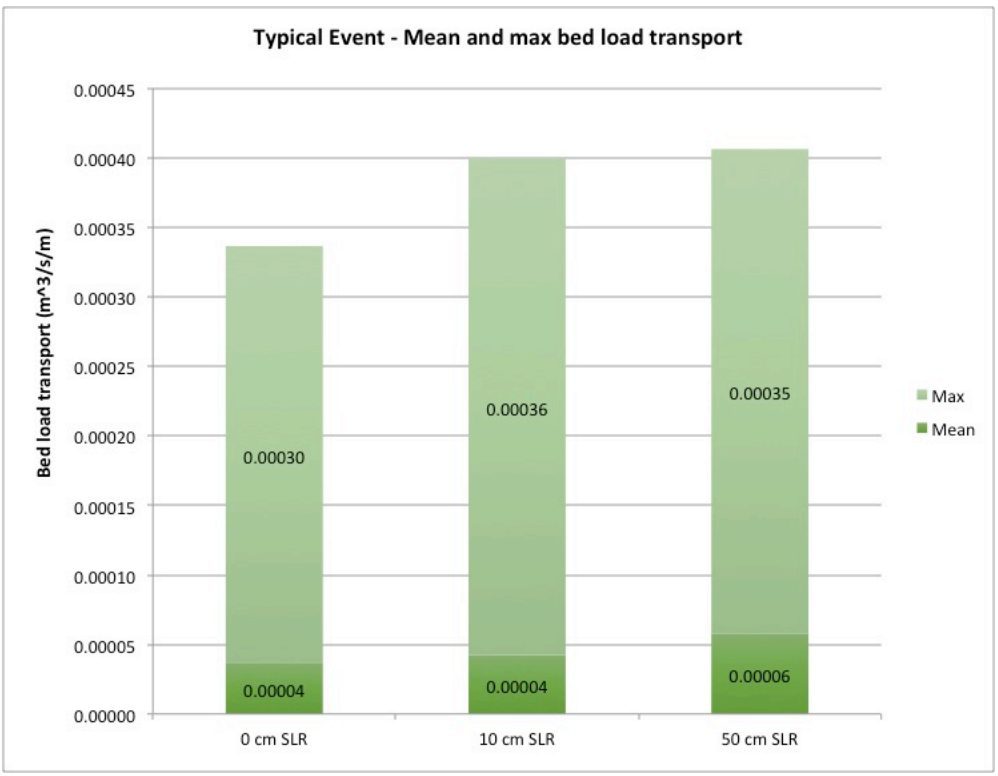

Figure 10.41 Mean and max bed load transport for typical event simulations for 0 m, 0.1 m, and 0.5 m SLR scenarios.

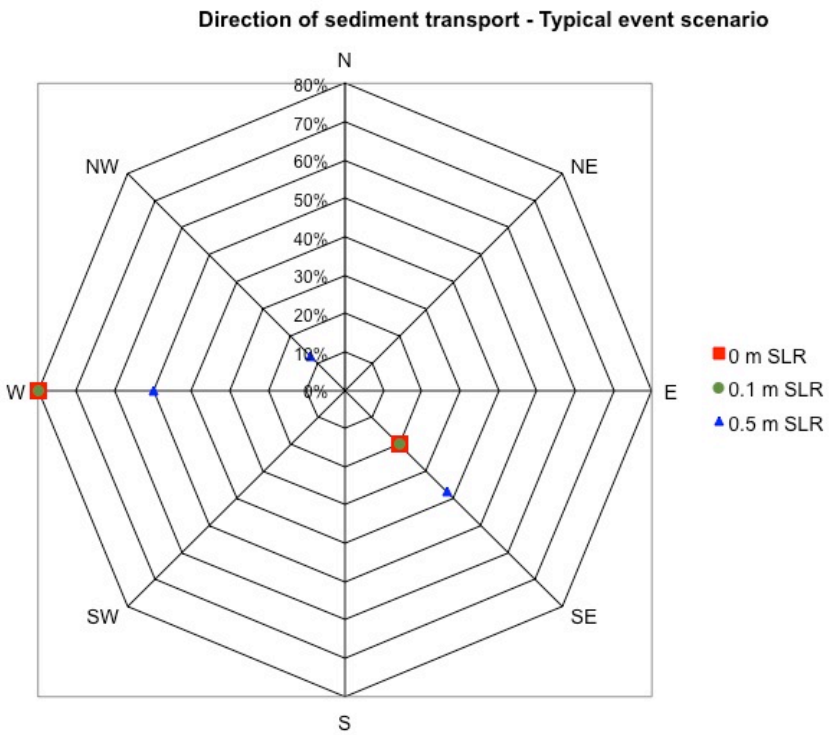

Figure 10.42 Compass rose plot illustrating direction of sediment transport at the sediment tracer injection point during the typical event simulation for all three SLR scenarios. **NB:** While in many cases, wind and wave directions are defined positive clockwise from true North (coming from), in MIKE 21 load directions are defined positive clockwise from true North (going against). For clarity, the output was adjusted to reflect load directions coming from, as opposed to going against. This means that, for example, for the 0 m SLR scenario, for 20% of the time, transport was from southeast to northwest and for 80% of the time, transport was from west to east (onshore).

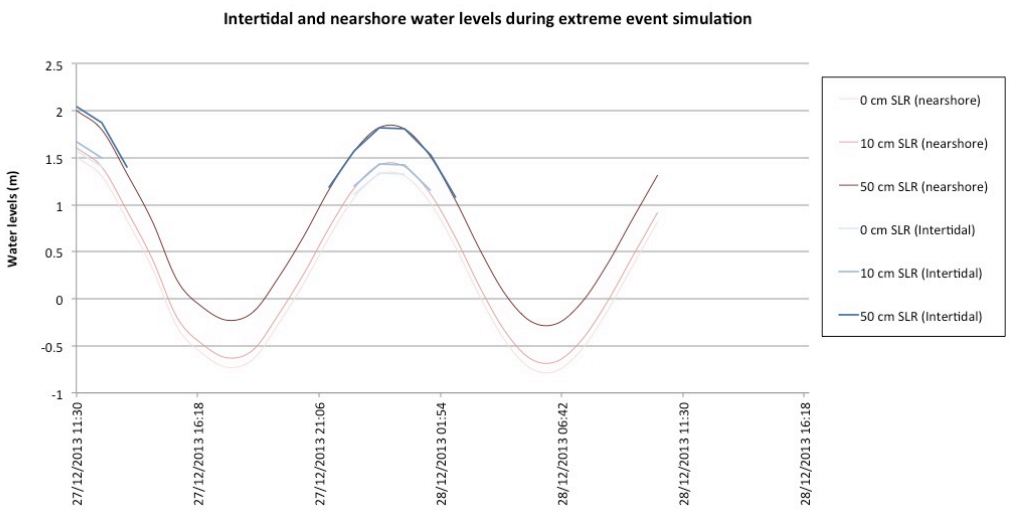

Figure 10.43 Time series showing water levels at the sediment tracer injection point during the extreme event simulation for all three SLR scenarios. Water levels are relative to MSL.

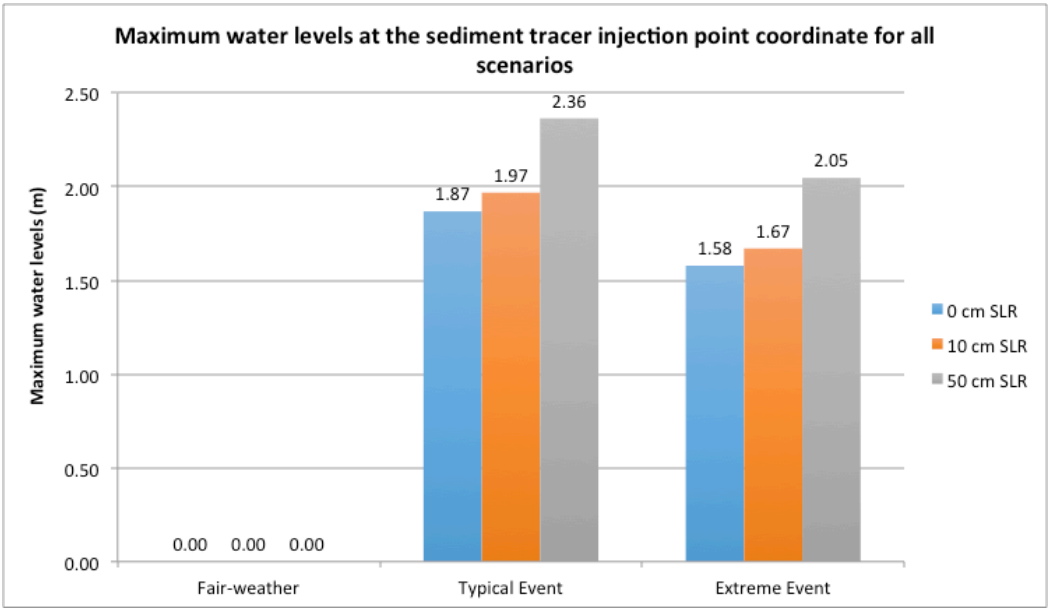

Figure 10.44 Maximum water levels reached at sediment tracer injection point coordinate for all nine scenarios. Water levels are relative to MSL.

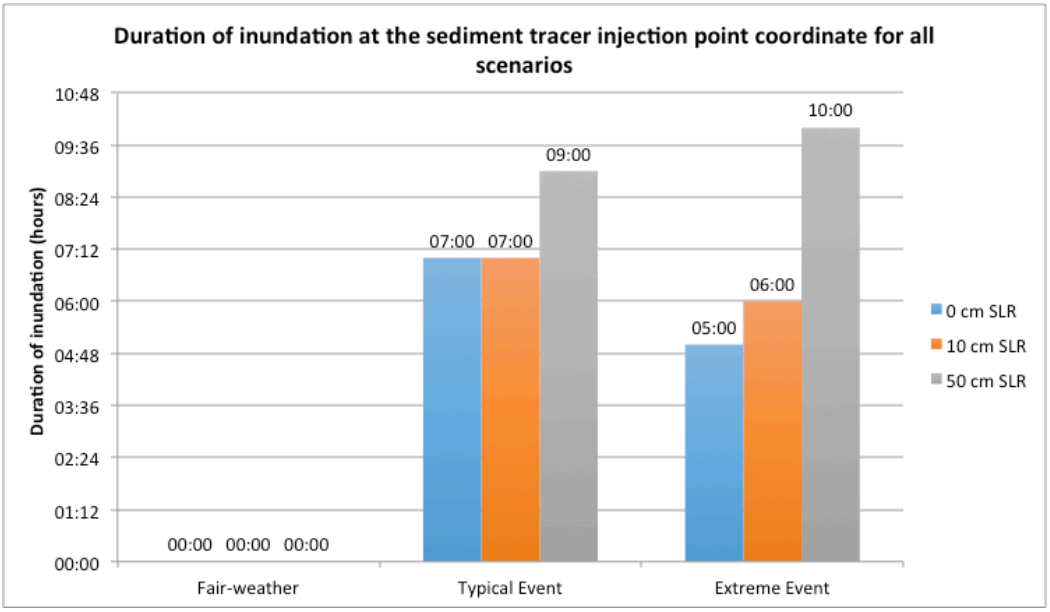

Figure 10.45 Duration of inundation at sediment tracer injection point coordinate for all nine scenarios. Water levels are relative to MSL.

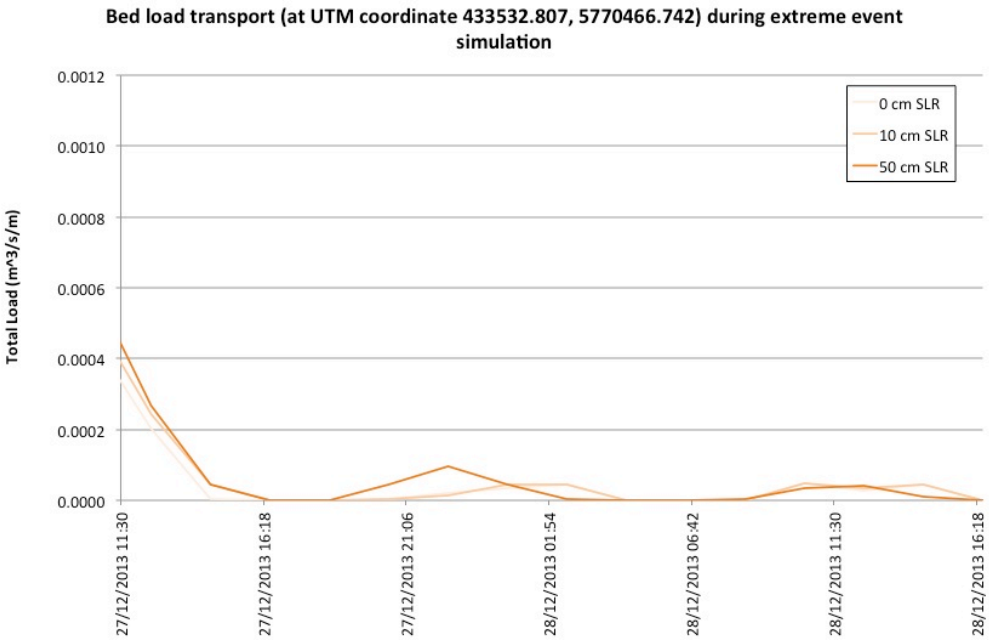

Figure 10.46 Time series showing transport magnitude at the sediment tracer injection point during the extreme event simulation for all three SLR scenarios.

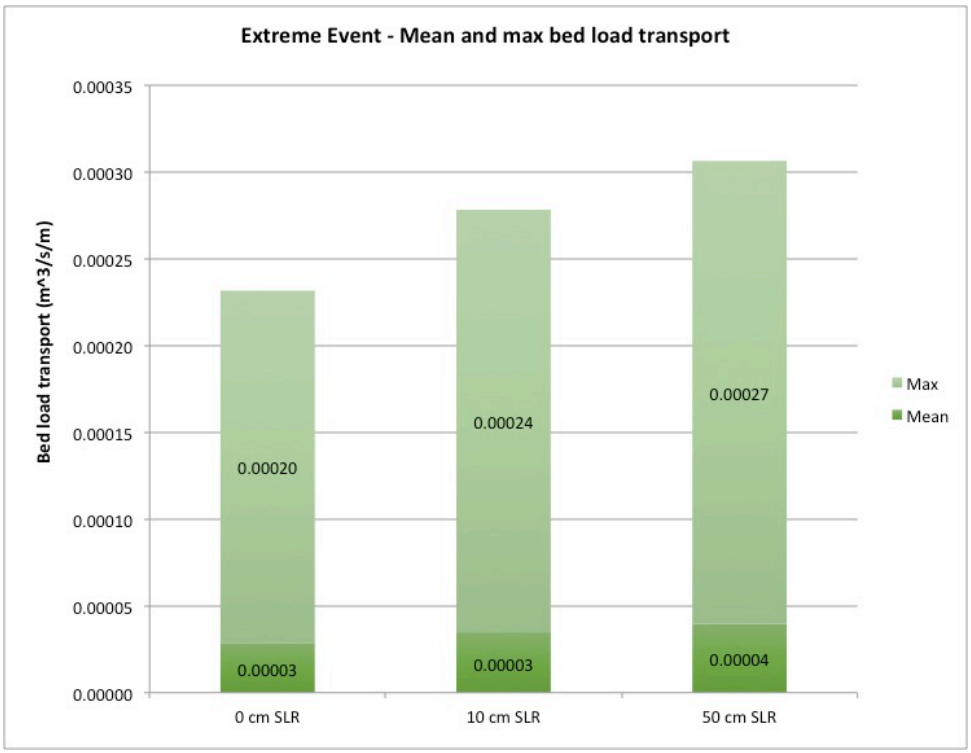

Figure 10.47 Mean and max bed load transport for extreme event simulations for 0 m, 0.1 m, and 0.5 m SLR scenarios.

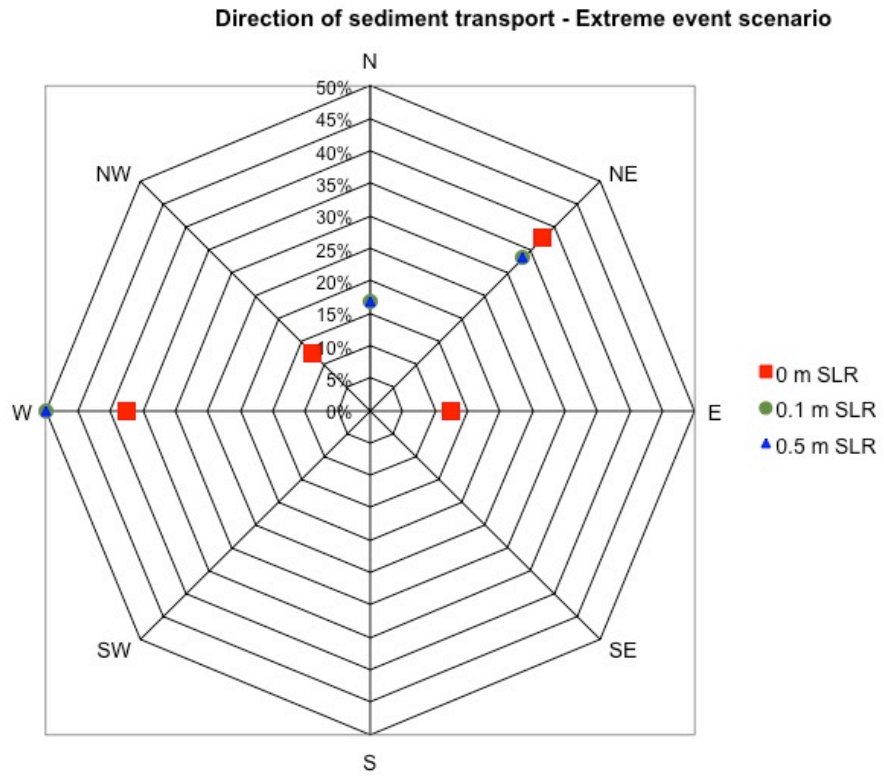

Figure 10.48 Compass rose plot illustrating direction of sediment transport at the sediment tracer injection point during the extreme event simulation for all three SLR scenarios.

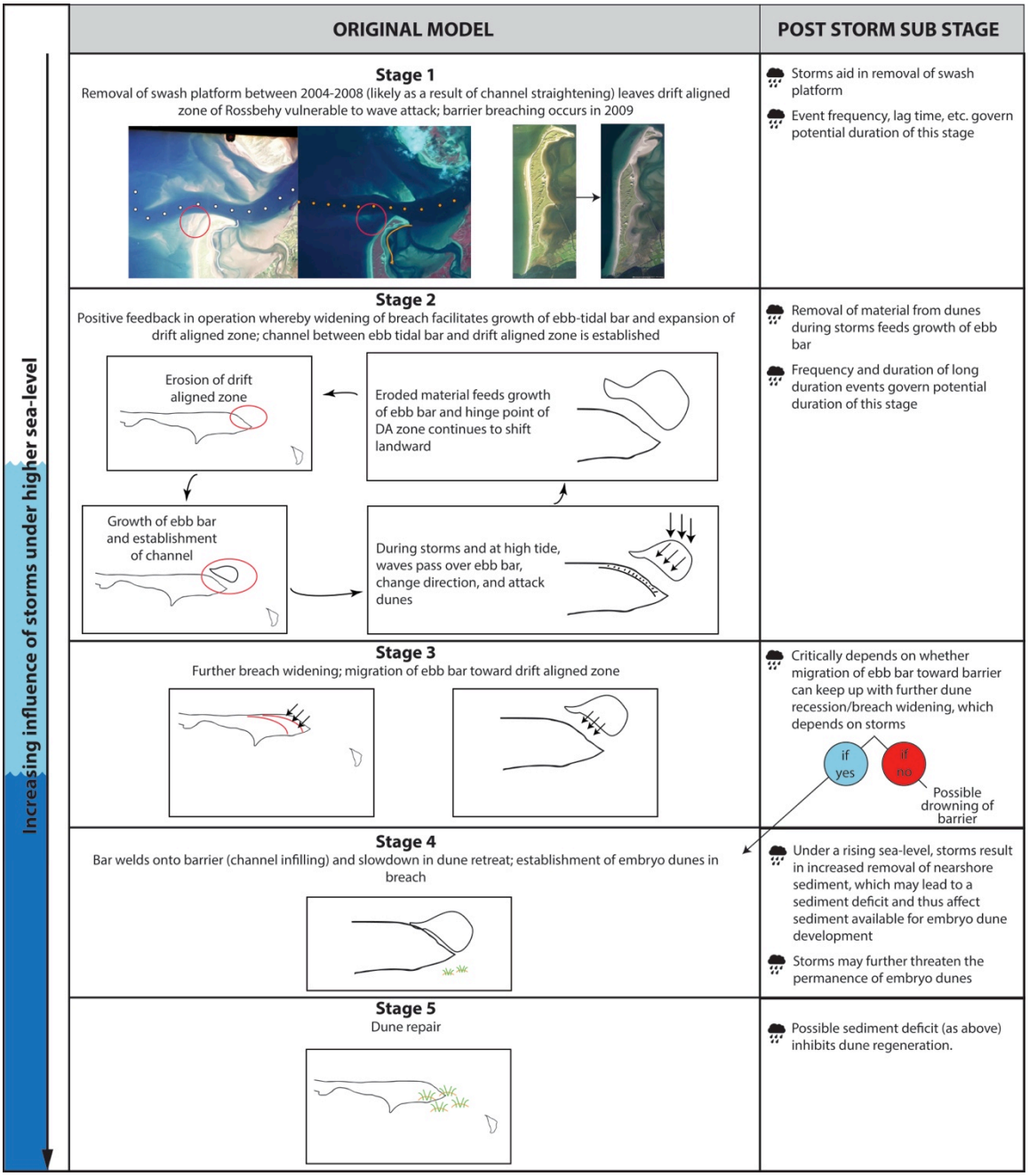

Figure 11.1 S-SLR conceptual model of evolution of Rossbehy in response to storms under a rising sea-level.